



**DATA BUOY COOPERATION PANEL**

**VARIETY IN BUOY TECHNOLOGY  
AND DATA APPLICATIONS**

**PRESENTATIONS AT THE DBCP  
TECHNICAL WORKSHOP**

**(Marathon, Florida, October 1998)**



**DATA BUOY CO-OPERATION PANEL**

**VARIETY IN BUOY TECHNOLOGY  
AND DATA APPLICATIONS**

**PRESENTATIONS AT THE DBCP  
TECHNICAL WORKSHOP**

**(Marathon, Florida, October 1998)**

**DBCP Technical Document No. 14**

**1999**

## NOTES

The designations employed and the presentation of material in this publication do not imply the expression of any opinion whatsoever on the part of the Secretariats of the Intergovernmental Oceanographic Commission (of UNESCO), and the World Meteorological Organization concerning the legal status of any country, territory, city or area, or of its authorities, or concerning the delimitation of its frontiers or boundaries.

*Editorial note:* This publication is for the greater part an offset reproduction of typescripts submitted by the authors and has been produced without additional revision by the Secretariats.



## FOREWORD

The success of technical workshops at the eleventh, twelfth and thirteenth sessions of the Data Buoy Cooperation Panel (DBCP) (respectively Pretoria, Henley-on-Thames and La Réunion, see DBCP Technical Publication No. 12) encouraged the panel to make such workshops a regular feature of its annual session, as a practical means of promoting cooperation and information exchange amongst all sections of the global buoy community, including buoy deployers, data users and communication systems providers.

Consequently, a technical workshop on *Variety in buoy technology and data applications* took place during the first day and a half of the fourteenth session of the panel, held in, Marathon, Florida, USA, in October 1998. Around 20 papers were read to more than 50 participants during the workshop, and the texts of 15 and abstracts of 4 of these are included in this DBCP technical publication. In all cases the papers have been reprinted as received, without additional editorial intervention.



## TABLE OF CONTENTS

### FOREWORD

### TABLE OF CONTENTS

### AGENDA

### PRESENTATIONS

1.	D.W. Jones and A.N. Bentley, UK Meteorological Office, United Kingdom <i>Open-Ocean Data Buoy</i> .....	1
2.	Peter Thomas, Central Institute of Technology, New Zealand <i>Issues Involved in the Design of an Autonomous Solar Electric Research Vessel for Gathering Surface from Remote Areas</i> .....	9
3.	David B. Gilhousen, National Data Buoy Center, USA <i>Dial-A Buoy Reaches Mariners</i> .....	19
4.	David Meldrum, Dunstaffnage Marine Laboratory, UK <i>Recent Drifter Developments at Dunstaffnage: the Smart Buoy and the Mini Drifter</i> ....	27
5.	Mark Bushnell, NOAA/AOML-GDC, USA <i>Recent Progress Using Orbcomm and Iridium for Drifting Buoy Data Transmission</i> ....	31
6.	Ngoc Huang and Jeff Wingwroth, TECHNOCEAN, NAL Research, USA <i>Data Relay Systems for Drifting Buoys Utilizing Low-Earth Orbit Satellites</i> .....	33
7.	Hal Brown, Ralph Cambre, Joel Chaffin and Charles Bond, National Data Buoy Center and Computer Sciences Corporation, Stennis Space Center, USA <i>A Buoy-Mounted Air Traffic Control Radio Relay System</i> .....	35
8.	M. Blaseckie, S.G.P. Skey, K. Berger-North, J. Ploeg and P.A. Bolduc, Axys Environmental Consulting Ltd., DFO/Canadian Coast Guard, Marine Environmental Data Service, Canada <i>The Cape Mudge Wave Experiments: Early Results</i> .....	41
9.	David Wang and David Gilhousen, Computer Sciences Corporation and National Data Buoy Center, Stennis Space Center, USA <i>Separation of Sea and Swell from NDBC Buoy Wave Data</i> .....	53
10.	Stephen E. Pazan and Peter P. Niiler, Ocean Prospects and Scripps Institution of Oceanography, USA <i>Recovery of Near Surface Velocity from Undrogued Drifters</i> .....	61
11.	John Stadler, Atlantic Oceanographic and Meteorological Laboratory, USA <i>Development of a Drifting Buoy Metadata File at the Global Drifter Center</i> .....	107
12.	M. Taillade, CLS/Service Argos, France <i>Preliminary Analysis of Argos 2 on NOAA K Performances</i> .....	109
13.	Christine M. Caruso, National Oceanic and Atmospheric Administration, National Weather Service and National Centers for Environmental Prediction Central Operations, USA <i>Interactive Real-time Quality Control of Surface Marine Data at the National Centers for Environmental Prediction</i> .....	123
14.	Sveng-Aage Malmberg and Hedinn Valdimarsson, Marine Research Institute, Iceland <i>Long Distance Drift from Icelandic Waters into the Labrador and Norwegian Seas 1995-1998</i> .....	131

15.	Mark Swenson and Donald V. Hanson, National Oceanic and Atmospheric Administration/AOML, USA <i>Mixed Layer Heat Budget in the Cold Tongue Region</i> .....	133
16.	David Cotton, Satellite Observing Systems, United Kingdom <i>The Global Inter-Calibration of Satellite and Buoy Measurements of Winds and Waves</i> .	135
17.	D.W. Jones and H.M. Tanner, UK Meteorological Office, United Kingdom <i>An Assessment of the Uncertainty in NWP Background Field Data Based on Duplicate Observations from Moored Buoys</i> .....	143
18.	Robert Molinari, Atlantic Oceanographic and Meteorological Laboratory, NOAA, USA <i>Profiling-ALACE Floats in the Atlantic Circulation and Climate Experiment</i> .....	155
19.	H. Paul Freitag, Linda J. Mangum, Nathan C.M. Franzen and Michael J. McPhaden, National Oceanic and Atmospheric Administration, Pacific Marine Environmental Laboratory, USA <i>TAO Array Enhancements and Expansions</i> .....	157

**LIST OF PARTICIPANTS**

**AGENDA FOR SCIENTIFIC AND TECHNICAL WORKSHOP  
OF THE DATA BUOY COOPERATION PANEL**

**VENUE: Marathon, Florida**

**DATE: October 12-13, 1998**

**THEME: Variety in Buoy Technology and Applications**

**WORKSHOP CHAIR: Eric Meindl, National Data Buoy Center (NWS/NOAA), U.S.A.**

**Monday, October 12, 1998**

**Session I Innovative Concepts in Moored and Drifting Buoy Design and Application  
Chair — D. Wynn Jones, UK Meteorological Office, U.K.**

**Open-Ocean Data Buoy**

D. W. Jones and A. N. Bentley, United Kingdom Meteorological Office, U.K.

**Issues Involved in the Design of an Autonomous Solar Electric Research Vessel for  
Gathering Surface Data from Remote Areas**

Peter Thomas, Central Institute of Technology, New Zealand

**Dial-A-Buoy Reaches Mariners**

David B. Gilhousen, National Data Buoy Center (NWS/NOAA), U.S.A.

**Recent Drifter Developments at Dunstaffnage: the Smart Buoy and the Mini Drifter**

David Meldrum, Dunstaffnage Marine Laboratory, Scotland - U.K.

**Recent Progress Using Orbcomm and Iridium for Drifting Buoy Data Transmission**

Mark Bushnell, Atlantic Oceanographic and Meteorological Laboratory (OAR/NOAA), U.S.A.

**Data Relay Systems for Drifting Buoys Utilizing Low-Earth Orbit Satellites**

Dr. Ngoc Huang (and Jeff Wingroth, TECHNOCEAN), NAL Research, U.S.A.

**An Air Traffic Control System Utilizing Moored Buoys**

Hal Brown, National Data Buoy Center (NWS/NOAA), U.S.A.

**Session II Applications of and Scientific Results Deriving from Buoy Data in Research or  
Operations Chair - Elizabeth Horton, U.S. Naval Oceanographic Office, U.S.A.**

**The Cape Mudge Wave Experiment: Early Results**

M. Blaseckie, S.G.P Skey, K. Berger-North, J. Ploeg and P.A. Bolduc, Axys Environmental Consulting Ltd, DFO/Canadian Coast Guard, and Marine Environmental Data Service, Canada

**Estimating Swell Information for NDBC's Web Site**

David Gilhousen and Dr. David Wang, National Data Buoy Center (NWS/NOAA) and Computer Sciences Corporation, U.S.A.

**Recovery of Near Surface Velocity from Undrogued Drifters**

Dr. Stephen Pazan and Dr. Peter Niiler, Ocean Prospects and Scripps Institution of Oceanography, U.S.A.

**Development of a Drifting Buoy Metadata File at the Global Drifter Center**

John Stadler, Atlantic Oceanographic and Meteorological Laboratory (OAR/NOAA), U.S.A.

**Preliminary Analysis of Argos 2 on NOAA K Performances**

M. Taillade, Service Argos, Inc., France



**Interactive Real-time Quality control of Surface Marine Data at the National Centers for Environmental Prediction**  
Christine M. Caruso, NOAA/NWS/NCEP/Central Operations, U.S.A.

**Long Distance Drift from Icelandic Waters into the Labrador and Norwegian Seas 1995-1998**  
Svend-Aage Malmberg and Heoinn Valdimarsson, Marine Research Institute, Reykjavik, Iceland

**Mixed Layer Heat Budget in the Cold Tongue Region\***  
Mark Swanson and Donald V. Hanson

**Tuesday, October 13, 1998**

**Session III      Buoy Data as a Complement to Remote Sensing, Modeling, and Other Disciplines**  
**Chair - Ron McLaren, Environment Canada**

**The Global Inter Calibration of Satellite and Buoy Measurements of Winds and Waves**  
David Cotton, Southampton Oceanography Centre, U.K.

**An Assessment of the Uncertainty in NWP Background Field Data Based on Duplicate Observations from Moored Buoys**  
D. W. Jones and H. M. Tanner, United Kingdom Meteorological Office, U.K.

**Profiling-ALACE Floats in the Atlantic Circulation and Climate Experiment**  
Dr. Robert Molinari, Atlantic Oceanographic and Meteorological Laboratory (OAR/NOAA), U.S.A.

**TAO Array Enhancements and Expansions**  
Paul Freitag, Pacific Marine Environmental Laboratory (OAR/NOAA), U.S.A.

---

\*No written material submitted for the proceedings.

# OPEN-OCEAN DATA BUOY

By D W Jones and A N Bentley

## 1. Abstract

Based on many years operational experience, The UK Meteorological Office (Met Office) has developed an Open-ocean Meteorological Data Buoy capable of continuous extended operation in the severe environment of the north-east Atlantic Ocean. The buoys are equipped with duplicated sensors and data collection systems. Each buoy also has two Meteosat DCP transmission systems, each of which transmits both sets of collected data every hour. This redundancy significantly reduces the potential for data loss due to any sensor failure, or failure of either of the data collection or transmission systems. The duplicate data sets also enable quality control and selection of the 'best' before coding and dissemination on the GTS. The paper includes a description of the main design features, the sensors and data acquisition systems. It also describes some of the enhancements, to both the buoys and the network, planned for implementation within the next year.

## 2. Introduction

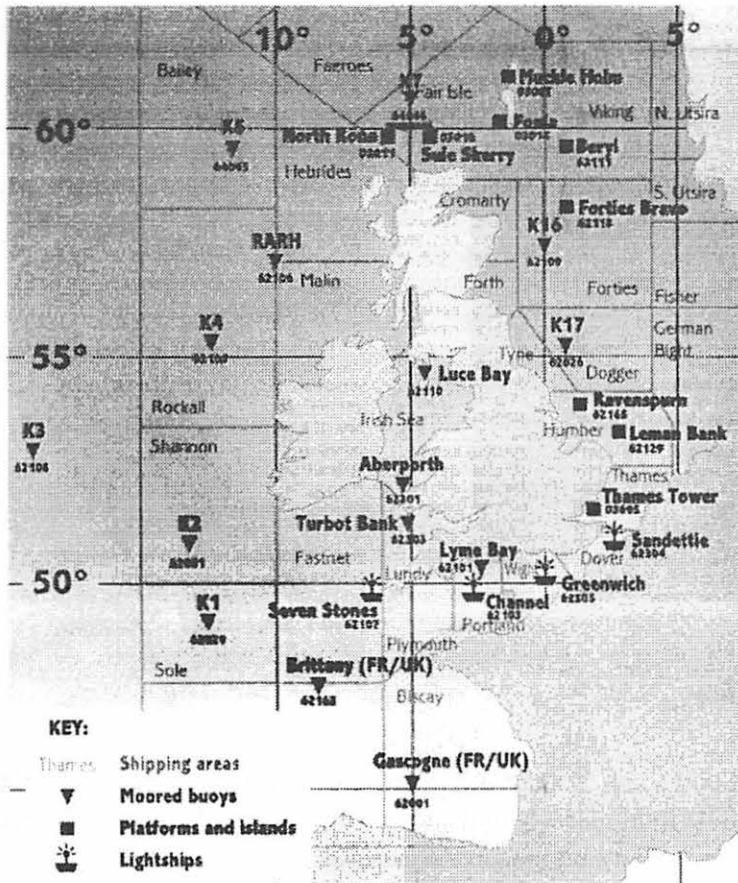


Figure 1 shows the UK Met Office (UKMO) network of marine automatic weather stations and their associated World Meteorological Organisation (WMO) numbers.

This paper describes the moored buoy part of this network with particular reference to the open-ocean buoy design which is used at all buoy stations except Lyme Bay, Aberporth and Luce Bay.

The buoys are also in use at the Brittany and Gascogne Stations as collaborative projects with Meteo France.

Figure 1 UK Met Office (UKMO) Network of Marine Automatic Weather Stations

### 3. The Open-Ocean and Inshore Buoys

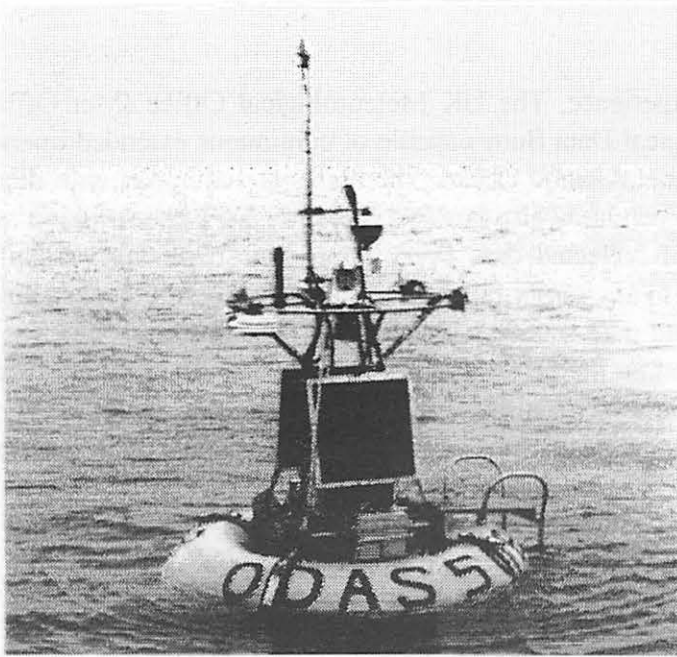


Figure 2 Inshore Design



Figure 3 Open Ocean Buoy

Figures 2 and 3 show the UKMO Inshore and Open-Ocean Buoys.

The inshore design (Figure 2) is a 2.5 metre diameter toroidal buoy using a single electronics payload and sensor suite with a UHF, line-of-site, communications link to a local shore station. These buoys are generally deployed in relatively shallow waters, up to 50 metres and have the advantage that in addition to providing automatic hourly reports they can also be interrogated.

The open-ocean buoy (Figure 3) has been designed to operate in virtually any water depth from 30 metres to 6,000 metres, in all sea conditions, at least all those encountered in the North- Eastern Atlantic.

It has a hull diameter of 2.8 metres, an overall height of 6.0 metres and it weights 4.1 tonnes, in its operational state.

Buoyancy is provided by a closed cell foam floatation collar protected by self-coloured elastomer skin approximately 10 mm thick. The total reserve buoyancy of the buoy is 5 tonnes which enables it to carry the entire mooring system without being submerged, for example, if the buoy is dragged out of its mooring depth. The hull has a cylindrical steel foot, which allows it to be free standing when out of the water, and fins which reduce rotational motion when it is at sea.

The superstructure is 3.0 metres high and manufactured from marine grade stainless steel; it is free standing when separated from the hull. It incorporates a single point lifting eye and is stressed to safely take the weight of the buoy and mooring during deployment and recovery. The superstructure incorporates a 'crow's nest' arrangement with a 1.5 metre diameter ring at its top, made from 1 inch stainless steel tube, on which wind sensors and antennae are mounted; this is 4 metres above nominal sea level when deployed. There are also lower bars for the mounting of barometric pressure, air temperature and humidity sensor housings.

The sensors and antennae are mounted by means of quick release clamps which are easy to operate in rough sea conditions and without the use of special tools. The superstructure also incorporates access ladders, solar panels, radar reflectors, and a single navigation lamp to meet the safety provision of ODAS Aids and Devices published by the Inter-Governmental Marine Consultative Organisation (IMCO).

In addition to the meteorological and oceanographic variables the buoys also report location using the GPS, plus house keeping data such as electronics supply voltage, electronics pod humidity and temperature, navigation lamp status, battery charge and discharge currents, transmission count and hull dry or flooded.

## 4. Sensors

All sensors, except the wave sensor, are duplicated and all except the wave and sea temperature are mounted externally and can be exchanged at sea. The variables reported and sensor types are given in Table 1. All sensors are calibrated at the UKMO test and calibration facility, before being used operationally. This includes a purpose built, vertical, wave sensor calibration rig which is capable of simulating sinusoidal and complex waves of up to 4 metres peak to trough and periods in the range 3 to 30 seconds. Check observations are also taken on station before and after sensors are exchanged.

Variable	Reported Value	Sensor Type
Wind Speed	The ten minute average preceding the observation time	Rotating cup anemometer.
Maximum Gust	The maximum 3 second value since the last synoptic observation.	Rotating cup anemometer.
Wind Direction	Averaged as for wind speed	Self referencing wind vane.
Barometric Pressure	A ten second average not corrected to mean sea level.	Aneroid capsule or vibrating cylinder.
Relative Humidity	An instantaneous value, taken at the observation time.	Electrical conductors set in a wafer of a chemically treated styrene copolymer with an integral non conducting substrate. Protected against salt water contamination.
Air Temperature	A ten second average.	Platinum resistance thermometer in an ODAS radiation screen.
Sea Surface Temperature	A ten second average at a nominal depth of 1 metre.	Platinum resistance thermometer mounted in a hull contact housing.
Significant Wave Height and Wave Period	4 x RMS value of the wave height, and the average crossing interval of the wave through the mean water level, for 17.5 minutes preceding the observation time.	An accelerometer the output of which is double integrated to produce heave.

Table 1 Variable, Reported Value and Sensor Type

## 5. The Electronics Payload

A schematic diagram of the open-ocean buoy electronics system can be seen at Figure 4. It is fully duplicated, with the exception of the wave sensor, with crossover interconnections for increased system integrity whenever possible.

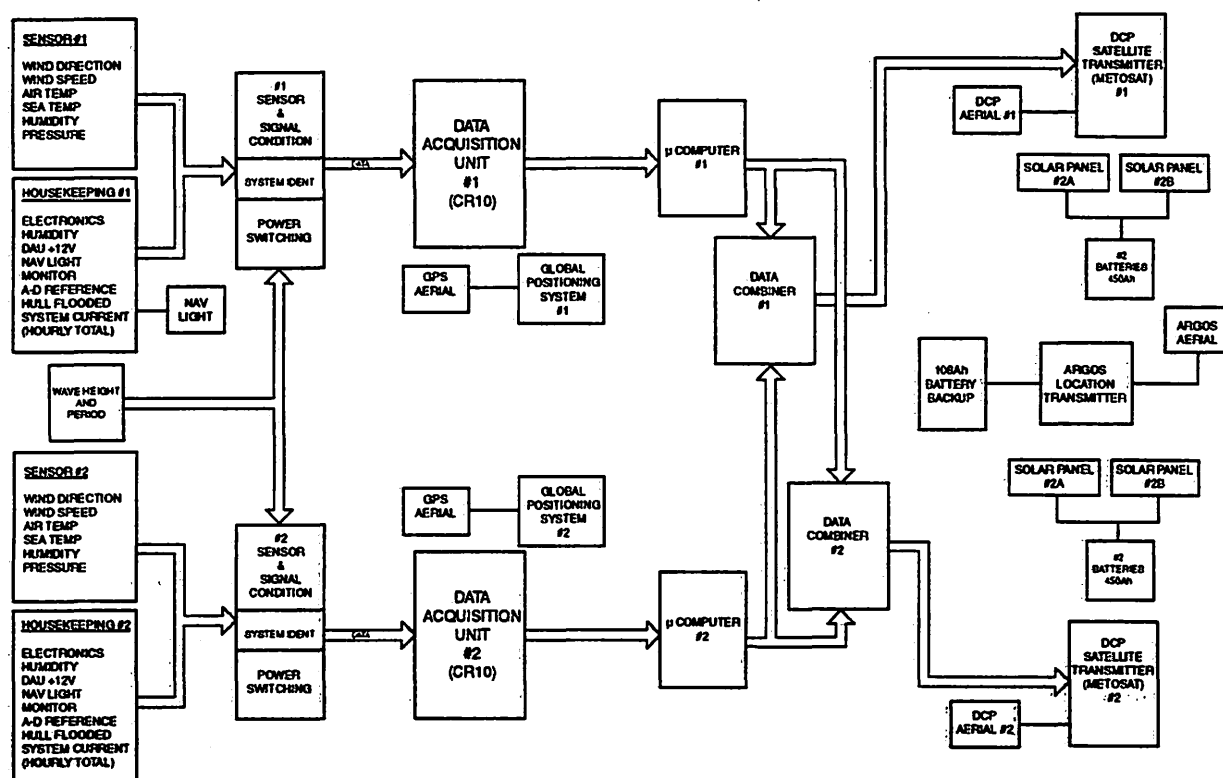


Figure 4 Schematic Diagram

Each data acquisition system is based upon a PC programmable, proprietary data logger, The CR10, manufactured by Campbell Scientific. The logger output is then converted to a unique marine automatic weather station (MAWS) code, within a programmable, single board microcomputer, which takes in position data directly from the GPS.

The data from each of the two microcomputers are then united within two data combiners, the outputs of both combiners are then passed to two DCP satellite transmitters. Consequently each transmission contains data from both suites of sensors and both data acquisition systems.

The power output of the DCP transmitter is 25 Watts. This has proved to be sufficient to ensure reliable operations for latitudes up to at least 60°. To ensure timely availability of the data, both for NWP models and forecasters, DCP transmission slots between HH-8 and HH +10 have been selected. Data are received at the ESOC reception facility at Darmstadt from where they are forwarded to the UKMO Communications Centre at Bracknell, for data selection and recoding into WMO FM13 Ship Code for retransmission on the Global Telecommunications System (GTS).



## **6. Location**

Being moored, the nominal location of the buoy is known, at least within the circle of movement which results from the inverse catenary mooring (see Section 10). However the activities of fishing boats and other unwarranted interference does occasionally result in buoys going adrift. Consequently two Global Positioning System (GPS) receivers are installed on the buoy and the location data are included in the transmitted message. As a backup, in the event of a buoy suffering major damage to the superstructure, an Argos PTT, with an independent power supply, is incorporated into the hatch cover of the hull.

## **7. Power Supply**

Each of the two independent sensor and electronic systems on the buoy have their own battery packs, each charged by two solar panels, one on each side of the superstructure. In the unlikely event of the total failure of the solar charging system, a fully charged set of the lead acid gel batteries have sufficient capacity to power the buoy for at least three months. Even at 60° north the solar panels supply sufficient charge to maintain the buoy throughout the winter.

## **8. The servicing of Open-Ocean Buoy stations**

The present practice is for a servicing visit to each station every six months for a routine change of external sensors. The upper moorings are inspected every 12 months and the complete buoy is exchanged every two years. The mooring is changed at three yearly intervals.

## **9. Data**

### **9.1. Data Coding**

Under normal circumstances, four sets of observational data are available every hour (two transmissions each containing data from both sets of sensors) at the UKMO Communications Centre. Clearly only one set of data is needed to compile an observation and so a selective process has to be implemented. Normally the FM13 coded observations are made from sensor suite 1 data via transmission 1. However, if the transmitter or data acquisition system or individual sensors in the sensor suite fail, the FM13 message is compiled from the best available data.

### **9.2. Data Quality Control**

In addition to reducing the potential data loss due to sensor failure, the duplication of sensors provide an opportunity to compare data, and thereby give enhanced confidence in the data quality. There are three levels of quality control used at present:

- WMO FM13 Synoptic Observations are routinely compared against data from the Background Field by the Met Office Quality Evaluation Section. In addition to identifying individual gross errors their process also produces monthly statistics of biases and variances.
- Snapshot checks of the meteorological and oceanographic data are undertaken daily by internal comparison of the duplicated sensor data. Any anomalies are checked immediately against synoptic charts and/or background fields and, if appropriate, changes to the preferred sensor data are made. These daily checks also include monitoring of buoy location and the engineering housekeeping data.
- Data received at UKMO Marine Operations facility, via a Meteosat Retransmission Link, enable the duplicated data to be checked for individual observations and graphically as a time series.

## 10. The Mooring

In water depths of 30 to 100 metres an all chain mooring is used, with a sub-surface float. where appropriate.

The mooring used in deeper water is an inverse catenary type (see Figure 5) with a 1 tonne reserve buoyancy sub-surface float. Moorings based on this principle are in widespread use by, for example, the NDBC and Environment Canada. The principle difference with the UKMO design is the use of a 1 tonne reserve buoyancy sub surface float and an acoustic release; although the continued use of these is currently under review .

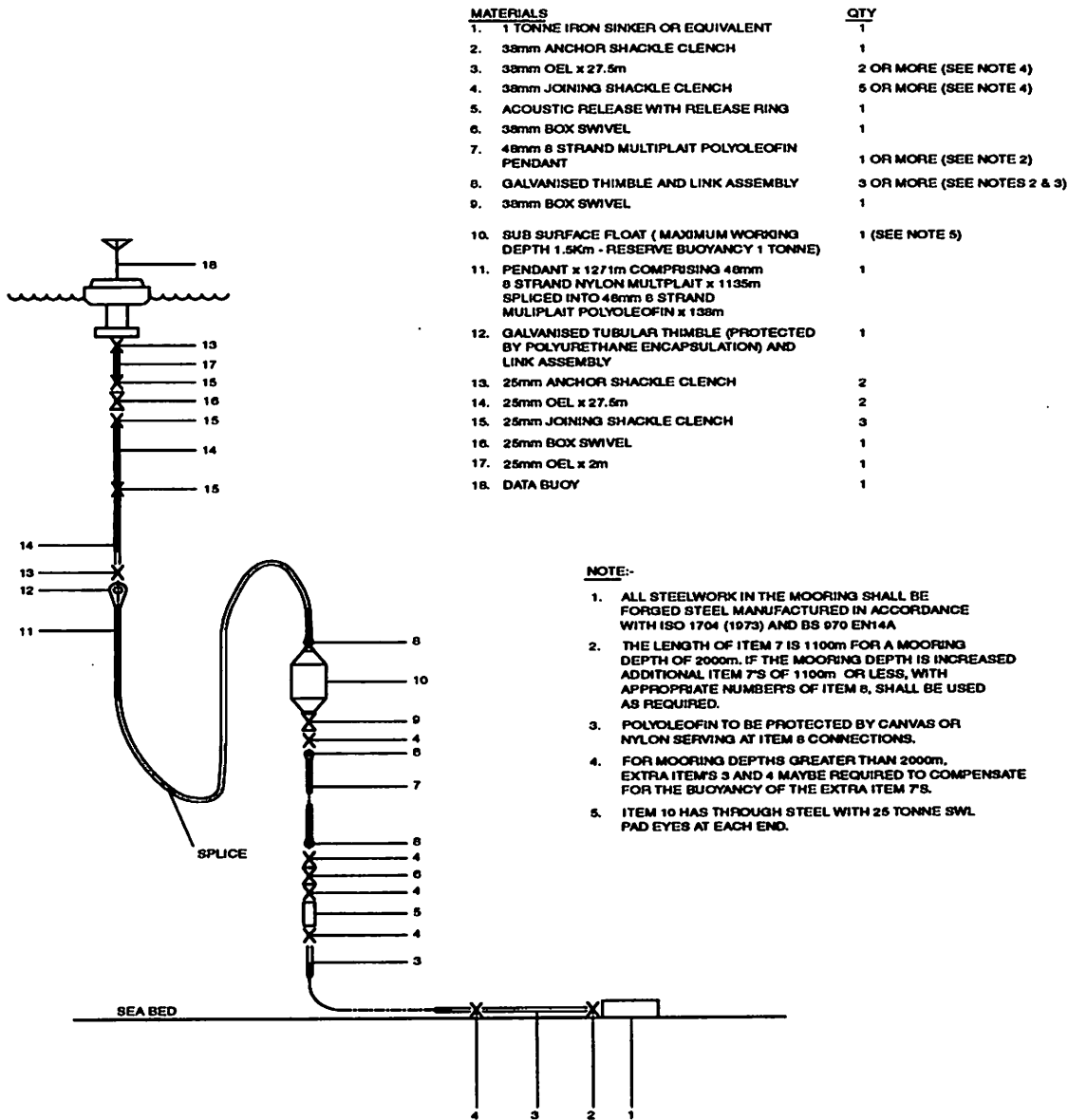
## 11. The Future

As with all operational programmes, enhancements aimed at improving the performance and/or the cost effectiveness are continually being sought. Developments now on trial are:-

- An alternative digital pressure sensor offering high accuracy and long term stability at much reduced cost.
- An improved static pressure head with a Goretex filter, to prevent water ingress, similar to that used on the WOCE drifting buoys.
- An active radar enhancer.
- A solid state wave sensor based on multiple accelerometer and tilt sensors. In addition to significant wave height. This will provide spectral and wave direction data, is a much smaller unit than the Datawell Heave Meter, presently in use, and if successful will permit the use of duplicate wave sensors.
- An Acoustic Doppler Current Profiler (ADCP).

## 12. Conclusion

The Met Office Open-Ocean Buoy is a successful design, having proved itself over many years as capable of providing reliable observations in the severe conditions encountered in the Northeast Atlantic. To date however, the buoys have been deployed to meet a meteorological operational requirements but as components of a long term operational programme they offer an opportunity to be developed as platforms for other oceanographic and environmental measurements.



MOORING DEPTH UP TO 6000m

**Figure 5 Inverse Catenary Type Mooring**



ISSUES INVOLVED IN THE DESIGN OF AN AUTONOMOUS SOLAR  
ELECTRIC RESEARCH VESSEL FOR GATHERING SURFACE DATA FROM  
REMOTE AREAS.

AUTHOR: PETER THOMAS

**ABSTRACT**

This paper outlines the major parameters involved in the design of the smallest conceivable autonomous solar electric research vessel capable of staying at sea for long periods. The design considerations are broken down into three main interrelated areas. These are: Hull Design, Navigation, Energy Management and Propulsion.

During this decade a number of technical innovations have matured to make it possible to produce an unmanned research vessel, powered by photo voltaic cells.

The specification for these unmanned vessels requires them to be capable of leaving their home port under their own power, navigating to a required destination, maintaining station at that location and eventually returning to their home port for a refit.

During their period at sea they radio back the data which they have gathered.

This paper discusses the issues involved in the design of the smallest conceivable vessel capable of performing these tasks. It is concerned only with the vessel as an ocean going research platform, it does not consider what instrumentation research workers may wish to install in it.

The problems involved can be divided into three (interrelated) areas. These are:

1. Hull design
2. Navigation
3. Energy Management and Propulsion



## Hull Design

Initial calculations showed a vessel 4 metres (13 feet) long should be capable of converting enough solar energy into electricity to be capable of powering itself over long periods. The vessel needs to be self righting under all conditions (this requirement ruled out the use of multihulls). If about  $\frac{1}{3}$  of the vessel's weight were to be dedicated to sealed deep cycle lead acid batteries, the vessel would be able to run through the night by consuming the surplus energy generated the previous day.

The positioning of the solar panel became a critical part of the hull design. The panels form an inverted V over the hull, with the angle of the apex  $90^\circ$ . There are a number of reasons for this.

1. More solar energy can be obtained when the sun is low in the sky.
2. The volume of air enclosed by the solar panels enables the vessel to meet its self righting requirements.
3. The steepness of the sides facilitates rapid salt water run off and does not allow the water to evaporate from the surface of the panels leaving behind pools of salt.
4. The slope is too steep and slippery for sea birds to stand on and foul the panels.
5. Wind striking the surface of the  $45^\circ$  panel produces equal capsizing and righting moments.

Keeping the vessel as small and low cost as possible means the energy equations for the vessel are tight. Most of the energy consumed by the vessel is consumed by the propulsion system. As a result the hull needs to be as efficient as we can make it.

The wetted surface has been reduced to a minimum by making the vessel round bilged. This reduced the frictional resistance to a minimum. Optimum prismatic coefficient and almost ideal angle of entry reduce the wave making losses as far as possible. There will be days when heavy cloud cover results in significantly reduced solar electric generation.

When this happens it is advisable to prevent the vessel drifting too far off course. This is achieved by a special rudder design.

The rudder is made in two halves. (Rather like a book). Under normal operation the rudder is turned as a book would be turned about its spine.

If the boat is required to maintain station the two halves of the rudder open up (like a book opening up) and the rudder acts as a drogue. When the drogue facility is no longer required two halves of the rudder close and the rudder operates normally.

The vessel is powered by a single permanent magnet brushed DC motor with direct drive via a manganese bronze log tube. The log tube is part of a single casting incorporating a bronze skeg and the sea water inlets for the cutlass bearing and the bottom bearing for rudder.

## Navigation

The vessel is self guided not radio controlled.

The required route is pre programmed into the GPS with all appropriate waypoints. The bearing to the next waypoint is calculated. This is the magnetic bearing and the boat takes into account variation due to the fact the magnetic poles are different from the true poles. The vessel uses a fluxgate (electronic) compass to determine the vessel's magnetic bearing. The compass takes into account the vessel magnetic deviation. So the bearings are magnetic bearings with both variation and deviation corrections made. Drift is also taken care of as the GPS recognises only the course over the ground, not the course through the water.

In addition to steering towards the next waypoint, the vessel also considers the cross track error (which is integral control). This cross track error is included to get the vessel rapidly back on course should it have been driven off course by adverse weather conditions. Should the vessel temporarily lose satellite coverage, the magnetic bearing to the next waypoint is stored in memory and the vessel continues to steer on its existing course until satellite coverage returns.

The steering servo system takes into account the fact that larger rudder movements are required when the vessel is moving slowly through the water than when the vessel's water speed is high. It does this by changing the gain of the servo system. If this was not done, the vessel would be underdamped at high speeds and overdamped at low speeds.

## **Energy Management and Propulsion**

Most of the energy consumed by the boat is used for propulsion. This provides a method of controlling energy consumption. The amount of electrical energy produced by the photo voltaic cells is weather dependent. The vessel carries sealed deep cycle lead acid batteries, which account for about  $\frac{1}{3}$  of the vessel's weight. This provides enough battery storage for the boat to run through the night. The weight of the batteries significantly lowers the centre of gravity of the boat to make it self righting under all conditions.

The vessel contains two battery systems. There is a 24 volt system and a 12 volt system. The 24 volt system runs everything on the boat. The output of this battery supplies the power for a 10 kHz 100V AC regulated sinusoidal supply. This supply uses class C push pull amplification running in parallel resonance. AC power is then reticulated round the vessel and each electrical system has its own ferrite transformer and rectifier. This provides electrical isolation between systems. In most cases, further DC analogue regulation is not required because the AC supply is already regulated. Also as it is run in parallel resonance which is fed from an above resonance series resonant circuit, the system is short circuit (and student) proof, thus eliminating the need for additional fault protection. It has a very high efficiency. The PWM supply for the main motor drive however runs directly from the 24 volt battery system. This is fitted with electronic over current limitation.

The 12 volt system normally does nothing. This is the uninterruptible power supply (UPS) which will maintain all essential services should adverse weather conditions result in failure of the 24 volt system. The essential services do not include the propulsion system and, without the main motor running, there is no point in running the steering system servo. However, services like the radio, energy management system. GPS, navigation lights, will run for weeks if necessary, even if the vessel were to obtain no solar energy at all.

The vessel carries six nitride treated, laser grooved monocrystalline silicon solar panels. Four panels are dedicated to the 24 volt system and two are dedicated to the 12 volt UPS system. Under normal circumstances the UPS battery will be fully charged on standby. In this situation the surplus energy from the two UPS solar panels is diverted into the 24 volt system. So the usual situation is to have a fully charged 12 volt UPS system and all six solar panels feeding the 24 volt system which supplies all the vessel's power.

The solar panels are fitted with auto tracking electronics. This ensures the panels are always running at maximum theoretical efficiency. For example a 36 cell solar panel may deliver maximum power when its output is 18 volts and say 5 amps (90w). If this solar panel were to be fed into a 12 volt battery the panel would still deliver only 5 amps but with a terminal voltage of 12 volts (60w) (current flowing is proportional to the number of photons striking the panels).

Unfortunately the nominal 18 volt panel output and the nominal battery terminal voltage are both variables. The vessel's auto tracking system ensures the panel is always running at max power output regardless of the panel and battery voltage. It is always tuned to peak power.

The vessel has two energy management systems. One system predicts how much energy should be available taking into account the latitude and longitude of the vessel, the vessel's course, the date and time. It assumes clear conditions and predicts how much energy should be available taking into account the air mass (the path length the sun's rays take through the atmosphere). The vessel measures how much energy it is receiving and compares this with the theoretical maximum. It then presumes this ratio of actual to optimum will continue until dusk. The programme continuously updates. From this ratio the vessel works out how much power it should be using so that it will not run out of energy before the next dawn.

In addition to this the vessel has a hardware back up system. This takes control initially, when the boat is first turned on, and remains in control until one hour after the next



dawn. Or it takes control if the vessel has an energy management crisis, ie. the main 24 volt battery system is either running flat or is getting overcharged. In which case, it provides rapid response to the crisis. It determines the degree of severity of the problem. It contains a self learning system so that the average values it proposes are based on what happened yesterday, which in turn was a response to what happened the day before, and so on. In this way it adjusts to changing latitudes and changing seasons.

## SOLAR BOAT SPECIFICATIONS

### *Mechanical specifications*

Name:	Solar Electric Research Vessel "GOODWILL"
Length (LOA):	4.0 metres (13 feet)
Length water line (LWL):	3.85 metres
Beam:	0.860 metres
Self righting:	All positions
Draft:	340 mm
Displacement:	200 Kgs
Hull material:	Fibre reinforced plastic
Antifouling coating:	Copper within the gel coat
Maximum speed:	5.5 knots (11 Km/hr)
Cruising speed:	4 knots (8 Km/hr)
Motive power:	Electricity

## SOLAR BOAT SPECIFICATIONS

### *Electrical specifications*

Motor:	24 Volt DC, permanent magnet
Maximum power:	280 watts
Cruising power:	100 watts
Number of solar cells:	6 monocrystalline laser grooved silicon panels
Total area of solar panels:	3.8 sq. metres
Maximum power generated per panel:	85 watts
Electrical storage:	3 x 65 Ah 12 volt sealed deep cycle lead acid batteries
Power reticulation:	100v AC 10 kHz

## SOLAR BOAT

### *On board systems*

- Primary energy management (software)
- Backup energy management electronics
- Battery charging and monitoring electronics
- Global positioning system  
*(Garmin GPS45 Personal Navigator)*
- Fluxgate compass  
*(Azimuth 1000 Digital Compass)*
- Satellite radio  
*(Argos satellite system for tracking and communicating with the boat)*
- Bilge pump electronics
- Navigation light and drogue motorelectronics
- Main motor electronics
- Steering motor electronics
- Microcontroller network
- 100v 100KHz AC inverter



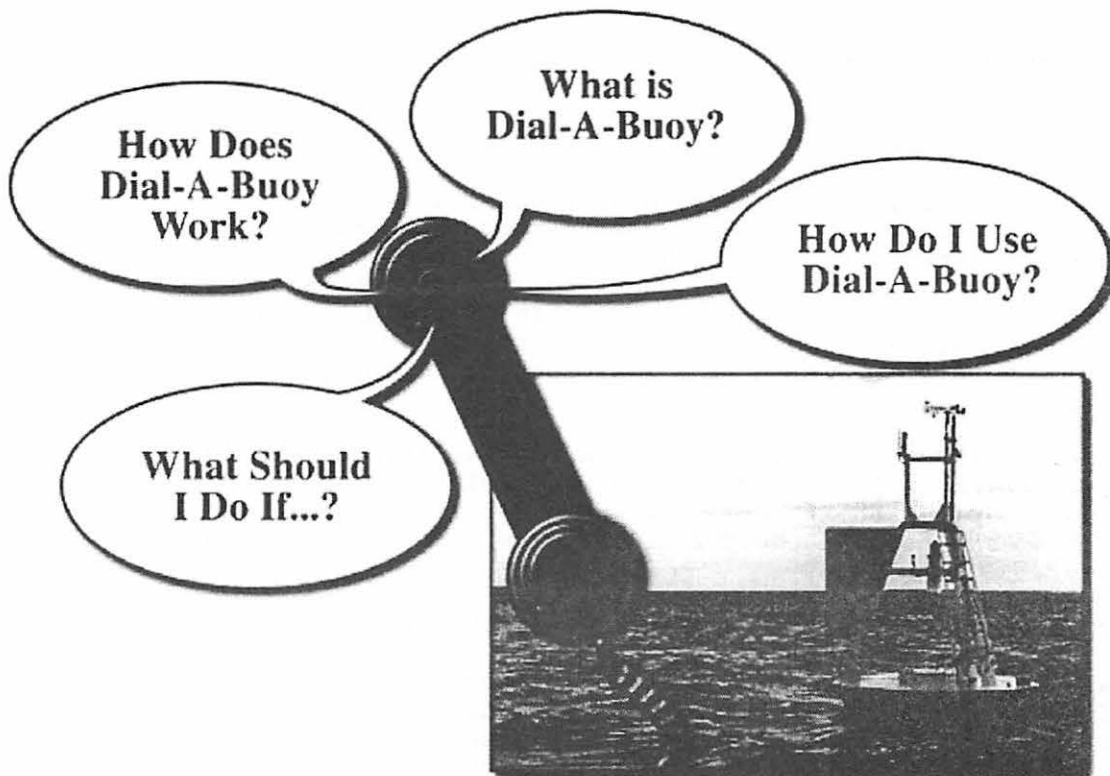
# **NATIONAL DATA BUOY CENTER**

## **Dial-A-Buoy**

---

### **How to Hear Our Observations on the Phone**

---



#### **What is Dial-A-Buoy?**

Mariners can now hear the latest coastal and offshore weather observations through a new telephone service called Dial-A-Buoy. Dial-A-Buoy provides wind and wave measurements taken within the last hour at 65 buoy and 54 Coastal-Marine Automated Network (C-MAN) stations. The stations are located in the Atlantic, Pacific, Gulf of Mexico, and the Great Lakes and are operated by the National Data Buoy Center (NDBC). NDBC, a part of the National Weather Service (NWS), created Dial-A-Buoy to give mariners an easy way to obtain the reports via a cell phone.

Large numbers of boaters use the observations, in combination with forecasts, to make decisions on whether it is safe to venture out. Some even claim that the reports have saved lives. Surfers use the reports to see if wave conditions are, or will soon be, promising. Many of these boaters and surfers live well inland, and knowing the conditions has saved them many wasted trips to the coast.

An increasingly popular way to obtain the observations has been through the Internet. In fact, NDBC's web site has received

more than a million hits a month. "Dial-A-Buoy is a logical extension to the Internet," states NDBC's David Gilhousen. "It will allow the mariner a way to get the conditions while offshore, at the marina, or away from the Internet."

Buoy reports include wind direction, speed, gust, significant wave height, swell and wind-wave heights and periods, air temperature, water temperature, and sea level pressure. Some buoys report wave directions. All C-MAN stations report the winds, air temperature, and pressure; some also report wave information, water temperature, visibility, and dew point.

#### **How do I use Dial-A-Buoy?**

To access Dial-A-Buoy, dial (228) 688-1948 using any touch tone or cell phone. Assuming you know the identifier of the station whose report you need, enter 1. Then, enter the five-digit (or character) station identifier, followed by the # sign, in response to the prompt. The system will ask you to confirm that your entry was correct by pressing 1. After a few seconds, you will hear the latest buoy or C-MAN observation read via computer-generated voice. Characters are entered simply by pressing the key containing the character. For Q, press "7", and for Z, presses "9". Please be patient and wait for the system to finish prompting you; Dial-A-Buoy will not understand your entry if you are too fast.

Dial-A-Buoy also can read the latest NWS marine forecast for most station locations. If this option is available, the system will prompt you to press the # key after the observation is read. Wait to hear the tone at the end of the prompt before pressing the # key.

When you are finished with Dial-A-Buoy, simply hang-up!

There are several ways to find the station locations and identifiers. For Internet users, maps showing buoy locations are given at <http://www.ndbc.noaa.gov/>. Telephone users have several options. They can enter a fax number to receive a location map by following the prompts. Or, they can enter a latitude and longitude and receive the closest station locations and identifiers.

#### **How Does Dial-A-Buoy Work?**

The Dial-A-Buoy system does not actually dial into a buoy or C-MAN station. The phone calls are answered by a computer at the Stennis Space Center in Mississippi, where NDBC is located. The computer runs Web-on-Call software to control the dialog and read the forecasts and observations from NDBC's web site. Web-on-Call, a commercial product from General Magic Corporation of Sunnyvale, California, controls the reading of Web pages over the phone.

Dial-A-Buoy is a proof-of-concept system that seeks involvement from the private sector. The eight-line system could be expanded through sponsorship by a private corporation such as a boating or meteorological organization. Alternatively, these organizations could offer a similar service at another location. This could easily be accomplished by running Web-on-Call software that would obtain the observations from NDBC's web site.

**What are some problems with Dial-A-Buoy?**

*I entered a station identifier, but heard a response "Sorry, I did not recognize that selection." You entered the station identifier too soon. Wait until the system finishes asking you for the identifier.*

*How do I enter characters for a Station Identifier?*

Characters are entered simply by pressing the key containing the character. For Q, press "7", and for Z, presses "9". For example, to enter CHLV2, press the keys 24582 followed by the # sign.

*I entered a valid station identifier, but heard a response saying that the topic was unavailable after about 6 second delay. Occasionally, the Internet gets very busy here at Stennis Space Center. The Web-On-Call software, which runs Dial-A-Buoy, has been programmed to give this response if it cannot obtain our web page to read in about 5 seconds. So, unfortunately, the answer is: Try again later.*

*I pressed the pound sign to get a marine forecast but heard the response, "Sorry I did not recognize that selection." You entered the pound sign too early. Wait until you hear a tone to press the pound sign.*

*How do I quit Dial-A-Buoy? Simply hang-up.*

*How do I hear the observations for another station? When you are finished hearing the observations or forecasts, the system will begin a long prompt saying, "To listen to this topic again, press 1....." If you press 6 at this point, Dial-A-Buoy will take you back to the beginning of the dialog.*

*This page was last modified on Monday, 10-Aug-98 12:53:20 CDT*

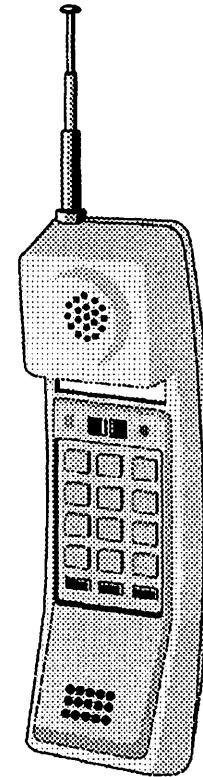
[HOME](#) | [Webmaster](#) | [Disclaimer](#) | [GUESTBOOK](#) | [FAQ](#)

[Home](#) | [Webmaster](#) | [Disclaimer](#) | [Guest Book](#) | [FAQ](#)

# NDBC'S DIAL-A-BUOY SYSTEM

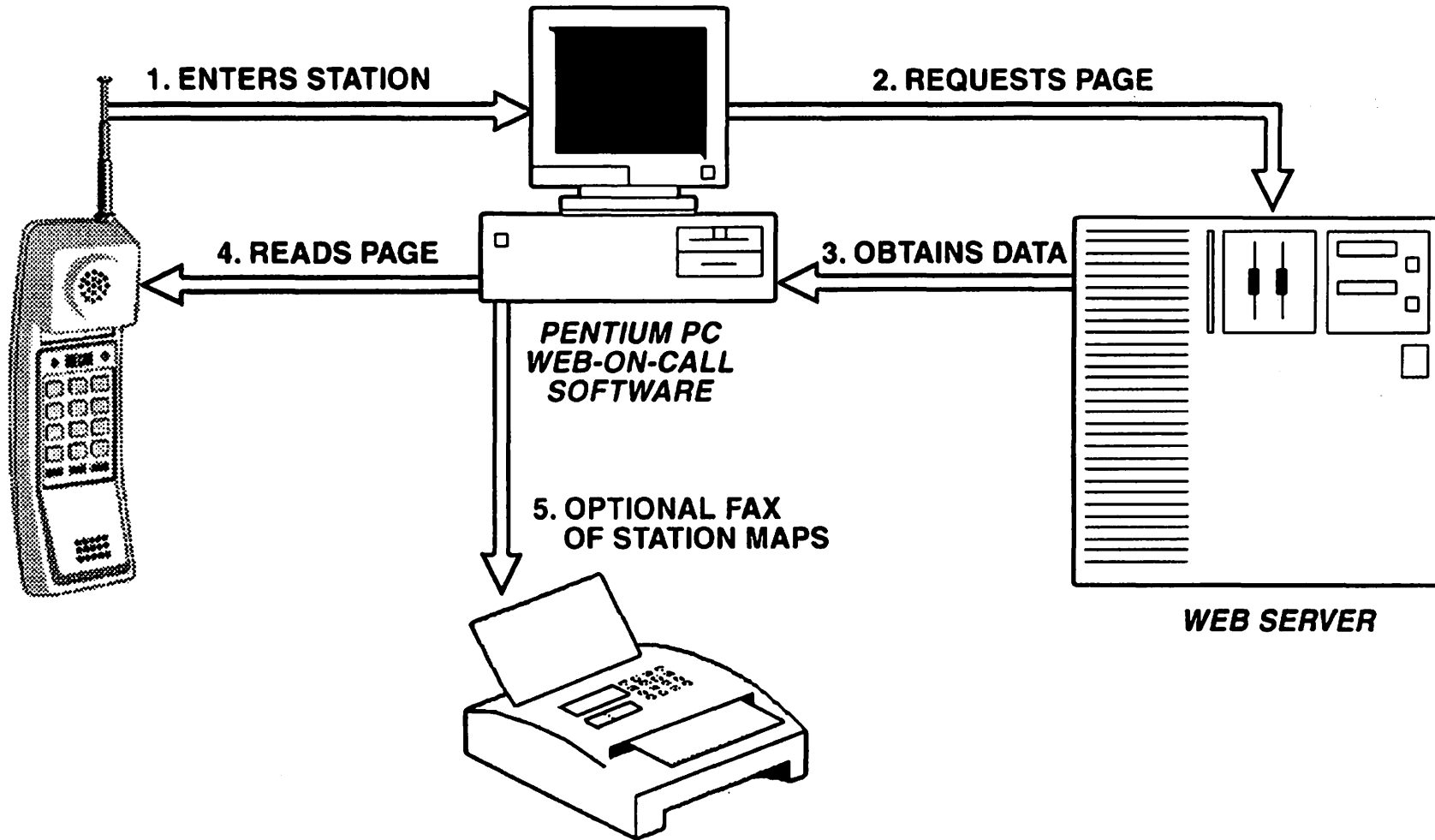
COMPUTER VOICE RESPONSE SYSTEM THAT

- **READS**
  - LATEST OBSERVATION
  - COASTAL-MARINE FORECASTS
  - CLOSEST STATIONS GIVEN POSITION
  
- **FAXES STATION LOCATION MAPS**





# DIAL-A-BUOY SYSTEM



# DIAL-A-BUOY REACTION

- **AVERAGES 700 CALLS A DAY**
- **REACHES MANY WHO CANNOT TRAVEL IN CYBERSPACE**
- **ONE USER COMMENT: "DIAL-A-BUOY IS A GREAT IDEA! AND "COOL" TOO. I WILL BE SURE TO TELL THE WIND-SURFING CROWD ABOUT IT . . . IT IS GREAT TO SEE A TRULY USEFUL EXPENDITURE OF TAX DOLLARS."**
- **PRIVATE SECTOR INTEREST:**
  - **NEW JERSEY COMPANY TO START 1-900 NUMBER**
  - **BOAT/US INTERESTED IN OFFERING SERVICE IN SELECTED AREAS**

## **WEB-ON-CALL, VERSION 2 IMPROVEMENTS**

- **USERS CAN ENTER STATION IDENTIFIER BEFORE THE PROMPT HAS FINISHED**
- **SYSTEM QUICKLY RECOGNIZES LINES WHERE THE USER HAS HUNG UP TO GIVE GREATER CAPACITY**
- **NDBC CAN TAILOR THE PROMPT AT THE END ALLOWING USERS TO EASILY REQUEST A SECOND STATION**
- **SYSTEM WILL ALLOW NDBC TO INCREASE THE TIME THAT *WEB-ON-CALL* WILL WAIT FOR A STATION PAGE TO BE OBTAINED FROM THE NDBC WEB SITE**



## Recent Drifter Developments at Dunstaffnage: the Smart Buoy and the Mini Drifter

David Meldrum  
Centre for Coastal and Marine Sciences  
Dunstaffnage Marine Laboratory  
Oban PA37 1QA  
Scotland

### INTRODUCTION

The increasing military requirement for rapid environmental assessment (REA) has stimulated the development of a number of expendable oceanographic sensor systems. At Dunstaffnage we have developed a 'smart' drifter for REA which evaluates the data from its sensor suite (thermistor string plus GPS receiver), according to user-specified criteria, and only transmits profiles which it considers will be of interest to the user. Currently, Argos is used as the communications channel. Satellite over-passes are predicted by the on board processor and data uploads scheduled accordingly. This approach optimises data transfer and minimises the risk of detection.

In a separate development, a mini-drifter has been produced for near-shore studies. Bi-directional UHF telemetry is used to receive DGPS corrections from a shore station. Corrected DGPS locations are broadcast over the return link and displayed in real time on a navigation chart using commercially available ship navigation software. The drifter has been used to study pollution trajectories close to fish farms.

### THE ADAPTIVE SAMPLING 'SMART' TZ BUOY

#### *Adaptive Sampling*

A basic belief in oceanography is that the oceans contain too much data for the entirety to be measured, recorded and processed in any simple-minded fashion. This is particularly true if the goals of operational ocean observation in support of climate modelling and prediction are to be realised cost-effectively. Even if enough ocean platforms (moored instruments and buoys, drifters, profilers, autonomous submersibles, ships) could be deployed to make measurements at the required accuracy and density, the data communications and processing burden would be overwhelming. Furthermore, much of these data would be uninteresting and of little or no impact on the analysis, and would only serve to consume valuable energy, communications bandwidth and data processing resources. The costs of this profligacy are even more damaging in the military case of 'Rapid Environmental Assessment' (REA), where unnecessary data transmissions increase the risk of detection and countermeasures, and impose additional burdens on an increasingly stressed communications system (Meldrum and Peppe, 1998).

Adaptive sampling aims to make the most efficient use of the energy and communications resource by selecting significant data at the point of measurement (by autonomous decision on board the measurement platform) and by transmitting these data alone. Data selection criteria are loaded into the platform prior to deployment, but may be updated via a two-way communications link if deemed necessary. From an energy point of view, the penalty resulting from the increased processing power that must be installed on the platform to drive the data selection process is more than offset by savings in the communications budget. If we add to these savings the decreased likelihood of detection, and the increased quality and relevance of the condensed data stream, the concept of adaptive sampling becomes even more compelling.

#### *The Prototype Adaptive Sampling Buoy (ASB)*

Under a study sponsored by the UK Defence Evaluation and Research Agency (DERA), DML has investigated the implementation of adaptive sampling using a number of artificial intelligence techniques. While some approaches, such as the NASA-developed CLIPS, looked promising, the compiled code sizes were in general considered too large for a small, low-power drifter. However, results of a case study were sufficiently encouraging for work to proceed to the construction of a prototype ASB.

For this practical case of the first prototype ASB at least, it was decided to write the adaptive sampling algorithm, as well as other parts of the firmware, in C. The code was then implemented on a low-power DML processor board featuring the 80C186EB processor, essentially a PC on a small card. This approach confers a number of benefits: in particular, the code can be developed and fully tested on a conventional PC before embedding in the target processor. For the prototype, the following rather arbitrary sampling rules were chosen to trigger 'significant' data selection:

- 1 sensor has changed by  $> 0.50$  C since last logged value;
- 2 sensors have changed by  $> 0.35$  C since last logged value;
- 3 sensors have changed by  $> 0.30$  C since last logged value;
- 4 sensors have changed by  $> 0.25$  C since last logged value;
- 5 sensors have changed by  $> 0.20$  C since last logged value;
- the drifter has moved by  $> 200$  m since last logged value;
- no data have been selected in the last 2 hours.

The firing of any of these rules is sufficient to cause the sampled sensor values to be added to the stack of significant data for transmission to the user.

In addition to the processor card, the prototype ASB sensor package included a low-power GPS receiver, a string of five thermistors and an Argos satellite transmitter. The prototype hardware and software was extensively exercised prior to trial deployments using a purpose-built hardware simulator which mimicked sensor inputs arising from simulated trajectories through both real and synthetic ocean datasets. These bench trials showed that the adaptively sampled dataset accurately reproduced the significant temperature structure of the source data, while considerably reducing the amount of data that needed to be transmitted (Figures 1 and 2).

Data telemetry for this phase of the project used the Argos system carried by the polar-orbiting NOAA satellites. Data transmission efficiency was significantly enhanced through the implementation on the ASB of an orbit-prediction routine to adapt the transmission schedule to satellite availability. The complete prototype system was packaged in a modified WOCE-pattern buoy hull (Sybrandy and Niiler, 1991) and successfully tested in inshore waters close to Dunstaffnage (Figure 3).

### The Sonobuoy-Sized ASB

The next phase of the project has been to repackage the above hardware in a much smaller A-size sonobuoy hull. This hull, and other elements of the hardware such as the thermistor string, flotation and antennae, were supplied by Metocean Ltd as part of a collaborative approach to the design of sonobuoy-sized drifters for REA. The DML electronics and firmware were redesigned and hulls in Canada in August 1997. Two A-size ASBs were successfully deployed in October 1997 alongside more conventional A-size Metocean drifters during a trial in the central Mediterranean (Figures 4 and 5).

Although the buoys are capable of being air-deployed using an integral parachute and pyro-triggered inflatable flotation, this feature was not required for the trial and fixed solid flotation was used. Data analysis from this and more recent trials has now been completed, and will be reported in more detail at a later date.

### THE MINI DRIFTER

In response to a requirement for the accurate tracking of pollutants emanating from fish farms, notably the drugs used in the eradication of sea lice, DML has developed a small DGPS drifter for inshore use. The value of the exercise has been enhanced by recruiting science students from our local high school to produce and evaluate the prototypes as a project within the Royal Society's Engineering Education Scheme.

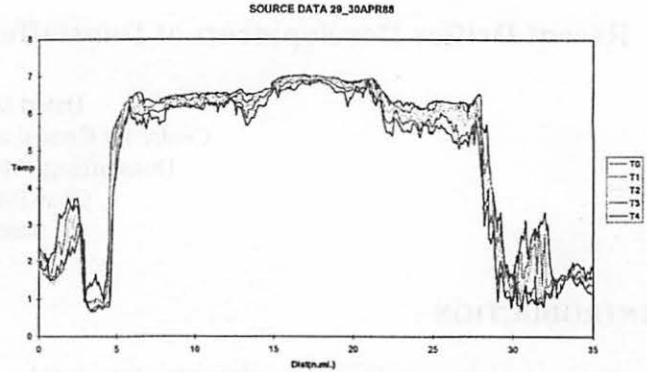


Figure 1. Temperature data at five depths for a simulated track through a real dataset.

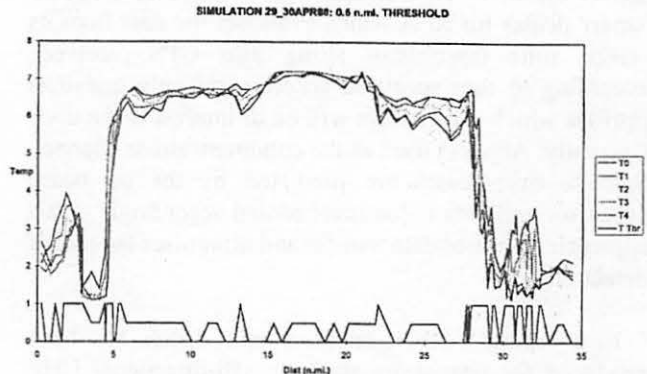


Figure 2. The much smaller adaptively sampled dataset successfully reproduces the salient features of the original data.

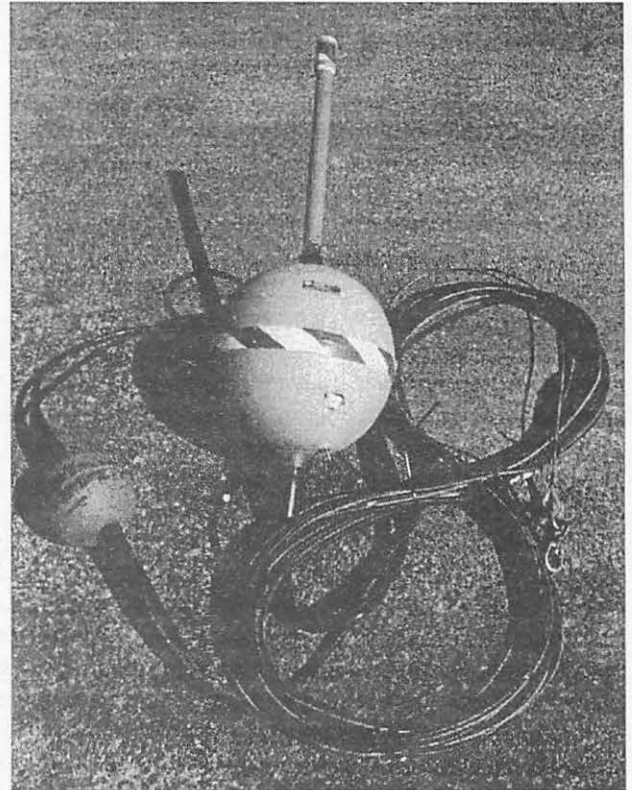
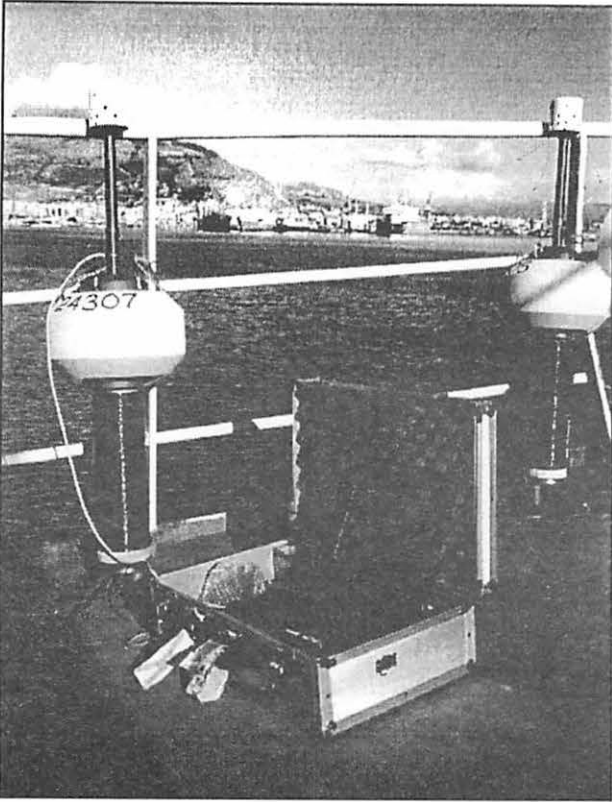
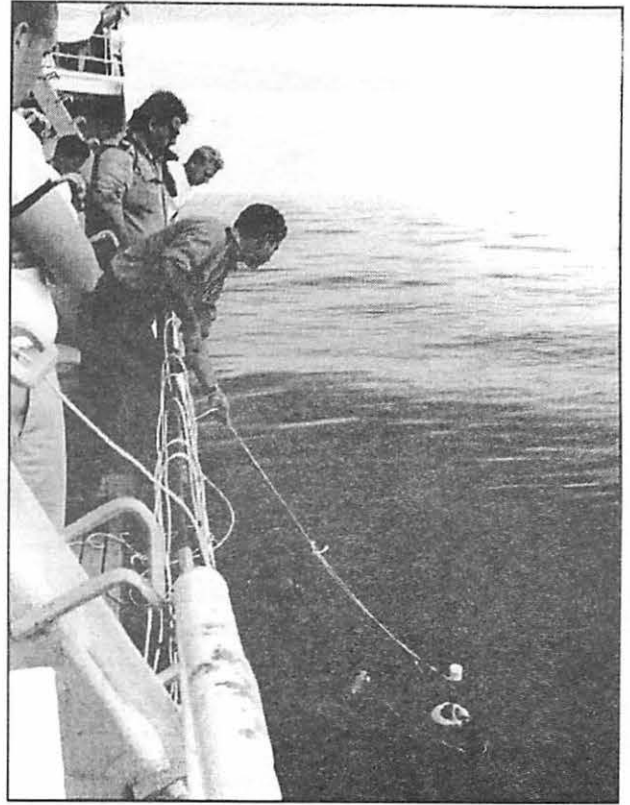


Figure 3. The prototype adaptive sampling drifter used in the first trials at Dunstaffnage.



*Figure 4. Prototype ASBs are programmed prior to deployment. In this case, the thermistor string is wound around the buoy hull.*



*Figure 5. A prototype ASB is recovered after deployment in the Mediterranean.*

The drifter consists simply of a plastic shipping container housing a battery, GPS receiver and UHF packet transceiver. A short mast carries both GPS and UHF antennae, and the complete assembly is attached to a drogue. A vehicle tyre inner tube is added for buoyancy. Both window-blind and holey-sock patterns have been used in the evaluation process (Figure 6).

In our application, differential GPS corrections have been generated at an onshore base station and transmitted to the drifter over the UHF link, thus allowing the on board GPS receiver to compute fixes with accuracies of better than 10 m. The fix data are then relayed to the shore station over the return UHF path.

A key feature of the mini drifter is the exploitation of commercially available navigation software (SeaPro, by Euronav Ltd) for data logging and real-time display. This is implemented rather easily by programming the GPS receiver to transmit its fixes in the NMEA format that is universally used by ship navigational equipment. The incoming NMEA data stream is then assimilated by the navigation package as though it were coming from a ship's receiver, and displayed accordingly.

Figures 7 and 8 show early trials of two mini drifters in Dunstaffnage Bay and the drift tracks that were recorded by the shore-based navigation package. The mini drifters have since been used extensively to complement existing

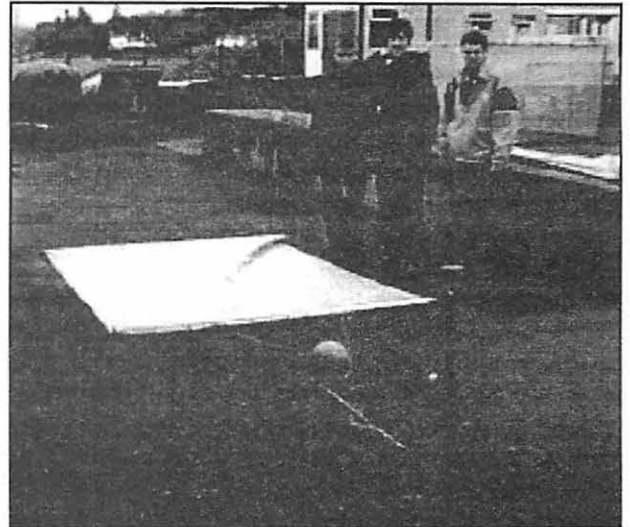
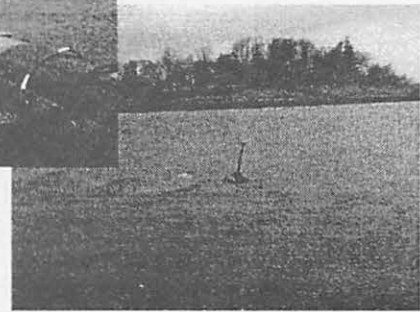
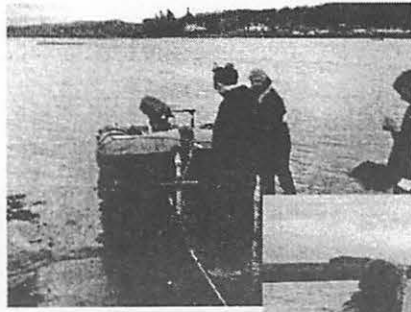


*Figure 6. Pupils from Oban High School prepare a mini drifter for deployment in Dunstaffnage Bay.*

techniques for the study of pollutant trajectories in the vicinity of fish farms..

#### ACKNOWLEDGEMENTS

The underpinning work on drifters was supported by the UK Natural Environment Research Council. The 'smart' buoy studies were carried out under DERA contracts



CENTRE FOR  
COASTAL &  
MARINE  
SCIENCES



Dunstaffnage  
Marine  
Laboratory

*Figure 7. The mini drifters are deployed for their first trial in Dunstaffnage Bay, Oban, Scotland.*

PDN1a/340, SSDW1/24 and SSDW1/505. The mini drifter was realised through collaboration with the pupils of Oban High School. All of the above has depended heavily on the painstaking effort of a number of colleagues here at DML and at DERA. In particular the invaluable and cheerful help given by Neil MacDougall of DML before his tragic death in a car accident is gratefully acknowledged.

#### REFERENCES

Meldrum, D T and Peppe, O, 1998. An adaptive sampling drifter for rapid environmental assessment. In: *Proceedings of Oceanology International 98, Brighton, 2, 25-30.* Spearhead Exhibitions Ltd, Kingston upon Thames, UK.

Sybrandy, A L and Niiler, P P, 1991. WOCE/TOGA Lagrangian drifter construction manual. WOCE Report No 63, Scripps Institution of Oceanography, La Jolla, California.

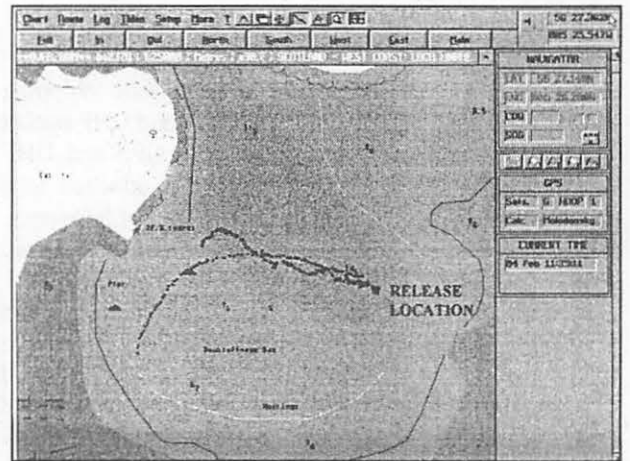


*Figure 8. Drift tracks of two mini drifters are superimposed on a navigation chart of Dunstaffnage Bay, using the SeaPro navigation package. The drifters were drogued at 2 and 5 m.*



## Recent Progress Using Orbcomm and Iridium for Drifting Buoy Data Transmission

Presented at DBCP-14, Marathon, Florida, October 1998

by

Mark Bushnell, NOAA/AOML-GDC

Oceanographers lack the resources to establish the array of drifting buoys needed to satisfy GOOS, GCOS and other program requirements. Drifter data transmission presently costs as much as the drifter, and so it is wise to examine the possibility of alternative data paths. Oceanographers have also promoted the use of drifting buoys among meteorological agencies by placing barometers and wind sensors on drifters. While this has resulted in additional deployments, it has also required more immediate data transmission, and again an alternative data collection system may reduce data latency.

A wide variety of satellite systems are presently proposed, and several are approaching or already claiming an operational status. Over 800 communication satellites are proposed for launch by the year 2000, and over 1300 by 2005. During the period 1990-1997, 17 companies filed applications for Low Earth Orbiting (LEO) or Mid-altitude Earth Orbiting (MEO) FCC licenses in the US alone. Three of the most promising systems are Orbcomm, Iridium, and Teledesic, and they are respectively thought of as paging, cell phone, and internet satellite services. The Global Drifter Center at AOML has efforts in place to examine both Orbcomm and Iridium.

On 02 August 1998 Orbcomm launched an additional 8 satellites using a L-1011 aircraft to deploy the Pegasus rocket, for a total of 20 satellites launched. After these eight achieve an operational status, globally a satellite will be available instantly about 70% of the time (17 hours/day). The planned constellation will consist of 48 satellites, a recent increase over the initial plan of 36. The next launch is scheduled for September 1998. Orbcomm satellites are capable of direct drifter-satellite-ground station data links, and store-and-forward messaging (Orbcomm Globalgrams) where the satellite records the data and later re-transmits it when passing a ground station.

Iridium completed the full deployment of its constellation of 66 satellites and 6 spare satellites (72 total) on 17 May 1998. Once the ground segment is completed, the system will claim an operational status on 23 September. Iridium satellites are capable of satellite-to-satellite communications, eliminating the orbital delays found in the Argos and Orbcomm systems. Each Iridium satellite projects 48 beams onto the earth to form 48 cells, which operate much like a conventional cellular phone system.

Four standard SVP type drifters fitted with Orbcomm/GPS transceivers have been obtained from Seimac, Inc. and tested at the GDC. The tests were carried out with the drifter in the water as well as ashore. Seimac has tested another 2 Orbcomm drifters, and the GDC has received over 600 data messages via Orbcomm satellites. Unfortunately, the transceivers used in the Seimac drifters were hard-wired for bent-pipe data transmissions only. As such, they are not capable of global deployment and would only function in regions close to a ground station.

Fortunately, Dr. Olson at the University of Miami had obtained 4 Orbcomm/GPS drifters built by Metocean, Inc. These were to be deployed in the US coastal waters to test US Coast Guard search and rescue current studies, yet their transceivers were configured for both bent-pipe and Globalgram transmissions. Dr. Olson agreed to swap drifters with the GDC, and so a second test using the Metocean drifters began.

During the course of the Metocean test, a potential problem with the GPS receiver was discovered. In order to reduce battery consumption, the controller only allows the GPS 6 minutes to acquire a position, and if it fails it shuts the GPS down and tries again one hour later. Most GPS receivers require a longer period of uninterrupted signal acquisition to obtain ephemeris and almanac data following a cold start. The concern was that if the drifter was shipped to a remote location, the GPS would fail to start, which in turn would disable the Orbcomm satellite pass predictions used aboard the drifter. Following the drifter tests, one of the Metocean drifters was placed aboard the R/V SEWARD JOHNSON while active, hoping to avoid the cold start problem. The SEWARD JOHNSON carried the active drifter on an open deck to the equatorial Pacific Ocean, and then deployed it.

Almost 600 data messages were obtained from the Metocean drifters during the course of the test and the following deployment. Most of these messages were bent-pipe messages, which is the default whenever possible, but 37 Globalgram messages from seven different Orbcomm satellites were obtained. The drifter performance after deployment was poor. The GPS position only updated about once per week, and the drifter only reported for about one month.

During the course of the Seimac and Metocean tests, the GDC received almost 200 Orbcomm Customer Service messages. Most often, these reported a brief service outage for one or more of the satellites.

**Data Relay Systems for Drifting Buoys Utilizing Low-Earth Orbit Satellites**  
Dr. Ngoc Huang (and Jeff Wingroth, TECHNOCEAN)  
NAL Research  
U.S.A.

**ABSTRACT ONLY SUBMITTED**

Increased demands for land mobile and personal communication services, coupled with advances in antenna design, digital compression techniques, on-board switching and on-board processing have changed approaches to satellite design. Satellite providers are moving away from deploying a few large geosynchronous (GEO) satellites to deploying tens, even hundreds of smaller satellites at low-Earth orbit (LEO) and medium-Earth orbit (MEO). A variety of commercial LEO/MEO satellite communications systems produced by the private sector for voice and data relay of all types are now in, or will soon achieve, operational status. They will offer considerable opportunity for drifting buoy applications in remote regions including two-way communications, real-time data transmissions, global coverage and reduced costs. They are much closer to Earth; therefore, low-power lightweight transmitters and receivers and omni-antennas can be used. NAL Research Corporation is planning to develop a satellite data relay system for drifting buoys utilizing commercial LEO satellite transceivers. The system will allow real-time data collection. In addition, drifting buoys can be monitored, adjusted and re-calibrated by scientists at their home laboratories or institutions. This paper presents a thorough study of various commercial LEO/MEO network capabilities and identifies the most applicable LEO system(s) for drifting buoy applications.



## A BUOY-MOUNTED AIR TRAFFIC CONTROL RADIO RELAY SYSTEM

Hal Brown,<sup>1</sup> Ralph Cambre,<sup>1</sup> Joel Chaffin,<sup>2</sup> and Charles Bond<sup>2</sup>

National Data Buoy Center<sup>1</sup> and Computer Sciences Corporation<sup>2</sup>  
Stennis Space Center, Mississippi, USA 39529-6000

### 1.0 INTRODUCTION

The National Data Buoy Center (NDBC) and the Federal Aviation Administration (FAA) have entered into an interagency agreement to implement the Gulf of Mexico Project (GOMP), a program to extend air/ground communications capabilities to presently uncovered areas of the Gulf of Mexico. The GOMP uses Large Navigational Buoy (LNB) hulls modified to accommodate air/ground communications equipment.

The Buoy Communications System (BCS) serves as a radio relay between the FAA Air Route Traffic Control Center (ARTCC) in Houston, TX, and aircraft flying over the Gulf of Mexico that are out of range of direct radio contact. The system provides direct voice communications between aircraft and the ARTCC in virtual real-time.

### 2.0 BACKGROUND

At the present time, foreign and domestic aircraft flying over a large portion of the Gulf have no radio contact with air traffic control (ATC) systems of the United States or other countries around the Gulf.

This lack of communications in some areas of the Gulf requires that aircraft be spaced at distances which ensure safety during passage through these areas. The present spacing requirements have resulted in the inability to increase the volume of air traffic in this area and in delays and cancellations for existing flights. Air traffic over the Gulf is projected to increase dramatically in the future, and the North American Free Trade Agreement (NAFTA) ensures that this will happen. The GOMP, by extending air/ground communications to these uncovered areas of the Gulf, will enable the closer spacing of aircraft over the Gulf, resulting in a higher traffic volume and the accompanying economic benefits of this traffic.

The primary means of air/ground communications is very high frequency/amplitude modulation (VHF/AM) radio, which is basically a line-of-sight system; that is, an unobstructed direct path must be between the aircraft and ground station to maintain radio contact. Aircraft flying at an altitude of 5,486 m (18,000 ft), for example, have line-of-sight contact with points at sea level to a distance of 117 km (189 mi). Some aircraft are equipped with high frequency (HF) communications equipment, which enable them to communicate with ground stations far beyond the line-of-sight limitations due to the nature of HF radio waves. However, while HF systems are capable of two-way communications over great distances, this equipment is not available on most foreign and domestic aircraft and is not available at FAA ATC Centers. In addition to its unavailability, HF systems are also adversely affected by weather and other conditions, resulting in an availability factor that is deemed unacceptable.

### 2.1 Proposed Solutions

Solutions were sought that were transparent to the existing ATC system (i.e., that required no changes in existing communications equipment and procedures). Several proposals, such as tall towers, permanent platforms, shore stations equipped with 1,000-watt transmitters and high-gain antennas, and buoy-mounted systems were studied.

The tall towers solution calls for placing VHF/AM antennas on top of existing television/microwave towers, which are approximately 610-m (2,000-ft) tall. There are several such towers located in the United States around the Gulf. Tests showed that the increased elevation of the antennas did not result in an appreciable increase in range, and this solution was rejected.

The permanent platform solution was studied and rejected. The platforms require a water depth of 150 ft

or less, severely limiting the deployment areas, and are prohibitively expensive.

The high power shore stations, while not achieving complete coverage, significantly extend the range of shore-based stations under optimum conditions. However, in certain climatic conditions, the performance is considerably degraded.

A combination of shore-based stations and Buoy Communications Systems (BCS) was selected as the most economically and technically feasible solution.

### 3.0 SYSTEM DESCRIPTION

The BCS consists of three major components: the buoy, communications equipment, and power system. The BCS, as do all NDBC-deployed buoys, has a meteorological system which reports hourly through the Geostationary Operational Environmental Satellite (GOES) system.

#### 3.1 Buoy Hull

The buoy hull is a U.S. Coast Guard (USCG) 12-m discus LNB. The hull is made of steel, and, after ballasting, weighs approximately 90,720 kg (200,000 lb). Several of these hulls were obtained by

NDBC for the FAA. The buoys were declared salvage material by the USCG.

#### 3.2 Communications System

The communications system consists of four Park Air Electronics Model 3070 VHF/AM transceivers for communications between the buoy and aircraft, four Westinghouse Wavetalk® L-Band satellite phones for communications between the buoy and the ARTCC, and the required voice relay (interface) equipment. The communications path between the buoy and aircraft is VHF/AM radio; between the buoy and the satellite earth station, L-Band satellite; and between the earth station and the ARTCC, telephone land lines (Figure 1).

The communications channel on the primary satellite is a dedicated circuit. When a pilot or air traffic controller keys the microphone, dialogue can be initiated with no delay. The buoy-located radio relay function is virtually transparent to users, with a 500 ms propagation delay being the only difference between this and a direct air-to-ground radio contact.

System status is transmitted as X.25 packet data via a dial-up L-Band satellite channel to the ARTCC and to NDBC. System status data are automatically

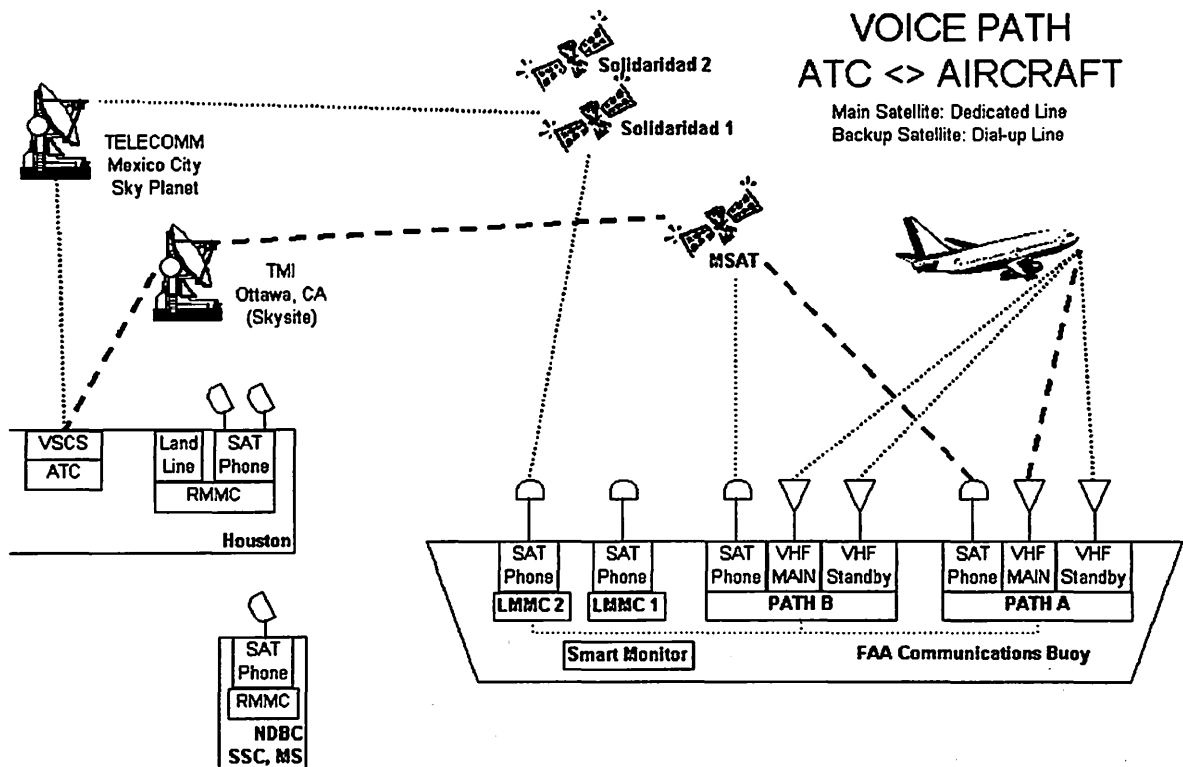


Figure 1.

transmitted at predetermined intervals, or can be obtained at any time by an interrogation command from the ARTCC (Figure 2).

Tests have shown that the Wavetalk® antenna can maintain a lock on the satellite with buoy motion of up to 50°/s angular velocity and 28°/s<sup>2</sup> angular acceleration.

Redundancy is provided for all BCS equipment. There are two paths of communication with the primary satellite. Each path consists of one satellite phone, two transceivers, and other associated equipment. A third satellite phone can provide communications via a backup satellite. The data path and the local maintenance monitoring and control (LMMC) system also have redundancy (Figure 3).

### 3.3 BCS Power System

NDBC has designed and tested a buoy-mounted direct current (DC) power system capable of providing the large amounts of average and peak power required by the BCS. The primary power system consists of a photovoltaic array, photovoltaic charge controllers, secondary batteries, and a power system monitor and

control unit. A backup power capability is provided by a 7.5-kW auxiliary diesel engine generator set. The primary power system provides continuous average power in excess of 800 watts at 24 VDC and satisfies peak demands up to 5,000 watts without the support of the diesel generator. A block diagram of the entire power system is shown in Figure 4.

The primary power system is designed for graceful degradation in case of component failure or damage. The system is divided into 14 separate diode isolated 24-VDC sources. Each of the sources consists of the following:

- A. Sixteen 12-V batteries (Sonnenschein Model 212/80A). Two 12-V batteries are connected in series to provide a 24-VDC unit, then eight of these 24-VDC units are connected in parallel.
- B. Sixteen solar panels (Type M55J), each of which, at peak power, produces 3.1 amperes at 17.5 VDC. To produce the nominal 24 VDC required to charge the batteries, two panels, called a set, are connected in series, and eight sets are connected in parallel. Each set is diode isolated from the others. The eight sets that make

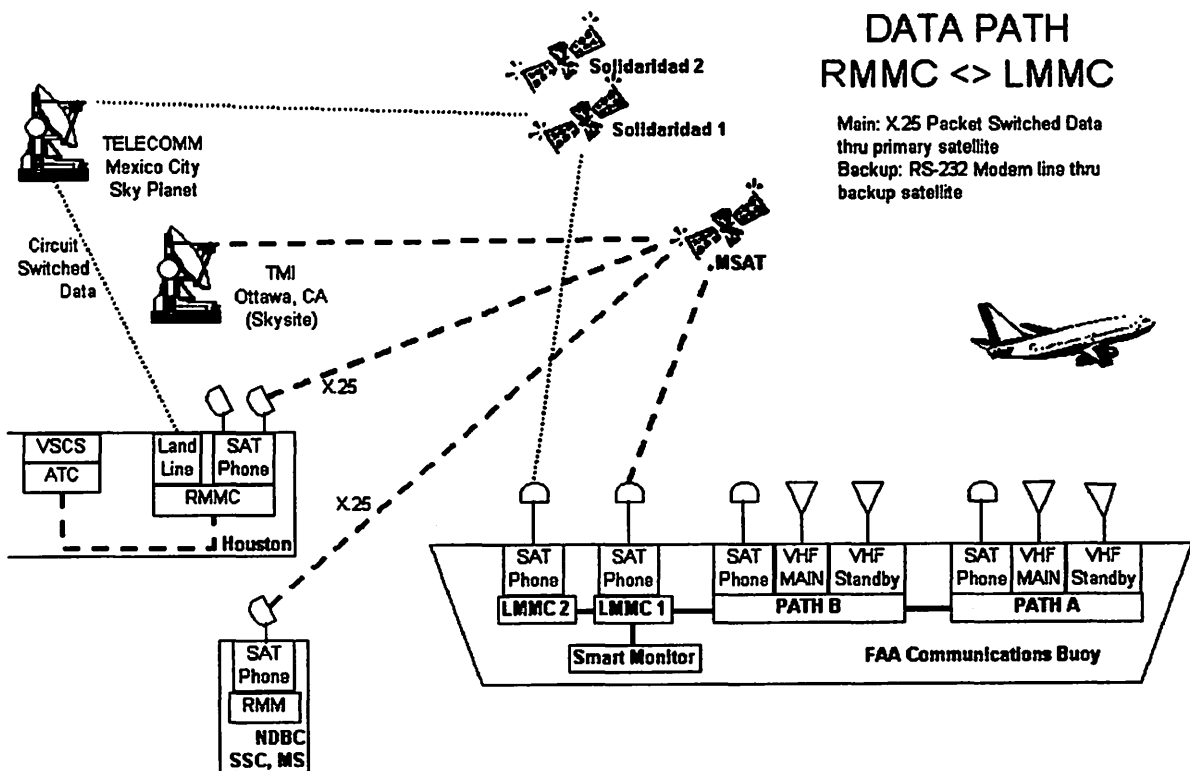


Figure 2.



**REMOTE BUOY COMMUNICATIONS SYSTEM**

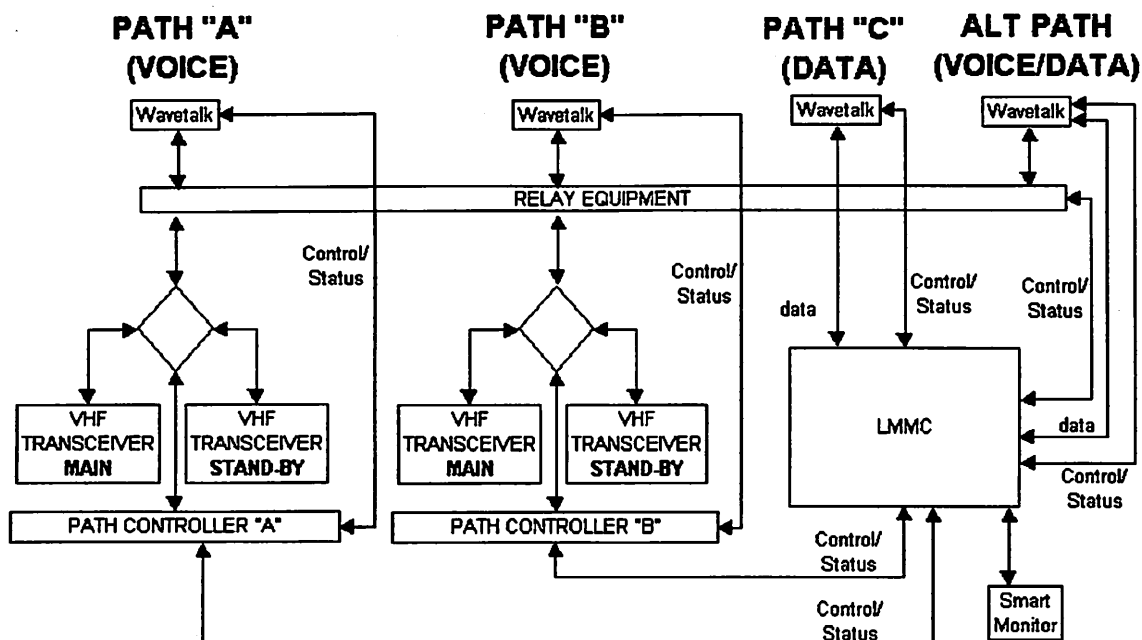


Figure 3.

up one solar power module are divided into two submodules for physical installation, with each submodule being installed on opposite sides of the buoy deck. This alleviates the possibility of an entire module being shadowed by the buoy superstructure, or of an entire module being disabled by external damage.

A total of 230 solar panels is installed parallel to the deck of the buoy and approximately 2.2 m above the deck. The panels shade the equipment compartments of the buoy, significantly reducing the buoy internal temperature.

C. A microprocessor-controlled photovoltaic controller (Morningstar) provides regulation of the secondary battery charging currents from the solar panel modules. The photovoltaic controllers manage battery charging by a constant-voltage Pierson-Moskowitz (P-M) algorithm that has

been optimized for photovoltaic systems. Battery charging is regulated by monitoring ambient temperature, battery type, system battery voltage, and battery equalization requirements.

The backup generator is a 7.5-kW keel-cooled marine diesel-electric generating set (genset). The genset alternator is brushless, synchronous, self-excited, self-voltage regulated and designed to accept inrush currents in excess of 500 percent of rated full load. The genset fuel tank is a bladder-style fuel tank, custom fit to the buoy fuel compartment. The bladder includes foam baffling for slosh suppression.

The genset is designed for continuous service. It is automatically activated for 30 minutes on a daily basis, and is programmed to come on line anytime the battery voltage drops below 23.5 VDC. The genset can also be started and stopped by a remote command from the ARTCC.



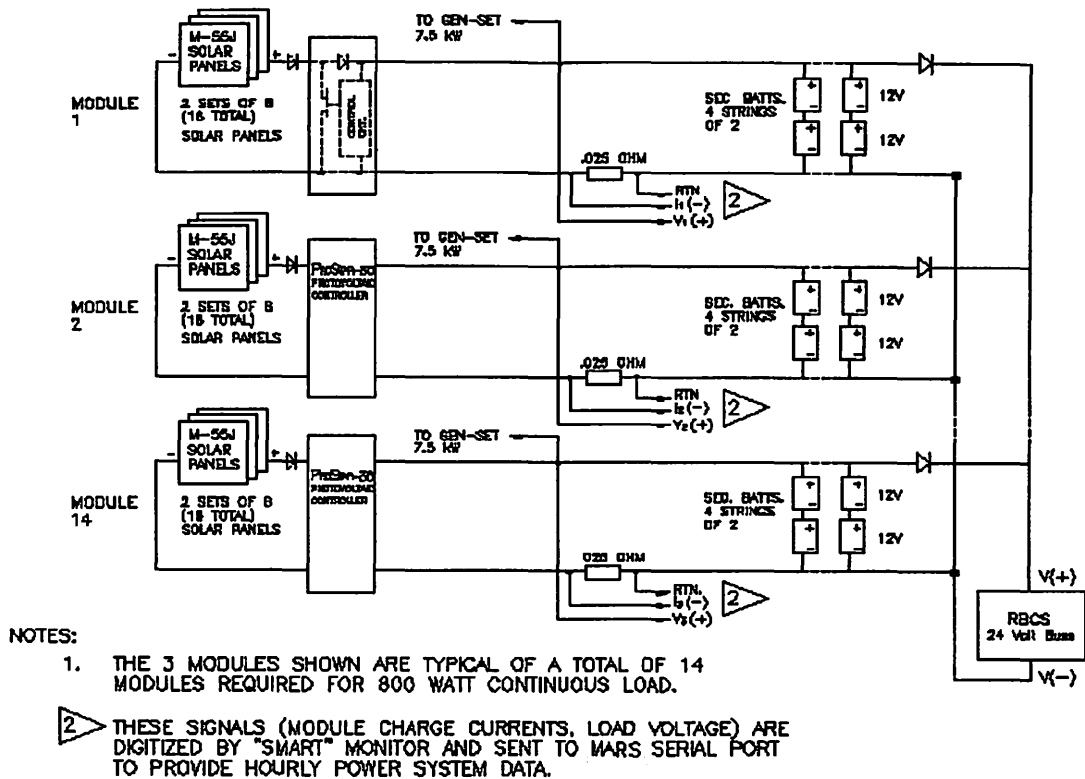


Figure 4.

A BCS primary power system (without the diesel generator) has been tested at sea. The system was installed aboard a 12-m LNB, which was then deployed in the Gulf at Main Pass Block 163, which is approximately 40 miles south of Pascagoula, MS. The test was conducted using a load bank sized to draw 880 watts (10 percent above the required system power output) and ran for approximately 5 months, from June 24 through November 20, 1996. The system satisfied all test requirements with no exceptions and no failures.

An auxiliary power system which uses excess power generated by the BCS system (available during periods of low BCS use) charges five 24-V secondary batteries in parallel, each consisting of two 12-V batteries in series. This power is available to operate fan ventilation for the BCS compartment.

The NDBC meteorological package on the buoy is powered by a separate 12-VDC power system

consisting of five solar panels, one controller, and six secondary batteries.

The operational status of the BCS power system is monitored by an NDBC-designed smart monitor that measures system battery voltage, charging currents, and other related parameters and reports these values through a Multifunction Acquisition and Reporting System (MARS)-based meteorological data system via the GOES to NDBC. Power system data will also be transmitted with the remote maintenance monitoring and control (RMMC) system data through the BCS via L-Band communications satellite to the ARTCC in Houston, TX.

The smart monitor will also control operation of the genset. It is programmed to run the genset on a predetermined daily operation schedule. The smart monitor will also start the genset anytime the system voltage drops below 23.5 VDC. The genset can be controlled remotely from the ARTCC in Houston via the communications satellite and through the NDBC

Operations desk via the GOES command receiver located on the buoy.

#### 4.0 METEOROLOGICAL DATA SYSTEM

NDBC installs meteorological (Met) packages on all buoys deployed by the Center. The Met package on this buoy consists of dual, sonic (no moving parts) anemometers, air temperature sensor, barometric pressure sensor, a directional wave system, and a MARS data collection platform. The system reports on an hourly basis through the GOES data collection system.

#### 5.0 BUOY COMMUNICATIONS SYSTEM STATUS

Factory acceptance testing of preproduction BCS No. 1 is now under way at NDBC. This system will be deployed at a site located in Main Pass Block 163 in

the Gulf. The location is approximately 25 km (40 mi) due south of Biloxi, MS, with a water depth of approximately 46 m (150 ft).

Preproduction BCS No. 2 is now being built. This system will use Cubic Communications ATC-100A transceivers. The transceiver uses digital signal processing as opposed to analog, and costs only about 20 percent of what analog transceivers cost. The FAA will study the feasibility of using such transceivers in the future. Digital VHF transceivers have not been certified for use in the ATC system.

When the system is declared operational, two or three FAA buoys will be deployed in the Gulf of Mexico at a latitude of 26°30', which is about 186 km (300 mi) south of the U.S. Gulf Coast, with one or two buoys located in the West Flight Information Region (FIR), and one in the East FIR (Figure 5). The water depth at these locations is approximately 3,124 m (10,250 ft).

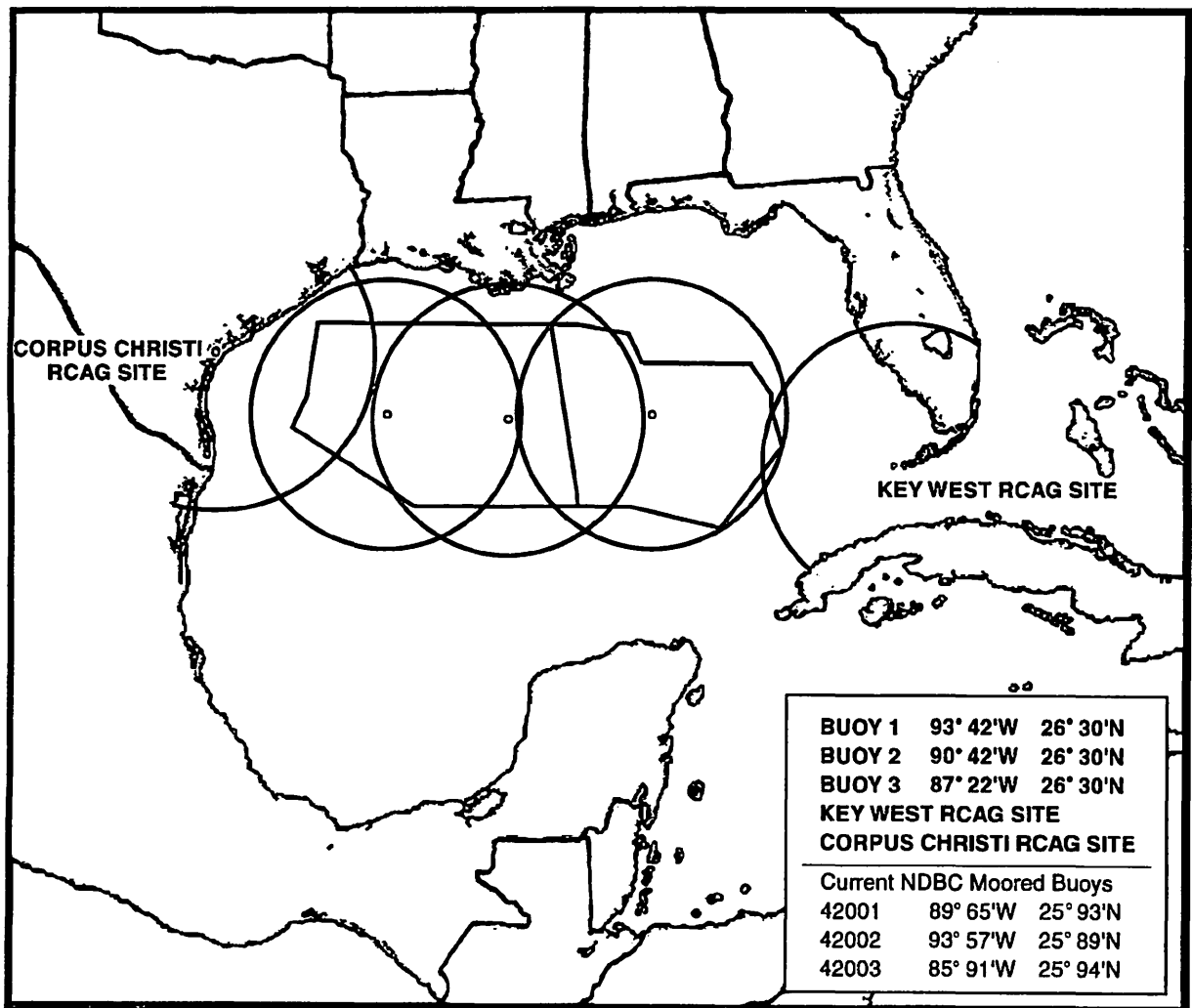


Figure 5.

## **The Cape Mudge Wave Experiments: Early Results**

by

**M. Blaseckie<sup>1</sup>, S.G.P. Skey<sup>1</sup>, K. Berger-North<sup>1</sup>, J. Ploeg<sup>2</sup> and P.A. Bolduc<sup>3</sup>**

### **1.0 Background**

On the West Coast of Canada between the northeastern end of Vancouver Island and the mainland, there is an important shipping route for all vessels (commercial and recreational) travelling up and down the coast. The southern end of this route is a narrow passage called Discovery Passage. To the north of Discovery Passage are Johnstone Strait and Queen Charlotte Strait, leading out into Queen Charlotte Sound, and to the south is the Strait of Georgia.

The tidal currents in Discovery Passage are extremely high, well known and predictable. They can reach speeds of 10 knots or so on the flood tide (southward flow) and slightly less on the ebb tide (northward flow). When a strong south wind coincides with a flood tide, an extreme wind-against-tide situation occurs, creating very hazardous wave conditions for all marine users. Slightly less extreme, but no less dangerous, conditions exist when northerly winds occur with an ebb tide.

In an attempt to monitor the wave conditions more specifically, and to provide round the clock accurate sea-states, in January 1997 a directional 0.9m diameter Datawell waverider buoy was installed near the southern end of the Discovery Passage in an area known as Wilby Shoals. The buoy was located 1/2 mile to the east of the entrance to Discovery Passage in a water depth of 30 m, with good open exposure to the south and south west, but limited exposure to the east and north. Figure 1 shows the location of the wave experiments. The reason that the waves were measured at Wilby Shoals and not in Discovery Passage itself are given below.

The wave data were transmitted to a meteorological station at Tyee Spit (on Vancouver Island about 5 miles to the west) where they were integrated with meteorological data gathered at Tyee Spit. The integrated data were then formatted for Environment Canada who accessed the data on an hourly basis via telephone modem. These data were then used in the Environment Canada and Canadian Coast Guard bulletins. All of these data were downloaded and archived by the Marine Environmental Data Service of the Department of Fisheries and Oceans.

Although the wave measurement program at the edge of Wilby Shoals was successful, and the buoy remained on station till the end of the project funding in May 1998, the wave conditions were very different from those experienced at the entrance to Discovery Passage. This was because the waves measured at the Wilby Shoals site were not affected by the strong tidal currents found in Discovery Passage.

---

<sup>1</sup> Axys Environmental Consulting Ltd., Sidney, B.C., Canada.

<sup>2</sup> Formerly with DFO/Canadian Coast Guard, Vancouver, B.C., Canada.

<sup>3</sup> Marine Environmental Data Service, Ottawa, Ontario, Canada.

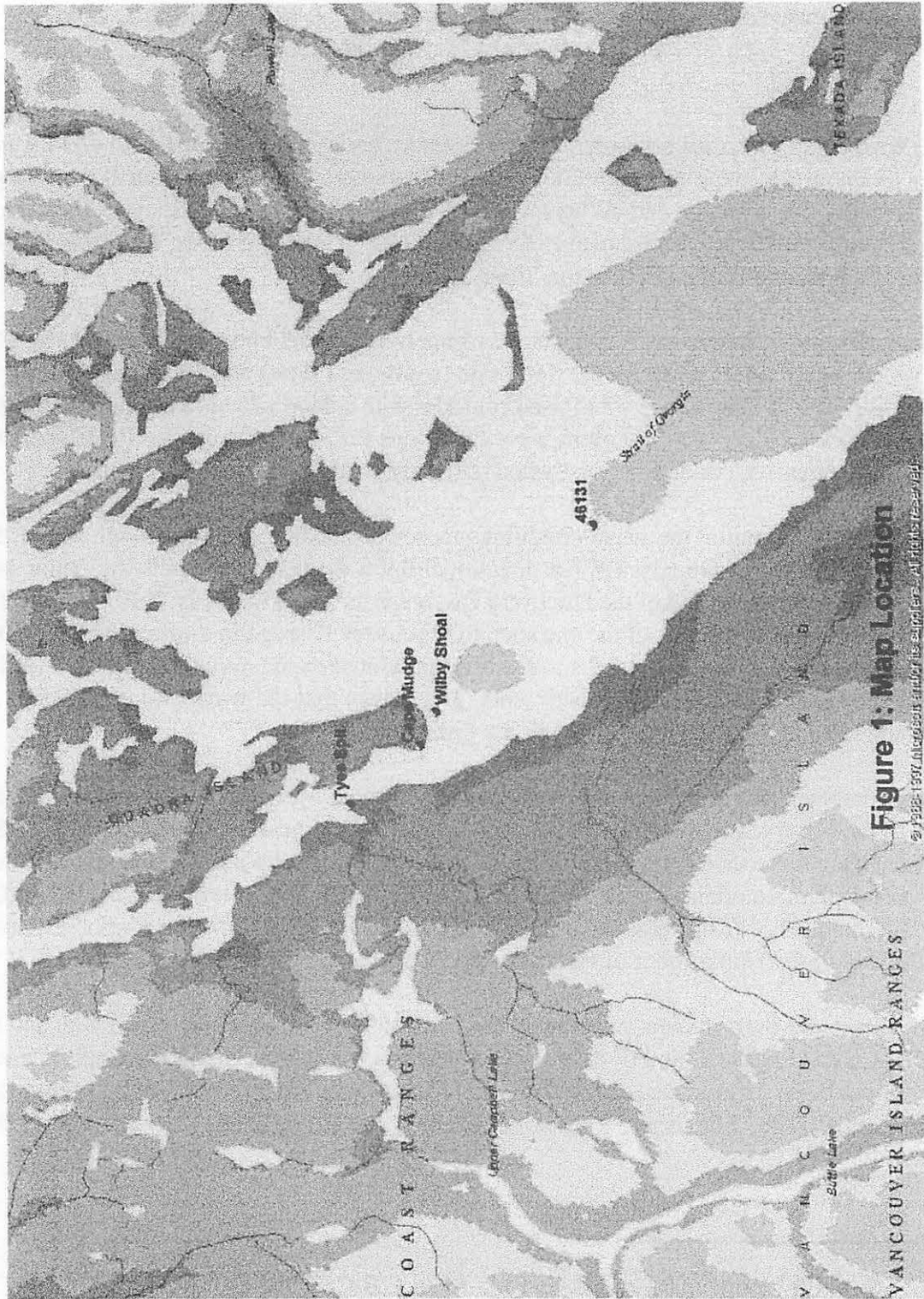


Figure 1: Map Location

© 1998-1999, Microson studies and its affiliates. All rights reserved.

To research this and provide a solution two supplementary studies were carried out. The first was to validate the data being gathered at Wilby Shoals with the data gathered at a buoy at Sentry Shoal 8 miles to the south. A second study was to modify the directional wave spectra gathered at Wilby Shoal by taking into account the tidal currents in the Discovery Passage.

## 2.0 Measurement of Waves in Discovery Passage

There are only three ways to measure waves. These are from the surface, from the subsurface and remotely. Each of these options is examined below.

### 2.1 Measurement from the surface

Traditional measurements of directional wave spectra from the surface use a small buoy (approximately 1 m diameter) in which a series of accelerometers are mounted. The motion of the buoy is assumed to represent the motion of the waves, and these motions are sensed by the accelerometers. Analysis of the accelerometer data lead to formation of directional wave spectra and information about wave height, period and direction. However these buoys are limited to working in maximum currents of no more than 6 knots (3 m/s) because in larger currents the strain on the mooring line is so great that it affects the ability of the buoy to move freely with the waves. In very high currents the buoy may be pulled under the surface. This is a severe limitation in Discovery Passage where the currents are much higher than the maximum practical values for a surface following buoy.

A further difficulty with measurement of waves from the surface in Discovery Passage is that with the high volume of marine traffic through the narrow passage, the buoy is very likely to get hit and destroyed. A significant problem for a proposed permanent wave monitoring program.

### 2.2 Measurement from Sub-Surface

In relatively shallow waters (<50 m) it is possible to measure waves by sensing the pressure differences on the bottom. Unfortunately Discovery Passage is too deep for this method being approximately 90 m. In some circumstances it is possible to mount a pressure sensor at mid depth on a mooring. However this method is not practical in areas with extremely high currents, because of the difficulty in maintaining the mooring. Also in Discovery Passage the presence of large numbers of tugs and barges with hanging towlines are likely to destroy any shallow sub-surface mooring.

### 2.3 Remotely Sensed measurements

Although shore based radar (CODAR) are mainly used for measuring currents through Doppler shift technology, they can measure waves. However since the primary returns indicate current speed and direction, in a high current regime the signal for the wave heights would be swamped.

A shore-based wave radar is also not suitable since the actual wave heights rely on a downward looking altimeter.

Given the above it is clear that it is not practically possible to physically measure the waves in Discovery Passage.

### 3.0 Wave Calibration and Validation

#### 3.1 Field Verification

##### 3.1.1 Verification of waves measured on Wilby Shoals

Axys installed the Datawell directional wave rider buoy on Wilby shoals near Cape Mudge at the entrance to discovery Channel in late January 1997 in 20 m of water (49°59'N 125°09'W). The wave data and sea temperature data are transmitted via VHF to the Canadian Helicopters hangar at Campbell River. At the hangar, wind speed and air temperature are also measured. The wind and temperature data are combined with the wave and sea temperature data and made available to Environment Canada and Coast Guard.

The Environment Canada Sentry Shoal ODAS weather buoy is located in Georgia Strait eight miles to the SE of Discovery Channel in 18 m of water. The following report gives a brief comparative analysis for data sampled in February and March 1998 for Discovery Channel (DISCO) and Sentry Shoal (46131).

##### 3.1.1.1 Data

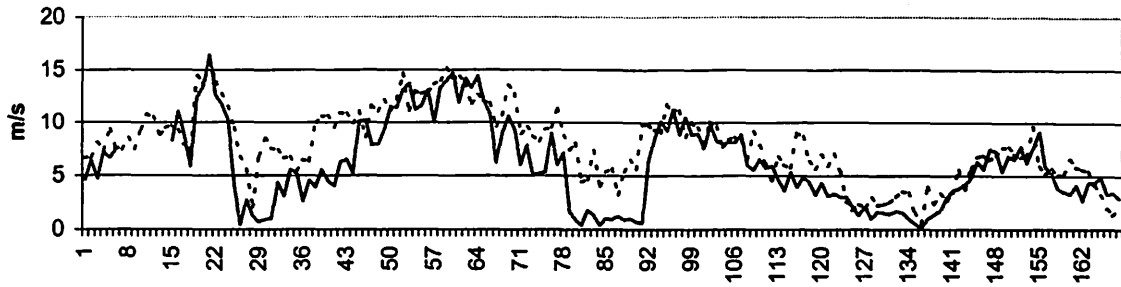
The data are gathered as follows:

- Winds: Wind speeds are calculated from a ten-minute mean, both at the Sentry Shoal buoy and at Discovery Channel.
- Waves: The sensor in the waverider buoy is comprised of 3 vertically stabilised accelerometers. The sensor in the 3 m buoy is a strap-down accelerometer. It does not measure wave direction. The significant wave height is calculated from a twenty minute record every hour. The significant wave can be regarded as the mean height of the highest third of the waves. This correlates with the "visual" appearance of the sea state. The value of the significant wave is a standard calculation from the spectral variance.
- Temperature: The air temperatures are calculated over a ten-minute mean.

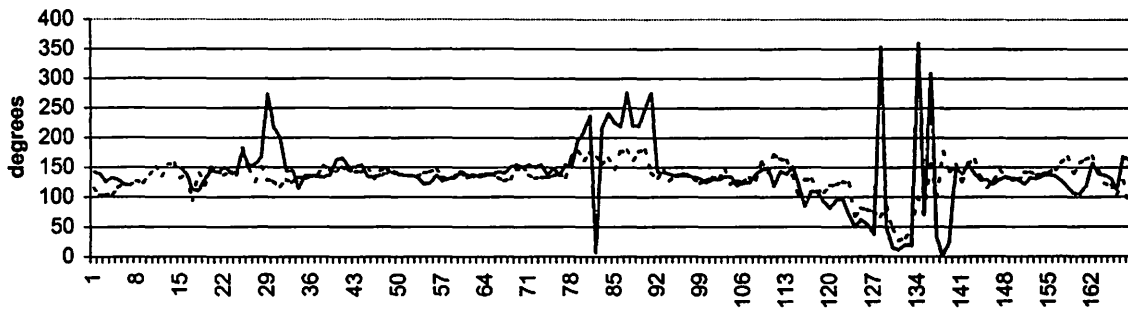
##### 3.1.1.2 Data Plots

Figure 2.1 shows time series data for wind speed (m/s) and direction (°), and significant wave height (m) for both Discovery Channel (DISCO) and Sentry Shoals (46131) for the period of analysis in February. Figure 2.2 shows similar parameters for March. The tidal current shown is for Discovery Passage.

Mid February 1998 Wind Speed

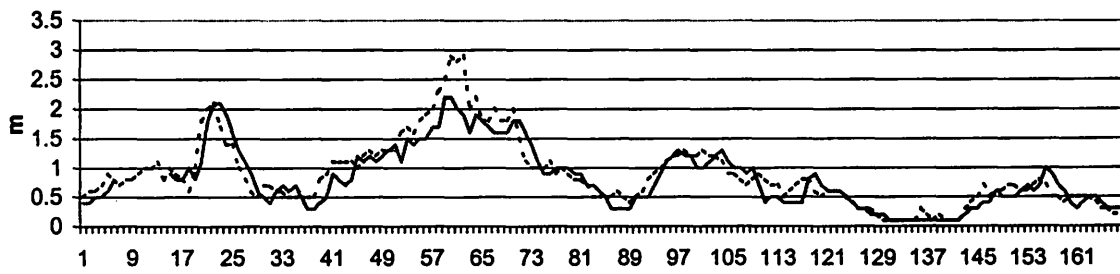


Mid February 1998 Wind Direction

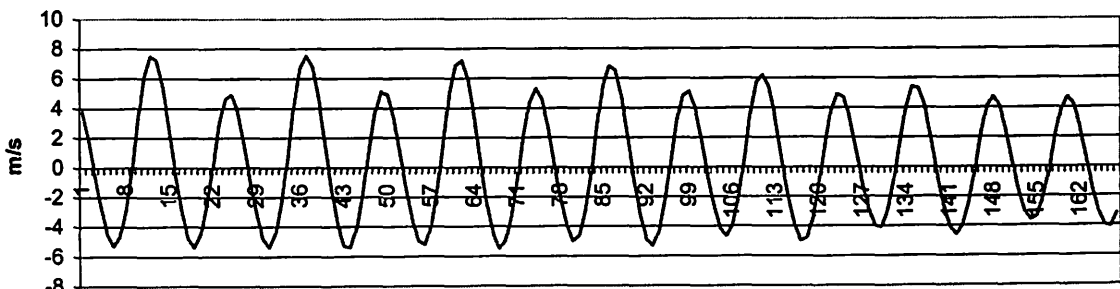


..... 46131  
—— DISCO

Mid February 1998 Hs

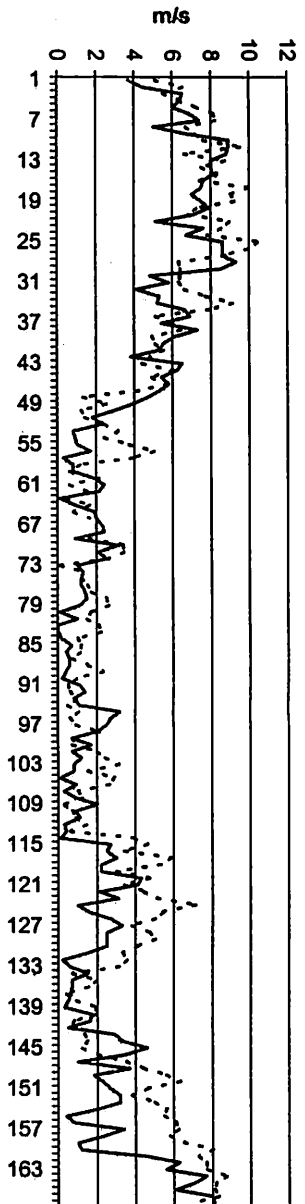


Mid February 1998 Tidal Current (Flood+)

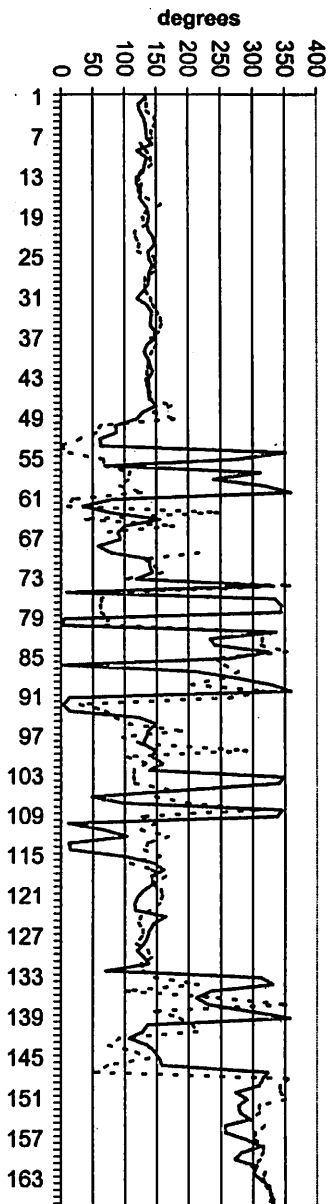


Hourly Data

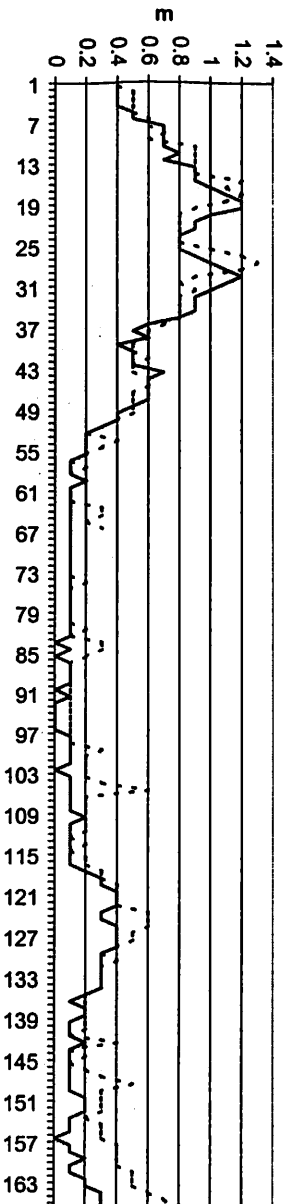
Figure 2.1



Mid March 1998 Wind Direction



..... 46131  
—— DISCO



Mid March 1998 Tidal Current  
(Flood+)

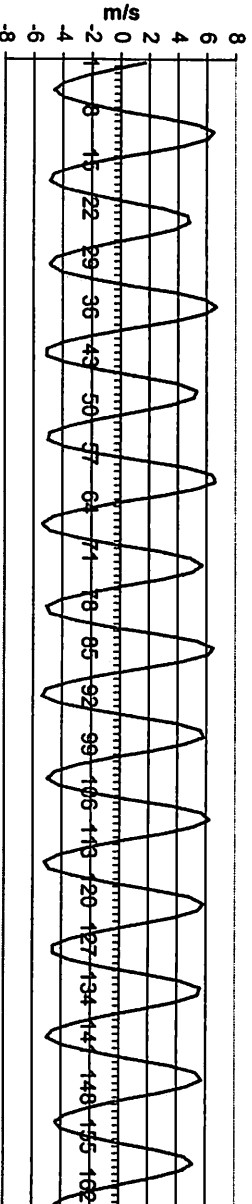


Figure 2.2



### 3.1.1.3      Analysis

#### a) Wind

The wind data do not show any surprises. The wind speed is generally higher at Sentry Shoals by a few metres/sec. The patterns for the wind speed are similar for both locations.

#### b) Waves

The wave heights from both sites are similar and display similar patterns. In particular it is important to compare the wave heights with the wind speed as well as the wind direction. When the wind direction is from the south or southeast, the wave heights at Discovery Channel are proportionally larger than for a similar wind speed from other directions. This is because the waverider is partially sheltered from winds from the west, north and northeast.

#### c) Sea Surface Temperature (SST);

The SST values (not shown here) from the buoy at Discovery Channel show a relationship with the tidal cycles. It appears that during the northerly flowing ebb tides the SST rises slightly. This might be explained by the movement of the warmer surface waters of the Georgia Strait.

#### d) Air Temperature

The air temperature values (not shown here) match each other quite well. The greater variability at Discovery Channel can be explained by the fact that these values are not over water values. They are measured on land at an elevation of 10 metres. The buoy-measured winds are at an elevation of approximately 5 m.

### 3.1.1.4      Summary

The data show that there is little substantive difference between the two sites, especially when the winds are from the southern sectors. The SST values may differ more markedly during the summer season, and are typically more variable at Discovery Channel on a diurnal basis.

## 3.2      Modification of Waves According to the Currents

It is known that a wave field is modified in the presence of currents. Recent research (Nwogu, O. 1993) has indicated that it is possible to predict how the directional wave spectra will change if the current speed and direction is known. At Discovery Passage the magnitude and direction of the currents are known and predictable, since tidal forces drive them. Also the directional wave spectra within 1/2 mile of Discovery Passage at Wilby Shoals are known. Thus by modifying the known wave spectra with known currents it may be possible to estimate the existing wave conditions in the passage.

This following section describes the modification of the Wilby Shoals directional wave spectra with Discovery Passage currents. It also describes an attempt to verify these modified waves with actual measured waves from a dedicated vessel over a flood tide event.

### 3.2.1 Discovery Passage Tidal Currents

The current speed and direction values for Discovery Passage were obtained from Fisheries and Oceans at the Institute of Ocean Sciences, Sidney, BC. The scientists there have modelled the entire Georgia Strait and are in the process of verifying the model. However at the time that the present work was taking place the verification process had not been completed. So in the meantime the known currents modelled from Seymour Narrows (a mile or so to the north of Discovery Passage) were modified for Discovery Passage. This modification, which took into account both height and temporal modifications was only approximate. However the opinion was that for this pilot project stage it would give a reasonable account of the currents at Discovery Passage.

The modifications for Discovery were a reduction from the Seymour Narrows predictions of a factor of 1/1.75 for flood speeds and of 1/2.20 for ebb speeds. The times were not adjusted since observed currents at both sites suggest time adjustment is small if not zero.

The outcome of this work was a database of hourly data for a whole year of current speed and direction at the entrance to Discovery Passage.

### 3.2.2 Modification Algorithm

The software required to modify the directional spectra was developed at the CHC of the NRC. Dr. Okey Nwogu's research both theoretical and in model tests in the wave tank at the NRC in Ottawa, indicated how the effects of current speed and direction modify wave spectra. The algorithm was made available to the project. These modifications include an algorithm that limits the steepness of the waves.

### 3.2.3 Integration of Current Speed and Direction Database and Wave Modification Algorithm.

The wave analysis software of NRC and the current speed and direction database was integrated with the existing system installed in place at the Base Station at Tyee Spit. The Base Station software took the hourly measured spectra from Wilby Shoals, and the predicted current speed and direction for the same hour from the database and then modified the spectra in accordance with the NRC algorithm. The resulting spectra were then analysed to provide a value of the "simulated" significant wave height. This wave height was then inserted into the hourly message that was formatted for Environment Canada and Canadian Coast Guard.

### 3.2.4 Real Time System

The system was installed and operated in real time for three months from January to the end of March 1998.

### 3.2.5 Verification

Once the system was operating, we planned to carry out a verification program. As discussed above since it was not possible to measure waves in Discovery Passage with any automatic systems, we had to use a dedicated vessel following a free-floating waverider.

### 3.3 Measurement of waves in Discovery Channel

The wave model validation trials were completed on Wednesday January 14/1998. The weather forecast for Tuesday pm was for gale to storm force SE winds in the northern Strait of Georgia continuing into Wednesday. The equipment used for the trial was a Datawell 0.7 m Waverider buoy with DIWAR radio receiver, autotrack GPS receiver and PC computer data logger/processor. The Waverider was prepared for a free floating deployment with 2 ballast chains secured beneath the buoy and a 15 m pickup line terminated with a Scotsman float. A portable autotrack GPS receiver was attached to the head of the buoy and programmed to log a position once a minute. All data was transmitted from the buoy to a logging station on the research vessel.

The timing of the currents at Discovery Passage was such that the turn of the tide was at 13:05 with the maximum flood current predicted for 15:41 hours. The predicted current speeds for the times of the trials, namely 13:30, 14:30 and 15:30 were approximately 0, 3.5 and 4.3 m/s (See Figure 3).

There were a total of three drift deployments run during the afternoon. The maximum currents as calculated from the GPS data were 3.5 knots at approximately 15:30. The weather for the first two tracks was clear with 15 knot SE winds. The weather for the third track deteriorated with winds gusting to 25 knots, rain squalls reducing visibility and coupled with maximum flood currents. Plots of the three buoy tracks are shown in Figure 4.

#### 3.3.1 Discussion

The following observations from the field evaluation were made:

- The current regime in the area was quite complex with a high degree of variability both spatially and temporally;
- High occurrence and rapid generation of potentially dangerous waves;
- Although the conditions the trials were not run under most serious wind/wave conditions likely to occur in the area, it would have been dangerous to consider the operations in much more than was encountered. The waves in the rip area although not large tend to be very steep and breaking.

### Tidal Currents for Discovery Passage During Validation Trials

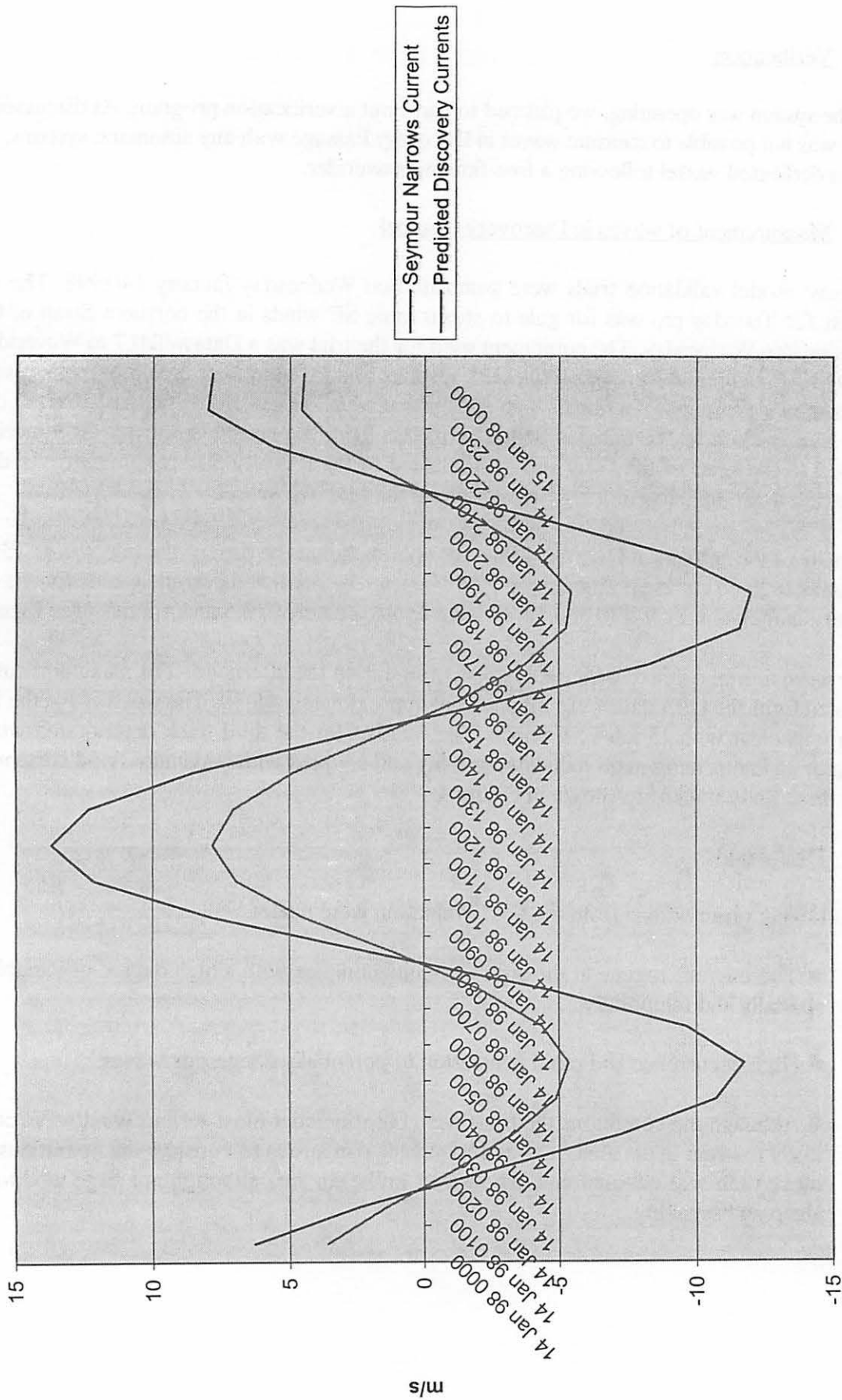


Figure 3

Observations from Drift Deployments

<b>Trial Run Time</b>	<b>Waverider (0.7 m)</b>	<b>Wilby Shoals Waverider (0.9 m) measured</b>	<b>Sentry Shoals (3 m Discus Buoy)</b>	<b>Discovery Passage (simulated)</b>
13:30/21:30 UTC	0.47m/5.9s	1.2m/3.9s	1.5m/5s	
14:30/22:30 UTC	1.02m/5.1s	1.3m/4.1s	1.0m/5s	
15:30/23:30 UTC	1.36m/4.9s	1.2m/4.9s	1.0m/4s	

3.3.2 Wave Modification Algorithm

The algorithm used (Nwogu, 1993) to modify the spectra was successful for situations where the currents were in the same direction as the winds, but only partially successful in true wind-versus-current situations. When the current values exceeded -1 m/s, the higher frequency end of the spectra reduced to zero. As the current speed increased to -2 or -3 m/s this end of the spectra shrank toward the lower frequency end such that at -3 m/s there was no spectra left at all.

The reason for this is that with adverse currents, there is maximum current speed at which the waves cannot propagate into the currents and will be reflected. Based on kinematic considerations alone, the maximum current speed is equal to the local group velocity. In deep water,

$$U_{\text{block}} = -0.25 \text{ Phase Velocity (without currents).}$$

As you approach that speed, however, there will be significant non-linear interactions and wave breaking. To properly study such steep waves in adverse currents, a fully non-linear wave current interaction model with wave breaking is required.

4.0 Summary and Conclusions

This program was unique and had a number of unique challenges. The observations from the field during moderate wind versus tide conditions underscored the difficulties in monitoring wave conditions in these situations, either from a research vessel or remotely via instrumentation.

The methodology used to simulate the actual spectra had a number of source errors. These were:

- No knowledge of the actual current speed and direction in the area. The data used was taken from an uncalibrated model which seemed to provide reasonable numbers;
- The current speeds and directions in the area were highly variable both temporally and spatially;
- The algorithm used (Nwogu, 1993) to modify the spectra was not a fully non-linear wave current interaction model with wave breaking.

As such, wave accuracy could not be expected to be within the 3% estimated by the waverider. From pragmatic considerations wave height values ( $H_s$ ) within 0.5 m would be considered acceptable.

Unfortunately the project funding was terminated before the analysis could be completed and modification model assessed further. However there was definitely enough information and positive results from this program to give a cautious thumbs-up for this pragmatic and possible method of trying to provide real-time values of wave heights within acceptable error limits in situations where strong currents and deep water prevent the waves from being measured directly.

## 5.0 References

Nwogu, O. 1993. Effect of steady currents on Directional Wave Spectra, OMAE, Volume 1, Offshore Technology, ASME.

Note: The above described work was sponsored by the DFO/Canadian Coast Guard and Axy Environmental Systems, with assistance from the Canadian Hydraulics Centre (CHC) of the National Research Council.

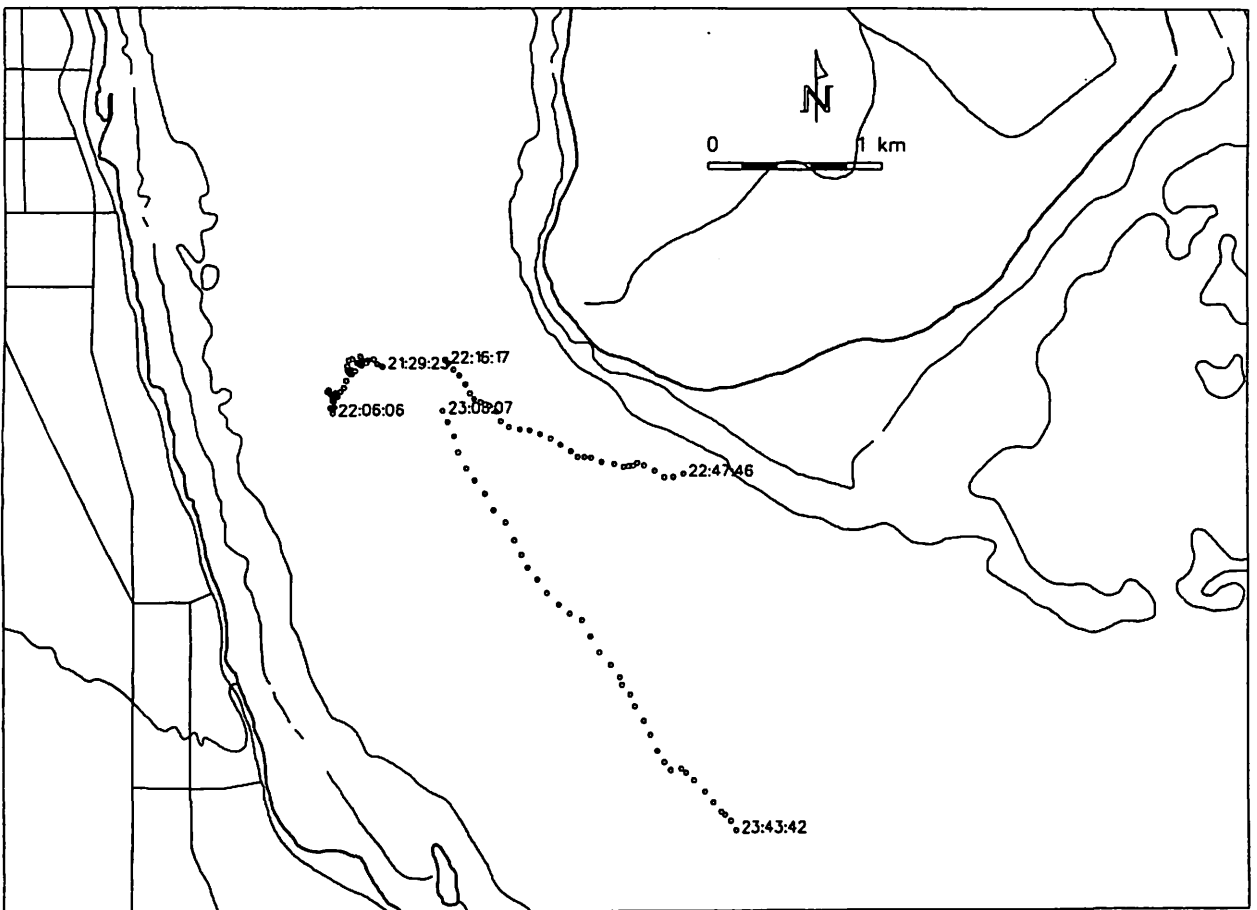


Figure 4: Buoy Tracks

## SEPARATION OF SEA AND SWELL FROM NDBC BUOY WAVE DATA

David Wang<sup>1</sup> and David Gilhousen<sup>2</sup>

Computer Sciences Corporation<sup>1</sup> and National Data Buoy Center<sup>2</sup>  
Stennis Space Center, Mississippi, USA 39529-6000

### 1.0 INTRODUCTION

The National Data Buoy Center (NDBC) operates more than 50 buoy stations reporting wave spectral data hourly. From these spectra, real-time reports of significant wave height and dominant wave period were posted on several Internet home pages for the last 2 years. One frequent request from the maritime public using these postings was to add swell height and period measurements. Indeed, wind seas and swells have different characteristics that are important for seakeeping safety, small boat operation, ship passages over harbor entrance, and surfing forecasting (Earle, 1984). The statistical description of individual wind sea and swell wave system provides information needed to investigate the influence of swell on wind sea growth and dissipation in open ocean (Hanson, 1996). The presence of swell could also affect the relationship between wind stress and sea state (Dobson, et al. 1994).

A wave identifying and tracking scheme was formulated for directional wave spectra (Gerling, 1992; Kline and Hanson, 1995; Hanson, 1996). This approach requires information of both directional wave and wind data that may not always be available. Earle (1984) proposed that the frequency separating wind seas and swells are related to the peak frequency of the Pierson-Moskowitz (P-M) spectral model, which can be determined for a given local wind speed. This approach is conceptually similar in that wind sea is part of the wave spectrum for which the wave phase velocity is less than the wind velocity component in the direction of wave propagation (The WAMDI Group, 1981; Dobson, et al. 1994). Vartdal and Barstow (1987) developed an algorithm, based on the shape of mean JONSWAP spectral model, to separate

wind seas and swells for a given wave spectrum that does not require wind data.

In this study, in addition to algorithms by Earle (1984) and Vartdal and Barstow (1987), a new algorithm for separating wind sea and swell based on wave steepness was introduced. Three algorithms were examined using directional wave and wind data collected from a buoy station off the Alabama coast in the Gulf of Mexico.

### 2.0 ALGORITHMS FOR SEPARATION OF WIND SEA AND SWELL

The separation of wind sea and swell is carried out by estimating separation frequency,  $f_s$ , for the wave spectra. Wave energy at frequencies higher than  $f_s$  is considered generated by local winds; wave energy at frequencies lower than  $f_s$  is considered generated by swell. Three algorithms for estimating  $f_s$  are introduced.

#### 2.1 P-M Algorithm

According to the P-M spectral model, the peak frequency of a fully developed sea is related to the local wind speed by

$$f_p = \frac{1.25}{U} \quad (1)$$

where  $f_p$  in Hz is the frequency of maximum spectral density and  $U$  in m/s is wind speed at the 10-m height. Earle (1984) recommended the separation frequency  $f_s$  as

$$f_s = C f_p \quad (2)$$

where  $C$  is an empirically determined constant. A value of 0.8 is used by Earle (1984). A similar approach with additional consideration of the wind and wave direction difference was developed by Vartdal and Barstow (1987).

Equation (2) with a value of 0.8 for  $C$  can be expressed as the relation of wave phase velocity,  $V_s$ , at  $f_s$  and wind speed, which is

$$V_s = 1.56U \quad (3)$$

This suggests that Earle's algorithm is similar to the concept that wind seas are reflected in a specific frequency range of the wave spectrum.

### 2.2 Spectral Shape Algorithm (SPSH)

The spectral shape algorithm, denoted as SPSH, was developed by Vartdal and Barstow (1987). This algorithm is based on the shape of the mean JONSWAP spectrum. The first step is to determine the lowest frequency  $f_1$  of wind-generated equilibrium range that has

$$s(f) * f^5 > 2.5 * 10^{-4} (m^2 Hz^4) \quad (4)$$

where  $s(f)$  is the measured wave spectral density in  $m^2/Hz$  and  $f$  is frequency in Hz. The value  $2.5 * 10^{-4}$  is half the asymptotic value of the P-M spectrum multiplied by  $f^5$ . The second step is to determine the wind sea peak,  $f_{wi}$ , that is the frequency of maximum  $S(f)$  in the range

$$0.75f_1 < f < 1.25f_1 \quad (5)$$

and takes

$$f_s = Cf_{wi} \quad (6)$$

as the separation frequency between swells and wind seas.  $C$  is an empirically determined constant. A value of 0.75 is used by Vartdal and Barstow (1987).

### 2.3 Wave Steepness Algorithm (STPN)

The wave steepness algorithm, denoted as STPN, is based on the assumption that wind seas have higher steepness and swells have a lower wave steepness. A representative parameter describing the steepness of random waves is defined as

$$steepness = \frac{H_s}{L} = \frac{2\pi H_s}{gT_z^2} \quad (7)$$

where  $H_s$  is the significant wave height,  $L$  is the

wave length associated with  $T_z$ , and  $T_z$  is the average wave period computed from the  $n$ th moment of wave spectrum by

$$H_s = 4\sqrt{m_0}, \quad T_z = \sqrt{\frac{m_0}{m_2}} \quad (8)$$

$$m_n = \int_{f_1}^{f_u} f^n s(f) df$$

where  $f_u$  and  $f_1$  are usually the upper and lower frequency limits of measured wave spectra, respectively. In this study, 0.03 and 0.4 Hz were used for the lower and upper limits, respectively. A frequency-dependent parameter representing wave steepness over frequencies ranging from a specified  $f$  to the upper limit  $f_u$  is defined as

$$\xi(f) = \frac{2\pi H_s(f)}{gT_z(f)^2} \quad (9)$$

where  $H_s(f)$  and  $T_z(f)$  are computed from

$$H_s(f) = 4\sqrt{m_0(f)}, \quad T_z(f) = \sqrt{\frac{m_0(f)}{m_2(f)}} \quad (10)$$

$$m_n(f) = \int_f^{f_u} f^n s(f) df$$

The separation frequency  $f_s$  is estimated by

$$f_s = Cf_x \quad (11)$$

where  $f_x$  is the frequency of maximum  $\xi(f)$ , and  $C$  is an empirically determined constant. A value of 0.95 is used in this study. This method does not require wind data and any assumption concerning wave spectrum.

### 3.0 FIELD DATA TESTING OF THE SEPARATION METHODS

The validity and reliability of the algorithms were examined using hourly measured wind and directional wave data measured from an NDBC buoy station during a meteorological frontal passage accompanied by rapid wind speed and direction shifts. The buoy was moored off the Alabama coast at a water depth of approximately 30 m. The buoy was equipped with an NDBC directional wave measurement system to estimate wave directions using the buoy's heave,



pitch, and roll motions. Winds were measured by an R.M. Young propeller-type anemometer mounted at the top of the buoy mast at approximately 5 m above the waterline. The 5-m measured wind speed was converted to wind speed at a 10-m height using a multiplication factor of 1.2.

As the wind direction remained approximately 140 degrees during the first 26 hours from December 13-15, 1995, the wind speed gradually increased from 5 to 15 m/s (see Figure 1a). The significant wave height increased from 0.5 to 4 m as the dominant wave period increased from approximately 4 to 8 s (see Figure 1b). The wave condition during this period was dominated by wind seas caused by the long-fetch southeasterly winds over the Gulf of Mexico. In the early hours of December 14, the wind speed quickly dropped to less than 4 m/s as wind direction shifted to approximately 290 degrees. Wind speed then increased to approximately 10 m/s, and both the wind speed and direction remained relatively steady for the

rest of the period. The wave conditions during this period consisted of southerly swell and a newly developed wind sea generated by the fetch-limited northwesterly winds.

Figure 2a shows a selected wave spectrum with significant wave height of 4.135 m and wind speed of 15.3 m/s before the frontal passage, which are the highest wave height and wind speed of the entire period. Figure 2b shows frequency-dependent mean wave direction that aligned well with the local wind direction as indicated by the horizontal dashed line. The separation frequencies derived from the P-M, SPSH, and STPN algorithms are indicated by the vertical dashed, dash-dotted, and solid lines, respectively. The vertical dotted line shows the frequency above which the deep-water wave phase velocity is less than the wind velocity component in the mean wave direction. As shown, separation frequencies from the above algorithms are lower than peak frequency at 0.13 Hz, indicating wave energy is mainly generated by the local wind.

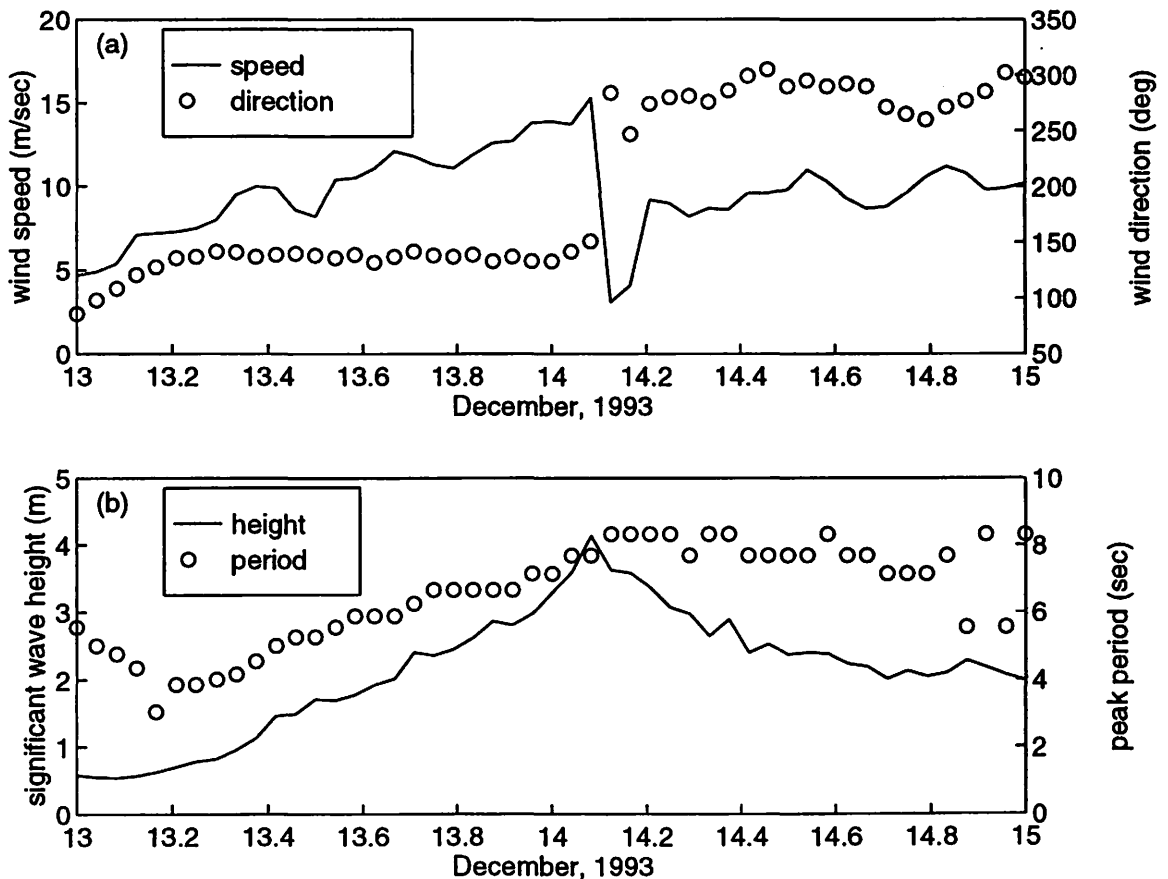


Figure 1. Time series of (a) wind speed and direction and (b) significant wave height and peak wave period.

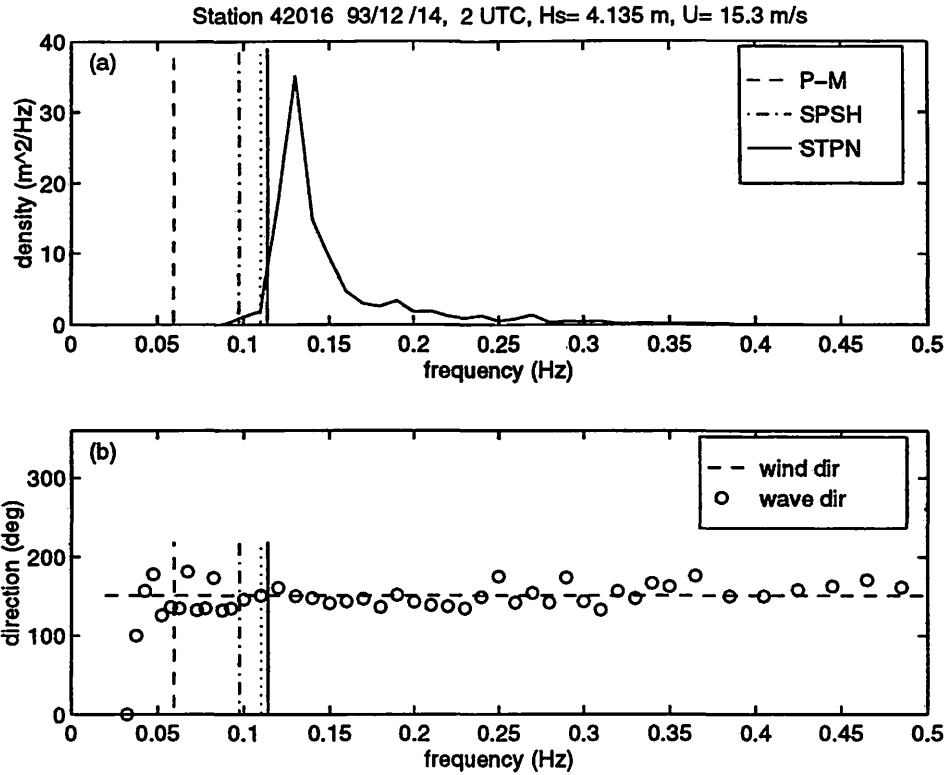


Figure 2. A selected (a) wave spectrum and (b) mean wave and wind directions before the frontal passage. The separation frequencies derived from the three algorithms are indicated by the vertical dashed, dash-dotted, and solid lines. The vertical dotted line indicates the frequency above which the wave phase velocity is less than the wind velocity component in the mean wave direction.

Figure 3 shows the selected wave spectrum and mean wave direction of a bimodal sea after the frontal passage. As indicated by the mean wave direction and local wind direction, wave energy at frequencies lower than 0.17 Hz has a major peak at 0.13 Hz, which was caused by swells coming from 160 degrees. Wave energy at frequencies higher than 0.17 Hz has a peak at 0.21 Hz, which was from wind seas generated by the local winds. The separation frequency derived from the STPN algorithm is 0.16 Hz, which properly separates the wind seas and swells. However, the separation frequencies from the P-M and SPSH algorithms do not separate the two energy sources properly. Using separation frequencies from these two algorithms for this bimodal wave spectrum overestimates wind sea energy and underestimates swell energy. Examinations of wave spectra from the rest of the period show similar results as the two examples discussed.

The significant wave height and average wave period for wind seas and swells can be computed

from Equation (8) by replacing  $f_l$  with  $f_s$  for wind seas and replacing  $f_u$  with  $f_s$  for swells, respectively. Figures 4 and 5 show the time series of wind sea significant wave height,  $H_{sw}$ , and swell significant wave height,  $H_{ss}$ , obtained using the separation frequencies by the three algorithms. For comparison, reference significant wave heights for wind sea and swells are also shown. The reference wave heights are obtained by considering  $f_s$  as the frequency above which the wave phase velocity is less than the local wind velocity component in the mean wave direction. This separation frequency is indicated by the dotted vertical line in Figures 2 and 3.

As shown in Figure 4, when wave field was dominated by the growing wind seas before the frontal passage, the  $H_{sw}$  derived from the three algorithms all agree well with the reference  $H_{sw}$ . During coexistence of wind seas and swells after the frontal passage, the  $H_{sw}$  by the P-M and SPSH algorithms is significantly higher than the reference  $H_{sw}$ . The  $H_{sw}$  by the STPN

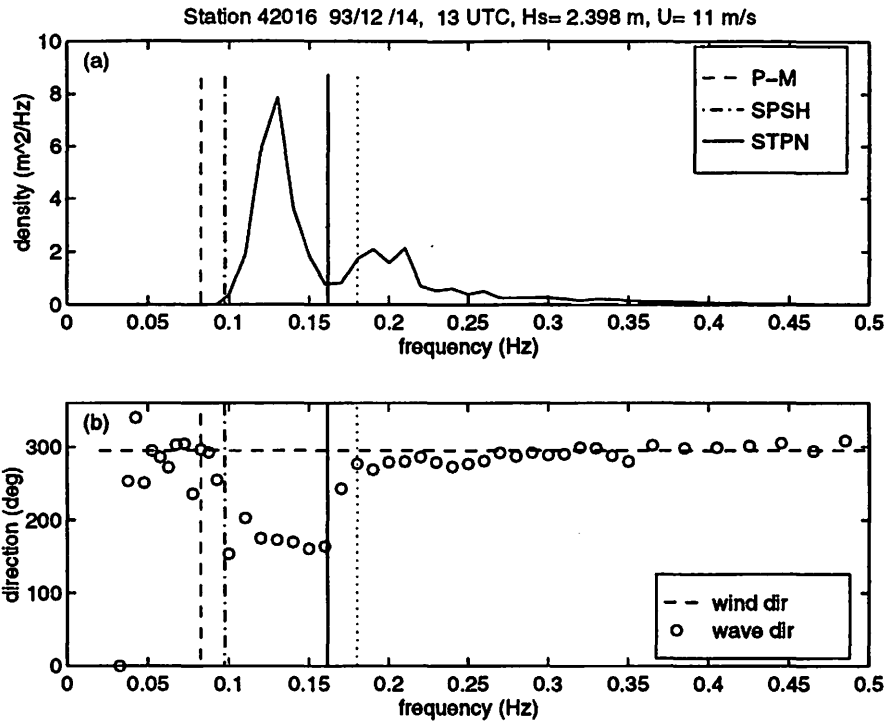


Figure 3. A selected (a) wave spectrum and (b) mean wave and wind directions after the frontal passage. The separation frequencies derived from the three algorithms are indicated by the vertical dashed, dash-dotted, and solid lines. The vertical dotted line indicates the frequency above which the wave phase velocity is less than the wind velocity component in the mean wave direction.

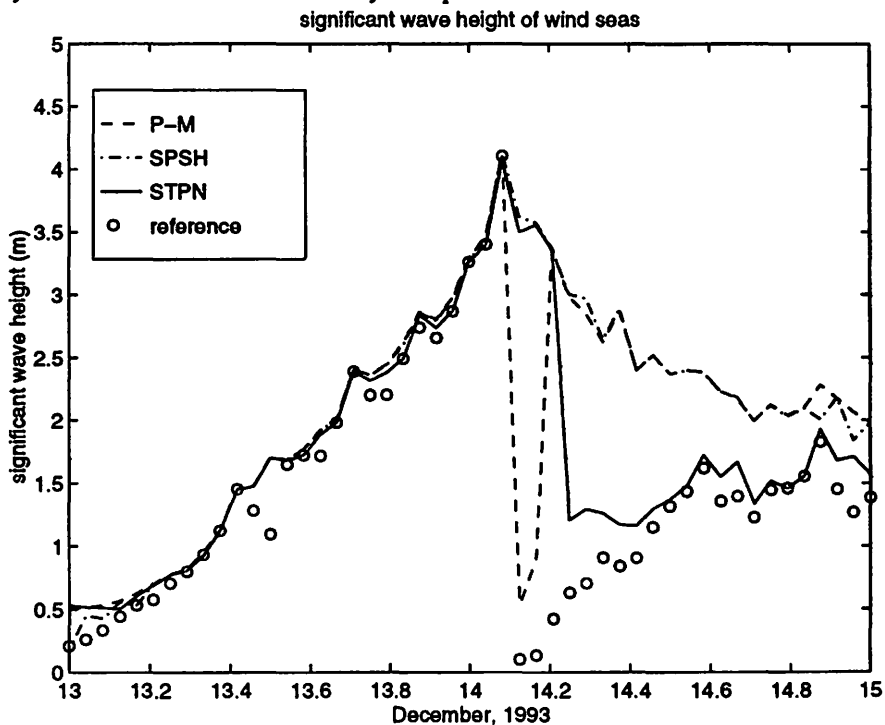


Figure 4. Time series of significant wave height of wind seas using the separation frequencies by the three algorithms. The reference significant wave heights for wind seas are obtained by using the separation frequency above which the wave phase velocity is less than the wind velocity component in the mean wave direction.

algorithm agrees well with the reference  $H_{sw}$ , except for a few hours when both wind speed and direction changed rapidly during the frontal passage.

As shown in Figure 5, when wave fields were dominated by the growing wind seas, the swell significant wave height,  $H_{ss}$ , by the three algorithms and the reference  $H_{ss}$  are generally less than 1 m, and the differences among them are insignificant. When the wave fields consisted of wind seas from fetch-limited wind seas and swells,  $H_{ss}$  by the STPN algorithm agrees well with the reference  $H_{ss}$ , while  $H_{ss}$  by the P-M and SPSH algorithms are significantly lower than the  $H_{ss}$  by the STPN and the reference  $H_{ss}$ .

Figures 6 and 7 show the time series of significant wave height and average wave period of wind seas and swells by the STPN algorithm, respectively. When wave conditions were dominated by wind seas before the frontal passage, the significant wave height and average wave period are almost the same as those of wind seas. During coexistence of wind seas and

swells after the passage on December 14, the separation algorithm provided a detailed description of the evolution of wave conditions. It shows the gradually decreasing significant wave height  $H_s$ , in fact, consisted of a growing  $H_{sw}$  and a decaying  $H_{ss}$  with an average wave period of approximately 4 s for wind seas and 7.5 s for swells.

#### 4.0 SUMMARY

Three empirically developed algorithms for separation of wind seas and swells were examined based on directional wave and wind data from an NDBC buoy station during a meteorological frontal passage. All three algorithms provide similar estimation of separation frequency when wave conditions were dominated by wind seas from a uniform and long-fetch wind field before the passage. However, when wave conditions were contributed by both wind seas and swells after the passage, only the algorithm based on wave steepness (STPN) provided proper and

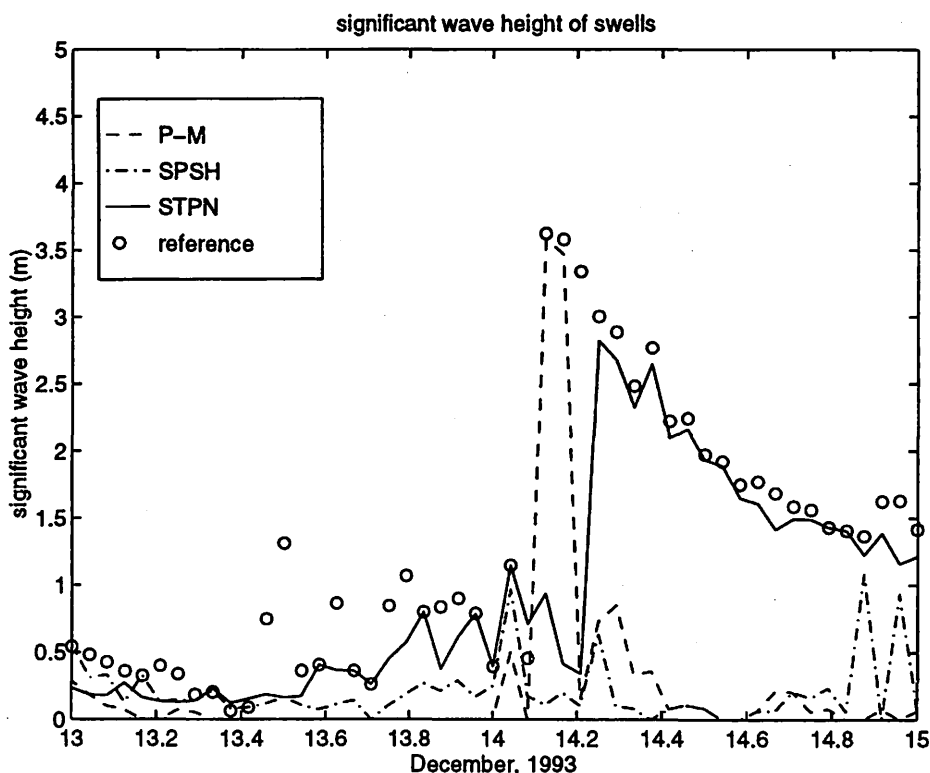


Figure 5. Time series of significant wave height of swells using the separation frequencies by the three algorithms. The reference significant wave height for swells are obtained by using the separation frequency below which the wave phase velocity is greater than the wind velocity component in the mean wave direction.

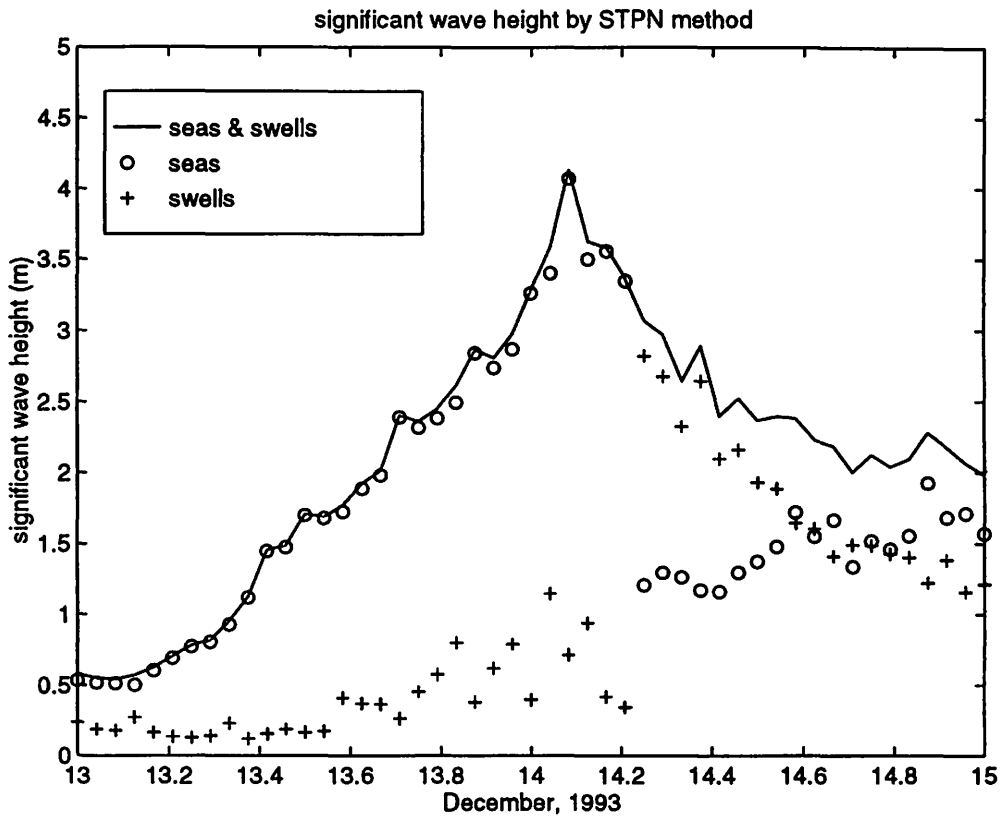


Figure 6. Time series of significant wave height of wind seas and swells by the wave steepness algorithm (STPN).

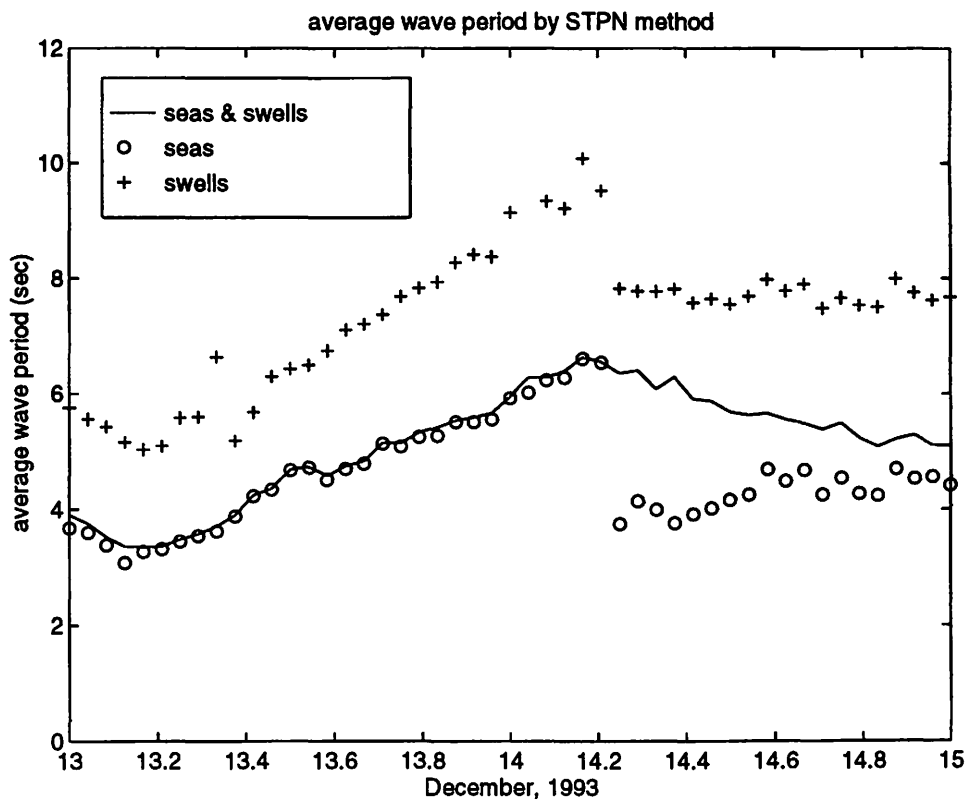


Figure 7. Time series of average wave period of wind seas and swells by the wave steepness algorithm (STPN).

consistent separations for wind seas and swells. The other two algorithms overestimated wind seas and underestimated swells.

The STPN algorithm, without the requirements of wave direction, wind data, and wave spectrum shape assumptions, shows the spectral-related steepness parameter can be used to separate wind seas and swells effectively. This simple algorithm can be easily implemented to report wave height and period of wind seas and swells in real time for operational purposes.

## 5.0 REFERENCES

- Dobson F.W., S.D. Smith, and R.J. Anderson, 1994: Measuring the relationship between wind stress and sea state in the open ocean in the presence of swell. *Atmosphere-Ocean* 32 (1), pp. 237-236.
- Earle, M.D., 1984: Development of algorithms for separation of sea and swell. Technical Report MEC-87-1, National Data Buoy Center, pp. 53.
- Gerling, T.W., 1992: Partitioning sequences and arrays of directional ocean waves spectra into component wave systems. *Journal of Atmospheric and Oceanic Technology*, Vol. 9, pp. 444-458.
- Hanson, J.L., 1996: Wave spectral partitioning applied to the analysis of complex wave conditions in the north Pacific Ocean, in *Proceedings, 8th Conference on Air-Sea Interaction and Symposium on Goals*, American Meteorological Society.
- Kline, S.A., and J.L. Hanson, 1995: Wave identification and tracking system. Technical Report STD-R-2436, The Johns Hopkins University, Applied Physics Laboratory; Laurel, MD.
- Vartdal, L., and S.F. Barstow, 1987: A separation algorithm for wind sea and swell for applications to directional Metocean data buoy. Technical Report, Oceanographic Center, SINTEF Group, Trondheim, Norway, pp. 104.
- The WAMDI Group, 1988: The WAM model-A third-generation ocean wave prediction model. *Journal of Physical Oceanography*, Vol. 18, pp. 1775-1810.

# Recovery of Near Surface Velocity from Undrogued Drifters

Stephen E. Pazan

*Ocean Prospects, Encinitas, California*

Peter P. Niiler

*Scripps Institution of Oceanography, La Jolla, California*

## ABSTRACT

We have quality controlled a global dataset of wind and buoy data, made comparisons of 15 m drogued and undrogued buoy observations, and developed both 1-D and 2-D linear regression models of the difference between drogued and undrogued drifter velocity as a function of wind and Coriolis parameter. Meridional and zonal surface wind velocity components from the global synoptic FNMOC model and the global synoptic ECMWF model were interpolated to each naval AN/WSQ-6 and WOCE/TOGA buoy position and date/time in the datasets. Seven 1-D linear regression models were evaluated for both the Navy vs. WOCE drogued-on dataset and the WOCE drogued-off vs. WOCE drogued-on dataset. Principal results from this analysis were: the constant term in the regression analysis was zero; the Navy buoys behaved like WOCE drogued-off buoys; either FNMOC or ECMWF winds were sufficient. The 2-D regression analysis on selected synoptic data was:

$$U_{undrogued} - U_{drogued} = B \cdot W,$$

where  $U_{undrogued} - U_{drogued}$  was ensemble mean buoy velocity difference and  $W$  was wind velocity; the real and imaginary parts of these quantities were the zonal and meridional components, respectively.  $B$  was the complex valued regression coefficient. We found that the absolute value of  $B$  was a function of the reciprocal of the square root of the Coriolis parameter,  $f$ , giving:

$$|B| = (B_0 + B_1 \cdot f^{-1/2}),$$

where the best fit gives  $B_0=0.003$ , and  $B_1=0.00016$  ( $\text{sec}^{1/2}$ ). A dataset assembled from undrogued (Navy) and drogued buoy pairs was analyzed and results confirm the amplitude of the mean coefficient. The analysis also found that the angle,  $\lambda$ , of the velocity difference with respect to the wind, was a function of the surface wind and the Coriolis parameter:

$$\lambda = \text{Phase}(B) = (\lambda_0 + \lambda_1 \cdot |W| \cdot f^{-1/2}),$$

where  $\lambda$  ranged from  $20^\circ$  to  $35^\circ$  to the left (right) of the wind north (south) of the equator from  $20^\circ$  to  $50^\circ$  in latitude; it is best fit by  $\lambda_0=15^\circ$  and  $\lambda_1=0.75$  (degrees  $\text{sec}^{1/2}/\text{m}$ ).

A parametric model of the Ekman spiral plus a leeway was used to evaluate the observed velocity differences. The parameters derived from non-linear regression analysis were consistent with Ralph & Niiler (1998), developed independently by analysis of drogued drifter data alone. We developed and evaluated a parametric model of buoy velocity difference:

$$\text{Buoy Velocity Difference} = u_{\text{difference}} = \Delta u_E \cos \phi + u_x \cos \lambda,$$

where  $\Delta u_E$  is the Ekman velocity difference between the surface and 15 m depth,  $u_x$  is leeway drift,  $\phi$  is the angle the buoy velocity difference makes with respect to  $\Delta u_E$ , and  $\lambda$  is the angle the velocity difference makes with respect to  $u_x$ . Buoy velocity difference is a function of the model parameters  $\alpha$ ,  $\beta$ ,  $\gamma$ ,  $\theta_0$  where:

$$u_x = \alpha \cdot u,$$

where  $u$  is the wind friction velocity. In the limit of small current rotation between the surface and 15m:

$$\Delta u_E \cong \gamma \beta^2 z = \xi \cdot z.$$

Current rotation with depth is parameterized by  $\gamma$ ;  $\theta_0$  is the complement of the angle of surface current relative to the wind. We found broad maxima in the reduction of variance of  $u_d$  for  $3 < \alpha < 6$ ,  $0.070 < \beta < 0.075 \text{ sec}^{-1/2}$ ,  $\gamma=1.1$ , and  $30^\circ < \theta_0 < 90^\circ$ .



## **1. Introduction**

In the past ten years oceanographers, meteorologists and the US Navy deployed a large number of ARGOS-tracked drifters into all of the major ocean basins. Data from these drifters has accumulated at Meteorological and Environmental Data Service (MEDS), Canada, which is the world responsible center for drifting buoy data. Between 1987 and 1994, location data is available from principally two very different types of drifters: the WOCE/TOGA Surface Velocity Program (SVP) drifter (1632 SVPs) (Sybrandy and Niiler, 1991) and the naval AN/WSQ-6 meteorological (WSQ) drifter (704 WSQs) (Selsor, 1993). This data is potentially a rich source of information on the circulation of the upper ocean, provided the drifter displacements can be interpreted as being caused by the horizontal movement of water at some known depth. Because of the complex action of the wind and waves on the drifter float the drogue tether causes a "leeway" of the drifter through the water, floating objects in the upper ocean can drift in very different manner from the movement of the water and leeway is not always well understood or documented. This is a study of the difference of the movement of drogued SVPs (called SVP hereinafter), whose water following characteristics are well documented (Niiler et al., 1995) and the movement of WSQs and SVPs that have lost their drogues (called SVPL hereinafter). The global near-surface velocity data set would be approximately doubled if the WSQ and the SVPL data could be combined with the SVP data.

The SVP is drogued to 15m depth with a drogue that has a drag area ratio of drogue area to the tether and surface float area greater than 40. When the drogue is attached to the SVP it follows the water to within  $\pm 0.1$  m/sec in 10 m/sec winds. This drogue is so large that it often drags the surface float under water (Niiler et al., 1995); its status is monitored by a sea-water switch which does not close if the drogue falls off. The WSQ has a much smaller drogue, the surface float does not submerge and the drogue status is not known.

Two principal physical effects determine the relative movement of objects strongly anchored to the water at 15 m depth and objects at the surface on which the water has a weak purchase. First, there is the effect of a wind-driven Ekman current that rotates into the direction of the wind from 15 m depth to the surface (Chereskin, 1995). The structure and strength of this rotation has been parametrized as a function of wind and Coriolis parameter from SVP drifter measurements in the tropical Pacific (Ralph and Niiler, 1998). Secondly, the direct action of the wind and waves can result in a relative movement, or "leeway", of an object through water either down-wind or sometimes even up-wave, depending upon the very specific conditions that prevail (Davis, 1984). We will use these basic principles in the analysis of the relative motion of the drifters that are drogued and the floats moving more freely on the surface. We focus on interpretations in terms of the surface wind from several operational products, as these are global and readily available for many years in the past and in the future. The data and methods are discussed in Section 2. In Section 3 the Ekman theory is reviewed and the statistical results of the analysis are in Section 4. Section 5 presents the statistical interpretation in terms of the Ekman spiral and a leeway.

## **2. Data and Procedures**

### ***2.1 SVP Lagrangian Drifter Data***

The World Ocean Circulation Experiment (WOCE) and the Tropical Ocean and Global Atmosphere (TOGA) Program have established a long term ocean observing system for monitoring ocean currents; this program, called the Surface Velocity Program (SVP), coordinates global deployment of Lagrangian drifters. In the United States, this is done principally from the Global Drifter Center (GDC) at the Atlantic Oceanographic and Meteorological Laboratory (AOML). The SVP has been deploying over 300 drifters per year since about 1991, principally in the global tropics (Niiler *et alia*, 1991). The WOCE

and TOGA projects deployed 2013 SVP Lagrangian drifters altogether during the period 1990-1994.

Considerable effort has gone into designing a Lagrangian drift buoy used in SVP (Niiler *et alia*, 1987). The SVP Global Drifter Program Lagrangian drifter, shown in Figure 1 (left), is light-weight, constructed of low-cost sea water compatible plastics; it is composed of a surface float, a tether and a drogue. Plastic impregnated wire rope tethers the surface float to the drogue. Its physical characteristics, including its drag area ratio, are tabulated in Table 1 (Niiler *et al.*, 1991). It has a mean time before failure of about one year, and it is easy to deploy from Volunteer Observing Ships (VOS). It is designed to follow water parcels vertically averaged over a drogue of height 6-7 m, centered 15 m below the surface (WCRP-26); the drag area ratio is an order of magnitude greater than the Naval AN/WSQ-6 buoys, as can be seen in Table 1. There were two principal design considerations: 1. the drogue leeway drift should be predictable; 2. the drifter should have a mean time to failure of many months in an open ocean environment. As a consequence, the final design incorporates the following features: 1. three dimensionally symmetric float; 2. thin and stiff wire tether; 3. dimensionally stable drogue with a high drag coefficient, the holey sock drogue, and 4. drag area ratio greater than 40. These features act to reduce the steady tension and eliminate any shock stress between surface and subsurface elements of the drifter, minimize surface wave effects, and reduce the drag of the tether and submerged floats relative to the drag of the drogue. During tests, a Velocity Measuring Current Meter (VMCM) attached to the top and bottom of the SVP drogue did not measure leeway drift greater than 0.01 m/sec in conditions of 10 m/sec winds.

We archived these data and data from 1632 SVP drifting buoys after they lost their drogues, a dataset comprising 1,844,144 drogued buoy observations and 848,416 undrogued buoy observations at synoptic time intervals; the quality control of these data

has been described in Poulain and Hansen (1996). Global monthly summaries of the WOCE/TOGA Lagrangian drifting buoy dataset are shown in Figure 2.

Each of the TOGA/WOCE Lagrangian drifters had a drogue on/drogue off sensor that determined whether the spherical surface float was out of water or underwater. So long as the drogue is attached, the surface float tended to submerge; if the surface float is continuously out of the water, the buoy was assumed to have lost its drogue. In 400 days of deployment about half of the WOCE buoys lost their drogues, consistent with previous findings, although the time to drogue loss might have been shorter in harsher environments (Poulain *et al.*, 1996), and after accounting for buoys which become inoperative due to other causes. The decline in drogued buoy population was highly variable; the decay was not exponential nor is it clearly linear. It can be said that it was consistent with a "noisy" linear decline, implying that a fixed number of buoys, not a fixed proportion of buoys, lose their drogues in any time interval; this was equivalent to the probability of drogue failure increasing with time. Niiler and Sybrandy (personal communication, 1998) have found, for six recovered drifters in the tropical Pacific of the same design and manufacture as those study herein that the tether connecting the buoy with its drogue was bitten by fish and appeared to be severed just above the subsurface float carrot.

## ***2.2 SVP Lagrangian Drifter Data Quality Control***

Quality control procedures developed by the Buoy Data Center at AOML have already examined the SVP data records for internal consistency, positioning errors and outliers. MEDS has done similar internal consistency, and made positioning error checks in the Navy buoy dataset, but there were problems in the Navy dataset which did not occur in the SVP dataset. Sometimes positions do not change from one observation to the next and at the end of a record there were often several observations from a single position; these were not included in the analysis. Each record was examined, occasionally revealing large shifts in position within a few hours. This was apparently because a new buoy had

been deployed with the same ARGOS ID after the old buoy deployment had terminated. Although the only buoy identifiers were the ARGOS identification numbers, the first observation of the new buoy deployment was identified by the large time and space interval between the last observation of one deployment and the first observation of the next deployment. Sometimes the day and month changed from December 31 to January 1 but the year didn't. This was rectified by resetting the year to the next year.

### **2.3 Naval AN/WSQ-6 Drifter Data**

METOCEAN Data Systems, Ltd., of Halifax, Nova Scotia, Canada manufactured the Naval AN/WSQ-6 drifter shown in Figure 1. The Naval Research Laboratory's (NRL) Tactical Oceanographic Warfare Support (TOWS) Program has managed and evaluated development of the Naval AN/WSQ-6 buoys (Selsor, 1993). They are self-contained drifters designed with power for a minimum of 90 days unattended collection of sea level pressure, SST and air temperature data from the open ocean; the deployed physical dimensions of the Naval AN/WSQ-6 drifter appear in Table 1. This study included data from the two principal manufacturer's versions of the Naval AN/WSQ-6, the CMOD and CMOD-I, although heavily weighted towards the former. For a more detailed discussion of the Navy drifters see Pazan and Niiler, 1998.

An important factor in Lagrangian drifter design is the "*drag area ratio*," which is the ratio of the drag area of the drogue to the sum of the drag areas of the tether system, submerged floats, and hull. Drag area is the frontal area of a buoy component times its drag coefficient. A drag area ratio larger than 40 is needed for small "leeway drift", the difference of velocity of the drifter and vertically integrated current velocity across the drogue; drag areas of each component of the Naval AN/WSQ-6 drifter and the drag area ratio of the drifter are tabulated in Table 1. Although the Naval AN/WSQ-6 drag area ratio is insufficient for a Lagrangian drifter, it is adequate for a Naval AN/WSQ-6 buoy designed

to be influenced by surface wind and wave forcing, as it was designed for meteorological observations.

Naval AN/WSQ-6 drifters are air deployed from P-3 aircraft, S-3 patrol aircraft, and various helicopter platforms (Selsor, 1993). The Naval AN/WSQ-6 buoy is drogued, usually with the aluminum cylindrical container used for packaging prior to deployment. A short wire cable connects the drogue to the nylon tether which is attached in turn to a toroidal surface flotation collar surrounding the spar shaped float. Over 95% of the total number constructed conform to this plan, although several variants have been proposed and built (*ibid.*, 1993); moreover, buoys deployed by the Navy conform to this plan even more consistently.

All Naval AN/WSQ-6 buoys are adaptable to several configurations (Selsor, 1994). For our data, the float assembly in each of these is the same, but the drogue, antenna and sensor arrangements differ; the configurations are further complicated by the presence or absence of protective netting on the tether and surface float variants.

During the period 1989-1994, 706 METOCEAN Naval AN/WSQ-6 buoys were deployed in the Atlantic, Pacific and Indian Ocean; these buoys returned 334,944 observations through the ARGOS satellite, shown in Figure 2. Data from 704 Navy buoys have been linearly interpolated to 196,885 synoptic 4-daily time intervals for consistency with both SVP datasets. A linear interpolation to synoptic times was used.

#### **2.4 Wind and Wave Data**

FNMOC produces marine synoptic six-hourly wind and wave analyses on a global grid; ECMWF produces marine synoptic 12-hourly wind analyses, also on a global grid. Since the buoy data positions either are archived at synoptic six-hourly intervals or interpolated to synoptic six-hourly intervals, we linearly interpolated synoptic wind and wave values to the location of individual buoy observations from the four surrounding

FNMOC or ECMWF grid field values. Wind or wave data were also interpolated in time when data were missing at any particular synoptic time or at every 06 GMT and 18 GMT synoptic time for ECMWF data.

### **2.5 Wind Data Quality Control**

We found occasional inconsistencies within the FNMOC wind and wave dataset. The FNMOC winds sometimes had the incorrect century, but this was trivial to correct. There have been other formatting errors, inconsistent with the official GRIB system, the WMO format for the storage of weather product information and the exchange of product messages in gridded binary form, which did not affect the data and were easy to manage. The FNMOC wind format was inadequately documented and changed between 1992 and 1993; the longitude and latitude axes were swapped between 1991 and 1992; and the longitude origin was displaced from the prime meridian by different amounts before and after 1992. There were also several GRIB encoding errors. After solving these problems, the FNMOC and ECMWF wind fields compared well. Correlations of FNMOC and ECMWF fields were tabulated in Table 2.

TABLE 2. ECMWF-FNMOC CORRELATION		
	ZONAL	MERIDIONAL
SVP/SVPL	96%	89%
SVP/NAVY	96%	94%

Wherever FNMOC and ECMWF winds disagreed by more than 1 m/s, the data report was disregarded in the final analysis; comparison of the wind datasets provides an extra quality control check on the wind data.

## **2.6 Data Selection Criteria**

There were three important considerations in the selection of potential study areas: 1. the buoys to be intercompared should have been close enough to be in the same ocean current; 2. the ocean region should have been one of low horizontal shear; 3. the ocean region should have relatively steady wind velocity and wave energy. These considerations generally excluded use of data from boundary currents or equatorial currents. The trade wind regions were favorable to this study because of the relatively large decorrelation scales and low horizontal shear of mean currents. Four selected regions of relatively low wind speed variability and wave height variability have been selected and shown as the boxed regions in Figure 3. Climatological horizontal shear in the upper ocean was low and observational density was relatively high in these regions, with the exception of the tropical Pacific, which was chosen to provide some insight into processes near the equator, although in fact our final selection process removed data in the tropical Pacific from consideration.

## **2.7 Statistical Procedures**

We have made statistical summaries of buoy drift velocity, ECMWF and FNMOC wind velocity and FNMOC wave height in  $2^\circ$  latitude  $\times$   $8^\circ$  longitude  $\times$  1 month bins. Binning generally removed mesoscale eddy variance through averaging, and therefore revealed underlying relationships which might otherwise be obscured by large incoherent motions. Because these statistical summaries included standard deviations as well as mean quantities, they were used to remove bias in the regression and estimate confidence limits. The summaries were of two kinds: first, separate drogued and SVPL (Navy) statistics were computed of all quantities associated with selected buoys; second, combined statistics were computed of all quantities associated with selected pairs of drogued and SVPL (Navy) buoys. The distribution of the first type of summary bins was roughly equivalent to the



distribution of observations. The second type of summary had a more restricted distribution; there were about 3001 of these bins in the SVP/SVPL buoy pair dataset, and about 565 of these bins in the SVP/Navy buoy pair dataset; eliminating null and suspect values, bins with less than 5 observations, reduced the numbers of bins actually used in the buoy pair analyses to 19, all from the SVP/SVPL buoy pair dataset.

In Figure 4 (right) residuals of buoy velocity difference have been plotted against the so-called "normal score." Residuals have been computed from a simple 1-D regression of global mean buoy drifter velocity differences on wind. No attempt was made to restrict the analysis to a subset of the data. The purpose of this initial analysis was to discover if different regions have statistically distinct populations. Residuals drawn from a Gaussian Normal population will describe a straight line if plotted against the "normal score"; this is not true of any other distribution. Figure 4 (bottom right) for the SVP/Navy Dataset looks very much like a bimodal distribution, being composed of two straight-line segments, and Figure 4 (top right) for the SVP/SVPL Dataset is also clearly not normally distributed. In each case, the segment at normal scores  $>1.5$  is gray shaded. In Figure 4(left)the gray-shaded residuals occupied areas in the Kuroshio, the Kuroshio Extension, the North Equatorial Current and the Gulf Stream, all areas of high shear which we predicted might prove difficult to model. The "normal score" plots confirm that drift in high-shear areas was statistically distinct from that in low-shear areas, and that a population drawn from low-shear geographic areas may have satisfied assumptions of statistical normality even if the global population didn't. The conclusion is that the regression analysis could be done best with a selected sub-population of either dataset and operational models of buoy drift should take geographical restrictions into account. However, it should be noted that this does not mean that the applicability of the regression is limited to the low-shear areas; the problem arises only when comparing data which may be drawn from statistically distinct samples. With this caveat in mind the results of the global models will be examined below.

### 3. Models of Drogued and Undrogued Buoy Drift

#### 3.1 Wind Driven Upper Ocean Circulation

In order to develop a model of the latitudinal dependence of the relationship between velocity difference and wind stress, it is useful to examine some theoretical relationships between near surface currents. The momentum balance of the large spatial scale, time-mean near surface circulation of the ocean is a linear relationship between the Coriolis force, pressure gradient and the vertical convergence of the turbulent stress due to the winds (Pedlosky, 1982).

$$\rho \cdot f \cdot \bar{u} = -g\rho_0 \bar{\nabla} \eta + \frac{\partial \bar{\tau}}{\partial z}. \quad (1)$$

When the local pressure gradient is not statistically or dynamically related to the local wind (Niiler et al., 1993; Luther et al., 1990) and it can be estimated from sea level or hydrographic measurements (Ralph and Niiler, 1998), it is, in principle, possible to estimate the vertical convergence of the wind-produced turbulent stress from the ageostrophic component of the directly measured current. This convergence of stress depends upon the processes by which vertical turbulence transports of momentum occur on time scales shorter than the time scale at which the Ekman balance ensues. Ralph and Niiler (1998) have made an analysis of the ensemble mean ageostrophic circulation measured by WOCE drifters at 15m depth in the tropical Pacific. They found that the best statistical model (49% of variance explained) was one in which both the amplitude of the current and its vertical scale were proportional to wind speed and inversely proportional to the square root of the Coriolis parameter,  $f=1.454 \times 10^{-4}(\text{sec.}^{-1}) \sin(\text{latitude})$ . When the ageostrophic currents at 15m depth were plotted as functions of a non-dimensional depth equal to 15m, divided by the scale depth, an increasing rotation to the right of the wind was observed as a function of this scaled, non-dimensional depth. In the discussion which

follows, let  $u_*$  be the wind friction velocity, where  $\tau = \rho_0 u_*^2$ ,  $A$  be the Austausch coefficient,  $q$  be the Ekman velocity scale and  $L$  the scale of the turbulent eddies.

The scale depth ( $L$ ) is in general a very complex functional of the generation, transport, and dissipation of mechanical and potential energy. However, an examination of scale depth in various limits provides a conceptual guide for the development of a statistical model. In the presence of strong winds non-stratified turbulence scales apply (e.g. Caldwell et al., 1972):  $q \sim u_*$ ;  $L \sim u_*/f$ ;  $A = qL \sim u_*^2/f$ . In the presence of strong buoyancy fluxes,  $B$ , Monin-Oubokov scalings are appropriate (McPhee, 1995)  $L \sim u_*^3/B$ . From these limiting scaling arguments it can be shown, viz. (1), that for non-stratified, turbulent layers the Ekman currents,  $u_E$ , are proportional to wind speed and the Ekman layer scale depth,  $H_E$  is proportional to wind speed divided by the Coriolis parameter:  $u_E \sim u_*$ ;  $H_E \sim u_*/f$ . This is the limiting case during the winter season in sub-polar gyres. During times of strong heating and light winds, as occur in spring and early summer for the establishment of the seasonal thermocline, the length scale is proportional to Monin-Oubokov scale. These results imply the remarkable result that the Ekman currents are independent of wind and their depth scale is proportional to the wind speed squared:  $u_E \sim (-B/f)$ ,  $H_E \sim u_*^2/(-Bf)$ ; under these special conditions the model for wind driven currents may not work. The physics that lead to the most statistically useful scaling in the tropical and mid-latitude ocean is a third limit. In this limit mixing of a negative buoyancy flux is done by shear of the near-inertial currents, as would occur in late summer conditions in the mid-latitude oceans, where a weak stratification,  $N$ , is maintained (Niiler and Krauss, 1976):

$$\begin{aligned} u_E &\sim u_* \cdot (f/N)^{-1/2}; \\ H_E &\sim u_* \cdot (Nf)^{1/2}, \end{aligned} \tag{2}$$

In summary, in the most generally applicable model, Ekman currents proportional to wind speed and inversely proportional to the square root of the Coriolis parameter. This analysis is appropriate for the computation of long term mean Ekman currents, although in

cases of strong negative buoyancy fluxes, the linear dependence of current on wind speed will weaken and be difficult to establish statistically.

## 4. Results and Discussions

### 4.1 One-dimensional Regression

In order to connect the results of this study with those of earlier studies, and to test certain statistical assumptions, a one-dimensional linear regression model following Poulain et al. (1996) has been used to determine the buoy velocity difference between  $U_{SVP}$ , the velocity (m/sec) of the buoy with a drogue, and  $U_{SVPL}$ , the velocity (m/sec) of the buoy without a drogue (or Navy buoy with small drogue), in terms of  $W$ , the wind velocity (m/sec):

$$U_{SVPL} - U_{SVP} = A + B \cdot W. \quad (3)$$

The A (m/sec), C (sec) and B coefficients were chosen to minimize the calculated residual variance estimates.

Results from an earlier study which was confined to the Norwegian Sea can be compared with results from this study; this earlier regression (Poulain et al., 1996) assumed the constant term was equal to 0 and was made for the period 1 August, 1991-31 December 1993 in the area 15°W-20°E, 60°N-74°N. The buoy drift velocity dataset was drawn from 461 pairs of six-hourly krigged drogued and SVPL drifter observations within 10 km radius of each other; the regression of these velocities was done upon UK Meteorological Office six-hourly wind products. The results the Norwegian Sea study were:

$$\text{Model 1: } U_{SVPL} = 0.84 \pm 0.04 U_{SVP} + 0.0105 \pm 0.0007 W_x, \quad R^2 = 67\%$$

$$V_{SVPL} = 0.58 \pm 0.05 V_{SVP} + 0.0119 \pm 0.0008 W_y, \quad R^2 = 54\%$$

$$\text{Model 2: } U_{\text{SVF}}=0.59\pm 0.03 \quad U_{\text{SVPL}} - 0.0039\pm 0.0007W_x, \quad R^2=53\%$$

$$V_{\text{SVF}}=0.43\pm 0.03 \quad V_{\text{SVPL}} - 0.0020\pm 0.0008W_y, \quad R^2=30\%$$

The statistic  $R^2$ , also called the "coefficient of determination," is an overall measure of the success of the regression in predicting the dependent variable from the predictors. The tabulated error is the standard deviation of the sampling distribution (also called the standard error) of the respective coefficient; 95% confidence limits for Poulain's results were calculated by using his tabulated standard deviations and assuming 459 degrees of freedom, two less than the number of observations in his dataset. This analysis showed that buoy drift velocity dependence upon wind velocity was statistically significant. Apparently drogued buoy drift direction and velocity were tied to upper ocean currents, which might or might not be aligned with the wind, whereas undrogued buoys were directly influenced by the wind.

We have calculated the regression of synoptic six-hourly SVP drogued buoy drift and Navy buoy drift on wind velocity for the period 1 January, 1990-31 December 1994. FNMOC or ECMWF six-hourly wind products were both used; since insignificant differences were discovered between analyses using these wind products, results are given below for analyses using FNMOC alone. Since we have been seeking the influence of the wind on SVPL or Navy buoys, we selected the wind at the position of the buoy most affected by the wind, the SVPL or Navy buoys in all the analyses that follow. The buoy drift velocity dataset was drawn from six-hourly WOCE/TOGA drogued buoy and Navy buoy observations in  $565^\circ$  latitude  $\times$   $8^\circ$  longitude bins. The median number of observations in a bin was 66 and the maximum was 394; bin averages were over all time. We are interested in the response of buoy drifter velocity differences to wind, and not in the response of buoy drifter velocity to wind and itself, as in the Norwegian Sea study; therefore, we will display results only for regression of velocity differences on wind:

$$U_{\text{NAVY}} - U_{\text{SVP}} = -0.0361 \pm 0.0144 + 0.0166 \pm 0.0029 W_x, \quad R^2 = 9\% \quad df = 331 \quad s = 26$$

$$V_{\text{NAVY}} - V_{\text{SVP}} = -0.0148 \pm 0.0110 + 0.0145 \pm 0.0034 W_y, \quad R^2 = 5\% \quad df = 357 \quad s = 21$$

We have included values for the degrees of freedom,  $df$ , and the standard deviation of the residual,  $\sigma$ . The former has been used to determine the 95% confidence limits of the regression coefficients. The percent of variance tabulated above is considerably less than the percent of variance explained in the North Atlantic. Reasons to expect this are: buoy observations in the 1-D analysis above were separated by up to 800 kilometers zonally, 200 kilometers meridionally and weeks in time. Additionally, the North Atlantic analysis was restricted to 14° of latitude in the Arctic, whereas the SVP/Navy data ranged from the tropics to 60° N, and as we will show later that the relationship between the velocity difference and wind is dependent on the Coriolis parameter. Finally, when stricter selection criteria were applied to the data and the binned means used in this analysis, the percent of variance explained increased.

The same model was tested with the binned SVP and SVPL dataset; this dataset was drawn from 3001 pairs of 2° latitude by 8° longitude binned SVP and SVPL velocity observations. The median number of observations in a bin was 75 and the maximum was 1679:

$$U_{\text{SVPL}} - U_{\text{SVP}} = 0.0009 \pm 0.0004 + 0.0135 \pm 0.0009 W_x, \quad R^2 = 13\% \quad df = 1710 \quad s = 1.5$$

$$V_{\text{SVPL}} - V_{\text{SVP}} = 0.0015 \pm 0.0034 + 0.0120 \pm 0.0012 W_y, \quad R^2 = 5\% \quad df = 1835 \quad s = 1.4$$

The percent of variance explained in this dataset by the first two models was very nearly the same as explained in the SVP and Navy dataset. The constant term evaluated to zero within 95% confidence. Agreement between the SVP/Navy Dataset and the SVP/SVPL Dataset is good. The regression coefficient of buoy drift on wind velocity was in agreement for any particular model regardless of dataset.

Wave drift has also been approximated from FNMOC wave height, direction, and period for every buoy location and time but the results are entirely negative; the inclusion of wave drift did not improve the predictability of any of the models. Such relationship as existed may be obscured by errors in the FNMOC wave field or may be because the wave field does not contain separate information from the winds on time scales less than several days.

In summary, results of these 1-D regression analyses are:

- For the purposes of this study, the constant term in the regression analysis may be assumed to be zero;
- Both coefficients and variance explained are the same within error for regressions using Navy buoy velocity or undrogued SVPL buoy velocity as dependent or predictor variables, i.e. the Navy buoys behave like SVPL buoys;
- The regression coefficients and variance explained are the same within errors for either FNMOC or ECMWF winds and for the purposes of this study, either FNMOC or ECMWF winds should be sufficient;
- Coefficients of dependence upon wind in SVP/SVPL buoys are the same within errors as found in the Norwegian Sea study;

We now explore the geographic segregation expected from the effects of earth's rotation.

#### ***4.2 Two-dimensional Regression on Synoptic Data: Amplitude***

Using the results of the 1-D study, a 2-dimensional regression model has been developed. We have let each buoy drift observation vector and each wind vector be a complex number; the real part of the number is the north-south component of the vector and the imaginary part of the number is the east-west component of the vector. We will use a complex variant of the model, in which each coefficient in equation 3 is complex-valued.

Following the results of the 1-D study in the previous section, the coefficient A was set equal to zero. Having confirmed the dependence of undrogued drift upon drogued drift in the 1-D study, the regressions of undrogued(drogued) drift on drogued (undrogued) drift were eliminated. The 2-d regression analyses were done on two scales; first, the data in each 2° latitude by 8° longitude bin was used to calculate a regression of either six-hourly synoptic drogued or six-hourly synoptic undrogued buoy drift on synoptic undrogued wind:

$$u_{SVPL} = B_{SVPL} \cdot W_{SVPL} \quad (4.1)$$

$$u_{SVP} = B_{SVP} \cdot W_{SVP} \quad (4.2)$$

Since we have been seeking the influence of the wind on SVPL or Navy buoys, we selected the wind at the position of the buoy most affected by the wind, SVPL or Navy. However, the average wind at the position of the SVPL buoy was constrained to be within 1 m/s of the wind at the SVP buoy; results should be nearly independent of the choice of wind,  $W_{SVPL}$  or  $W_{SVP}$ . The phase angle of the complex linear regression coefficient was the angle of the response of the buoy drift to the wind.

In order to find the underlying relationship between the buoy drift and wind forcing, it was necessary a priori to reduce the noise created by eddies and shears of strong currents. From the many bins, 27 were found which met the following criteria:

- The wind should explain over 60% of the variance of the SVPL buoy drift, e.g., there was a wind-driven circulation;
- The number of 5-day observations in a bin were at least 15 or more;
- The percent of observations contributed by one buoy could not be more than 20% of the total. The latter criterion was suggested by previous experience with drifting buoy data analysis;



- In rare instances where the SVP buoy drift was highly correlated with the wind the velocity difference relationship is obscured - velocity difference becomes a small difference between two large numbers - and these instances were also rejected;
- Any instance of retrograde motion of an SVPL buoy was rejected on the grounds that such a dynamics was unphysical and probably represented an error in wind or buoy drift or both.

The distribution of these bins is displayed as open circles in Figure 3; the selected bins were extra-tropical, ranging 20° to nearly 60° in latitude away from the equator. The number of observations/ bin in exceeded 15 and often exceeded 100. Each bin yielded an estimate of the complex coefficient B of the vector regression equation using singular-value decomposition and assuming a Gaussian normal error distribution for binned mean drifter velocity differences: Since each bin extended over only 2° of latitude, it was not necessary for this equation to have a term which depends upon the latitude. As will be explained later, the dependence on wind is best examined in terms of the phase and amplitude of the complex coefficients, rather than the real and imaginary parts. The results of this analysis are displayed in in terms of amplitude and phase of  $B_{\text{difference}}$  rather than real and imaginary components. Taking the difference of equation 4.1 and equation 4.2, we have:

$$\begin{aligned} u_{\text{difference}} &= u_{SVPL} - u_{SVP} \\ &= B_{\text{difference}} \cdot W_{SVPD} \\ &= |B_{\text{difference}}| \cdot e^{2\pi i \lambda / 360} \cdot W_{SVPL} \end{aligned} \quad (5)$$

The complex coefficient  $B_{\text{difference}}$  is the difference between the coefficients  $B_{SVPL}$  and  $B_{SVP}$ .  $\lambda$  is the phase of  $B_{\text{difference}}$  in degrees. Figure 5 (bottom) displays a scatterplot of amplitudes of  $B_{\text{difference}}$  vs. latitude for 27 selected bins; a least-squares best fit to a linear Ekman model of latitudinal variation of the amplitude of  $B_{\text{difference}}$  explains 34% of the

variance in  $B_{\text{difference}}$ . The model is explained in the next section. Estimates of the 95% confidence limits of  $B_{\text{difference}}$  are shown in this figure; the mean confidence limit so estimated is approximately 0.001 m/sec. We also computed the regression of binned mean  $u_{\text{difference}}$  on wind and a function of the Coriolis parameter, which solved the problem on a global scale, instead of the sub-bin scale for which equation 4.1 and equation 4.2 were solved as discussed above. Data was summarized by computing the mean and standard deviation of buoy drift and wind,  $W$ , in the every bin; the first 1-dimensional regression results were derived from such summaries. The 2-dimensional analyses used similar summaries, which differ in that buoy drift and wind were complex quantities. These results explained over 47% of the variance in the amplitude of  $u_{\text{difference}}$  if a term explaining variability with the Coriolis parameter was included. In order to explain these results more completely it is now necessary to examine the nature of variability with the Coriolis parameter in more detail.

#### 4.3 Undrogued-Drogued Buoy Velocity Differences

Following the above analysis the equations for the latitudinal dependence of the coefficient  $B$  in equation 5 can be rewritten:

$$u_{\text{difference}} = (B_0 + B_1 \cdot f^{-1/2}) \cdot e^{2\pi i \lambda / 360} \cdot W_{\text{SVPL}}, \quad (6.1)$$

$$\lambda = \lambda_0 + \lambda_1 \cdot |W_{\text{SVPL}}| \cdot f^{-1/2}, \quad (6.2)$$

where  $u_{\text{difference}}$  and  $W_{\text{SVPL}}$  are complex valued, but all other parameters are real valued. Observed amplitudes of  $B$  are plotted versus latitude in Figure 5 (bottom) and can be used to solve for the amplitude of the coefficients in equation 6, assuming the complex phases

( $\lambda$ ) of  $B_0$  and  $B_1$  are identical. This is essential since the theoretical analysis above has shown that  $\lambda$  varies inversely with the scale depth, and the scale depth is a linear function of both the wind speed,  $W_{SVPL}$ , and the reciprocal of the square root of the Coriolis parameter,  $f^{1/2}$ . Linear regression returns  $B_0=-0.003$ ,  $B_1=0.00016$  ( $\text{sec}^{1/2}$ ), where  $f$  is the Coriolis parameter. There was evidence that the standard error of the coefficients returned by this regression overestimates the error over much of the latitude range because the envelope of points in Figure 5 (bottom) expands from lower to higher latitudes. Taking this into account and disregarding five extreme outliers of  $B$ , more than  $3\sigma$  from the model curve of  $B$  derived from  $B_0$  and  $B_1$ , above, the values of  $B$  converge to an amplitude of 2 at  $20^\circ$  latitude and are enveloped by a lower curve (upper curve for absolute latitudes less than  $20^\circ$ ) described by  $B_0=-.017$ ,  $B_1=0.00026$  ( $\text{sec}^{1/2}$ ) and an upper curve (lower curve for absolute latitudes less than  $20^\circ$ ) described by  $B_0=0.009$ ,  $B_1=0.00009$  ( $\text{sec}^{1/2}$ ). The envelope enclosed over 80% of the data and was used to make an estimate of confidence limits for the amplitude of the wind coefficient. The difference in the lower and upper bounds of the wind coefficient  $|B|$  defined the longitudinal axis of an error ellipse:

$$\begin{aligned} \epsilon_{B|} &= \left| 0.026 - 0.00017 \cdot f^{-1/2} \right| \quad \text{if } \epsilon_{B|} \geq .1 \\ \epsilon_{B|} &= .001; \quad \text{otherwise} \end{aligned} \quad (7)$$

$\epsilon_{B|}$  is constrained by the mean 95% confidence limit on  $|B|$  values shown in Figure 5 (bottom). It follows that the longitudinal axis of the velocity difference error ellipse (along the direction of  $U_D$ ) was:

$$\epsilon_{U_D|} = \epsilon_{B|} \cdot |W| \quad (8)$$

The error will be discussed further in Section 4.5, below.

#### 4.4 Two-dimensional Regression on Binned Means: Amplitude

A regression was also made of binned mean drifter velocity difference on binned mean buoy wind; this analysis assumes equation 6.1 and equation 6.2 held for mean buoy drift and mean wind, just as it did for synoptic buoy drift and synoptic wind. A scatterplot of the mean buoy velocity difference vs. the mean SVPL buoy wind for the same selected bins as used in the analysis above is shown in Figure 5(top); because no latitudinal dependence is included, the plot shows a trend equivalent to a low absolute B-value of 0.87. Including latitudinal dependence would require a 3-dimensional graph; the complex multiple regression equation is:

$$\overline{u_{\text{difference}}} = (B_0 + B_1 \cdot f^{-1/2}) \cdot \overline{W_{\text{SVPL}}} \quad (9)$$

Solutions to equation 9 are limited because the complex  $B_0$  and  $B_1$  coefficients in this equation cannot reproduce the variation in  $\lambda$  which can be explained by equation 6.2. The full solution of equation 9 for binned means is displayed in Figure 5(bottom) as the dashed line indicating the regression on binned means ( $A=0$ ). As can be seen, the solution is very close to the best fit to the regression coefficients computed from six-hourly synoptic data. As a check on the assumption of no constant term in equation 9, we have also plotted the regression on binned means assuming  $A \neq 0$ . These regressions explain over 47% of the variance.

#### 4.5 Two-dimensional Regression: Angle of Response

The angle of response,  $\lambda$ , of SVPL and Navy buoy drifter velocity difference to vector wind is shown in Figure 6. The angle of response is the phase angle of the complex B coefficient, given by

$$\lambda = \text{ArcTan}(\text{Imaginary}(B) / \text{Real}(B)), \quad (10)$$

For heuristic reasons, we have displayed the scatterplot of the response angle derived from synoptic data vs. latitude in Figure 6 (top); no relationship can be seen between the phase angle and latitude. However, as implied in the discussion in section 3.1, the angle depends upon both the Ekman depth and the inverse square-root of the Coriolis parameter. The relationship in equation 2 suggested dependence of the response angle upon the product of the wind and the reciprocal of the square root of the sine of the latitude, shown in Figure 6 (bottom). This quantity,  $\xi$ , is proportional to the Ekman depth,  $H_E$ , defined in equation 2. Scatter is still great and the percent of variance explained in this figure is low, but a Student's T-test shows that the trend exists with greater than 95% confidence. Deviation from the trend in this figure may be because the relationship does not hold under all ocean conditions. No clear estimate of the variation of the angle of response with latitude could be obtained from the binned mean regression analyses; this is not surprising since it is obvious this complex regression would only show a clear relationship if there were a clear trend in Figure 6 (top). The best estimate of a fixed angle of response from this analysis is approximately  $25^\circ$ , in the middle of the range of observed angles.

The range of the angles of response shown in Figure 6 at any latitude was  $10^\circ$ ; the precision of this estimate could be improved but not the accuracy. The transverse axis of the error ellipse for B is:

$$\epsilon_{B_r} = 0.1745 \cdot |B| \quad (11)$$

Therefore the transverse axis of the velocity difference error ellipse was:

$$\epsilon_{U_{D_r}} = \epsilon_{B_r} \cdot |W| \quad (12)$$

#### 4.6 The Most Likely Exponent of the Coriolis Parameter

As has been discussed earlier we expect the buoy velocity difference to be proportional to the reciprocal of the square-root of the Coriolis parameter. We have tested the assumption that the exponent should be  $-1/2$  and show the results in Figure 7. The amplitude of the regression coefficients,  $|B|$ , obtained from the synoptic analyses are modeled by the equation

$$|B| = B_0 + B_1 \cdot \sin(\text{latitude})^e, \quad (13)$$

where values of  $|B|$  were taken from the observed coefficients for selected bins (section 4.2). Rearranging terms and taking the natural logarithm of both sides of the equation reveals a regression equation which can be solved for  $B$  and  $e$ :

$$\ln(B - B_0) = \ln B_1 + e \ln(\sin(\text{latitude})). \quad (14)$$

$B_0$  is set to  $-1$ , which is greater than its lower bound and the equation is solved for  $e$ , a process equivalent to finding the best straight-line fit to the scatterplot in Figure 7. The results indicated  $e = -.53$  was an optimal fit.

### 5. Model of Ekman Surface Current and Leeway Drift

#### 5.1 Model Theory

The drift velocity of a SVPL or Navy buoy is composed of the wind forced leeway drift plus the Ekman and geostrophic currents. Since the geostrophic current can be taken constant from the ocean surface to the drogue depth, the geostrophic component of SVPL or Navy buoy drift can be taken equal to the geostrophic component of SVP buoy drift and removed from consideration. A plan view of SVP and SVPL or Navy buoy drift vectors are shown in Figure 8, in which wind is directed towards the top of the figure by convention. In this figure the Ekman current vector of the SVPL or Navy buoy,  $u_0$ , and

of a buoy drogued at 15 m,  $u_{15}$ , approximately have absolute value equal to (Ralph & Niiler, 1998):

$$u_0 = u_{15} = \frac{\beta u_*}{\sqrt{f}}, \quad (15)$$

where the coefficient  $\beta$  parameterizes the effects of a vertical density gradient. We use an empirical expression for the friction velocity,

$$u_* = W \sqrt{\frac{C_D \cdot \rho_a}{\rho_w}}, \quad (16)$$

where  $C_D$  is the stress drag coefficient, set equal to  $1.2 \times 10^{-3}$ ,  $\rho_a$  is air density,  $\rho_w$  is water density, and  $W$  is the wind velocity. The figure shows that the difference between SVPL or Navy buoy drift and SVP buoy drift, the total buoy velocity difference, is equal to the sum of the vectors  $\Delta u_E$  and  $u_s$ . Leeway drift is parameterized by the coefficient,  $\alpha$ , in an expression which states that there is a drift of flotsam down wind,

$$u_s = \alpha u_* \quad (17)$$

The Ekman velocity difference,  $\Delta u_E$ , is the vector difference between  $u_0$  and  $u_{15}$ . We derive an expression for  $\Delta u_E$ , starting with the geometric identities:

$$\lambda_0 = \frac{\pi}{2} - \frac{\Delta\theta}{2}, \quad (18.1)$$

$$\lambda_1 = \frac{\pi}{2} - \theta, \quad (18.2)$$

$$\phi + \lambda = \pi - \lambda_1 - \lambda_0, \quad (18.3)$$

$$\theta + \Delta\theta = \theta_0 = \theta + 2\zeta, \quad (18.4)$$

where  $\zeta = \frac{\Delta\theta}{2}$ . The rotation,  $\Delta\theta$ , of the Ekman current vector with depth is parameterized by a constant  $\gamma$  (Ralph & Niiler, 1998):

$$\Delta\theta = \gamma z/z_0, \quad (19)$$

Applying the definition of  $z_0$  as the scale depth  $\frac{u_*}{\beta\sqrt{f}}$ . Combining 18.1 and 18.3 and eliminating  $\lambda_0$ , then using 18.2 to eliminate  $\lambda_1$ :

$$\phi + \lambda = \theta + \zeta, \quad (20)$$

where  $\theta + \Delta\theta = \theta_0$  by definition. Then by trigonometry and the above results, we find:

$$\alpha u \sin[\theta_0 - \zeta - \phi] = \Delta u_E \sin \phi, \quad (21)$$

which implicitly relates  $\Delta u_E$  and  $u_s$ , and an expression for  $\Delta u_E$ :

$$\Delta u_E = 2u_{15} \cdot \sin \zeta. \quad (22)$$

For small  $\zeta$ , and using equation 15, this expression becomes

$$\Delta u_E \cong \gamma \beta^2 z = \xi \cdot z. \quad (23)$$

where  $\xi$  is here defined as  $\gamma\beta^2$ .

The line DB represents the total buoy drifter velocity difference vector in Figure 8, identical to the quantity  $u_{\text{difference}}$  in equation 5. Using trigonometric identities to find BE and DE and summing these segments to find DB:

$$\text{BuoyVelocityDifference} = u_{\text{difference}} = \Delta u_E \cos \phi + \alpha u_s \cos \lambda. \quad (24)$$

We will first demonstrate that  $u_{\text{difference}}$  is a function of the parameters  $\alpha$ ,  $\beta$ ,  $\gamma$ , and  $\theta_0$ , and then discover the statistically optimal values of these parameters in that order. By



examination, equations 15, 22 and 23 determine the first term  $\Delta u_E$  to be a function of  $f$ ,  $\alpha$ ,  $\beta$  and  $\gamma$  (or  $\xi$ ). When calculating values for  $\Delta u_E$ ,  $u_w$  and  $f$  are determined by the data and values for  $C_D$ ,  $\rho_\alpha$ , and  $\rho_w$  are selected from published values. The coefficients  $\alpha$ ,  $\beta$  and  $\gamma$  are unknown and must be determined from the SVP and SVPL or Navy buoy drift data. The factor  $\cos\phi$  must be calculated; using trigonometric identities, an expression for the unknown  $\phi$  can be derived from equation 21.  $\zeta$  is proportional to  $\gamma$  by definition, making  $\phi$  a function of  $\theta_0$  and  $\gamma$ . The velocity difference angle,  $\lambda$ , is implicitly determined by equation 20 if the angles  $\phi$ ,  $\zeta$ , and  $\theta$  are known. Since  $\theta$  is a function of  $\gamma$ ,  $\theta_0$  and observables, the assertion that  $u_{\text{difference}}$  is a function of  $\alpha$ ,  $\beta$ ,  $\theta_0$  and  $\gamma$  alone is demonstrated. Determining the values of these parameters which minimize the model error,

$$\chi^2 = \sum (u_{\text{difference}} - \Delta u_E \cos\phi - u_w \cos\lambda)^2, \quad (25)$$

is the object of our analysis. We used the same selected, binned, mean dataset for the analysis as was used in Section 4.

### 5.2 Model Parameter Results

The Ekman current vectors of SVP buoys in three typical ocean conditions are shown in the left panel of Figure 9. The model equations, depending as they do on solutions of equations containing transcendentals, so the model solution for  $u_{\text{difference}}$  was determined by implicitly solving equation 24 for optimal values of  $\alpha$ ,  $\beta$ ,  $\theta_0$  and  $\gamma$ , using the selected datapoints shown in Figure 5 and discussed in Section 4.2. The minimum variance of the difference between the modelled values of  $u_{\text{difference}}$  and the observed values of  $u_{\text{difference}}$ ,  $\chi^2$ , was mapped against the unknowns. Since equation 23 suggests that the parameter  $\xi$

encapsulates the functionality of the terms  $\gamma$  and  $\beta$ ,  $\chi^2$  is mapped against  $\alpha$  and  $\xi$  in Figure 10. In this figure no single minimum of  $\chi^2$  appears; instead a minimum of values of  $\chi^2$  are found along an approximate straight line:

$$\xi = 0.0072 - 0.33\alpha, \quad (26)$$

drawn by inspection. The variation of  $\chi^2$  is so small along the axis of this "valley" all  $\alpha, \xi$  pairs which satisfy this equation are nearly degenerate solutions. The near degeneracy makes it difficult to independently solve for a unique pair of  $\alpha, \xi$ , but for values of  $\chi^2 < 370$ ,  $\alpha$  ranges between 3 and 6. Ralph and Niiler (1998) found that  $\beta = 0.065$  ( $\text{sec}^{-1/2}$ ) and estimated  $\gamma = 1.2$ ; a line is drawn for the corresponding value of  $\xi$ , 0.00507, for  $\alpha$  between 3 and 6. Restricting  $\xi$  to the "valley" between the lines  $\xi_1 = 0.0067 - 0.33 \cdot \alpha$  and  $\xi_2 = 0.0077 - 0.33 \cdot \alpha$ ,  $\chi^2$  is mapped against  $\beta$  and  $\gamma$  in Figure 11. The corresponding result of Ralph and Niiler (1998) is marked by a cross in Figure 11. Isoleths of  $\xi$  are shown as dashed lines; the corresponding  $\alpha$ , according to equation 27, is also annotated on the bottom end of the dashed lines. There is little model error variance dependence upon  $\beta$  and  $\gamma$  within the  $\chi^2 < 400$  contour, but the absolute minimum,  $\chi^2 < 370$ , lies in the range  $0.070 < \beta < 0.075$ , and  $\gamma = 1.1$ . Restricting  $\xi_1 < \xi < \xi_2$  as before,  $\chi^2$  is mapped against  $\xi$  and  $\theta_0$  in Figure 12. The variation of  $\chi^2$  is so small for values of  $\theta_0 > 30^\circ$  that all such  $\theta_0$  to the physically reasonable limit of  $90^\circ$  appear to be degenerate solutions. In summary, the  $\alpha, \beta$  and  $\gamma$  which are possible values for the velocity difference model are constrained by equation 29 and  $3 < \alpha < 6$ ,  $0.070 < \beta < 0.075$ ,  $\gamma = 1.1$ , and  $30^\circ < \theta_0 < 90^\circ$ . For these values, equation 25 explains 35% of the variance in observed  $u_{\text{difference}}$ . Ralph and Niiler (1998)

found that equation 15 explained 49% of the variance of  $u_{1,5}$ ; given that we are attempting to explain the variance of the difference of two velocities,  $u_{\text{difference}}$ , not the variance of a single velocity,  $u_{1,5}$ , the lesser amount of variance explained is expected.

*Acknowledgements.* This work has been supported by the Naval Research Laboratory, contract N00014-95-C-6002. We wish to thank Harry Selsor, the COTR for this contract, deserves thanks for his constant encouragement and help. Thanks to Harley Hurlburt, Charlie Barron Joseph Metzger, Steve Piacsek and Alex Warn-Varnas for informative discussions. Thanks to Andre Bolduc (MEDS), Dennis Laws (FNMOC), and Roy Lowry (Bidston UK) for their help with data issues. Thanks to Andy Sybrandy, Elise Ralph, Sharon Lukas and Judy Gauke of SIO for their help with the SVP dataset.

#### REFERENCES

- Caldwell, D., C.W. Van Atta, and K. Holland, A laboratory study of the turbulent Ekman boundary layer, *Geophys. Fluid Dyn.*, **3**, 123-160, 1972.
- Chereskin, T., 1995, Direct evidence for an Ekman balance in the California Current, *J. Geophys. Res.*, **100**, 18261-18269.
- Davis, R.E., Drifter observations of coastal surface currents during CODE: The statistical and dynamical views, *J. Geophys. Res.*, **90**, 4756-4772, 1985.
- Ekman, V.W., On the influence of the Earth's rotation on ocean-currents, *Ark. Mat. Ast. Fys.*, **2**, 1-52, 1905.
- Luther, D., A. Chave, J. Filloux, and P. Spain, Evidence for local and non-local barotropic responses to atmospheric forcing during BEMPEX, *Geophys. Res. Letts.*, **17**, 949-952, 1990.

- McPhee, M.G., 1995. On the turbulent mixing length in the ocean boundary layer, *J. Phys. Ocean.*, **24**, 2014-2031.
- Niiler, P.P., and E.B. Kraus. *One-dimensional models of the upper ocean. In: Modelling and Prediction of the Upper Layers of the Ocean*, edited by E.B. Kraus. Pergamon Press, 1977, pp. 143-172.
- Niiler, P.P., R.E. Davis, and H.J. White, 1987. Water-following characteristics of a mixed-layer drifter. *Deep-Sea Research*, **34**, 1867-1881.
- Niiler, P.P., J.D. Paduan, A.L. Sybrandy and L. Sombardier, 1991. *The WOCE/TOGA Lagrangian surface drifter*. Proceedings of Oceans 91, Hawaii, October 91, 839-843.
- Niiler, P.P., J. Filloux, W. Liu, R.M. Samuelson, 1993. Wind forced variability of the deep eastern North Pacific: Observations of sea floor pressure and abyssal currents. *J. Geophys. Res.*, **98**, 22589-22602.
- Niiler, P.P., A.L. Sybrandy, K. Bi, P. Poulain, and D. Bitterman, 1995. Measurements of the water-following capability of holey-sock and TRISTAR drifters. *Deep-Sea Research*, **42**, No. 11/12: 1951-1964.
- Pazan, S.E. and P.P. Niiler, 1998. *Final report on Comparison of Drogued and Undrogued Drift Buoys*, Naval Research Laboratory, Code 7406, Stennis Space Center, MS 39529-5004. 51 pp.
- Pedlosky, J., *Geophysical Fluid Dynamics*. New York:Springer-Verlag, 1982. 623 pp.
- Poulain, P.-M. and D.V. Hansen, 1996. Quality control and interpolation of WOCE/TOGA drifter data. *J. Atm.Oc.Tech.* **13**, 900-909.
- Poulain, P.-M., A. Warn-Varnas, and P.P. Niiler, 1996. Near-surface circulation of the Nordic seas as measured by Lagrangian drifters. *JGR*, **101**, No. C8: 18,237-18,259.

Ralph, E.A., and P.P. Niiler, Wind driven currents in the tropical Pacific, *J. Phys. Ocean.*,  
in press, 1998.

Selsor, H.D., 1993. Data from the sea: Navy drift buoy program. *Sea Technology*.  
December, 1993, 53-58.

Sybrandy, Andrew L. and Pearn P. Niiler, 1991. *The WOCE/TOGA SVP Lagrangian  
drifter construction manual*. La Jolla, Calif. : University of California, San  
Diego, Scripps Institution of Oceanography, Scripps Institution of Oceanography  
reference; 91-6, 58 p.

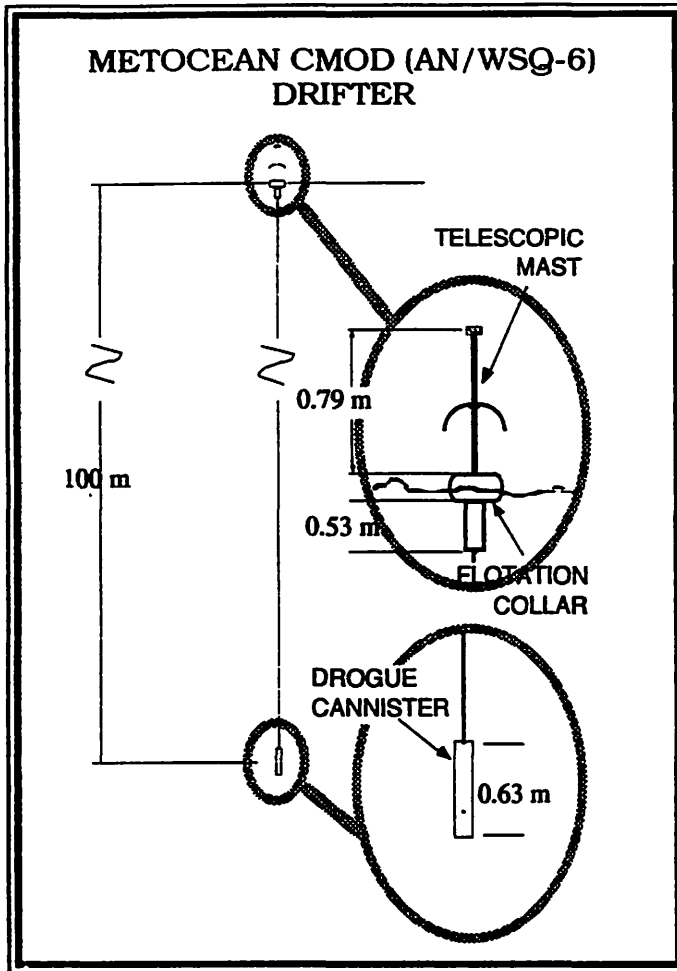


Figure 1 (right) AN/WSQ-6 drifter buoy design; this schematic is after ARGOS 61532, deployed February 9, 1992. Its manufacturer's designation is CMOD I, a multi-parameter, satellite reporting mini buoy series for Tactical Oceanographic Warfare Support. (from METOCEAN Ltd.) CMOD II is much the same except for a larger flotation collar.

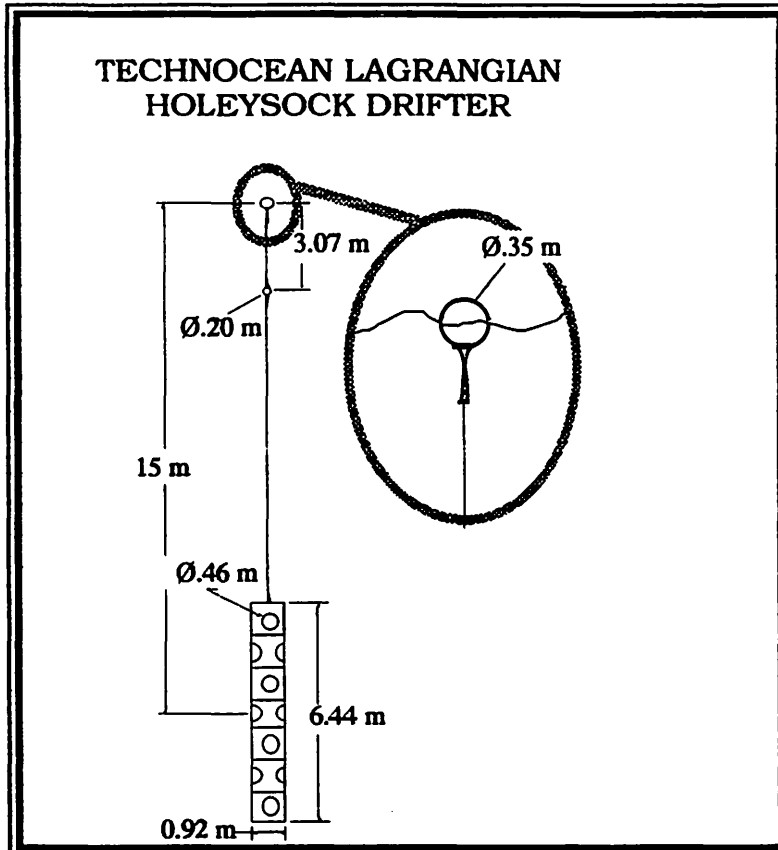


Figure 1 (left) SVP Technocean Holesock drifter buoy design; this is after ARGOS buoy 1425, deployed January 12, 1994. Note the enormous size of the drogue relative to that of the Metocean AN/WSQ-6 (CMOD). It has a subsurface float and Urethane carrots at all float-tether connections mediating the stress on the tether. The exploded 4x view of the surface float is included in order to enable a better intercomparison with other buoy schematics.

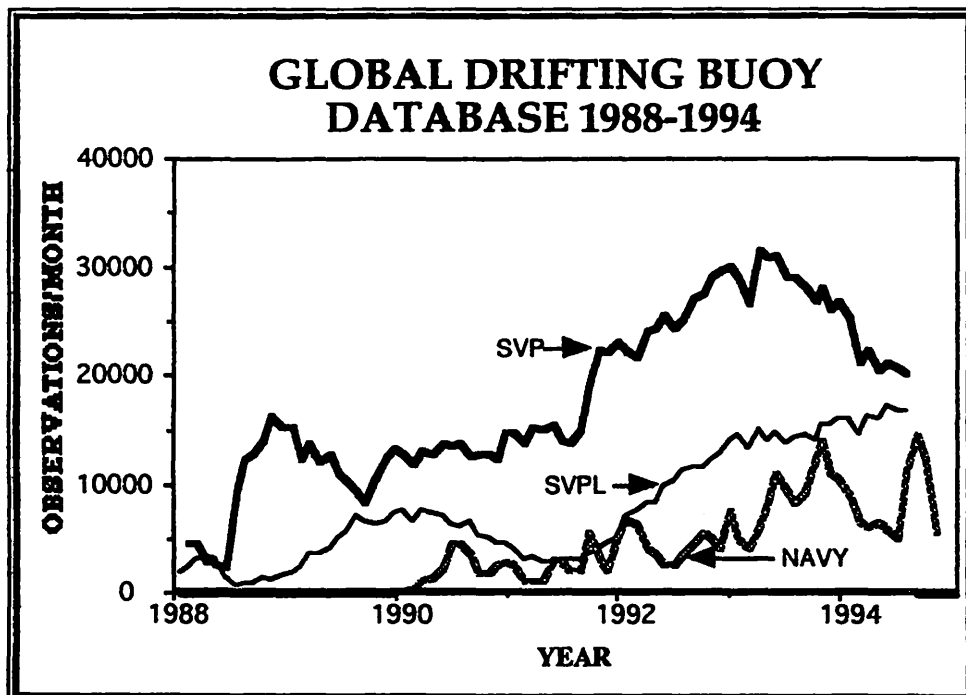


Figure 2. Global monthly summary of the number of drifting buoy observations per month in the Ocean Prospects data archive. The SVP and SVPL datasets are comprised of Lagrangian drifters deployed by the WOCE/TOGA scientific programs. Observations from a Lagrangian drifter are counted among the SVPL (undrogued) drifters after an on-board sensor indicates the buoy's drogue has been lost. The Navy dataset is comprised of AN/WSQ-6 drifters.



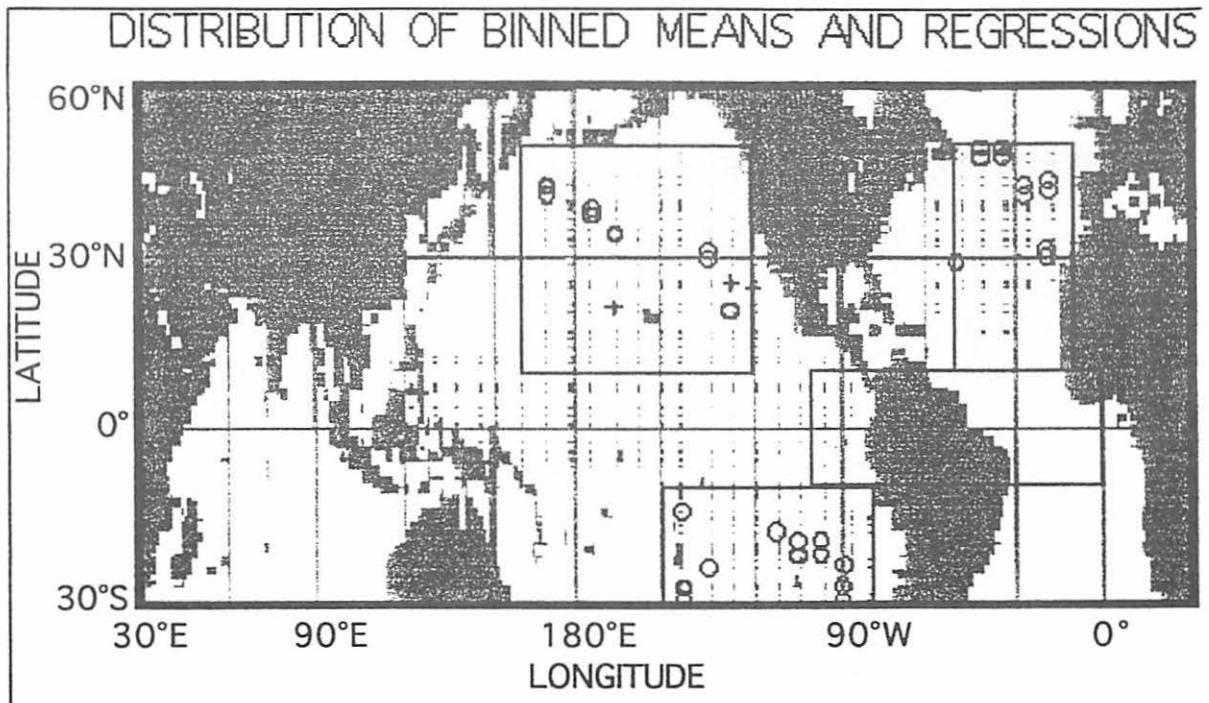


Figure 3. Distribution of binned means and regressions where both SVPL or Navy buoy data and SVP buoy velocity data exist in a single 2° latitude by 8° longitude bin; selected bins are black circles (SVP/SVPL) and crosses (SVP/NAVY).

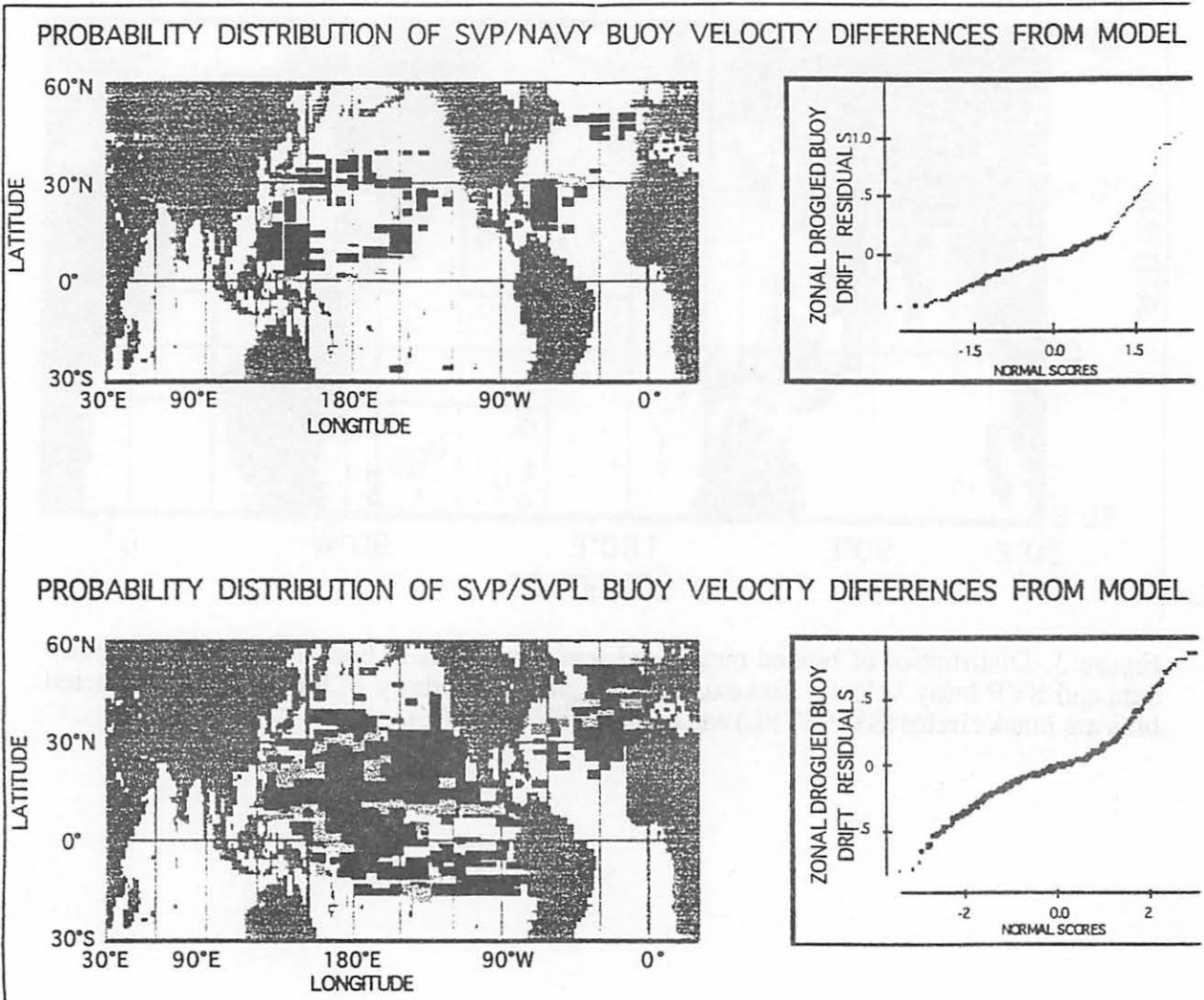


Figure 4. (RIGHT) The graph of residuals vs. the normal score statistic is a straight line if the assumption that the distribution of residuals from the regression are normal is true. (LEFT) Spatial distribution of 2° latitude by 8° longitude by 1 month summaries used in the regression analysis. Light shades denote regions where an anomalous relationship holds between wind and zonal SVP buoy drifter velocity.

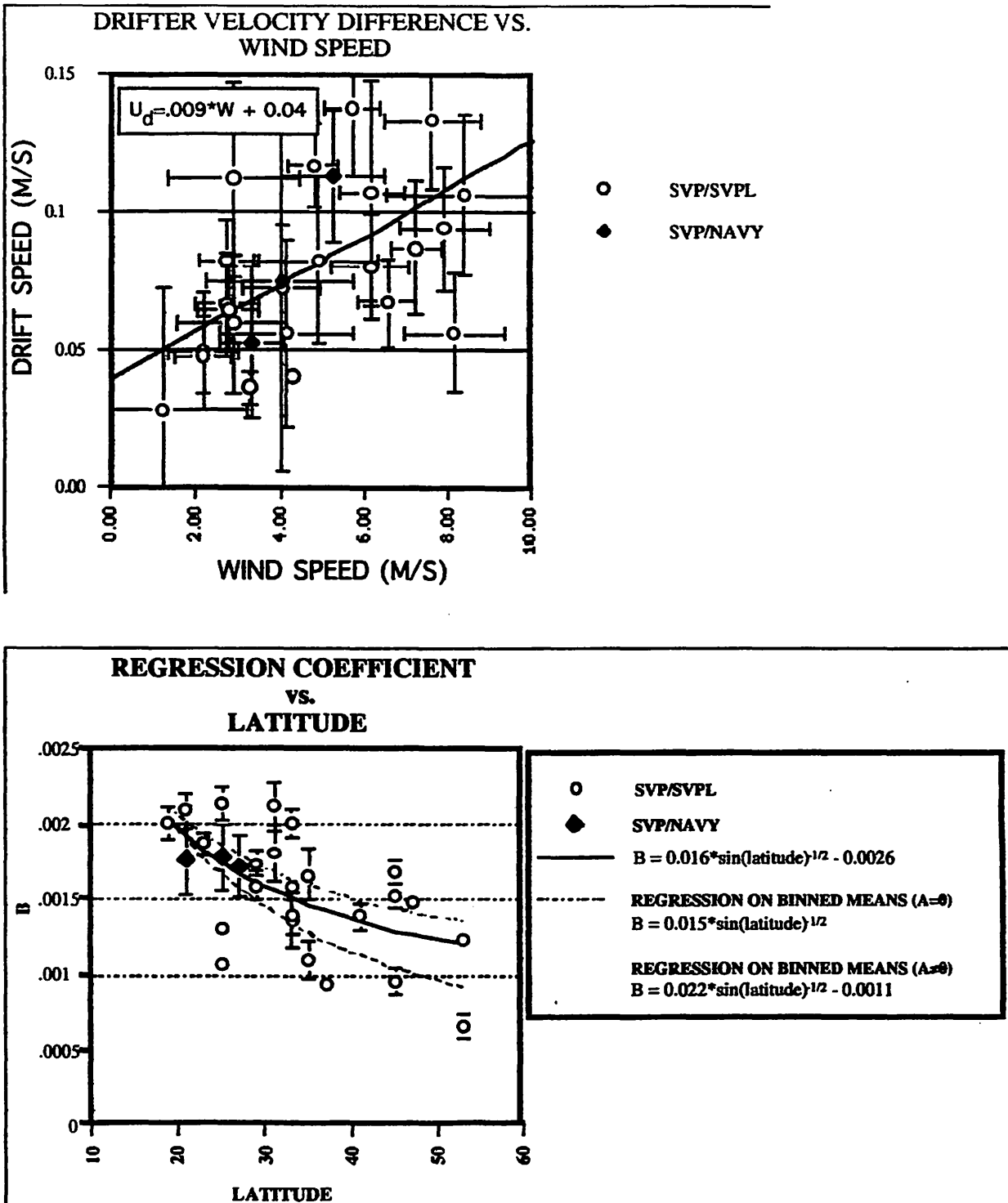


Figure 5 (TOP) SVP/SVPL (circle) and SVP/NAVY (diamond) buoy drifter velocity difference on wind; error bars are 95% confidence limits. (BOTTOM) SVP/SVPL (circle) and SVP/NAVY (diamond) regression coefficients of vector buoy drifter velocity difference on vector wind vs. latitude; error bars are 95% confidence limits. The model assumes an inverse square-root dependence upon the Coriolis parameter.

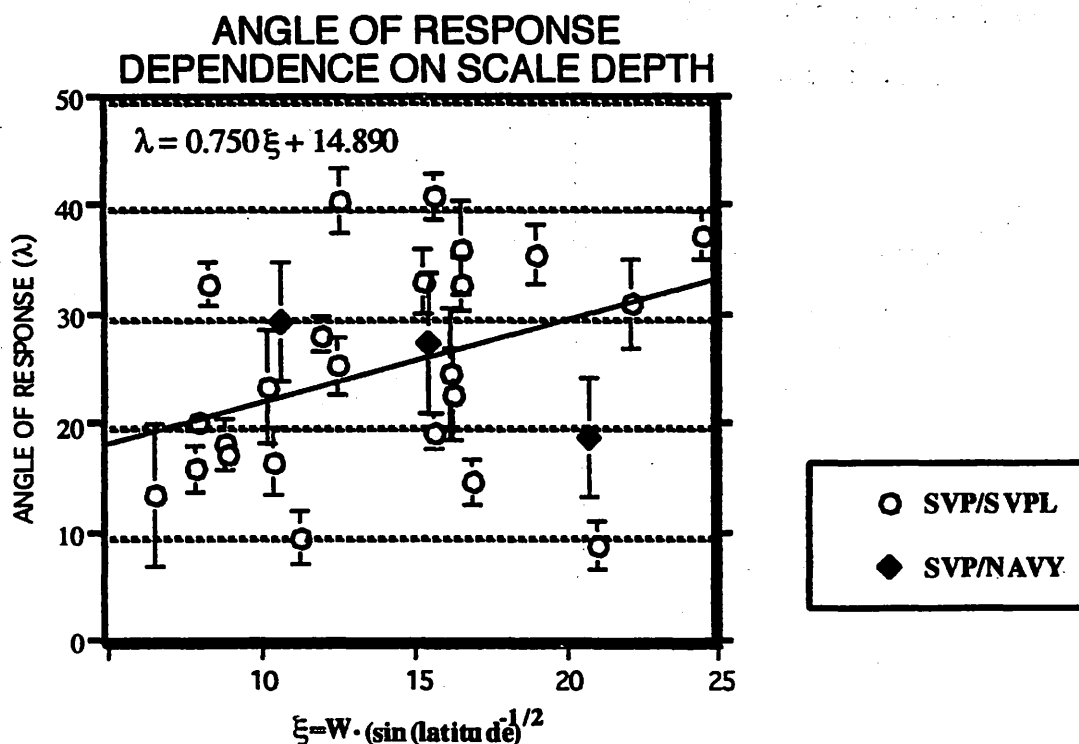
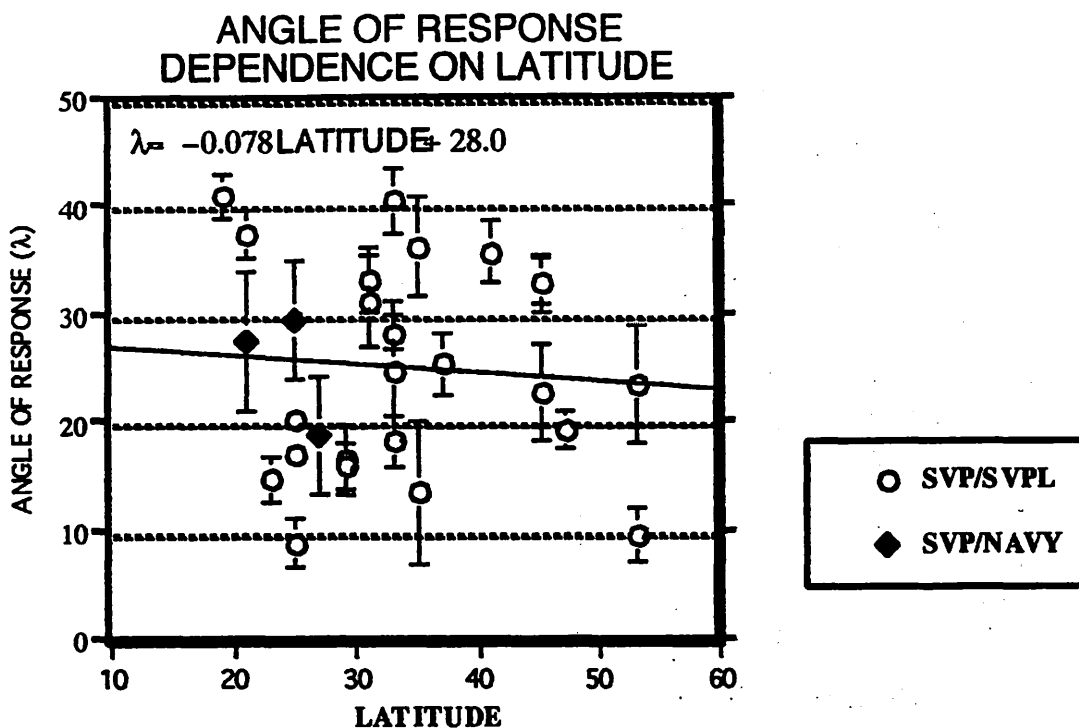


Figure 6. SVP/SVPL (circle) and SVP/NAVY (diamond) angle of response of vector buoy drifter velocity difference to vector wind vs. latitude; error bars are 95% confidence limits. The angle is left (right) of the wind in the northern (southern) hemisphere. There is no significant trend of  $\lambda$  vs. latitude (top), but there is a significant trend of  $\lambda$  vs. the scale depth  $\xi$  (bottom) with 98% confidence.

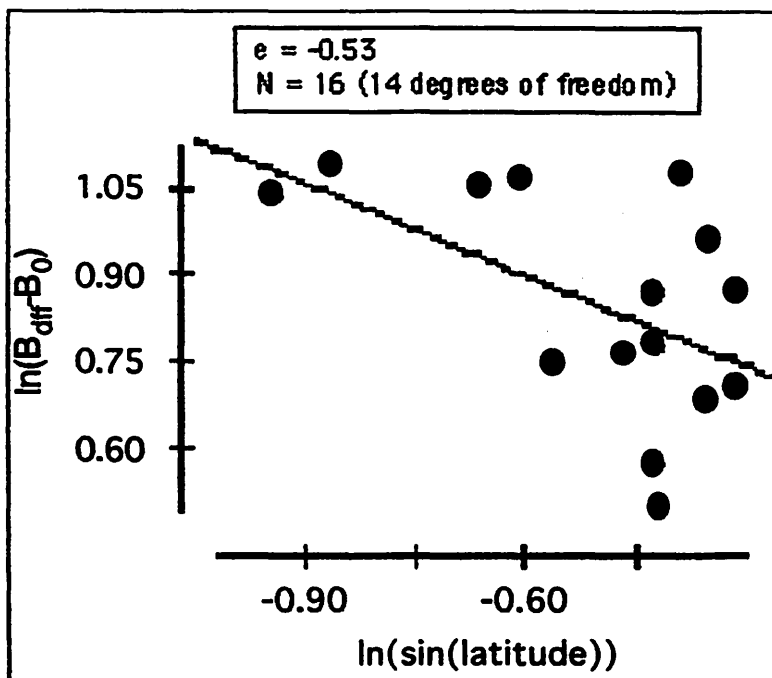


Figure 7. Given observed regression coefficients,  $B$ , of difference velocity on wind at different latitudes, the least-squares solution for the exponent of  $\sin(\text{latitude})$  is  $-0.53$ , supporting the choice of an exponent of  $-1/2$  in the difference velocity model.

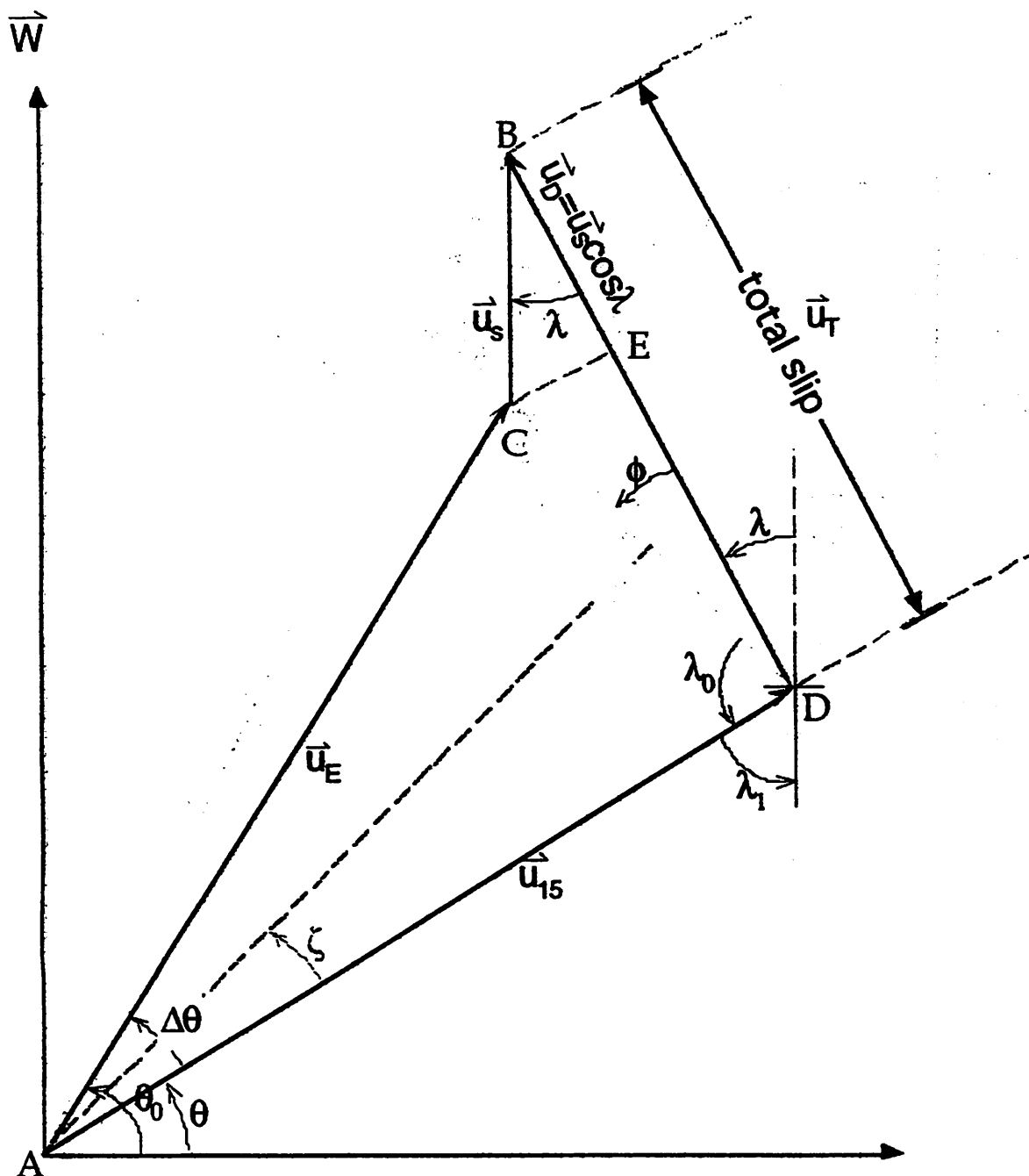


Figure 8. SVPL (undrogued) buoy drift,  $u_e$ , and SVP (drogued) buoy drift at 15 m. depth,  $u_{15}$ , relative to the wind vector,  $W$ . The buoy drift difference vector,  $u_D$ , is the vector difference  $u_{15} - u_e$ . The SVPL drift vector is the vector sum of the Ekman drift,  $u_s$ , and the leeway drift,  $u_l$ .  $\lambda$  is the difference velocity drift response angle with respect to the wind.

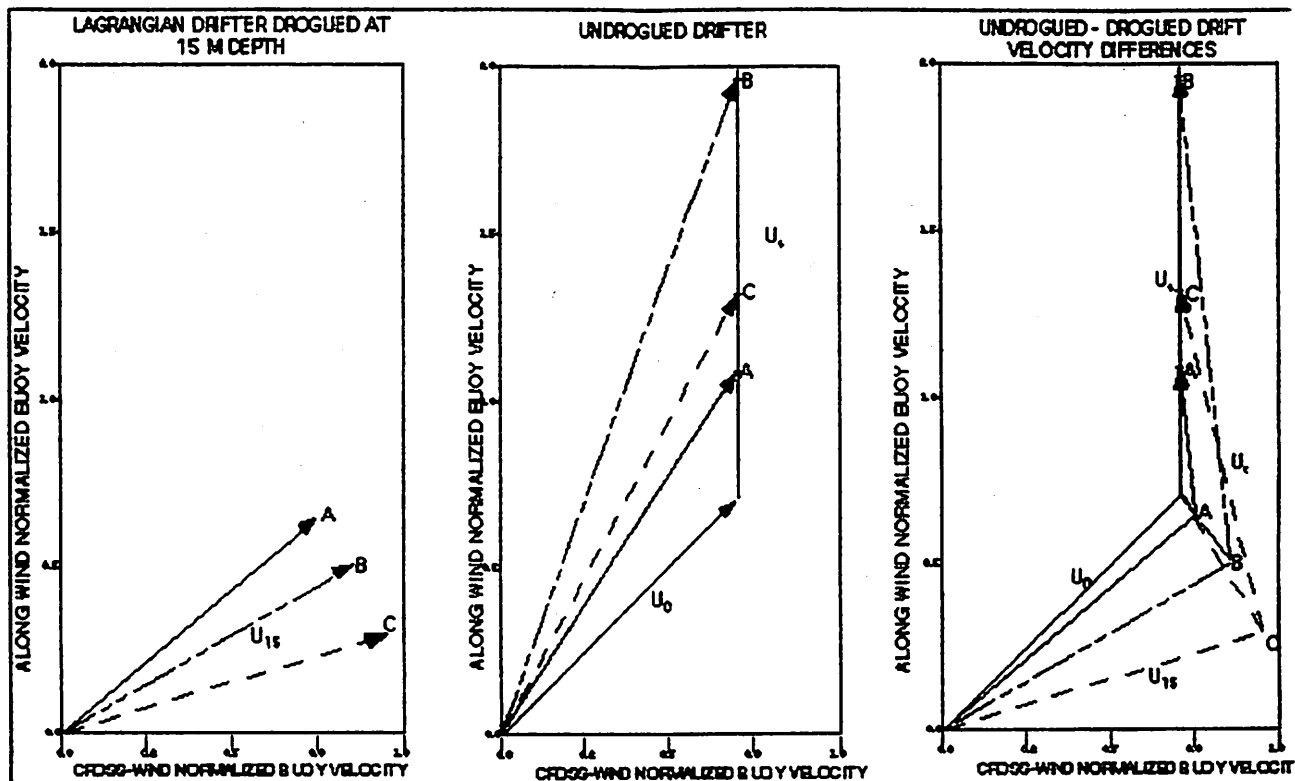


Figure 9. Buoy drift normalized by the Ekman velocity scale in three extreme upper ocean states representing the range of validity of the model: A. Ekman depth of 100m, strong winds very close to the equator; B. Ekman depth of 30 m, strong winds at high latitudes; C. Ekman depth of 15 m, weak winds in the tropics. (LEFT) normalized Ekman velocity,  $u_{15}$ , displaying the range of rotations with respect to the wind; (MIDDLE) the SVPL buoy velocity is a summation of surface layer Ekman velocity,  $u_0$ , and along wind leeway drift,  $u_1$ ; (RIGHT) total difference,  $u_2$ , between SVPL (undrogued) and SVP (drogued) buoy drift.

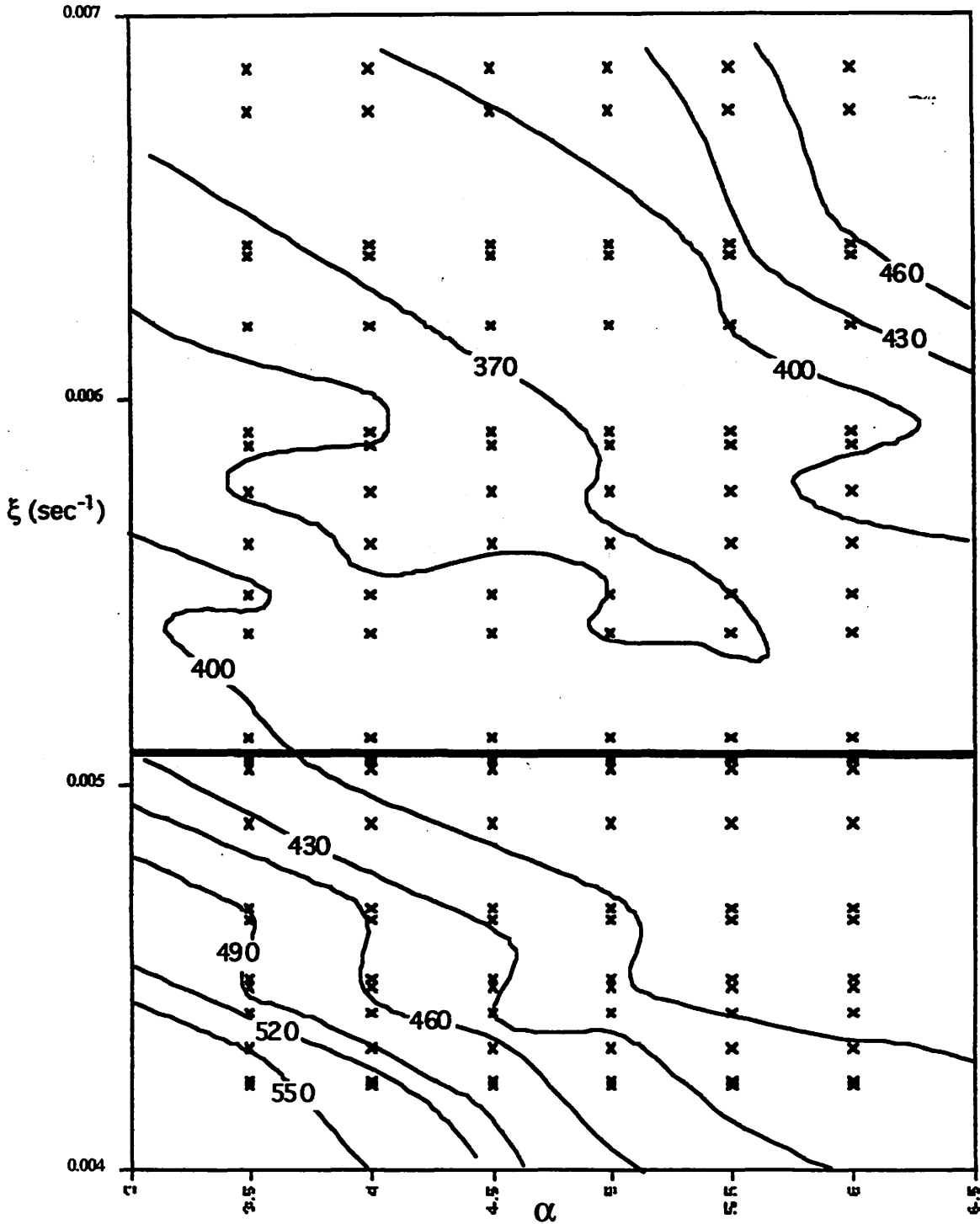


Figure 10. Error variance as a function of model parameters. The straight dashed line,  $\xi = 0.0072 - 0.32\alpha$ , follows the minimum in the model error variance. The parameter  $\xi$  is defined as the product of the model parameters,  $\gamma\beta^2$ . The horizontal line in the lower left is the range of  $\xi$ ,  $\alpha$  from Ralph & Niiler, 1998.



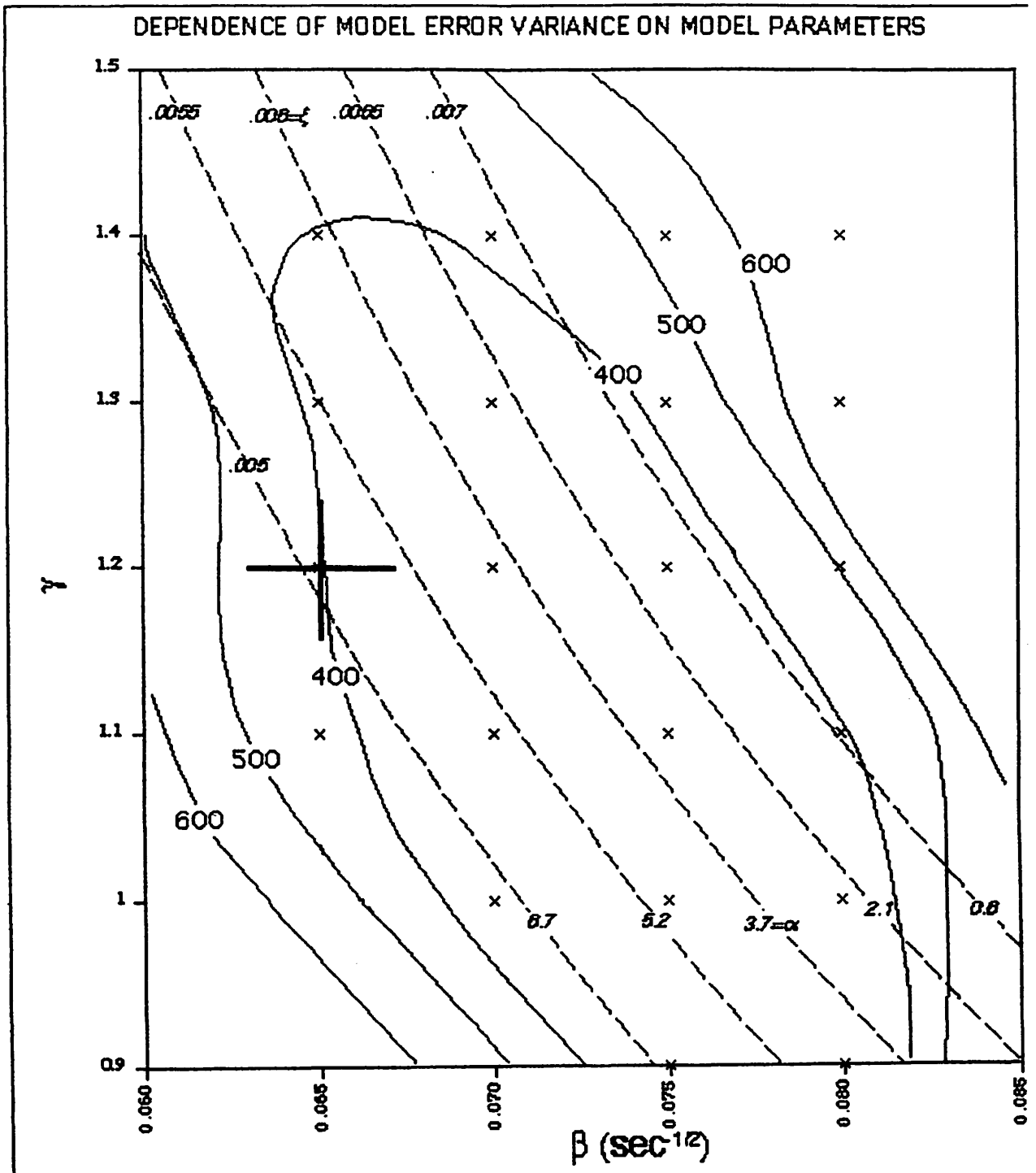


Figure 11. Model error variance,  $\chi^2$ , near the dashed line in Figure 10; isopleths of  $\xi$  are shown as dashed lines here. Derived values of  $\alpha$  are assigned to each isopleth (see text). The cross (+) is located at a reported value of  $\beta$  and  $\gamma$  (Ralph & Niiler, 1998). There is little model error variance dependence upon  $\beta$  and  $\gamma$  for  $\chi^2 < 400$ .

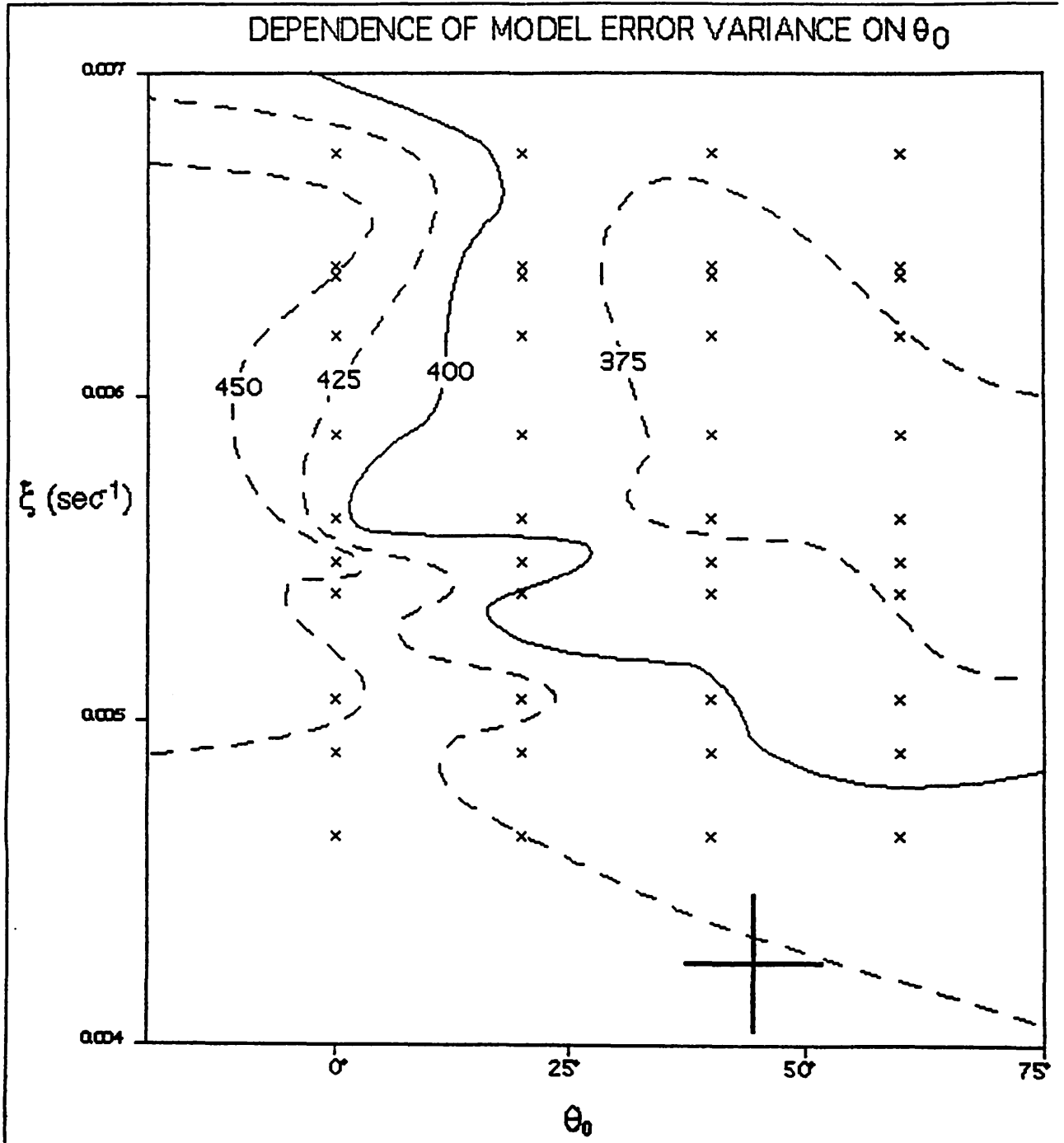


Figure 12. Model error variance as a function of  $\theta_0$  and  $\xi$  near the optimal values of  $\alpha$ ,  $\beta$  and  $\gamma$ . Gradients in model error variance is small but there is a slight tendency towards larger  $\theta_0$ .

Table 1. Drag area ratio of the AN/WSQ-6 (CMOD-II variant) (from data supplied by METOCLEAN Data Systems) and drag area ratio of the TOGA/WOCE SVP Lagrangian Drifter (from Niiler et al., 1991). Earlier models of the AN/WSQ-6 buoy had a smaller float collar, frontal area, and therefore larger drag ratio.						
BUOY TYPE	Drag Components	Length (cm)	Diameter (cm)	Frontal Area (cm <sup>2</sup> )	Drag Coefficient	Drag Area (cm <sup>2</sup> )
AN/WSQ-6	Hull	60.6	10.2	618	0.471	290
	Floatation Collar	19	35.5	674	0.47	317
	VEXAR H-30 fish netting	UNKNOWN				
	Tether	400	0.5	200	1.4	280
	Total Tether Drag Area					>887
	Drogue	91.45	12.4	1134	0.4-1.0	<1134
	Ratio of Drogue Drag Area to Tether Drag Area					<1.28
SVP	Drag area ratio of the TOGA/WOCE SVP Lagrangian Drifter (from Niiler et al., 1991)					
	Surface Float	n/a	34.29	923.5	0.47	434
	Subsurface Float	n/a	20.32	324.3	0.47	152.4
	Urethane below Surface Float	40	n/a	220.3	1	220.3
	Urethane above Subsurface Float	25	n/a	220.3	1	220.3
	Urethane below Subsurface Float	40	3.81	152.4	1	152.4
	Small Hydraulic Hose	163.6	1.49	243.8	1.4	341.3
	Tether	856.06	0.56	475.6	1.4	665.9
	Total Tether Drag Area					2186.6
	Drogue Section:					
	Urethane above Drogue	40	4/-4	161/5	1	161.5
Drogue	644	92	59248	1.4	82947.2	
Total Drogue Drag Area					83108.7	
Ratio of Drogue Area to Tether Drag Area					38	



**Development of a Drifting Buoy Metadata File at the Global Drifter Center**

John Stadler

Atlantic Oceanographic and Meteorological Laboratory (OAR/NOAA)

U.S.A.

**ABSTRACT ONLY SUBMITTED**

The Global Drifter Center at the Atlantic Oceanographic and Meteorological Laboratory maintains a database on drifting buoys deployed worldwide. The metadata component of this database includes technical specifications, program information, deployment information and shipping history, for more than 5200 drifting buoys. Historically, this metadata included drifting buoys of many different designs, and maintenance of the information was inconsistent. During the past year, a concerted effort has been made to update the metadata and fill in gaps in the data. Several significant changes have been made in the way in which the metadata is maintained: 1) the metadata was redesigned to take advantage of the relational capabilities of the software being used, resulting in a more compact database; 2) a unique identification number was created for each drifter; 3) criteria were established for inclusion of new drifters into the metadata; and 4) a standardized specification sheet, to be filled out by the manufacturer, was developed to provide a complete technical description of each new drifter. The goal of this presentation is to provide an overview of the structure of the metadata and the types of data that it contains.



## Preliminary analysis of Argos 2 on NOAA K performances

M. Taillade  
CLS / Service Argos

taillade@cls.cnes.fr

### 1. Space segment status and performance

#### 1.1. Status

Figure 1 shows the status of the Argos space segment:

- before May 1998, data were processed in global and regional mode from three satellites (NOAA 14 and 12 operational, NOAA 11 as backup third satellite), data from NOAA 10 being received from local user terminals (LUTs) only;
- between May and December 1st 1998, data were processed in global and regional mode from four satellites (NOAA 15 under test, NOAA 14 and 12 operational, NOAA 11 as backup third satellite), data from NOAA 10 being received from LUTs only;
- from December 1st 1998, data will again be processed in global and regional mode from three satellites (NOAA 15 and 14 operational, NOAA 12 as backup third satellite), data from NOAA 10 and 11 being received from LUTs only.

Satellite status	Before May 98		After December 1st 98
Under Test		15 NOAA K	
Operational	14 - NOAA J 12 - NOAA D	14 - NOAA J 12 - NOAA D	15 NOAA K 14 - NOAA J
Back up Third satellite	11 - NOAA H 10 - NOAA G	11 - NOAA H 10 - NOAA G	12 - NOAA D 11 - NOAA H 10 - NOAA G
Decommissioned	9 - NOAA F	9 - NOAA F	9 - NOAA F

figure 1: Argos space segment status

## 1.2. Data collection performance

Performance in terms of passes per day and with respect to latitude for two-, three- and four-satellite service is shown in figure 2 below.

### **Number of Satellite passes per day**

Latitude of the transmitter in degrees satellites	Mean number of passes per 24 hours		
	with 2 satellites	with 3 satellites	with 4
0	7	10	14
± 15	8	12	16
± 30	9	13	18
± 45	11	16	22
± 55	16	24	32
± 65	22	33	44
± 75	28	42	56
± 90	28	42	56

The number of satellite passes depends on the latitude of the transmitter

figure 3: Data collection performances

## 1.3. Data collection processing performance

Figure 3 shows the total messages received by each satellite from each orbitography beacon during August 1998. Results vary by a few per cent from one satellite to another.

This confirms that whatever the mode—under test, operational or backup—the four satellites offer similar data collection processing performance.



Nb of messages per month PTT ID								
	15 K	12 D	11 H	14 J	15 K	12 D	11 H	14 J
117	2979	2952	2976	3051	1%		1%	3%
110	3800	3788	3884	3980	0%		3%	5%
119	5278	5274	5423	5721	0%		3%	8%
111	3474	3488	3596	3459	0%		3%	-1%
108	5699	5765	5789	5929	-1%		0%	3%
1	3397	3450	3484	3563	-2%		1%	3%
118	3766	3874	3760	4252	-3%		-3%	10%
109	2788	2899	2693	3108	-4%		-7%	7%
149	2719	2838	2644	2934	-4%		-7%	3%
112	3961	4137	3961	4250	-4%		-4%	3%
<b>Total</b>	<b>37861</b>	<b>38465</b>	<b>38210</b>	<b>40247</b>	<b>-2%</b>		<b>-1%</b>	<b>5%</b>

figure 4: Data collection processing performances for orbitography platforms

## 2. Second-generation Argos instrument

NOAA K was launched in May 1998 carrying Argos 2, the first second-generation Argos instrument.

The main enhancements to this new instrument are:

- more receiving channels (increased from four to eight);
- wider receiver bandwidth (increased from 24 kHz to 80 kHz – see figure 4);
- greater receiver sensitivity (increased by 2 dB).

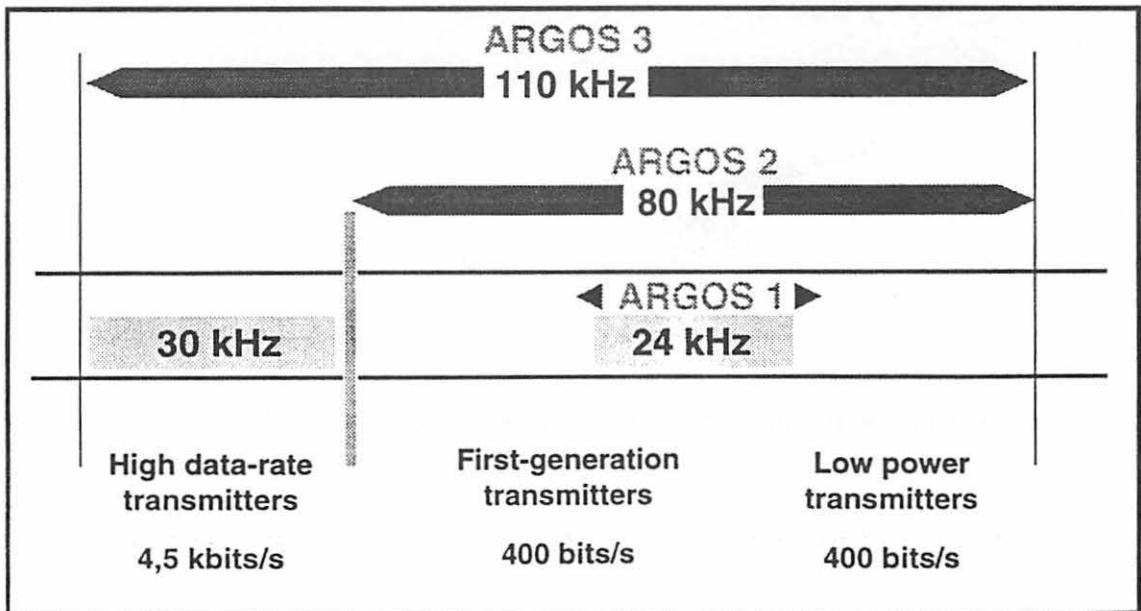


figure 4: Argos 1, Argos 2 and Argos 3 receiver bandwidth comparison

These enhancements have brought two main improvements for users over the Argos 1 instrument:

- a) more transmitters (PTTs) are within view of a satellite at any one time (factor-of-three-to-four increase);
- b) messages are more easily received from low-power PTTs, and more messages can be received from a single PTT.

### 3. Increased receiving capacity

#### 3.1. Current situation

Figure 5 shows the Argos 2 frequency band occupation during the satellites' 101-minute orbit period (each point on the graph represents a received message).

All messages are within the Argos 1 band, i.e., 12 kHz either side of 401.650 MHz.

We should note:

- That the group of PTTs belonging to the Brazilian program is operating in the Argos 2 band with the Brazilian SCD1 satellite and Argos 2. These two space systems are compatible.
- The curve of messages received by test PTT N° 1 in Toulouse, France (see paragraph ...).

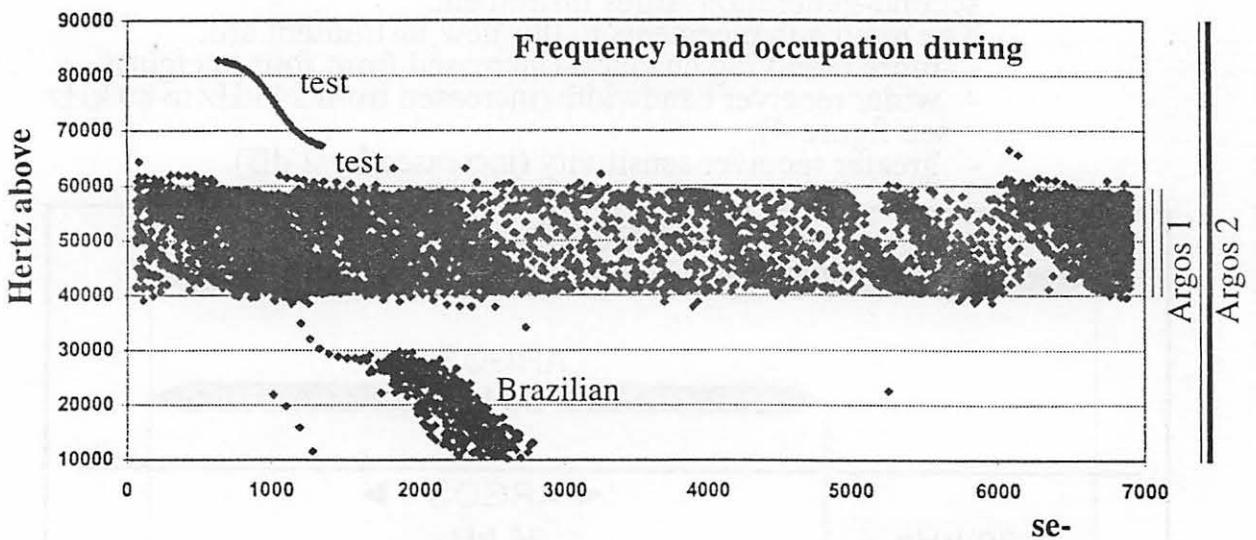


figure 5: Current frequency band occupation during an Argos 2 orbit

### 3.2. Capacity verification

Figure 6 shows occupation in the Argos 2 band for a satellite pass within view from Toulouse (lasting about 800 seconds) with a number of PTTs simulating Argos 2's maximum expected capacity.

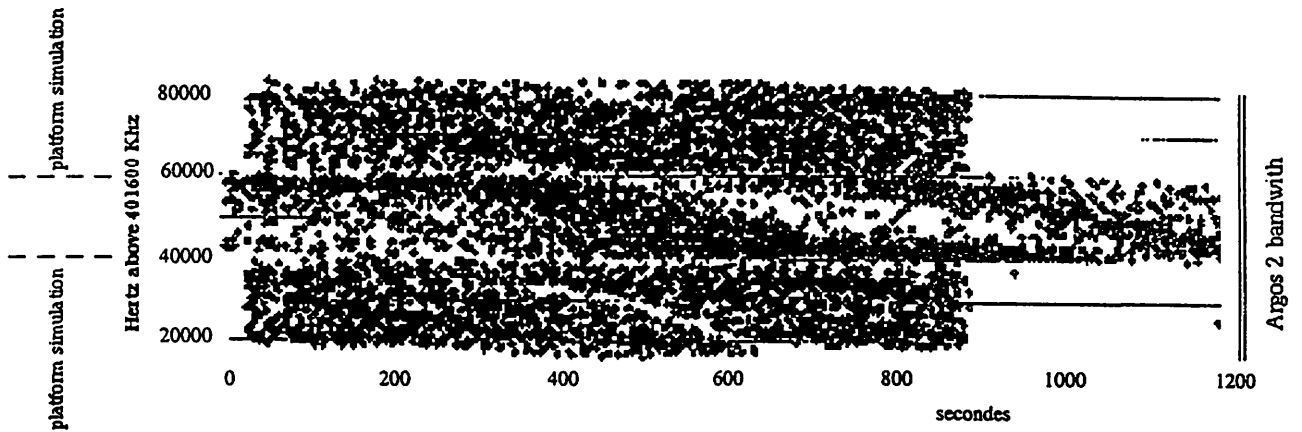


figure6: Simulation of Argos 2 maximum occupation in visibility of Toulouse

This simulation is based on a transmitter and a processor that generates a set of virtual PTTs that behave like real PTTs during a satellite pass.

Analysis focused on the number of messages transmitted by the simulator and received by the location system (satellite and processing).

This analysis showed that Argos 2 technical operating specifications were satisfied under maximum load.

### 3.3. Strategy for widening range of PTT frequencies in the Argos 2 band

#### 3.4. Test

Two Argos transmitters were activated during NOAA K passes. The transmitters could send the same number of messages simultaneously—one operating in the Argos 1 frequency band, the other in the Argos 2 band—using the same power and repetition period. Message content was identical in each case.

Transm. power	Power dBm	Transmitter 1 Received msg nb.	Transmitter 2 Received msg nb.	Messages nb. difference
2 watts	33	90	99	10%
	31	94	104	11%
1 watt	30	115	132	15%
500 mW	27	59	110	86%
500 mW	27	119	182	53%
	26	274	414	51%

Inside Argos 1      Outside  
 Bandwith            Argos 1  
                                  Bandwith

table 7: Transmission tests during NOAA K passes

Table 7 (transmission tests during NOAA K passes) shows the number of messages received from each transmitter, with signal powers varying from 500 milliwatts to two watts.

The last column shows the difference, in per cent, in number of messages received.

These results demonstrate that low-power PTTs work better transmitting in a clear frequency band (here Argos 2) than when they share the same band with many other, more powerful PTTs all operating at the same frequency (401.650 MHz).

#### 3.5. Approach

These results support the approach decided by the Argos Operations Committee in Anchorage in July 1998:

“The Argos Operations Committee, recognizing the need to optimize the use of the frequency bandwidth currently allocated to the Argos System (401.650 MHz +/- 12 kHz) resolves:

- that the central frequency to be used by future Argos Data Collection Platforms be 401.650 MHz, 401.648 MHz and 401.652 MHz. All three frequencies being equally used,
- that CLS shall take the necessary measures for manufacturers to develop corresponding Argos DCPs,
- that CLS should undertake the necessary studies to further optimize the utilization of the band allocated to the Argos System.”

## 4. Argos 1/ Argos 2 comparative sensitivity analysis

### 4.1. Principle

To analyze sensitivity, we need to compare PTT performance when transmitting to satellites flying Argos 2 and Argos 1 instruments.

Unfortunately, a PTT is never in the same position relative to the satellite during each successive pass, so signal attenuation is well above the difference in sensitivity (2 dB) normally observed between the two instruments under laboratory conditions.

To eliminate propagation errors and thus be able to analyze the performance of each satellite when receiving from the same PTT, we compiled a list of parameters for each PTT active over a one-month period (see table 8 - some of these parameters will serve to refine our analysis later).

<b>List of parameters for each platform</b>	
<b>Platform data</b>	Platform ID number Programm ID number Program name Type of processing (loc123, loc 1230, .....,data collection.) Type of Service (Standard, Limited, Back up) Repetition period Type of platform (marine, terrestrial animal, bird, buoy ...) Platform latitude Platform longitude
<b>General data collection performances</b>	Monthly total number of day with data collection for all satellites Monthly total number of passes with data collection for all satellites
<b>Data collection performances for satellite (i)</b>	Satellite identification (i) Monthly total number of day with data collection for satellite (i) Monthly total number of passes with data collection for satellite (i) Monthly total number of passes with location for satellite (i) Monthly total number of messages for satellite (i) Monthly mean number of message per pass for satellite (i)

table 8: List of parameters compiled each month for each platform

## 4.2. Theoretical visibility

Our analysis is based on a PTT located at a latitude of 45°. Satellite passes with an elevation angle of under 3° were eliminated.

Using real orbit parameter data, we calculated the theoretical total time each satellite was within view of the PTT during the month.

Results are given in the table 9 below.

Satellites	K NOAA 15	D NOAA 12	H NOAA 11	J NOAA 14
Visibilité cumulée (Heure)	32:10:49	32:12:11	33:52:25	34:00:40
	-0,07%		5,19%	5,61%

table 9: Platform visibility theoretical total time from each satellite

NOAA 11 and 14 are nearly 20 kilometers higher, and their total visibility is 5% better than NOAA 12 and 15.

These figures give us some idea of the degree of theoretical error introduced by differences in satellite visibility.

## 4.3. Satellite performance

We compared the performance of satellites D, J and H to that of NOAA K, on the basis of the **mean number of messages received per pass** by each satellite from the same PTT during August 1998.

This parameter is a very good indicator of system performance, because it significantly affects both data collection and location results (at least four messages must be received during a pass to attempt type 1, 2, 3 or 0 location, at least three for type A location, and at least two for type B location).

## 4.4. Orbitography beacon performance

The orbitography network comprises high-power beacons that offer a high level of performance.

Because these beacons are more powerful, the mean number of messages received per pass by each satellite is not a significant indicator of sensitivity. However, results do give an overall indication of performance with a uniform set of reference beacons.

Table .. shows for each orbitography beacon:  
 - the mean number  $N_i$  of messages received per pass by each satellite (i) during August 1998;  
 - the difference in per cent between satellites K and D, K and H, and K and J, where:

$$d(K-j) = (N_K - N_i) / N_i \text{ for } i = D, H, J.$$

Orbitography platforms	IDs	12	11	14	15	d(K-D)	d(K-H)	d(K-J)
		D Nd	H Nh	J Nj	K Nk			
Canberra	112	23,3	23,8	23,8	23,3	0%	-2%	-2%
?	117	21,5	22,7	22,5	23,2	7%	2%	3%
Hartbees	111	22,5	22,8	22,5	22,0	-2%	-3%	-2%
Kuerguelen	119	21,9	22,7	22,9	22,0	0%	-3%	-4%
Mojave	110	22,2	21,4	23,0	21,2	-5%	-1%	-8%
Kourou	109	21,5	19,5	22,0	20,4	-5%	5%	-7%
Wallops	118	21,4	20,3	21,9	19,6	-9%	-3%	-10%
Gilmore	108	18,1	18,3	18,8	17,8	-1%	-3%	-5%
Toulouse	1	18,0	17,5	18,4	17,0	-6%	-3%	-8%
Perth	149	17,2	16,5	17,1	16,3	-6%	-1%	-5%
<b>Total</b>		<b>208</b>	<b>205</b>	<b>213</b>	<b>203</b>	<b>-2%</b>	<b>-1%</b>	<b>-5%</b>

table 10: Mean number of messages received per pass from orbitography network

The difference in the mean number of messages received per pass does not exceed 10% from one satellite to another over the entire network.

As expected, these results show that NOAA K generally does not provide better performance than the other satellites with high-power PTTs.

## 5. Analysis based on low-power PTTs

Here, our analysis covered a set of 303 bird-tracking transmitters operating with three satellites during August 1998.

We only considered PTTs for which messages were received from at least 24 passes during the month (thus eliminating transmitters yielding abnormal results).

### 5.1. Analysis of $d(K-j)$ as a function of PTT latitude

We plotted the parameters  $d(K-D)$ ,  $d(K-H)$  and  $d(K-J)$  on the figures 11, 12 and 13. These parameters measure the performance of each satellite in comparison with NOAA K as a function of latitude.

We can see from these curves that:

- performance is apparently unaffected by PTT latitude;
- results are significantly better with NOAA K, i.e., Argos 2 as opposed to Argos 1 on NOAA D, J and H.

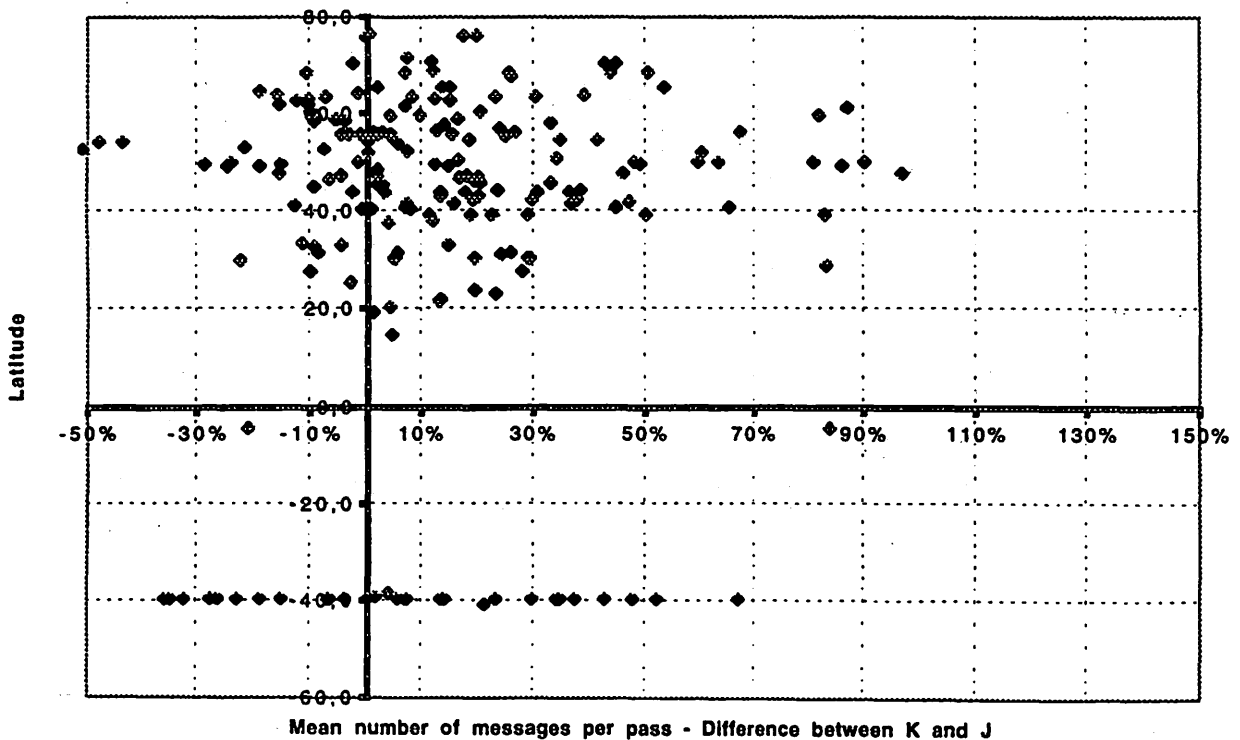
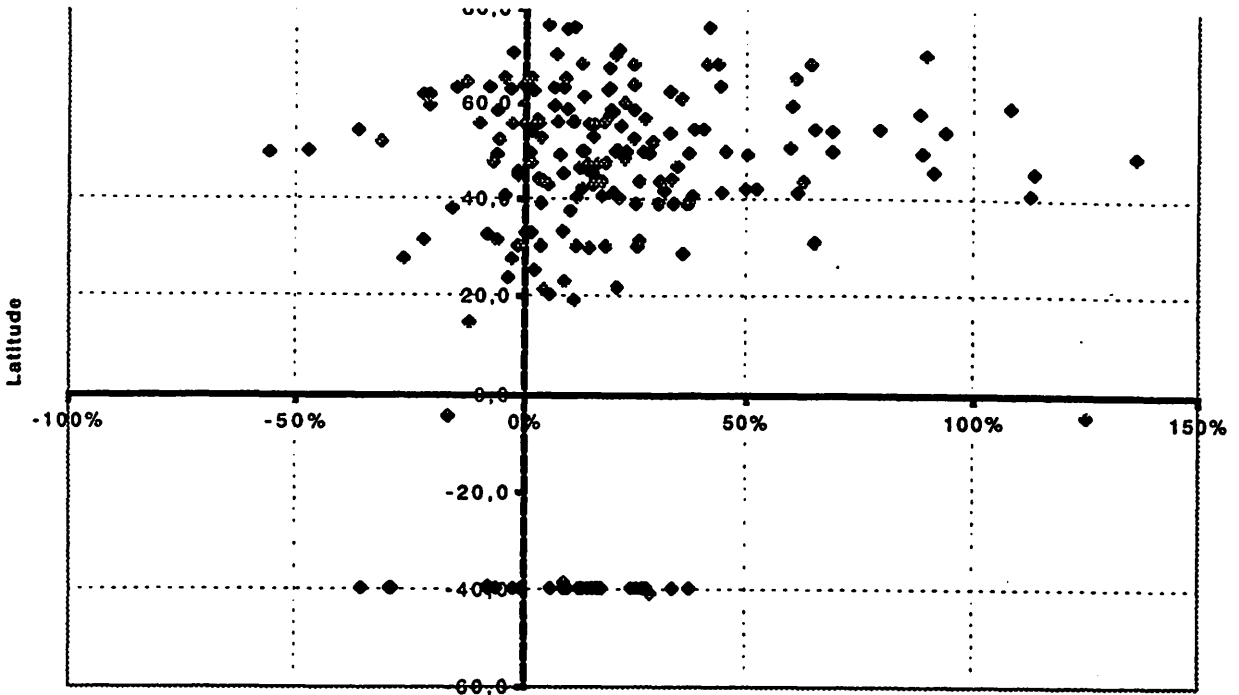


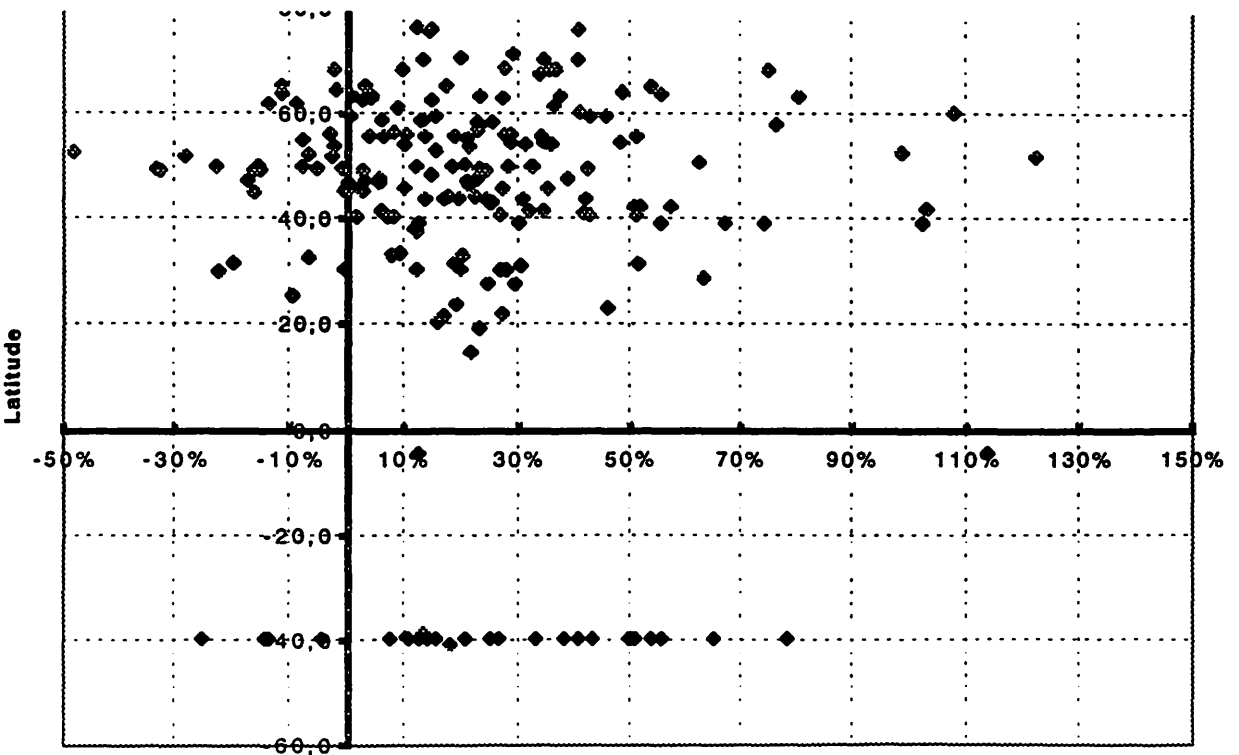
table 11: K (Argos 2) and J (Argos 1) comparison for low power platforms function of latitude





mean number of messages per pass - difference between K and D

table 12: K (Argos 2) and D (Argos 1) comparison for low power platforms function of latitude



Mean number of messages per pass - Difference between K and H

table 13: K (Argos 2) and H (Argos 1) comparison for low power platforms function of latitude

## 5.2. Analysis of $d(K-i)$ as a function of number of PTTs

### 5.2.1. Analysis

To plot curves 14 we:

- created a three-column table for each (K- i) pair;
- entered values of  $d(K- i)$  in decreasing order in the first column;
- entered the corresponding cumulative number of PTTs in the second column, starting with the highest  $d(K- i)$  values;
- converted this number into a percentage of the full set of PTTs in the third column.

Curves 14 allow us to compare the performance of Argos 2 (on NOAA K) and Argos 1 (on the other satellites) directly in terms of mean number of messages per pass.

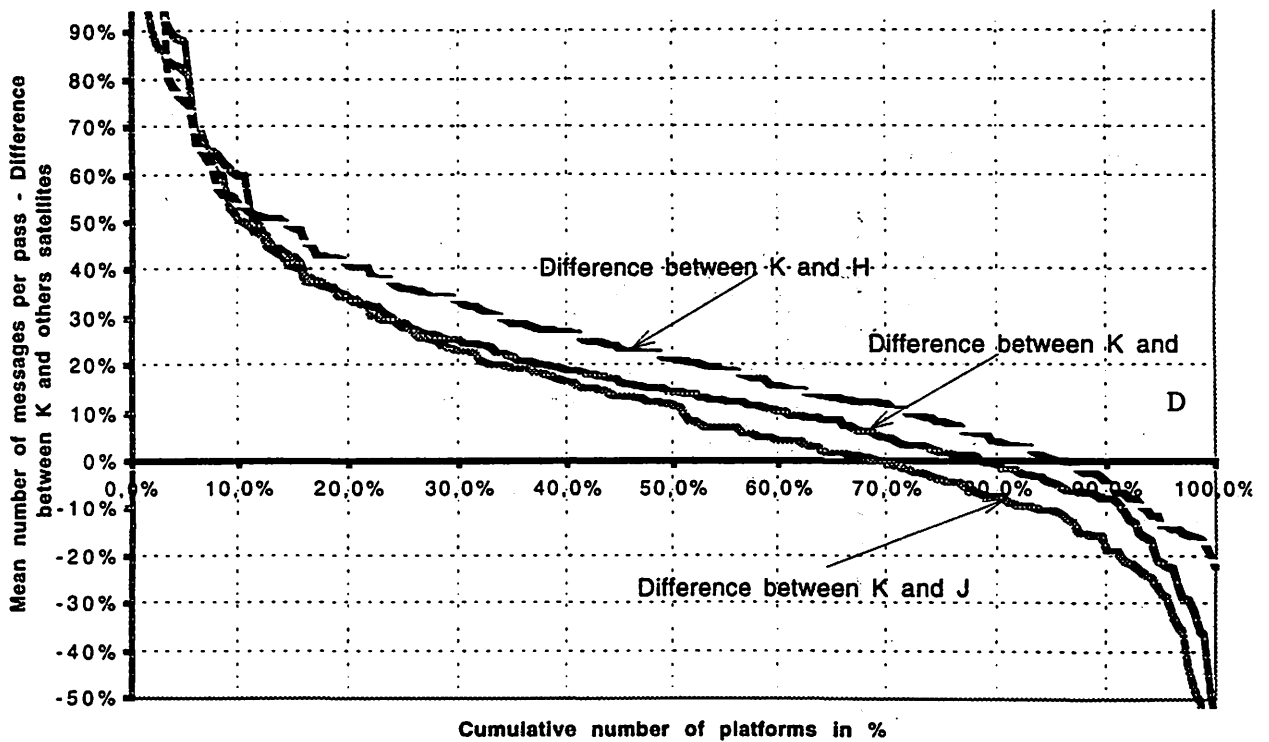


figure 14: Argos 2 on K sensitivity compared to Argos 1 on H, D and J

## 6 Preliminary results

We can conclude from this preliminary study on a set of low-power PTTs that Argos 2 performs better than Argos 1 with 70% of transmitters in the sample (70% with respect to NOAA H, 80% with respect to NOAA D and 85% with respect to NOAA J).

Comparative values for each transmitter and each satellite with respect to NOAA K are given by curves 14.

For example, we can see that the mean number of messages per pass increases by:

- at least 50% for 10% of transmitters;
- 35% for 20% of transmitters;
- and 10% for 50% of transmitters.

This study should be pursued as soon as NOAA K switches to operational status.

By having a larger data set of platforms we should then be able to explore:

- why PTT performance varies from one satellite to another;
- why some transmitters perform less well;
- how far location accuracy improves;
- variations in location classes;
- performance with other types of transmitter samples.



Interactive Real-time Quality Control of Surface Marine Data  
at the National Centers for Environmental Prediction

Christine M. Caruso

National Oceanic and Atmospheric Administration  
National Weather Service (NWS)  
National Centers for Environmental Prediction (NCEP)  
NCEP Central Operations (NCO)  
Camp Springs, Maryland, USA

## 1. Introduction

The accuracy of numerical prediction models which produce meteorological and oceanographic forecasts are dependent on; (1) the models' skill at sufficiently describing the physics of the atmosphere/ocean, and (2) the quality and quantity of the data used in their analyses and initializations. Although ever increasing numbers of marine observations are being transmitted, the ocean observing network for providing operational measurements on a routine basis is still very sparse both spatially and temporally when compared to observations over land. Therefore, considerable effort is made to quality control (QC) those available surface synoptic observations over the oceans. These quality-assured data must also be delivered to the numerical prediction models in a timely manner in order to be useful.

National weather and oceanographic centers are faced with two tasks which greatly affect their marine operations; (1) the time-critical QC of marine observations available for ingestion into numerical prediction models, and (2) the timely dissemination of both the QC'ed data and the forecast guidance based on the output from these numerical models (Richardson and Feit, 1990). This paper describes the Quality Improvement Performance System (QUIPS) being used by the NWS/NCEP/Marine Prediction Center (MPC) for the real-time QC of global surface marine observations collected by ships, buoys, and Coastal Marine Automated Network (CMAN) stations. Also described are the next-generation interactive QC system currently under development by NCO and the importance of buoy observations to weather forecasting.

## 2. Background

QUIPS was developed in 1987 by Compass Systems, Inc. for the National Ocean Service's Ocean Products Branch (OPB). The first version of QUIPS only allowed for the QC of sea-level pressure (SLP) reported by ships, moored and drifting buoys, and

CMAN stations. This version ran on a MicroVAX 3100 workstation using the VMS operating system. The ability to QC air temperature (AT), wind direction and speed (WD and WS), and sea surface temperature (SST) was added into the second version of QUIPS in 1991, and the software was moved to a VAXstation 4000 workstation, also running under VMS. Using QUIPS, OPB meteorologists performed real-time QC of all surface marine data received from ships, moored and drifting buoys, and CMAN stations. In October 1995, OPB was disestablished and the QC function, including personnel, hardware, and software, was transferred to the NWS. The meteorologists who perform the real-time QC are employed by MPC and the QUIPS software and hardware are maintained by NCO.

## 3. Data Collection, Coverage, and Use

Conventional surface marine data reported by ships, moored and drifting buoys, and CMAN stations are transmitted to NCEP via radio, satellite, and the Global Telecommunications System (GTS). In addition, observations from the Navy and Coast Guard are sent via the Automated Weather Network. These data are used by MPC and NWS field office meteorologists and by NWS numerical models to produce analyses and forecasts. The data are also used to validate satellite-derived measurements and are used in climate and global change studies. Upon arrival at NCEP, the raw bulletins containing surface marine data are decoded and stored into BUFR (Binary Universal Form for the Representation of meteorological data) format files on NWS Cray supercomputers.

The spatial and temporal coverage of the existing conventional ocean network is sparse when compared to equivalent measurements over land (Waters et al., 1993). Additional marine platforms have increased the number of observations received, and the number of observations which may be stored in the NWS database has increased, so that the number of surface marine observations stored each month has

risen from 140,000 observations in 1993 to 355,000 observations in 1998 (these numbers don't include duplicate observations or observations from ships identified by the callsign 'SHIP'). However, the additional observations are primarily seen in the North Atlantic and North Pacific Oceans, and many of the drifting buoys reports only include SST measurements. With the exception of observations from ATLAS buoys moored in the tropical Pacific, all surface marine reports must include a sea-level or surface pressure observation in order to be assimilated by NWS's Global Data Assimilation System (GDAS). A standard atmosphere pressure of 1013.25 mb is attached to reports from ATLAS buoys so that other measured parameters from these buoys may be used by NWS assimilation schemes and numerical models. Reports that include SST only are used in production of a one-week SST analysis which is updated daily and produced by the Climate Modeling Branch of NCEP's Environmental Modeling Center (Reynolds and Smith, 1994). This SST analysis is used to provide boundary conditions to NWS's Aviation (AVN)/Medium Range Forecast (MRF) model.

#### 4. Surface Data QC

Given the sparse nature of surface marine data, every effort must be made to ensure that these data will be used by the NWS assimilation schemes and numerical models. The accuracy of surface marine reports must also be known if marine forecasters are to produce accurate analyses and forecasts. As such, considerable effort is made to QC surface marine data. MPC meteorologists QC surface marine data via QUIPS throughout the day. Several times each synoptic period, real-time surface marine data are retrieved from the Cray BUFR files and downloaded to the VAXstations. At the beginning of each synoptic period, 6 hour forecasts (valid for the current synoptic period) of SLP, AT, SST, and u- and v-wind components from either NWS's GDAS or AVN model are downloaded from the Cray to the VAXstations. In QUIPS's preprocessing step, the surface marine data are compared to the first guess fields (first guess u- and v-winds are converted to WD and WS and the first guess fields are interpolated to the platform locations, but no time interpolation is performed). Data that vary from the first guess fields by predetermined threshold values (see Table 1) are flagged for review by the QC meteorologist. An average of 3200 surface marine reports (including duplicate observations and reports from callsign 'SHIP') are received on the VAXstations for QC each synoptic period (in 1993, the average number of surface marine reports received per synoptic

period was 1300). Of these reports, approximately 10 percent are flagged for manual review via QUIPS.

Table 1. Flagging Criteria used by QUIPS

<u>Parameter</u>	<u>Threshold</u>
SLP	+/- 4 mb
AT	+/- 8 deg C
WD	140 degrees
WS	+/- 15 kts
SST	+/- 6 deg C

Upon activation of QUIPS, a color-coded world map allows the meteorologist to select any flagged reports for QC. Menu driven commands, activated by a mouse, assist the meteorologist in determining the accuracy of the flagged data. QUIPS can display a map centered on the flagged report, which shows station plots of the flagged report and all neighboring platforms (see Figure 1). The background first guess fields (contours, vectors, and grid point data) can be overlaid on this map. These features allow the meteorologist to buddy-check the flagged report and make an initial determination as to whether the report or the first guess is correct. The meteorologist can check the history of each platform (up to 8 days of history are saved on the VAXstations for each platform) to see if there's a bias for the parameter in question. If the platform history indicates there may be a position error, the meteorologist can display the cruise track of the platform over the last 8 days (see Figure 2) and correct position errors via this display. The meteorologist can also display a line graph showing the platform's SLP, AT, WD, WS, and SST over the last 8 days versus the first guess fields interpolated to the platform's location. This line graph also indicates whether there's a bias with any of the observed parameters. Every effort is made to correct manual errors in reports sent by ships, such as transposed digits, incorrect signs on temperatures, bad callsigns, and incorrect hemisphere on the ship's location. If a report is determined to be a duplicate, the report may be manually flagged as such so that it won't be used by the data assimilation schemes and numerical models (due to the number of duplicate reports received from drifting buoys, duplicate buoy observations are automatically flagged to ease the meteorologist's workload). Finally, the meteorologist has near-global coverage of satellite imagery (visible, infrared, and water vapor) available on nearby monitors for additional comparisons as necessary.

Once the meteorologist has determined the quality of a flagged report, keep or reject flags may be

set on the SLP, AT, WD, WS, and SST (see Figure 3), or observations may be corrected when obvious errors are detected. Upon completion of QC, all QC flags and corrections are written to an ASCII text file which is then uploaded to the Cray. Whenever any computer program retrieves data from the Cray BUFR database, the QC flags and corrections will be applied, so that the program, whether it is a data assimilation scheme, numerical model, forecast product, or code that just plots data on a map, will include the QC'ed data. A manual reject flag set on a platform's observed SLP will force the GDAS to exclude that entire report, whereas a manual keep flag on SLP will force the GDAS to use the SLP and any other parameters that have keep flags set on them. If no flag is set on a particular parameter, the GDAS has automated QC codes which will decide whether to keep or reject a particular parameter. Automated QC decisions have lower weight in the GDAS than do manual QC decisions.

### 5. Monthly statistics

Surface platform statistics (differences between observations and first guesses) are computed each synoptic period for the 5 parameters listed in Table 1 and are saved, along with the observed parameters, into an archive on the Cray. At the beginning of each month, monthly statistics are produced for the previous month using the archived data and statistics, with separate statistics compiled for buoys. The monthly buoy statistics are broken down by WMO identification and parameter (wind vector and the 5 listed in Table 1) and include the number of reports received, number possibly used by the GDAS, number of gross errors, and other statistics. These statistics are posted to the Data Buoy Cooperation Panel's (DBCP) bulletin board for automatic distribution to representatives on the DBCP mailing list. Another set of monthly statistics (forwarded to the United Kingdom Meteorological Office (UKMO)) includes information on all 4 types of marine platforms (ships, moored and drifting buoys, and CMAN stations) and is also broken down by callsign/WMO identification and parameter. For platforms to be included on this list, NCEP must have received at least 20 observations for the month for a particular parameter and either have at least 25% of the observations for a particular parameter be gross errors (GE) or meet one of the criteria for bias or standard deviation (std. dev.) (see Table 2 (bias and GE criteria are absolute values)). NCO plans to include these statistics on an Internet web site in the near future to allow for wider dissemination.

Table 2: Criteria for UKMO statistics

	<u>Bias</u>	<u>Std. Dev.</u>	<u>GE</u>
SLP	4.0 mb	6.0 mb	15.0 mb
AT	4.0 deg C	6.0 deg C	15.0 deg C
WS	5.0 m/s		15.0 m/s
WD	30.0 deg.	80 deg	100 deg
SST	4.0 deg C	6.0 deg C	15.0 deg C

### 6. QUIPS - The Next Generation

The increasing volume of surface marine data, along with the need to have these data QC'ed before they are used by forecasters and numerical models, requires that a fast, reliable QC system be available for real-time operational use. The current system, QUIPS, runs on VMS VAXstations that are 7-8 years old and not powerful when compared to the newer Unix-based Hewlett-Packard (HP) workstations used by MPC. The preprocessing step for QUIPS takes too long to run on the VAXstations, resulting in a very limited amount of time available for the meteorologist to QC the data before the first numerical model starts during the 0000 UTC and 1200 UTC synoptic periods. The VAXstations have limited active memory, which puts a limit on how much data can be stored for any one synoptic period (for QUIPS, this limit is currently 4000 reports). If QUIPS reaches this data limit, it hangs and can't be used until the next synoptic period when the VAXstation's memory is cleared. This rarely happens but is a concern due to the ever increasing volume of data. Also, memory limitations have delayed implementation of satellite image overlays and loops in QUIPS. Because of these concerns, a new interactive QC system to replace QUIPS is being developed by NCO on a Unix HP workstation. The increased memory on the HP will allow overlaying and looping of satellite images and a faster run-time for the preprocessing step, thus providing more time for QC of surface marine data. HP memory allocation is handled dynamically, so there is no limit to the number of reports received each synoptic period. The new QC system has graphical displays similar to QUIPS and has the same functionality as QUIPS, but should be easier to use. Buttons that allow the user to process data are displayed at all times on a toolbar at the top of the graphical display, whereas QUIPS has pop-up menus and requires the use of 2 mouse buttons to activate the menus and correct data. A prototype for the new QC system is currently undergoing testing and evaluation.

## 7. The Advantages of Buoy Data

Surface marine meteorological and oceanographic data, as measured by moored and drifting buoys, are invaluable for several reasons. Not only are the data used to initialize numerical forecast models (atmospheric, oceanographic, and coupled air-sea), but they are vital to the forecasters trying to determine initial conditions over oceanic areas. An accurate analysis of synoptic data is absolutely necessary if one is to develop an accurate forecast. Buoys provide data at times when other surface marine data aren't available. Ships usually send reports only at synoptic times, whereas moored and drifting buoys and CMAN stations send reports much more frequently. Ships send reports from the usual shipping lanes, which are primarily in the North Atlantic and North Pacific Oceans, but buoys can be placed anywhere on the globe to take measurements. Perhaps most importantly, buoys don't move out of the way to avoid oncoming severe weather. Ship captains paying attention to the marine forecasts will steer around intense cyclones and tropical systems, although there have been a few notable exceptions to this (lucky for those who desire surface marine data near the storm center, but unlucky for the unfortunate crew aboard the ship!). Moored and drifting buoys lying in the path of severe weather stay there on the ocean's surface and send valuable data as the storms pass overhead. While the ability of satellite-based instruments to see through clouds and precipitation to measure data is improving, buoys still provide the most reliable data when storms pass over them.

## 8. Acknowledgments

The author expresses her appreciation to the following people who have provided input and feedback for this paper: James Partain, for providing input on the importance of buoy data; Bill Woodward, Cynthia Nelson, and Joseph Irwin, for helping convince the powers that be to send the author to the DBCP meeting, and Marshall Waters and Cynthia Nelson for proofreading and reviewing the paper. QUIPS was developed under contract to Compass Systems, Inc.

## 9. References

Richardson, W.S. and D.M. Feit, 1990: Expert Systems for Quality Control and Marine Forecast Guidance. Third workshop on Operational Meteorology, Montreal, Canada.

Waters, M.P., C.M. Caruso, W.H. Gemmill, W.S. Richardson, and W.G. Pichel, 1993: An Interactive Information and Processing System for the Real-Time Quality Control of Marine Meteorological and Oceanographic Data. Ninth International Conference on Interactive Information and Processing Systems for Meteorology, Oceanography, and Hydrology, Anaheim, California, USA.

Reynolds, R.W. and T.M. Smith, 1994: Improved global sea surface temperature analyses. *J. Climate*, 7, 929-948.





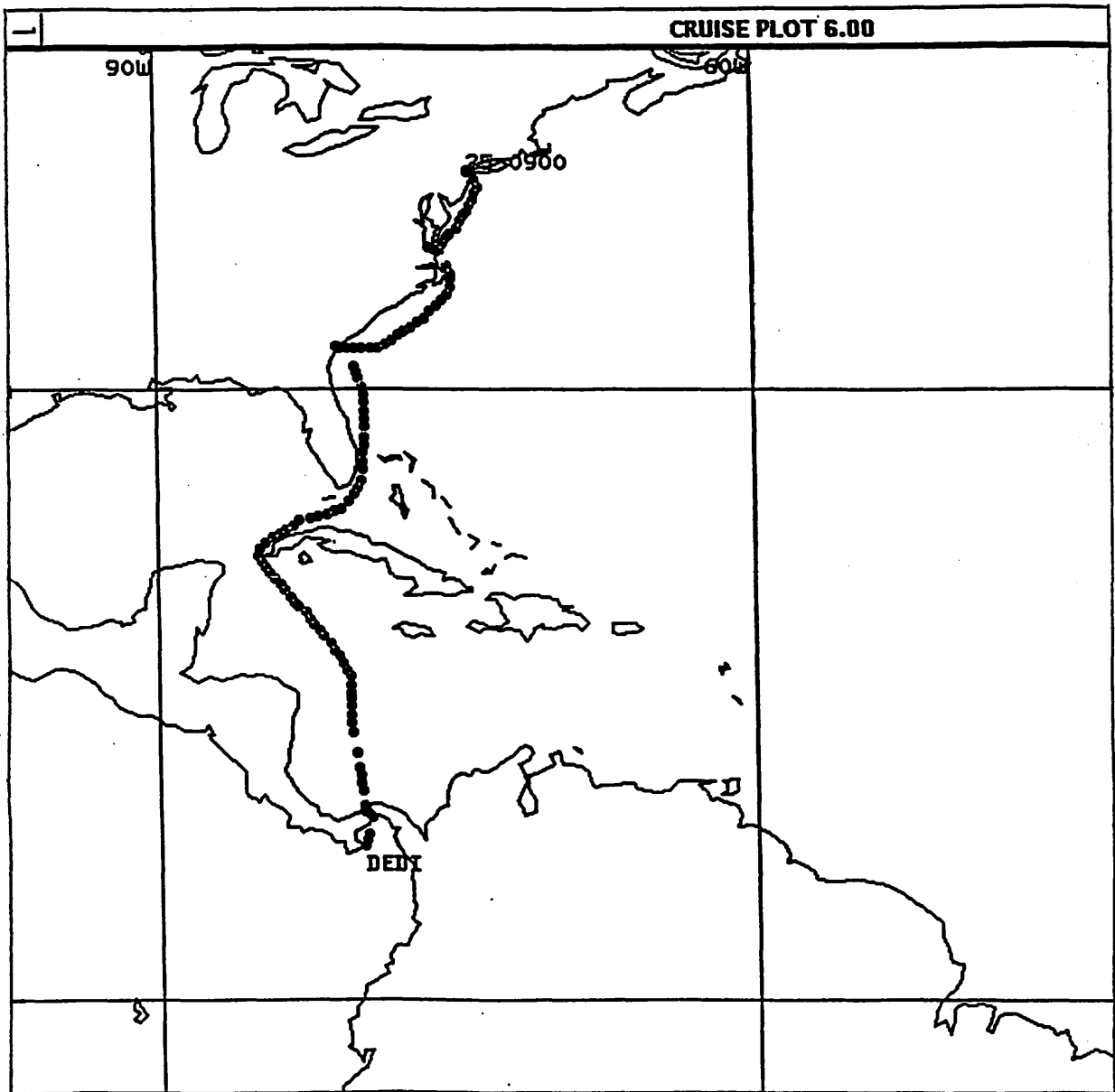


Figure 2. Cruise track showing position of ship DEDI over 8 days (latest observation is at New York Harbor).

DATE/TIME:	1993 01 12 1200	5	413
CALL LETTERS:	LDWR	RW+	
LATITUDE:	66.00N	1	
LONGITUDE:	2.00E	5	
PRESSURE DIFFERENCE:	-8.2	LDWR	
AIR TEMP DIFFERENCE:	-2.2	REJ	KEP
WIND DIR DIFFERENCE:	48.	<input type="radio"/>	<input checked="" type="radio"/>
WIND SPD DIFFERENCE:	7.	<input type="radio"/>	<input type="radio"/>
SEA TEMP DIFFERENCE:	-0.9	<input type="radio"/>	<input type="radio"/>
NAME:	POLARFRONT	REJ ALL	DUP
(DIFF=OBS-MODEL FIELD)		<input type="radio"/>	<input type="radio"/>

File Edit Commands Options Print Help

STATION EDIT PROCESS 6.04  
(MIDDLE MOUSE BUTTON TO DISPLAY MENU AT ANY TIME)  
(USE OFF-PICK LEFT MOUSE BUTTON TO ENTER KEYBOARD-SCREEN MODE)  
ON POINT= 96 OF 149 SELECTED. LOOKING AT 91 OUT OF 857 REPORTS  
PRIORITY POINT MODE-- USE LEFT MOUSE BUTTON TO SELECT

REPORT TYPE	000020A	EDIT FLAG	0000400	EDIT CHANGE	0000000
PRIORITY	96	RECEIPT GMT	1993 01 12 1200		
CALL SIGN	LDWR	OBSERV GMT	1993 01 12 1200		
LATITUDE	66.00N	LONGITUDE	2.00E		
SURF PRES/FCST	941.3	949.5 PRESS CHANGE	20	PRESS TENDENCY	6
VISIBILITY	400	WEATHER	81	CLOUD COVER	100
AIR TEMP/FCST	4.7	6.9 DEW POINT	1.4		
WIND DIR /FCST	100	148 WIND SPD /FCST	18	11	
SEA TEMP/FCST	5.4	6.3			

ALL STATIONS DETECTABL

Figure 3. Top: Keep/reject flag set and differences between observed data and first guess values. Bottom: Platform data and first guess values.



**Svend-Aage Malmberg and Héðinn Valdimarsson  
Marine Research Institute, Reykjavík, Iceland**

**Long distance drift from Icelandic waters  
into the Labrador and Norwegian Seas 1995-1998**

The drift of three selected SVP WOCE drifters is described, all deployed in Icelandic waters in August/September 1995 and still operating in late August 1998. These drifters are Clearwater drifters made available by prof. Peter Niiler and Mark Bushnell through the 1325 Scripps Institution of Oceanography (SIO), La Jolla programme which was carried out in co-operation with the 1119 Marine Research Institute, Reykjavík (MRI-R) programme. All together 120 drifters were deployed seasonally in Icelandic waters during the years 1995-1998, 60 Clearwater drifters and 60 Technocean drifters. Just a few drifters had a lifetime exceeding one year not to speak about three years as those described in the present report.

First, a drifter deployed in August 1995 off West-Iceland is considered (23508 Fig. 1). It drifted westwards to Greenland and followed the East and West Greenland Currents along Greenland and around Cap Farwell during 90 days. From there it drifted after some eddy drift in the Labrador Sea southwards to 46°N off Newfoundland where it in August 1997 after 360 days drift bent eastwards again. It crossed the Mid-Atlantic Ridge 1998 after 600 days just south of the Charlie-Gibbs Fracture Zone at about 52°N and continued northwards in the Iceland Basin up to 58°N; 28°W after 870 days, i.e. on the eastern side of the Reykjanes Ridge, there trapped in eddy circulation for a while. From there it crossed the Reykjanes Ridge and continued northwards on the western side of the ridge to 65°N (June 1998) closing the loop of the "Sub Polar Gyre". There it turned again southwards with the East Greenland Current and around Cap Farwell into the West Greenland Current (August 1998) just along the same paths as almost 1000 days or 32 months

before, which corresponds to about 6 km per day or 6-7 cm/sec. in overall average. The East and West Greenland Currents and the Labrador Current show the highest velocities or 20-30 cm/sec.

Secondly, two other long distance drifters considered in this report drifted eastwards into the Norwegian Sea and Norwegian waters (Fig. 2). They (23525, 23577) were deployed in the waters west of Iceland in August/September 1995 and drifted with the North Icelandic Irminger Current into North Icelandic waters in three to six months. From there they continued eastwards and southwards with the East Icelandic Current into the Faroe Current north of the Faroes (1996-1997) and further eastwards into Norwegian waters at 63-64°N. They continued northwards along Norway with the Norwegian Atlantic Current and further into the waters west of Spitzbergen after 1000-1100 days (August 1998). One of these drifters was for a time captured by eddies in the Lofot Basin. The overall mean drift speed corresponds to 3.6 km per day or 4.0 cm/sec., but the highest velocities were obtained in the East Icelandic Current north of the Faroes and in the Norwegian Atlantic Current or up to 15 cm/sec.

These results of drifters deployed in Icelandic waters in August/September 1995 reveal at least two exiting items, i.e. a long lifetime and a drift around the Sub-Polar Gyre in the Irminger and Labrador Seas in about 1000 days as well as into the Norwegian Sea northwards to Spitsbergen, also in about 1000 days. This drift was along known pathways of ocean circulation in the area. The steering by the bottom topography is also very evident.

At last, comparing the drift velocity of the drifters with the "Great Salinity Anomalies" in the northern North Atlantic in the seventies (Dickson et al. 1988) and eighties (Belkin et al. 1998) a good agreement is observed for those drifters deployed in Icelandic waters and drifting into Norwegian waters in 2-3 years. This may be due to an advective nature of the circulation in general. The drifter drifting around the Irminger and Labrador Seas reveal a much higher velocity than the salinity anomalies or 2-3 years against up to 8 years respectively. This may be due to the diffusive nature of the salinity anomalies in general vs. an advection nature of the drifter.

**References:**

- Dickson, R.R., J. Meincke, S.A. Malmberg, A. Lee, 1988. "The Great Salinity Anomaly" in the northern North Atlantic, 1968-1982. *Progress in Oceanography*, 20 (2), 103-151.
- Belkin, I.M., S. Levitus, J. Antanov, S.A. Malmberg, 1998. "Great Salinity Anomalies" in the North Atlantic. *Progress in Oceanography*, 41, 1-68.



**Mixed Layer Heat Budget in the Cold Tongue Region**  
Mark Swenson and Donald V. Hanson

PRESENTED AT THE WORKSHOP, HOWEVER, NO WRITTEN MATERIAL  
SUBMITTED.





## **The Global Inter-Calibration of Satellite and Buoy Measurements of Winds and Waves**

David Cotton  
Satellite Observing Systems, Godalming, Surrey GU7 1EL, UK  
d.cotton@satobsys.co.uk  
<http://www.satobsys.co.uk>

### **Abstract**

*The main purpose of this paper is to propose an international co-operative programme for the calibration/validation of altimeter and buoy sea state data (wave height, wind speed wave period). The principal objective of this programme is to apply a consistent calibration procedure across all altimeter and buoy measurements of winds and waves, generate a series of calibration corrections, and so provide users of wave data with the means to achieve consistent measurements of sea state across all altimeter and buoy data sets. We propose that this objective be achieved through a co-operative agreement for data exchange and that the results made freely available to users.*

*Through this paper we hope to initiate discussion and we invite expressions of interest in the co-operation proposal. The author would welcome any comments from readers.*

*A feasibility study for such a calibration programme was funded under the UK BNSC "ENVISAT Exploitation Programme". Results from this study can be found under" [http://www.soc.soton.ac.uk/JRD/SAT/envisat/envexp\\_html](http://www.soc.soton.ac.uk/JRD/SAT/envisat/envexp_html)"*

### **Introduction - An Ideal Global Wave Data Set?**

When formulating this proposal, the author first considered what qualities an "ideal" global scale wave data set (of significant wave height and wave period) might have. It is clear that any such list of desired qualities would be highly subjective and dependant upon the required uses of the data set. However, some requirements can be regarded as more or less universal and the list below summarises the more important of these:

1. Full global coverage.
2. Data available in near real time
3. Accuracy/reliability independent of location, conditions or time.
4. Long term, continuous data set.
5. Accuracy of significant wave height- < 0.5 m (in range 0.5 - 20.0 m).
6. Accuracy of wave period < 0.5 s.
7. Resolution in time and space variable according to need.

The possible uses of such a data set include ship routing, local wave forecasts/hindcasts, assimilation into local and global wave models, climate studies including estimation of extreme values.

These requirements cannot all be met by any existing individual wave data set, but they could be achieved through a combination of satellite altimeter and buoy data, if they were properly inter-calibrated. This paper therefore proposes an international co-operation by which wave buoy and satellite altimeter data could be merged to generate such a data set. The proposal is initially restricted to buoy comparisons with a satellite altimeter derived data set of significant wave height, wind speed, and wave period, and does not include at this stage directional and spectral parameters, which can be derived, with the help of models, from Synthetic Aperture Radar (SAR) measurements. This is because, whilst the procedures and principles of this proposal could equally be applied to SAR wave spectra data, the radar altimeter data set (covering 1985-89, 1991 to the present day, and assured into the next decade - see table 1) can be considered as a truly independent data set, and the altimeter can be regarded as a continuous and long term operational instrument. In contrast the processing of satellite borne SAR data to produce directional spectra requires a first guess from model output, so that SAR data cannot be regarded as truly independent from models. Neither can the satellite SAR yet be regarded as an operational instrument for continuous long term monitoring of the global ocean.

In the remaining sections of the paper we first consider the separate characteristics of satellite altimeter and wave buoy data, before providing more specific detail of the proposal for a co-operative calibration programme and discussing the benefits and likely costs of this programme

### **Characteristics of Satellite Altimeter Wave Data**

Satellite radar altimeters have been shown to provide accurate and reliable measurements of significant wave height, with r.r.m.s. values, m in comparisons with buoy measurements (*Cotton et al., 1997*), of 0.3. Recent work (*Davies et al., 1997*) has also demonstrated that a zero upcrossing wave period can be extracted from altimeters, with r. r.m.s. values from comparisons with buoys of 0.5 s to 0.8 s. Satellite altimeters have been providing near continuous global measurements of ocean waves since early 1985 (table 1), enabling researchers to look at wave climate on a global scale. Although satellites cannot provide continuous coverage at a particular point, they provide genuine global coverage and, after suitable averaging, these data can be used to generate global climatological wave charts.

However, satellite altimeter wave measurements require correction in order to bring them into agreement with *in situ* data, and the coefficients for these corrections vary from satellite to satellite (*Carter et al, 1992; Cotton and Carter, 1994; Gower, 1996; Cotton, 1998*). Moreover it has not been possible to validate these corrections for the full range of data recorded by the altimeter. There also remains some uncertainty as to whether the accuracy of the altimeter measurements may be dependent upon the nature of the sea surface (P. Janssen, ECMWF, pers comm.). Consequently there does not exist a single agreed set of corrections which could be applied with absolute confidence by the users.

Altimeter Satellite	(Scheduled) Dates	Agencies Responsible for Data
GEOS-3	1976-79	NOAA
SEASAT	1978	NOAA
GEOSAT	1985-89	NOAA
ERS-1	1991-96	ESA
ERS-2	1996->	ESA
TOPEX/Poseidon	1992->	CNES/NASA
GEOSAT Follow On	1998->	US Navy/NOAA
JASON	(2000)	CNES/NASA
ENVISAT	(2000+)	ESA

*Table 1. Past, present (and future) satellite radar altimeter data sets. (NOAA - US National Oceanic and Atmospheric Administration, ESA - European Space Agency, CNES - Centre National d' Etudes Spatial, France, NASA - US National Aeronautic and Space Administration)*

A limitation of altimeter data is that some locations are never visited, and those that are are only revisited infrequently (e.g. once every 10, 17 or 35 days, depending upon the orbital cycle). Moreover altimeter measurement may be degraded in certain conditions (e.g. heavy rain) and cannot make wave measurements close to coastlines (within 10-35 km, depending on whether the satellite track is moving on, or off, the land). As noted before, the altimeter can only measure significant wave height, now wave period, and wind speed. It cannot provide further spectral or directional information.

### **Characteristics of Offshore Buoy Wave Data**

A number of open ocean instrumental wave buoy programmes are currently in operation over the world's oceans. Wave buoys have provided vital data to meteorological and other agencies for many years. They are able to provide continuous time series of data at important locations (some for periods of over 25 years), are regularly maintained and carefully calibrated with known errors. There is, however, an uneven distribution of buoys, with a large concentration in coastal/shelf areas, and very sparse coverage in the Southern Hemisphere. Buoys cannot therefore be used to provide spatial picture of wave fields on a global scale.

A further potential problem follows from the fact that the global network of buoys is deployed, maintained and calibrated by a number of different national agencies. It is possible therefore, that calibration differences may exist between buoys operated by the various agencies.

### **A Proposal for a Co-operative Inter-calibration Programme**

We therefore propose a practical and valuable co-operative programme of cross-calibration between satellite altimeter and open ocean buoy wave data, whereby co-located and contemporaneous altimeter and buoy data are extracted,

quality tested, and compiled into data sets which are then inter-compared using rigorous statistical techniques. The results will provide calibration corrections which enable all satellite wave data to be brought into agreement with chosen in-situ data sets. The differences between the individual *in situ* data sets will be established through the separate comparisons with the satellite data.

The programme could be established through a partnership between satellite agencies, buoy operators and scientific institutes (the last responsible for carrying out the calibrations). These partners would come to an agreement on data exchange between each other, and on dissemination of results and data sets to the larger scientific community.

### *Proposed Operational Strategy*

The programme is straight forward in concept, and simple in terms of operational requirements. We would suggest that co-operating buoy networks and satellite agencies make their data available to the co-ordinating/calibrating institute(s) by electronic file transfer (ftp). Quality tested altimeter data from each satellite would be extracted at every buoy location. Buoy data for the times of the satellite passes would then be extracted from the buoy data sets and merged with the satellite data. We would envisage maintaining separate merged sets for each buoy network, for the use of the individual operators. At regular intervals the accumulated altimeter and buoy wind and wave data for each network would be intercompared using principle components regression techniques, to establish accuracies and calibration coefficients. Results would be analysed to provide information for both users of satellite data and buoy data, which would be presented on a regularly up-dated web page. Access to results and co-located data sets would ideally be open to all, but could if necessary be restricted for commercially sensitive data. A trial version of this strategy has now been successfully operating for a period of 10 months, under a co-operation between Southampton Oceanography Centre (SOC) and the UK Meteorological Office.

### **Benefits**

The chief beneficiaries of this programme would be four scientific communities: climate researchers, users of satellite data, users of buoy data, and wave modellers. The benefit to the first community is the generation of a consistent global data set, enabling researchers to look for local and global signatures of climate change, confident in the accuracy of their data, and their relationship to other data sets. The users of satellite data would gain calibration corrections for each satellite data set, bringing them into agreement with the standard *in situ* data set, a check for drift on these calibration corrections throughout the lifetime of the mission, and a data set for testing for dependencies of accuracy upon local environmental conditions (sea state, air/sea temperature). The data set would also be invaluable for those trying to generate improved altimeter wind speed algorithms, or to develop new algorithms to measure other sea state parameters (e.g. wind stress, wave slopes). As discussed above, this programme would also benefit users of buoy data, providing a cross check between the calibrations of buoys within different networks, or buoys of different designs. They would also potentially provide a link between time series of wave data at a single point to variability at different locations. Finally, wave modellers would benefit, through gaining access

to a globally consistent *in situ* data set, against which to validate their model output. Without such geographical consistency, it is not possible for them to be certain that their models are accurately representing conditions in all oceanic regions.

### **Costs**

Assuming that data could be freely exchanged between the co-operating partners, then the overall cost of the programme would be minimal. If funding were available to support the programme, it could be used to cover the expense of a central scientific officer responsible for administration and co-ordination, and for the maintenance of a central WWW site. Further funding could support coordination meetings, ftp facilities and/or web sites to encourage agencies to participate where resources are limited.

### **Conclusions**

There is considerable scope for a useful co-operation between data buoy operators and satellite wind/wave data users. Satellite data provide global coverage, but not continuous time series. Each satellite must be separately calibrated by reference to sea truth data, and these calibrations must be repeated throughout the life of the satellite to check for calibration drift. However, when calibrated, they can be expected to provide geographically consistent accuracy over all of the world's oceans. In contrast, buoy data provide poor spatial coverage, but temporal continuity. Buoys from each network are regularly maintained and calibrated, but they are independently calibrated and so it is possible that calibration differences may exist between buoy data from different networks. Satellite data can be used as a reference to make this link. Thus satellite and buoys can be used together in a mutually beneficial cross calibration exercise. Different satellite data sets can be calibrated and tested for drift by comparison against reliable buoy data, buoy data from different sources can be cross checked by reference to satellite data which can be expected to be globally consistent.

The benefits of such a programme would be significant. Wind and wave data from satellites and buoys have an important role to play in monitoring climate, as well as routine input to global models. However, whilst individual data sets continue to be calibrated independently, applying different techniques and using different reference data, it is not possible to combine these data into a consistent single data set. This programme would generate such a consistent data set, enabling researchers to look for local and global signatures of climate change, confident in the accuracy of their data, and their relationship to other data sets.

If the aims of this proposal are to be achieved, the support of buoy, satellite data and calibrating institutes/ agencies, and data users is required. To this end, details of this proposal have been presented to the Data Buoy Co-operation Panel, to the CEOS (Committee of Earth Observing Satellites) working group on calibration and validation, and to a number of satellite and buoy agencies. Calibration proposals have also been submitted in response to Announcements of Opportunity issued for forthcoming altimeter satellites, JASON and ENVISAT.

Comments, suggestions and expressions of interest to the author would be most welcome. The appendix at the end of the paper includes a questionnaire which interested parties are invited to complete.

### **References**

Carter D.J.T., P. G. Challenor, and M.A. Srokosz, 1992, An assessment of Geosat wave height and wind speed measurements, *J. Geophys. Res.*, **97**, No C7, 11,383-11,392.

Cotton P.D. and Carter D.J.T., 1994, Cross calibration of Topex, ERS-1 and Geosat wave heights, *J. Geophys. Res.*, **99**, No C12, 25,025-25,033.

Cotton, P.D., P.G. Challenor, and D. J. T. Carter, 1997, An assessment of the accuracy and reliability of Geosat, ERS-1, ERS-2 and Topex altimeter measurements of significant wave height and wind speed, *Proceedings of CEOS Wind and Wave Validation Workshop*, 3-5 June 1997, ESA WPP-147, ESTEC, Noordwijk, The Netherlands.

Cotton, P.D., 1998, A feasibility study for a global satellite buoy intercalibration experiment - A report for the BNSC ENVISAT exploitation programme, Southampton Oceanography Centre Research and Consultancy Report no. 27, Southampton S014 3ZH, UK.

Davies, C.G., P.G. Challenor and P.D. Cotton, 1997, Measurements of wave period from radar altimeters, in *Ocean Wave Measurement and Analysis, proceedings of the third international symposium "WAVES 97"*, editors B.L. Edge, and J.M. Hemsley, American Society of Civil Engineers, Virginia, USA.

Gower, J.F.R., 1996 Intercalibration of wave and wind data from TOPEX/Poseidon and moored buoys off the west coast of Canada, *J. Geophys. Res.*, **101**, No C2, 3817-3829.

**Appendix**

**Satellite/Buoy Wave Calibration Proposal**  
Data Buoy Co-operation Panel, Scientific and Technical Workshop, October 1998,  
Marathon, Florida, USA,

**Questionnaire**

Please return to David Cotton, Satellite Observing Systems, 15, Church Street,  
Godalming, Surrey GU7 1EL, UK (phone +44 1483 421213, fax +44 1483  
428691, or email d.cotton@satobsys.co.uk)

- 1. Name and Institute/Company (full address), plus email**
  
- 2. Would you be interested in joining a satellite/buoy wave calibration programme? In what way could you participate?**
  
- 3. Are you responsible for data that you would be prepared to make available? Please give details.**
  
- 4. Would you be prepared to send a letter of support, to support applications for funding?**
  
- 5. Can you suggest possible sources for funding?**
  
- 6. Can you suggest other possible data sources?**
  
- 7. Any other comments?**

Many thanks for your help!





## ***An Assessment of the Uncertainty in NWP Background Field Data Based on Duplicate Observations from Moored Buoys***

**D.W. Jones and H.M.Tanner**

### **Abstract**

Numerical Weather Prediction Background and First Guess Field data are universally accepted as an invaluable tool in data quality evaluation and control, particularly for the data sparse regions of the world's oceans. Comparisons of buoy observation data with the BGFs form the basis of the routine statistics produced world-wide by a number of Principal Meteorological and Oceanographic Centres and on which data are accepted or rejected and changes of platform status requested. However, whilst the BGFs represent our best estimate of the 'truth' over long periods, at any one time they may deviate significantly from the actual 'true' value. An assessment of the variance of the BGF data has been made based on comparisons with the duplicated sensors deployed on the UK Open Ocean Buoys. The data from both sensors usually agree much more closely with each other than they do with the BGF, and an analysis of the variances of the respective differences gives estimates of the uncertainty in the individual sensor values and of the BGF.

This analysis is also extended to give estimates of the uncertainty in drifting buoy data computed using the estimates of the BGF variances derived from the moored buoys.

### **Introduction**

The UK Meteorological Office has for many years operated a network of Marine Automatic Weather Stations in the waters around the British Isles. Details of this network and the Open Ocean Buoy that forms a major component of it is described in "Open Ocean Data Buoy" by D W Jones and A N Bentley, DBCP XIV Scientific and Technical Workshop, October 1998.

With the exception of the wave measurements these buoys are all equipped with duplicated sensors, data acquisition, and telemetry systems, providing two independent measurements of each of the variables recorded.

### **1. MSL Pressure Observations - Monthly Quality Control**

Assessing the accuracy of observational data, particularly those from the data sparse regions of the world's oceans, is very difficult because of the lack of knowledge the 'true' value. Numerical Weather Prediction (NWP) Background and First Guess Field (BGF) data are therefore universally accepted as an invaluable tool in data quality evaluation and control. Comparison of buoy observations with the BGF form the basis of the routine statistics produced world-wide by a number of Principal Meteorological and Oceanographic Centres. The observations, e.g. pressure, from the two systems on the Open Ocean Buoys can be compared with the BGF for any period. The differences between the two systems on the buoys and the difference between either system on the buoy and the BGF can be computed. Figures 1 - 3 show data from June 1998 from the Open Ocean Buoy station, K3, about 550km west of Ireland.

Figure 1 shows the differences between the observations made by the two pressure measurement systems on the buoy. The graph shows that the differences are small, ranging from +0.6 to -0.6 hPa. Figures 2 and 3 show the differences between each system on the buoy and the BGF. These differences are much larger, ranging from +1.7 to -1.7 hPa. These three graphs clearly show that uncertainties exist within the BGF. This study attempts to quantify these uncertainties.

Figure 1

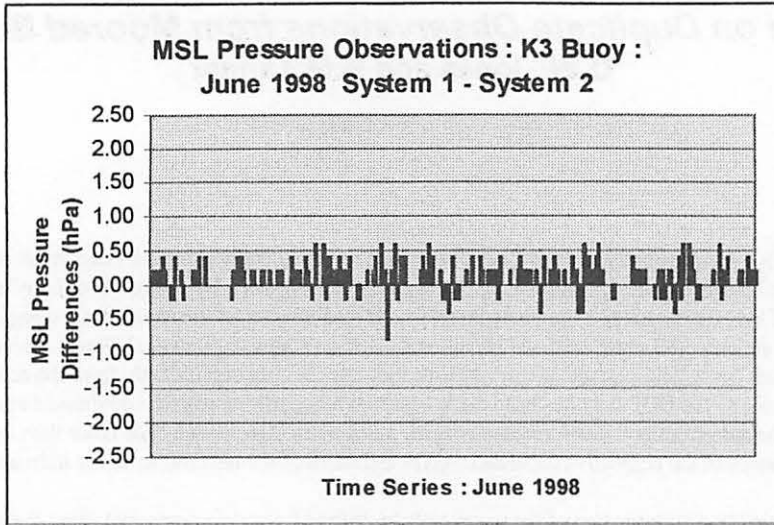


Figure 2

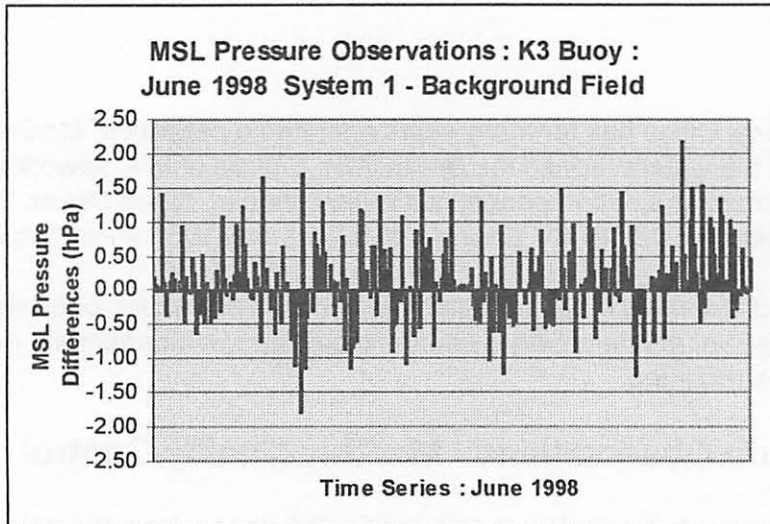
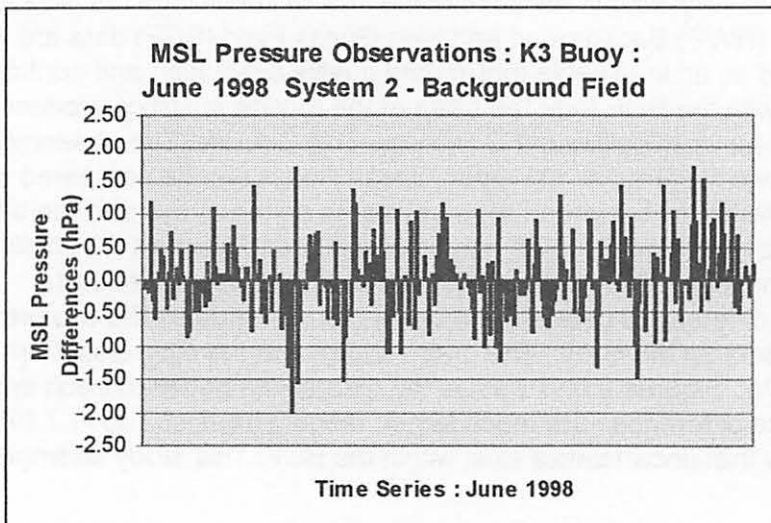


Figure 3



In order to make an overall assessment of the quality of observations, data are compared with NWP Background Fields, but this does not identify uniquely where the errors, implied by the differences, lie. However by calculating the variances of the differences between the data from two independent measurement systems and between each system and the BGF we can estimate the uncertainties in each.

The UK Open Ocean buoys are equipped with two identical and independent observing systems; this allows a comparison of three independent sets of data. The calculation assumes that the data are a sample of the entire population.

**The Variance of data is calculated by:**

$$\frac{n \sum x^2 - (\sum x)^2}{n^2}$$

**where:      x = individual item  
              n = number of items**

The variance is calculated for the differences between system 1 - system 2, system 1 - BGF and system 2 - BGF. Variances are additive so by solving the system of three equations illustrated below, the isolated variance against 'truth' for system 1, system 2 and BGF can be computed

**Total Variance (System 1 - BGF) = Variance of System 1 + Variance of BGF  
Total Variance (System 2 - BGF) = Variance of System 2 + Variance of BGF  
Total Variance (System 1 - System 2) = Variance of System 1 + Variance of System 2**

The main assumption is that the mean BGF value over the month represents our best estimate of the 'true' atmospheric value. This theory also assumes that all three systems are completely independent and are therefore given equal weighting. This methodological approach was devised and implemented by Jones & Bentley, September 1993, 2<sup>nd</sup> Data Collection System Users' Conference, Athens.

This process has been performed for MSL Pressure observations in the North Atlantic. Periods have been chosen for analysis when the buoys have been recently deployed or serviced, and are therefore equipped with newly calibrated sensors:

<b>Brittany Buoy</b>	<b>November 1997</b>
<b>K1</b>	<b>June 1998</b>
<b>K2</b>	<b>August 1997</b>
<b>K3</b>	<b>February 1998</b>
<b>K4</b>	<b>April 1998</b>
<b>K5</b>	<b>October 1997</b>
<b>RARH</b>	<b>October 1997</b>

### Assumptions:

A number of assumptions exist within this methodology.

1. NWP Background Field represents the best estimate of 'truth', at least when averaged over a period of a month.
2. Observations from the two sets of sensors on the moored buoys are independent measurements.
3. Both sets of pressure sensors are working correctly, and no faults identified in the measurement process.
4. The uncertainties in the BGF and the buoys' measurement systems are stable in space and time.

## 2. Regional Variation in Variance of MSL Pressure Observations

It is important to determine whether there are any regional differences in variance of the BGF, and of the buoys' measurement systems. This can be assessed as the Open Ocean stations extend from 47° 32'N (Brittany) to 59°05' N (K5); any regional differences in variance across this range of latitudes, will be seen from a comparison of the estimated variance from each individual buoy station. The statistically estimated variances of the buoy measurement systems 1 and 2 and the BGF, versus 'truth', for barometric pressure for all buoy stations in the Northeast Atlantic, are shown in Table 1, and in Figure 4:

Table 1

Buoy Station	Latitude of Buoy Station	System 1	System 2	BGF
Brittany	47 32 N	0.002	0.058	0.610
K1	48 42 N	0.004	0.037	0.515
K2	51 01 N	0.002	0.089	0.681
K3	53 30 N	-0.007	0.067	0.661
K4	55 25 N	-0.011	0.049	0.513
RARH	57 00 N	0.006	0.023	0.410
K5	59 05 N	0.008	0.046	0.458
<b>Average Variance</b>		<b>0.001</b>	<b>0.053</b>	<b>0.550</b>

Figure 4

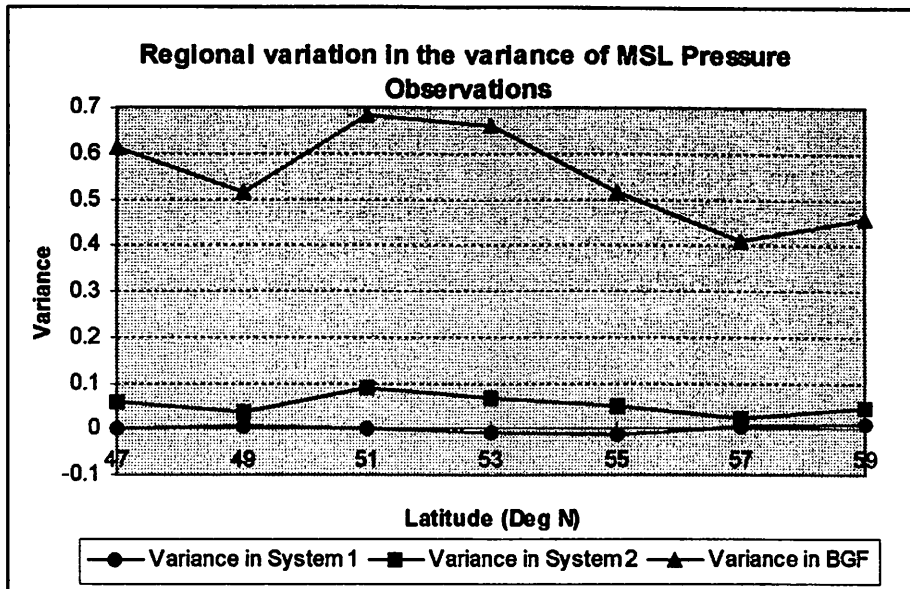


Table 1 and Figure 4 clearly show that the variance of the BGF and the variances of either measurement system differ by up to an order of magnitude, indicating that much of the uncertainty lies with the BGF. Although some degree of variation in space is evident from Table 1 and Figure 4, the general trend appears to suggest that the variance in MSL Pressure does not show any significant regional variation. Therefore, variance can be assumed to be spatially stable. The average variances for the two systems on the buoys and the BGF are therefore assumed to represent the Open Ocean Buoy estimate of variance for the North Atlantic.

Figure 4 and Table 1 show two limitations with the methodology. The computed values would indicate that system 1 variance is always smaller than the variance in system 2. This could be a consequence of the fact that, as a default, it is the observations made by system 1 that are incorporated into the NWP Model run. system 2 is only included in the NWP Model run if a pressure measurement failure has occurred. Therefore, some bias towards the observations made by system 1 may exist. The variances also show that in two instances, negative values are calculated. When calculating variances for sets of data, negative variances cannot exist, as the calculation uses squares and square roots, which inherently do not produce negative figures. However, the approach used in this study is a simple arithmetic operation. Inevitably there will be residual 'noise' within the measurements, and hence within the computed differences, which do not fully comply with the assumptions listed in section 1. Consequently negative values may result from the subtraction of two numbers of similar magnitude. However, the negative values are very small (averaging just -0.009) and only account for 2 out of the 21 values.

The systematically lower values produced for system 1 may also be an indication that the assumption that we are dealing with three independent measurements is not entirely robust; the model may be slightly biased by the observation data themselves. However, the differences between the variances in the BGF and the variances in either measurement system are so large that it is concluded that these methodological uncertainties are minimal.

### 3. Variation in Variance of MSL Pressure Observations over time

As stated previously, for the periods chosen for analysis, all the buoys have either been recently deployed or recently serviced with new sensors. It is important to assess whether the variance in BGF varies significantly over time, and test the assumption that variance in MSL Pressure is temporally stable. Each of the seven buoys are assessed for changes in variance for both the sensor systems and the BGF, from the time of deployment or servicing visit, until the next sensor change. Average variances are calculated in monthly groups and the results are shown below in figures 5 to 11.

Figure 5

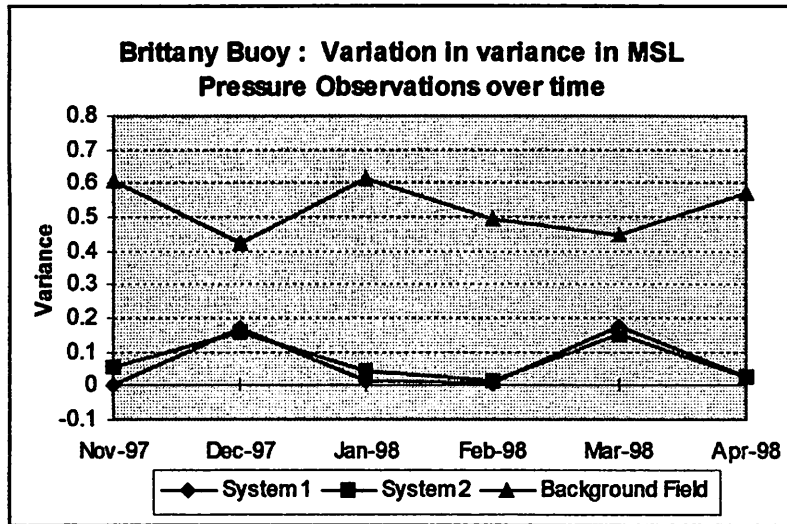


Figure 6

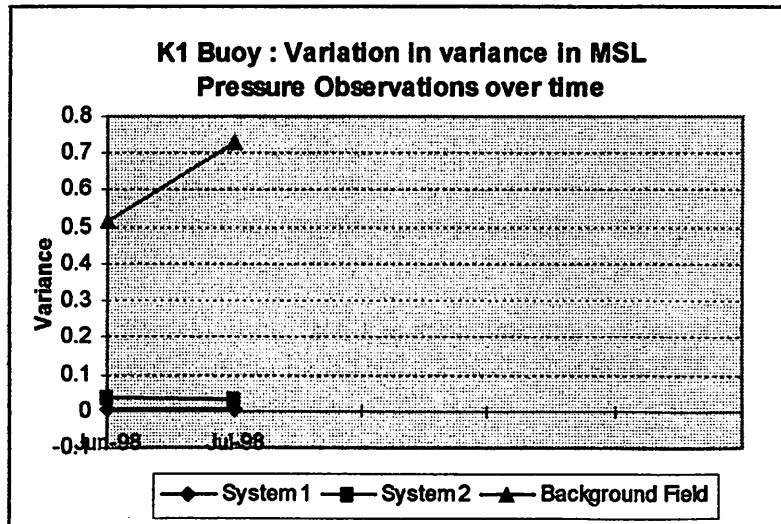




Figure 7

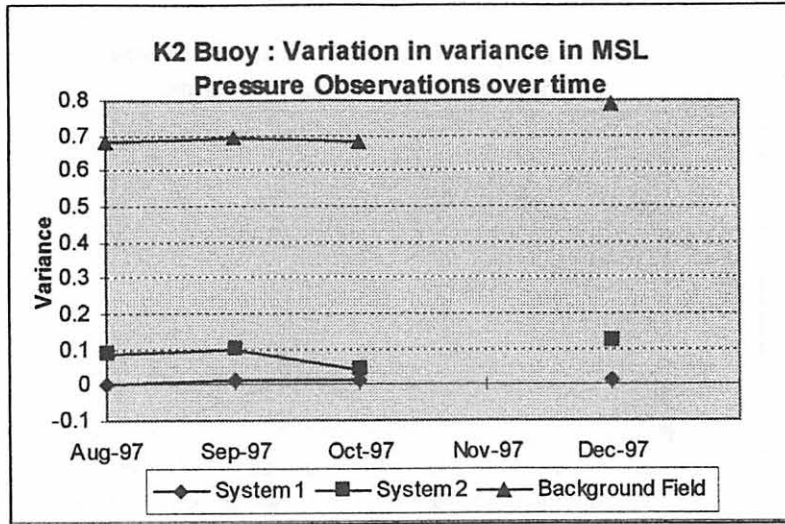


Figure 8

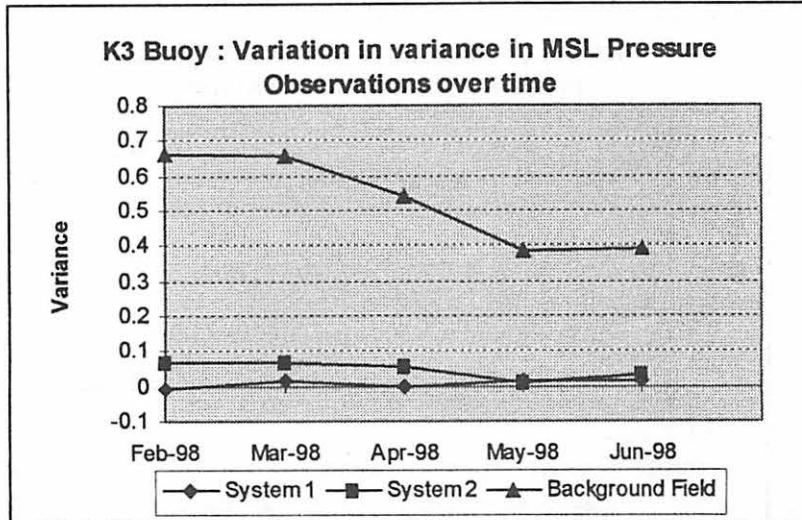


Figure 9

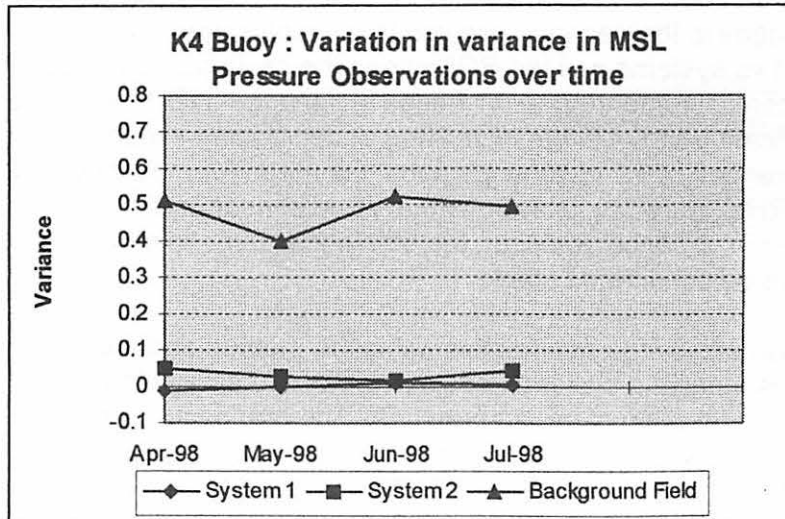


Figure 10

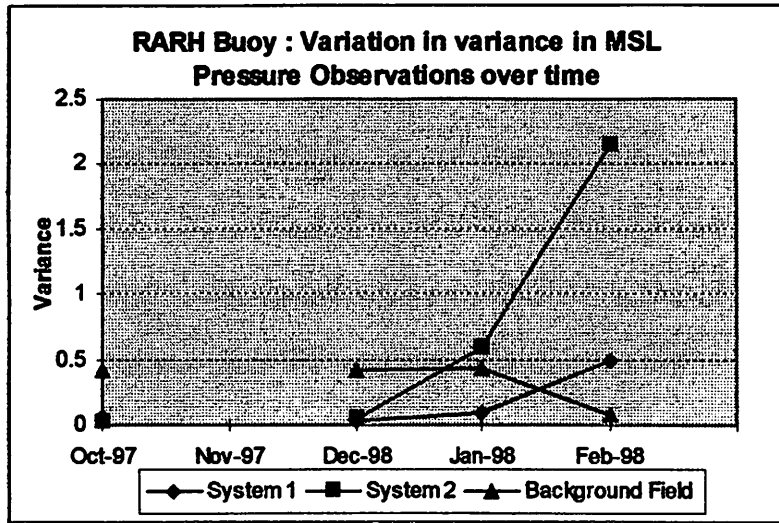
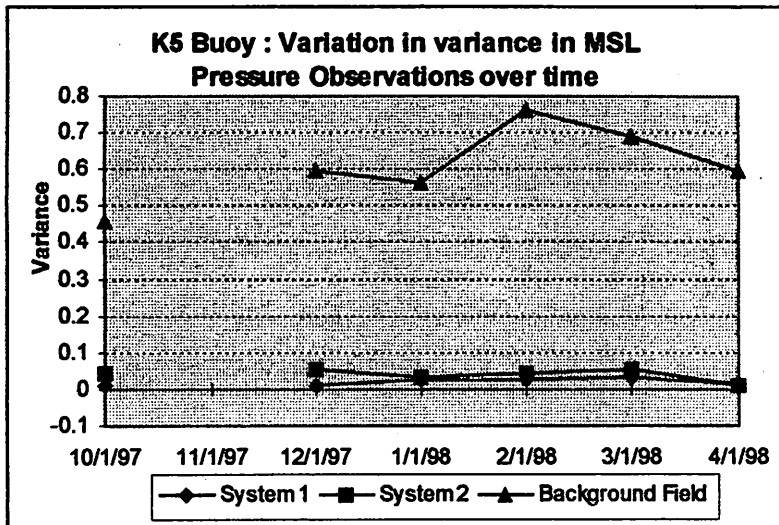


Figure 11



If any major changes in the variance occur in these tables, then this would indicate that the variances in the two systems and the BGF cannot be assumed to be stable over time. Figures 5 - 11 show that there is some degree of change in variance over time for each buoy, however, there is no significant trend of either increasing or decreasing variance. The variation typically amounts to differences of 0.2 in variance about the mean for most buoy data. The only exception is RARH (Figure 10), which obviously had sensor problems on system 2. Therefore, although changes in variance do occur, the differences over time do not possess a clear trend and can therefore be considered stable.

Figures 5 - 11 also show the uncertainties within the method and the assumptions as noted in Section 2. The variances in system 1 observations were always lower than the variance in system 2, with the exception of six occurrences. The graphs also show the presence of some negative values, all of which were for system 1. However, the negative values only accounted for 3.2% of the cases and averaged just -0.007.



#### 4. Average Variance for NWP Background Field

As there appears to be no evidence of either a regional variation in variance or any evidence of the variation in variance over time, an average estimated individual variance for NWP Background Field can be assumed to represent the average variance in BGF for the Northeast Atlantic region. The average variance for BGF is calculated to be **0.550** with a standard deviation of **0.103**.

#### 5. Estimating the Variance of Drifting Buoy Observations from the variance of Monthly Buoy QC Statistics

Now, that we have computed an average BGF variance, and we have determined that the variance in the BGF does not vary significantly in space and time, we can extend the study to include Drifting Buoy observations. The source of the data is the Monthly Statistics for EGOS Drifting Buoys in the North Atlantic, from November 1996 - August 1998. Any drifting buoy data that have been observed to be 'suspect' by Quality Control, have been excluded from the calculations. The Monthly Statistics provide standard deviations of the differences between the Drifter observations and the BGF, from which variances can be derived. The average calculated variance for the BGF has been subtracted from this total variance, to leave the individual variance for the Drifting Buoy observations. The average variance for all Drifting Buoy observations from November 1996 - August 1998 was computed to be **0.770**. The annual variation in the variance in Drifting Buoy observations is shown in Figure 12.

Figure 12

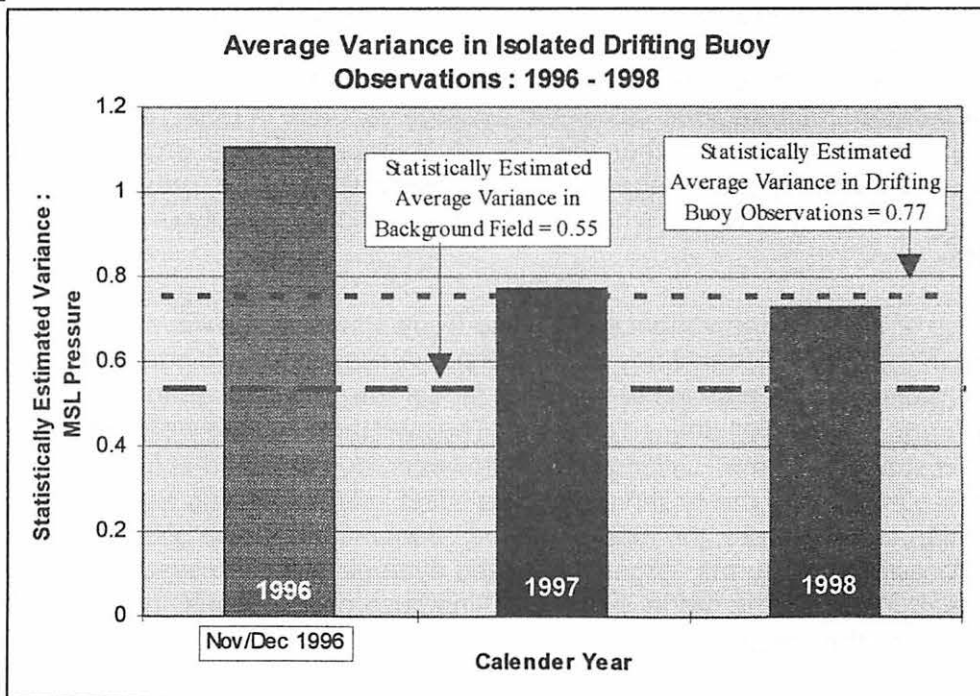


Figure 12 initially shows a trend of reducing variance in time from 1996 to 1998. However, 1996 only consists of two months worth of data, so this is misleading. The graph clearly shows that the variance in Drifting Buoy observations is always greater than the variance in BGF, shown by the red line. A more effective display of the variance in Drifting Buoy observations is shown by examining the monthly calculated variances shown in Figure 13.

Figure 13

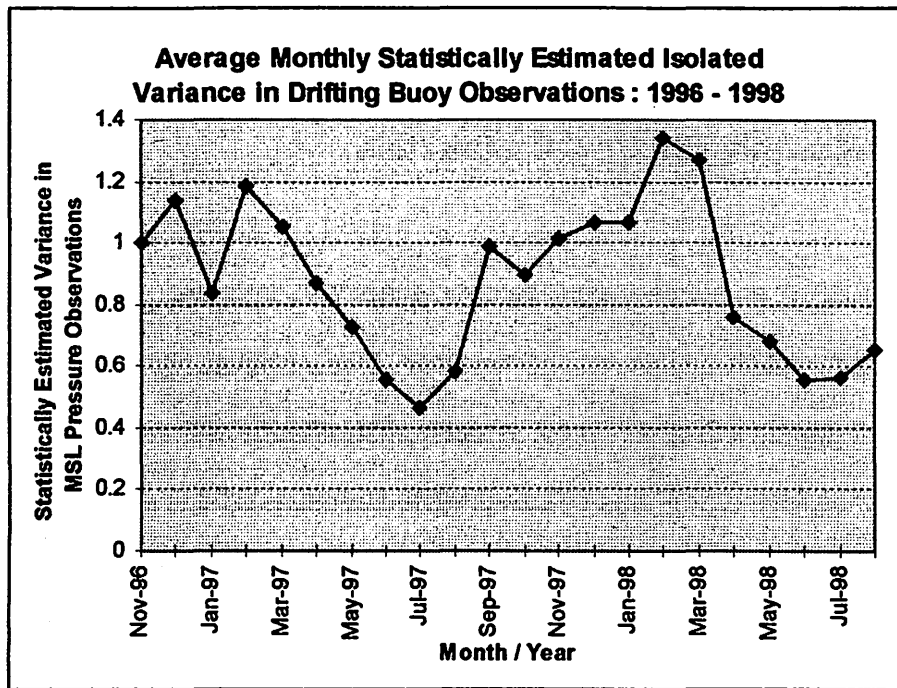


Figure 13 shows the monthly variation of the variance in the Drifting Buoy observations. A seasonal trend is evident from the graph. Higher variance is shown in winter time from January to March, and lower variances are shown in the summer, from June to August. The lower variances are comparable with the calculated average variance in BGF. This seasonal trend is plausible, as in the winter, the weather would be stormier producing a larger wave regime, which could reduce the accuracy of averaged pressure observations. Also, pressure systems develop and migrate more rapidly in winter, which would again effect the quality of pressure observations.

Figure 13 also shows that the variance in Drifting Buoy observations never fall to values near the variance in the Open Ocean Buoy observations. A reason for this could be related to the accuracy of matching observations to the NWP Model Run. Open Ocean Buoys report hourly observations and have a well-defined location. They will therefore be well matched with the model runs in space and time. Drifting Buoys, however, do not report at fixed times and it is possible for the model and the observation to be offset in time. Drifting Buoys also have a varying location and therefore, the model and the observation may be offset in space. The seasonal effect of winter storms, larger waves and dynamic pressure systems would exaggerate the problems of matching the model with the drifting buoy observations, in space and time, thereby increasing the variances.

## 6. Comparing the Differences between the Moored Buoy Observations and Background Field with the Differences between Drifting Buoy Observations and Background Field.

In June 1998, an Open Ocean Buoy, K3, and a Drifting Buoy, 44771, were in very close proximity in the North Atlantic. K3 is moored at 53°50'N, 19°30'W and Drifter 44771 was located at 54°00'N, 19°01'W at the end of June 1998. The close proximity of these two types of meteorological buoy provides an opportunity to compare the pressure observations at the same point in space and time.

Figure 14

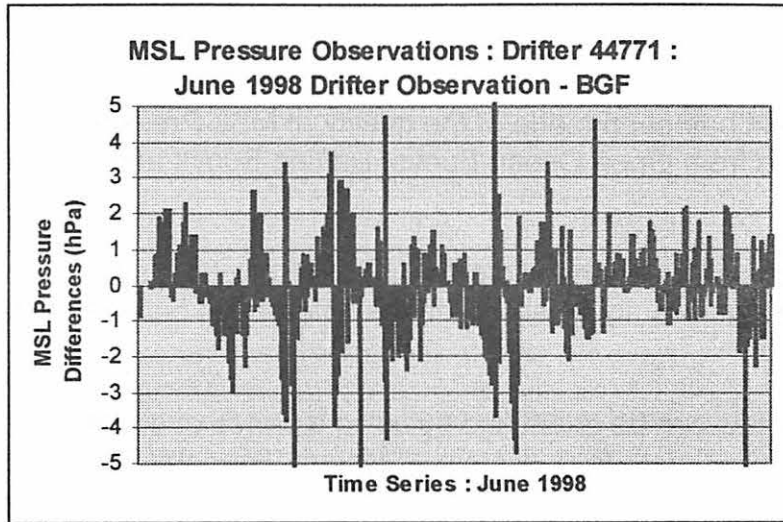


Figure 14 shows the differences between the Drifting Buoy observations and the Background Field. The differences generally range from +4.8 to -5 hPa, with a few anomalous differences of up to 30 hPa. The latter have been excluded from the statistics

Figure 15

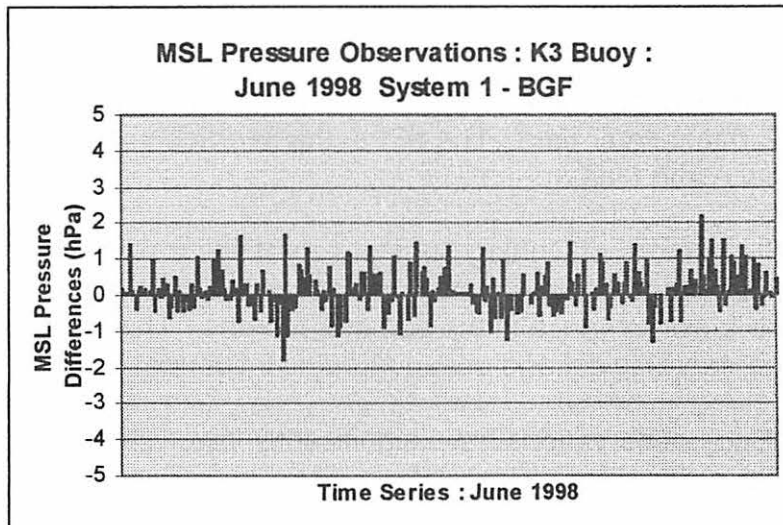


Figure 15 shows the differences between the Open Ocean Buoy observations and the Background Field. The differences generally range from +2.2 to -1.8 hPa.

These two graphs clearly show that improved pressure observations are available from the Moored Buoys compared with those from the Drifting Buoys. The range of differences between the Open Ocean Buoy observations and the BGF are half the value of the differences between the Drifting Buoy observations and the BGF. This observation supports the analysis with the computed variances in Section 5, that the average variance for Drifting Buoy observations was significantly higher than the average variance for the Open Ocean Buoy observations.

## **7. Summary**

- 1. An assessment has been made of the quality of MSL Pressure observations in the Northeast Atlantic from Open Ocean Buoys, Drifting Buoys and the NWP Background Field.**
- 2. The differences between the two pressure measurement systems on the Open Ocean Buoy are significantly smaller than the differences between either system and the Background Field.**
- 3. The uncertainties can be quantified by using a series of equations to calculate the individual variances in data from system 1, system 2 and the Background Field.**
- 4. Assumptions are made that the BGF represents the best estimate of 'truth', that the three observations are independent, and that any uncertainties that do exist are small.**
- 5. The average variance in Background Field is calculated to be 0.550, which is an order of magnitude greater than the average variance in system 1 and 2, at 0.001 and 0.053 respectively.**
- 6. There is no evidence that there is any regional variation in variance, or that there is any variation in variance over time. Therefore, the average variance in BGF is assumed to be stable in space and time.**
- 7. The individual variances of Drifting Buoy observations are computed, and average 0.770. Regional variations in the variance are observed, with higher variance in the winter months and lower variance in the summer months. This is probably a consequence of meteorological and oceanographic influences.**
- 8. Open Ocean Buoy observations have significantly lower variances than the Drifting buoy observations.**

**Profiling-ALACE Floats in the Atlantic Circulation and Climate Experiment**  
Dr. Robert Molinari  
Atlantic Oceanographic and Meteorological Laboratory (OAR/NOAA)  
U.S.A.

**ABSTRACT ONLY SUBMITTED**

The Atlantic Circulation and Climate Experiment (ACCE) represents the last field phase of the World Ocean Circulation Experiment (WOCE). The objectives of ACCE are to obtain a better understanding of the dynamics of the circulation of the Atlantic and how this circulation interacts with the atmosphere to generate climate variability. A Profiling-ALACE (PALACE) float array is a major component of ACCE. The main objective of this component is to characterize the internal oceanic processes that impact on sea-surface temperature variability. To achieve this objective, a basin-wide deployment of floats from 6S to the subpolar Atlantic was begun in 1997. The complete array will be in place in the fall of 1998. PALACE floats are designed to remain at a resting depth for some 10 to 14 days. For ACCE the depth was typically 1000m. After this preset time, the float ascends to the surface obtaining a temperature profile (in addition many of the floats were equipped with salinity sensors). The float remains at the surface for one-day transmitting its data through ARGOS. The float then returns to its resting depth to begin the cycle again. Thus, in addition to the profiles, float trajectories are available to characterize the circulation at 1000m. The resulting data will be used (1) to test hypotheses on the forcing mechanisms for temperature, salinity and current structure, (2) for ground truthing of satellite altimetry data and (3) for operational climate forecasting.



DBCP Scientific and Technical Workshop  
12-13 October 1998  
Marathon, FL

### **TAO Array Enhancements and Expansions**

H. Paul Freitag  
Linda J. Mangum  
Nathan C. M. Franzen  
Michael J. McPhaden

National Oceanic and Atmospheric Administration  
Pacific Marine Environmental Laboratory  
7600 Sand Point Way NE  
Seattle, WA 98115

#### *Introduction*

The Tropical Atmosphere-Ocean (TAO) Array consists of approximately 70 deep-ocean moorings spanning the equatorial Pacific Ocean between 8°N and 8°S from 95°W to 137°E (Figure 1). The purpose of the array is to provide high quality, in-situ, real-time data in the equatorial Pacific Ocean for short-term climate studies, most notably those relating to the El Nino/Southern Oscillation (ENSO) phenomenon. It is also a component of the Global Ocean Observing System (GOOS) and the Global Climate Observing System (GCOS). TAO measurements consist primarily of surface winds, sea surface temperature, upper ocean temperature, air temperature, and relative humidity. At a few selected sites, upper-ocean currents are measured from surface moorings instrumented with mechanical current meters and from subsurface moorings with Acoustic Doppler Current Profilers (ADCP). Daily-mean data and the most recent hourly surface data are telemetered in real time via Service Argos several (typically 2 or 3) times per day. The data are placed on the Global Telecommunications System (GTS) for distribution to operational centers where they are assimilated into weather and climate forecast models. No ocean velocity data are telemetered in real time, but are available after the moorings are recovered. The focus of this report is to review several enhancements and expansions to the TAO Array which are underway.

#### *Enhancements to ATLAS Moorings*

Since its beginning in 1984, the TAO Array has been mainly comprised of standard ATLAS moorings. Measurements from these moorings include surface winds, air temperature, humidity, sea surface temperature (SST) at hourly intervals, and daily mean subsurface temperatures. Subsurface measurements are made along a 500m temperature cable which runs parallel to the mooring line.

Newly designed ATLAS moorings, known as Next Generation ATLAS moorings, have been enhanced to include additional surface and subsurface measurements, increased sampling rates and elimination of the subsurface electromechanical conducting cable for temperature measurement. Options to the standard suite of measurements include shortwave radiation, rainfall rate and surface salinity. Daily mean, standard deviation and maximum shortwave radiation values are telemetered in real time (Figure 2a). These statistics are based upon 2-min average values which are stored onboard and available when the moorings are recovered. Telemetered rainfall data include daily mean and standard deviation rainfall rates and daily percent time raining (Figure 2b). These statistics are based upon 1-min average rainfall accumulation values which are stored onboard and available when the moorings are recovered. Daily mean conductivity values are telemetered in real time, and when combined with mean temperatures provide mean salinity values (Figure 2c). Conductivity and ocean temperature are sampled and recorded onboard at 10-min intervals (Figure 3). Two-minute averages of wind vectors, air temperature and relative humidity are also recorded onboard at 10-min intervals. Although not available at this time, optional longwave radiation and telemetered current velocity measurements are being developed.

The elimination of the subsurface temperature cable is made possible by inductive coupling of subsurface temperature and conductivity modules to surface instrumentation via the mooring cable itself. This advancement affords several advantages over the standard ATLAS mooring: lower drag on the mooring, which increases the reliability of the mooring system; decreased mooring weight and volume which lowers shipping costs; and decreased time required to deploy a mooring, which saves research vessel time.

At present, nearly all TAO moorings are taut-line design, but reverse catenary (or slack-line) moorings are being tested along side the traditional moorings at a few sites. Reverse catenary moorings have the advantage of being able to adjust to higher current regimes, and can be deployed for longer periods, since the instrumentation in the upper 500m can be serviced without replacing the entire mooring. A disadvantage of reverse catenary moorings is that subsurface sensors, in particular the deeper sensors, may experience large vertical excursions as the mooring reacts to varying currents. Next Generation ATLAS moorings are deployed with high accuracy pressure sensors at the deepest 2 (on taut-line moorings) or 3 (on reverse catenary moorings) subsurface temperature modules. Vertical excursions at 500m on a taut-line mooring are typically 10m or less, but can be as large as 75m on a reverse catenary mooring. Efforts are underway to develop depth and/or temperature algorithms for real-time correction of subsurface data (Figure 4). Before reverse catenary moorings can be deployed on a regular basis within the TAO Array, it will be necessary for Service Argos to include these algorithms in their processing to insure that TAO subsurface temperature data put on the GTS are reported at correct depths.

#### *Expansions of TAO Mooring Technology*

Since 1997, TAO has been involved with several new measurement programs (Figure 5). The Pilot Research Moored Array in the Tropical Atlantic (PIRATA) is a collaboration between TAO, Brazil (Instituto Nacional de Pesquisas Espaciais - INPE), and Directoria de Hidrografia e Navegacao - DHN)) and France (L'Institut Francais de Recherche pour le Developpement en Cooperation - ORSTOM). The focus of PIRATA is to study ocean-atmosphere interactions in the tropical Atlantic that are relevant to regional climate variability on seasonal, interannual and



longer time scales. At present, 5 Next Generation ATLAS moorings are deployed in PIRATA. When completed in 1999, the array will consist of 12 ATLAS moorings, each of which will measure, radiation, rainfall, and salinity at the surface and 3 subsurface depths, in addition to the standard TAO measurements.

Three Next Generation ATLAS moorings were deployed in 1998 as an element of the South China Sea Monsoon Experiment (SCSMEX) in collaboration with the National Taiwan University (NTU). SCSMEX is a large scale international monsoon experiment, the objective of which is improved understanding of the key physical processes responsible for the onset, maintenance and variability of the monsoon over Southeast Asia and southern China.

The addition of shortwave radiation measurement from ATLAS buoys was a collaborative effort between TAO and the US Department of Energy Atmospheric Radiation Measurements (ARM) Ocean Project. Seven TAO moorings along the 165°E meridian are providing long time series of surface insolation in support of ARM's research objective of understanding the surface radiation budget and cloud forcing in the tropical western Pacific.

Rainfall and surface salinity measurements are being made from a subset of the TAO Array in cooperation with NASA's Tropical Rainfall Measuring Mission (TRMM). These data will be used to address TRMM objectives of characterizing the time and space scales of rainfall variability in the tropical Pacific, for documenting and understanding the impact of rainfall on the ocean, and for better understanding the role of the hydrologic cycle in the climate system. Measurements are currently being made at 13 mooring sites, primarily along the 165°E meridian and along the equator. By boreal spring 2000, the array of rainfall and surface salinity measurements may be expanded to include all equatorial sites as well as all along the 140°W and 95°W meridians.

Moored bio-optical, nutrient and chemical sensors have been deployed at a few sites within the TAO array. This collaborative effort between PMEL and the Monterey Bay Aquarium Research Institute supports both NOAA's Ocean Atmosphere Carbon Exchange Studies (OACES) Program in the understanding of primary productivity and the exchange of carbon dioxide between ocean and atmosphere, and the NASA SeaWiFS (ocean color) satellite program, providing sea surface pigment distributions for verification of satellite measurements.

The Japan Marine Science and Technology Center (JAMSTEC) has deployed prototype moorings of their Triangle Trans-Ocean buoy network (TRITON), which have been designed to mirror TAO measurements. Initial ATLAS/TRITON comparisons from 4 collocated sites along the 156°E meridian over the 4-month long deployments were very good. Beginning in 1999, most TAO sites west of the 165°E meridian will have collocated ATLAS and TRITON moorings for a comparison period of about 1 year. After continuity of measurements has been assured, JAMSTEC will assume primary responsibility for these sites. Data will continue to be available on the GTS and via the TAO web site.

A high-latitude version of an ATLAS mooring was deployed by PMEL in September 1998 at Ocean Weather Station PAPA (50°N 145°W) in the northeast Pacific as a component of the National Ocean Partnership Program (NOPP) in September 1998. This mooring features a mooring system designed to withstand the harsher environment of the north Pacific, duplication of

surface sensors, and the addition of long wave radiation and barometric pressure measurements. The development of subsurface acoustic telemetry between this surface mooring and a nearby subsurface mooring is also being tested from this platform. The higher data telemetry rate from the NOPP mooring, which consists of continuous 3-hour mean and latest spot samples, is supported via GOES telemetry. TAO plans to have operational data put onto the GTS and is seeking help and advice from DBCP members who may be able to perform this task.

*Summary*

The TAO Project is improving and expanding measurements made within the tropical Pacific moored array. New technologies are actively being explored to increase the reliability of measurements, add optional measurements, and to increase the volume of data telemetered in real time. At the same time, new research opportunities in other climatic regions are being pursued.

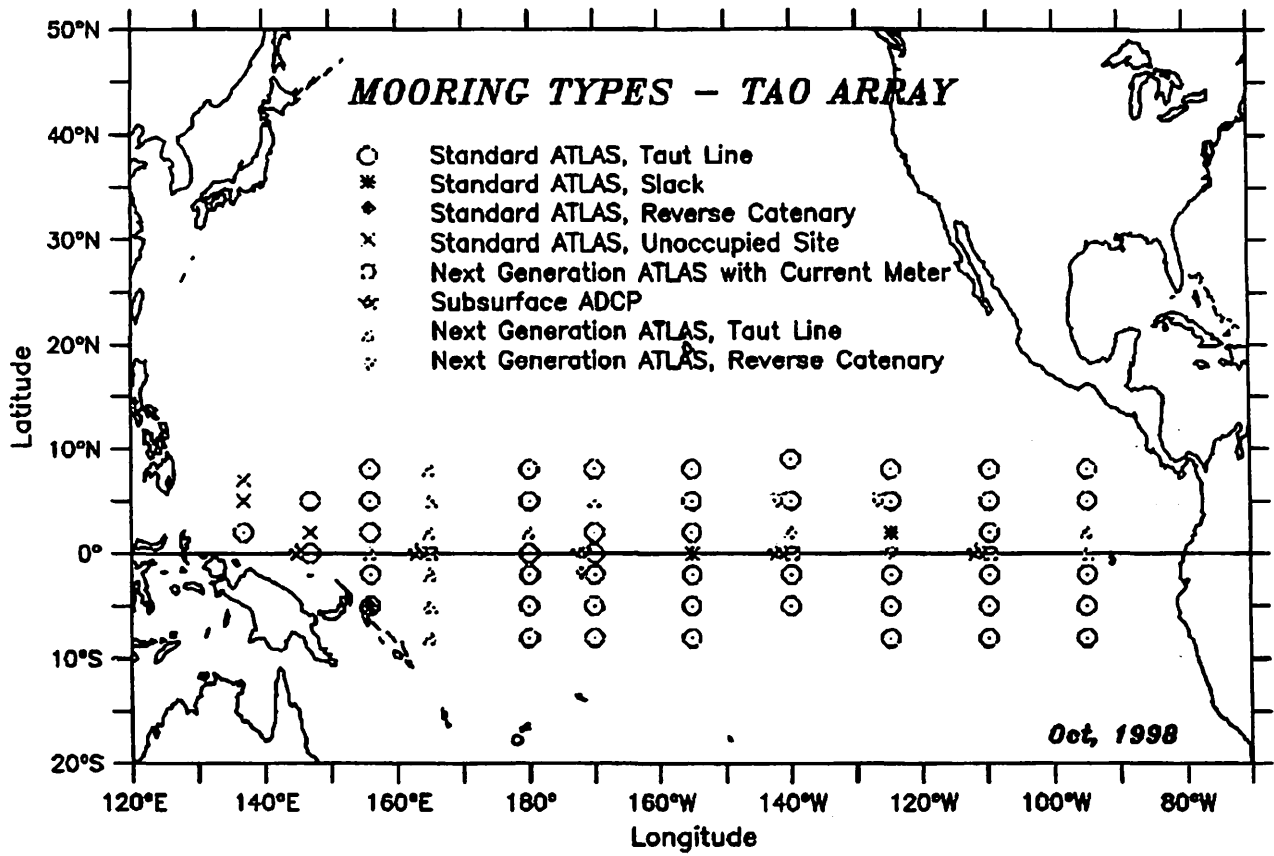


Figure 1: Location and types of moorings within the TAO Array.

### ATLAS II Radiation Data for 5n165e

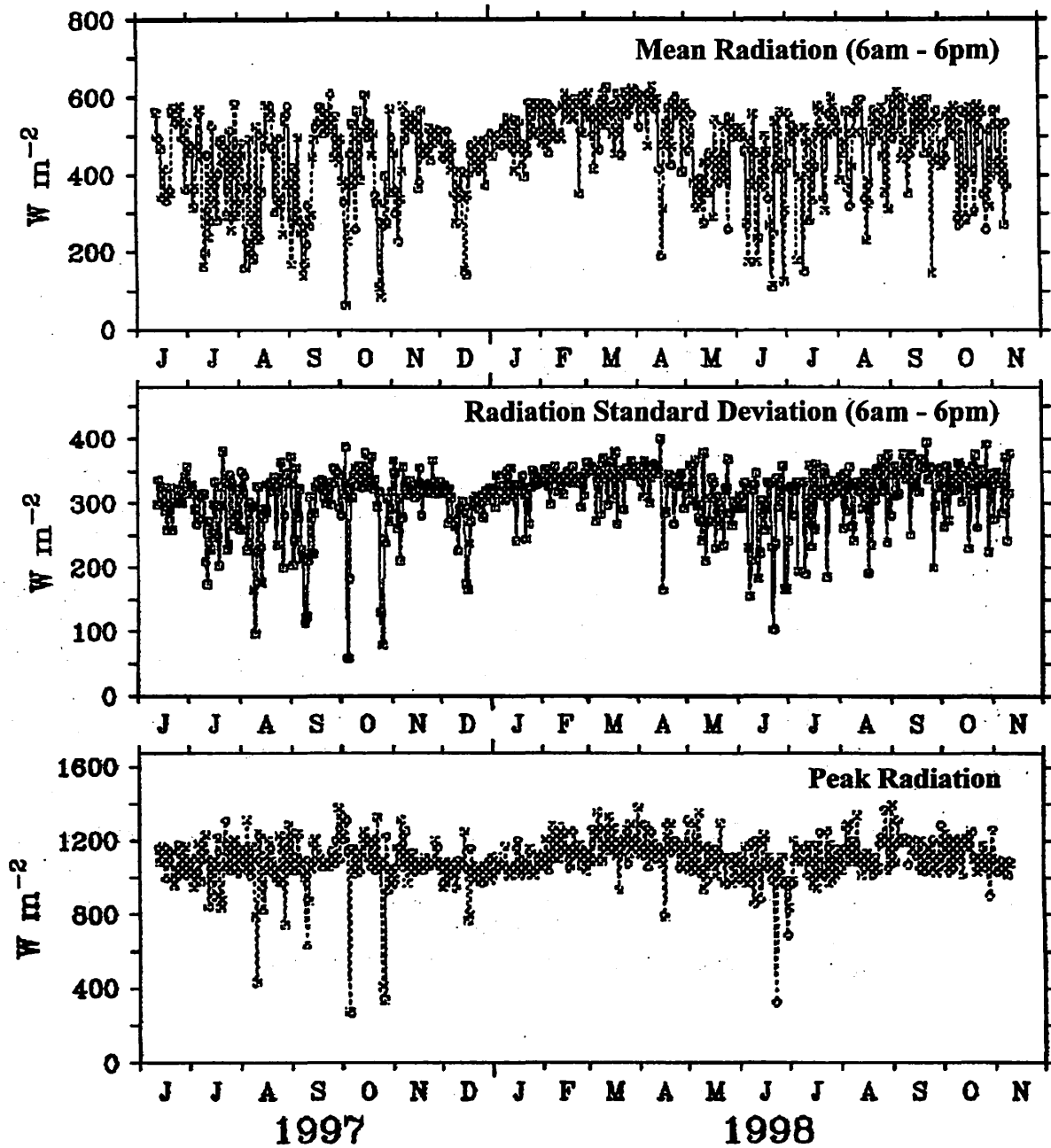


Figure 2a: Daily shortwave radiation data telemetered from a Next Generation ATLAS mooring.

### ATLAS II Rainfall Data for 5n165e

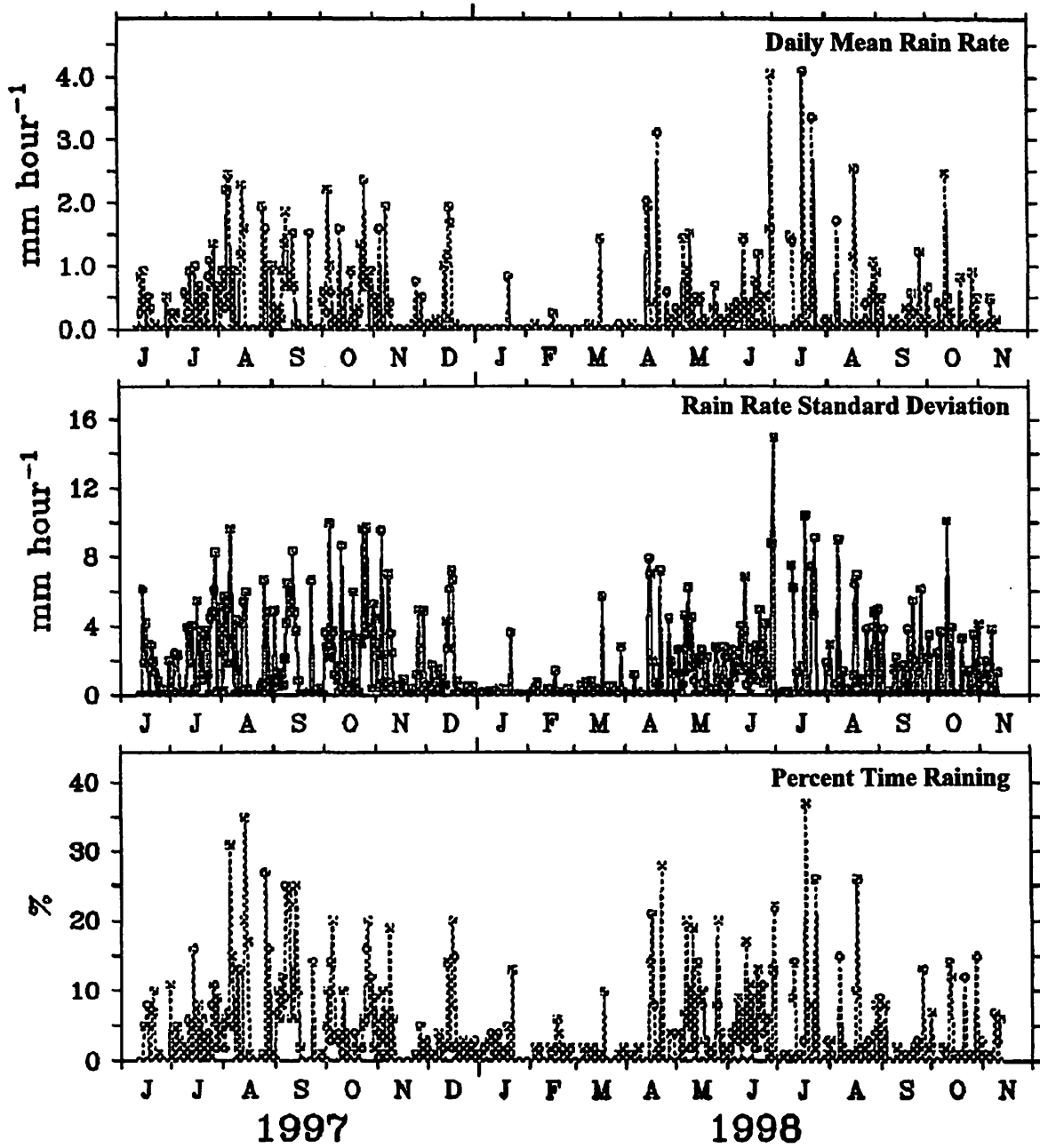
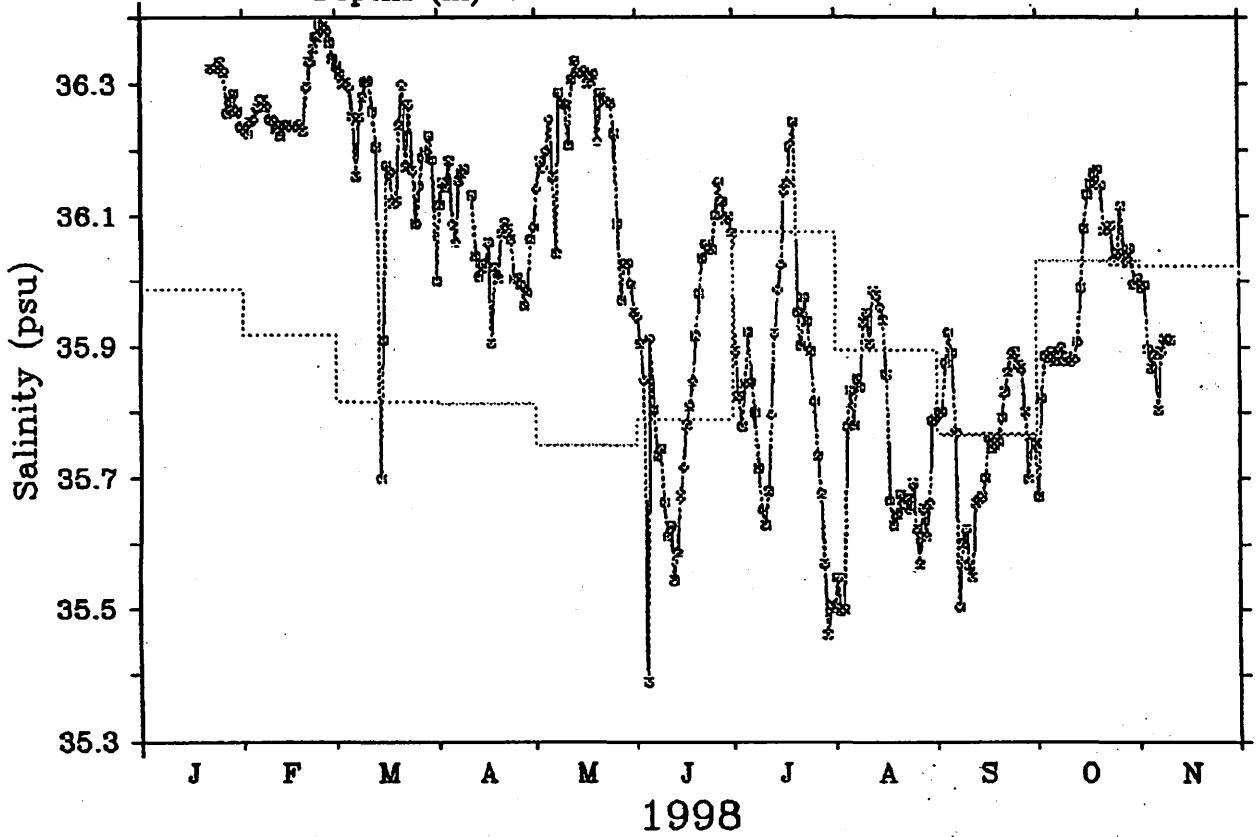


Figure 2b: Daily rainfall data telemetered from a Next Generation ATLAS mooring.

### ATLAS II Salinity (psu) for 0n35w

Depths (m): 1

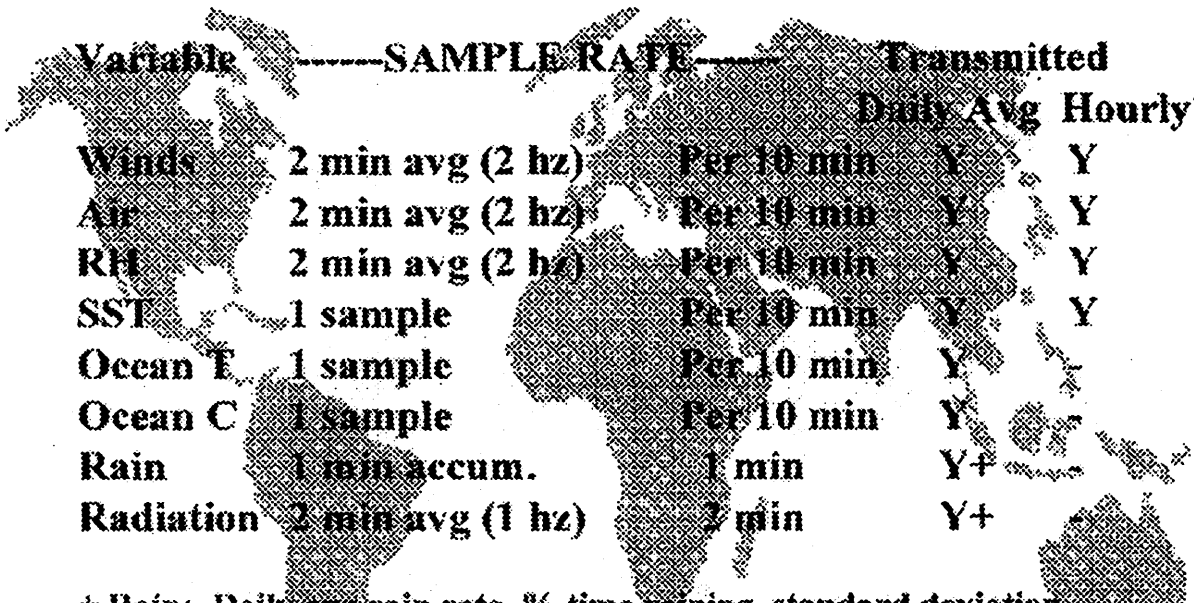


TAO Project Office/PMEL/NOAA

Nov 12 1998

Figure 2c: Daily salinity data telemetered from a Next Generation ATLAS mooring.

## Next Generation ATLAS



Variable	SAMPLE RATE		Transmitted	
			Daily Avg	Hourly*
Winds	2 min avg (2 hz)	Per 10 min	Y	Y
Air	2 min avg (2 hz)	Per 10 min	Y	Y
RH	2 min avg (2 hz)	Per 10 min	Y	Y
SST	1 sample	Per 10 min	Y	Y
Ocean T	1 sample	Per 10 min	Y	
Ocean C	1 sample	Per 10 min	Y	
Rain	1 min accum.	1 min	Y+	
Radiation	2 min avg (1 hz)	2 min	Y+	

+ Rain: Daily avg rain rate, % time raining, standard deviation

+ Radiation: Avg. from 6 am-6 pm (local), max. 2 minute value, st. dev.

\* Most recent hourly value (minute 00) received on each satellite pass.

Complete high resolution record only available after buoy is recovered.

Figure 3: Data sample rates and transmitted data from Next Generation ATLAS moorings.

# ATLAS NextGen Corrections ( $^{\circ}\text{C}$ ) for 5n140w

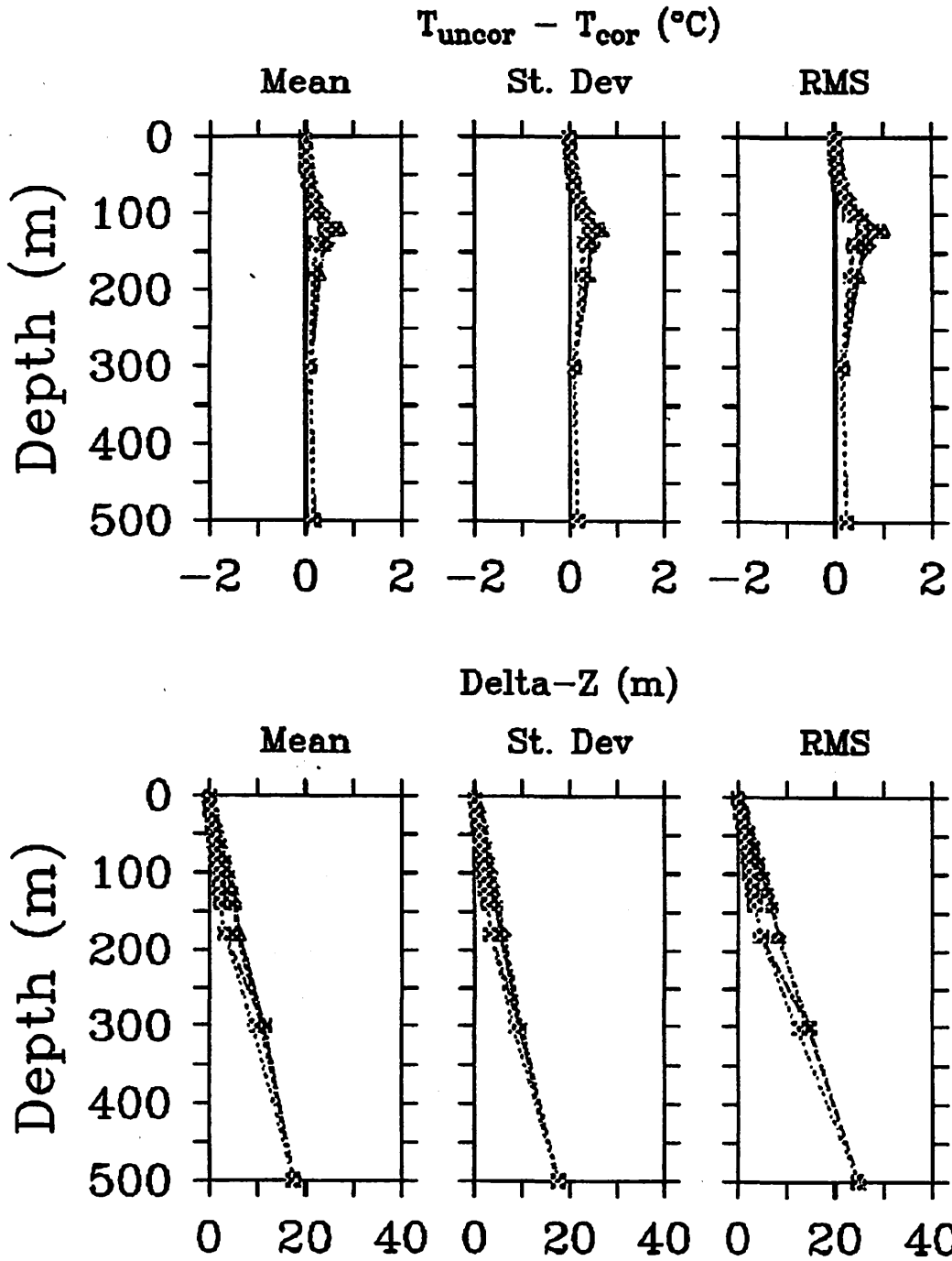


Figure 4: Lower panels: Mean standard deviation and RMS depth variation of ATLAS modules on a reverse catenary mooring. Pressure was measured at 180m, 300m, and 500m, and extrapolated upward. Alternate depth profiles were computed for cases when one or more measured pressures were not available. Upper panel: Temperature corrections computed from depth profiles and vertical temperature gradients.



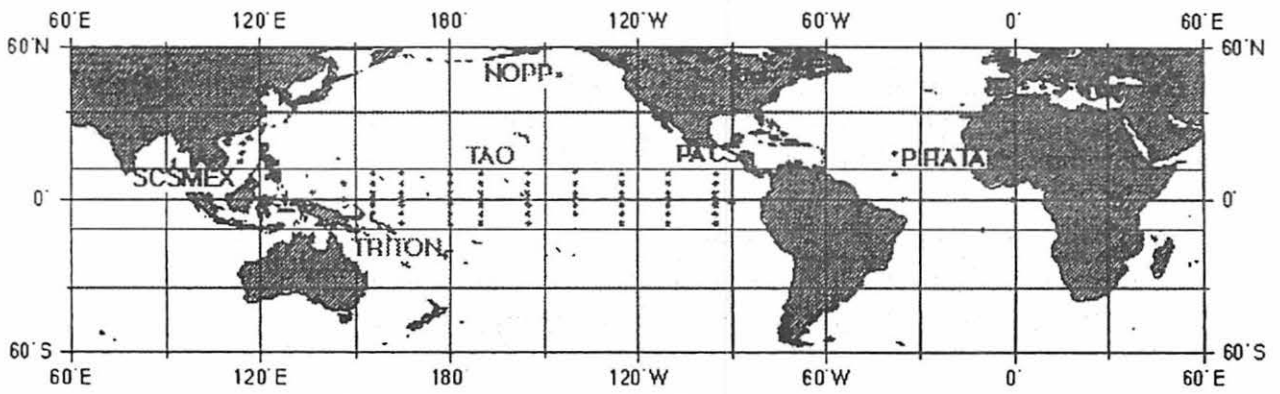


Figure 5: Expansions of TAO mooring technology.

99-005

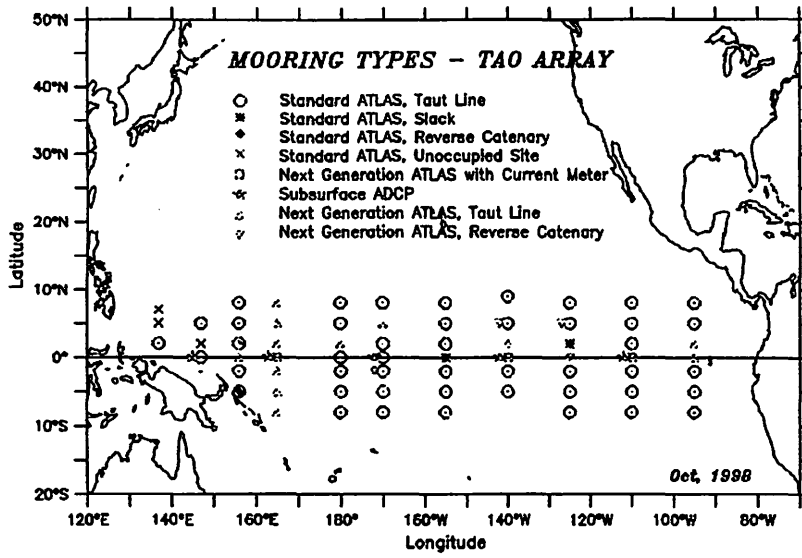
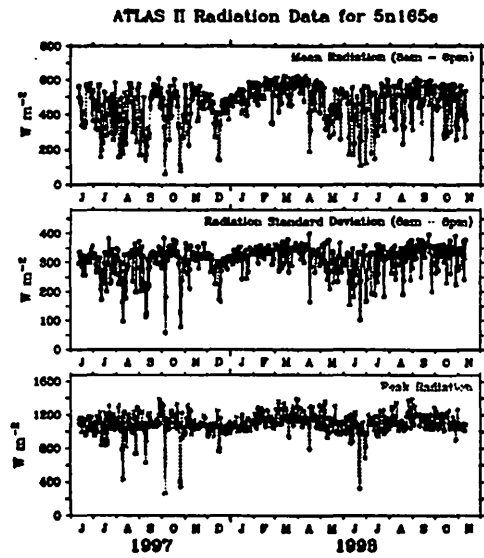


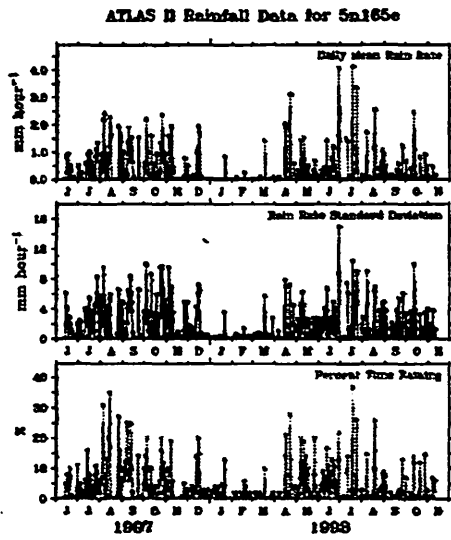
Figure 1: Location and types of moorings within the TAO Array.



NSF Project Office/PDEL/NOAA

Nov 13 1998

Figure 2a: Daily shortwave radiation data telemetered from a Next Generation ATLAS mooring.



NO Project 05165/002/0004

Dec 12 1968

Figure 2b: Daily rainfall data telemetered from a Next Generation ATLAS mooring.

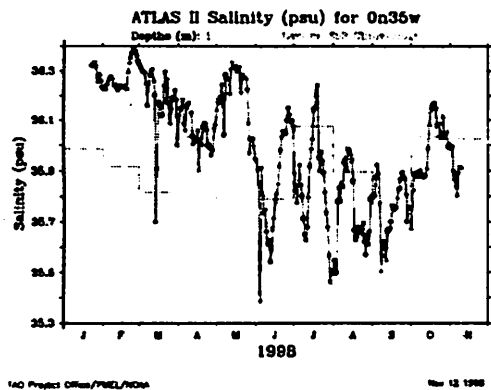
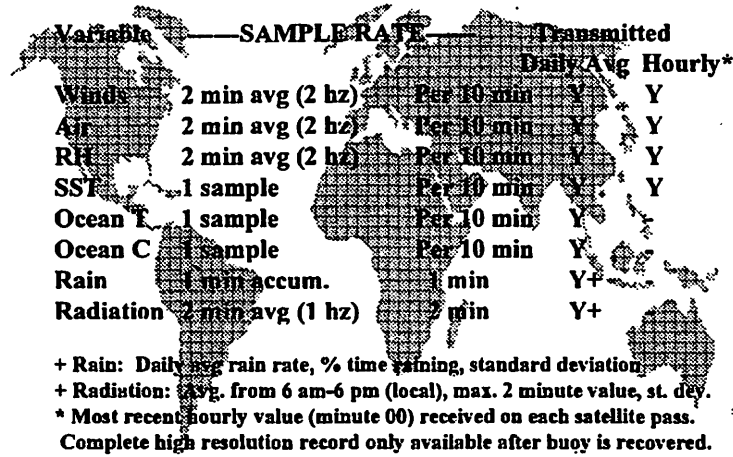


Figure 2c: Daily salinity data telemetered from a Next Generation ATLAS mooring.

## Next Generation ATLAS



Variable	SAMPLE RATE		Transmitted	
			Daily Avg	Hourly*
Winds	2 min avg (2 hz)	Per 10 min	Y	Y
Air	2 min avg (2 hz)	Per 10 min	Y	Y
RH	2 min avg (2 hz)	Per 10 min	Y	Y
SST	1 sample	Per 10 min	Y	Y
Ocean T	1 sample	Per 10 min	Y	
Ocean C	1 sample	Per 10 min	Y	
Rain	1 min accum.	1 min	Y+	
Radiation	2 min avg (1 hz)	2 min	Y+	

+ Rain: Daily avg rain rate, % time raining, standard deviation  
 + Radiation: Avg. from 6 am-6 pm (local), max. 2 minute value, st. dev.  
 \* Most recent hourly value (minute 00) received on each satellite pass.  
 Complete high resolution record only available after buoy is recovered.

Figure 3: Data sample rates and transmitted data from Next Generation ATLAS moorings.

ATLAS NextGen Corrections (°C) for 5n140w

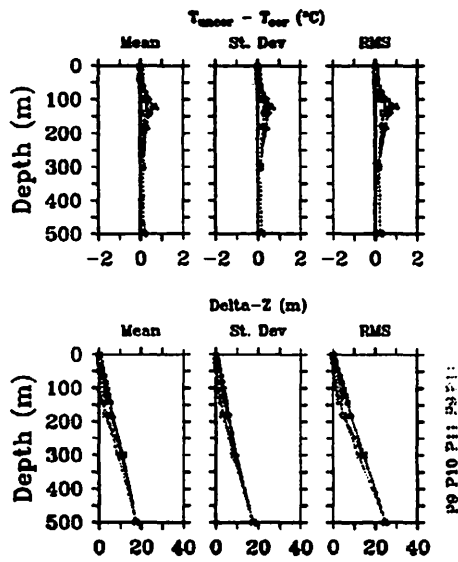


Figure 4: Lower panels: Mean standard deviation and RMS depth variation of ATLAS modules on a reverse catenary mooring. Pressure was measured at 180m, 300m and 500m, and extrapolated upward. Alternate depth profiles were computed for cases when one or more measured pressures were not available. Upper panel: Temperature corrections computed from depth profiles and vertical temperature gradients.

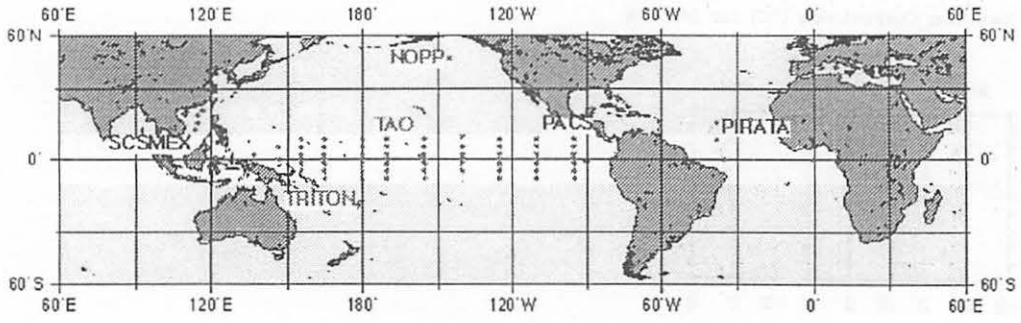
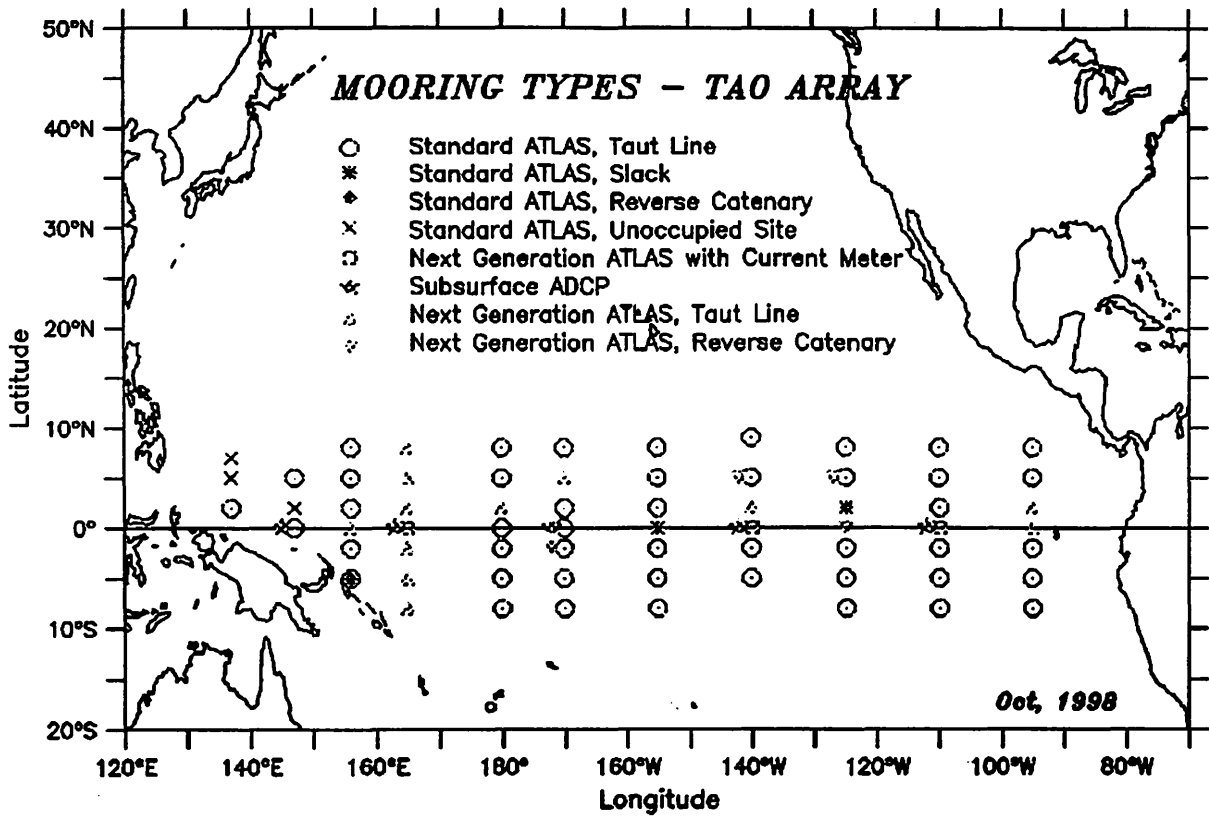


Figure 5: Expansions of TAO mooring technology.





### ATLAS II Radiation Data for 5n165e

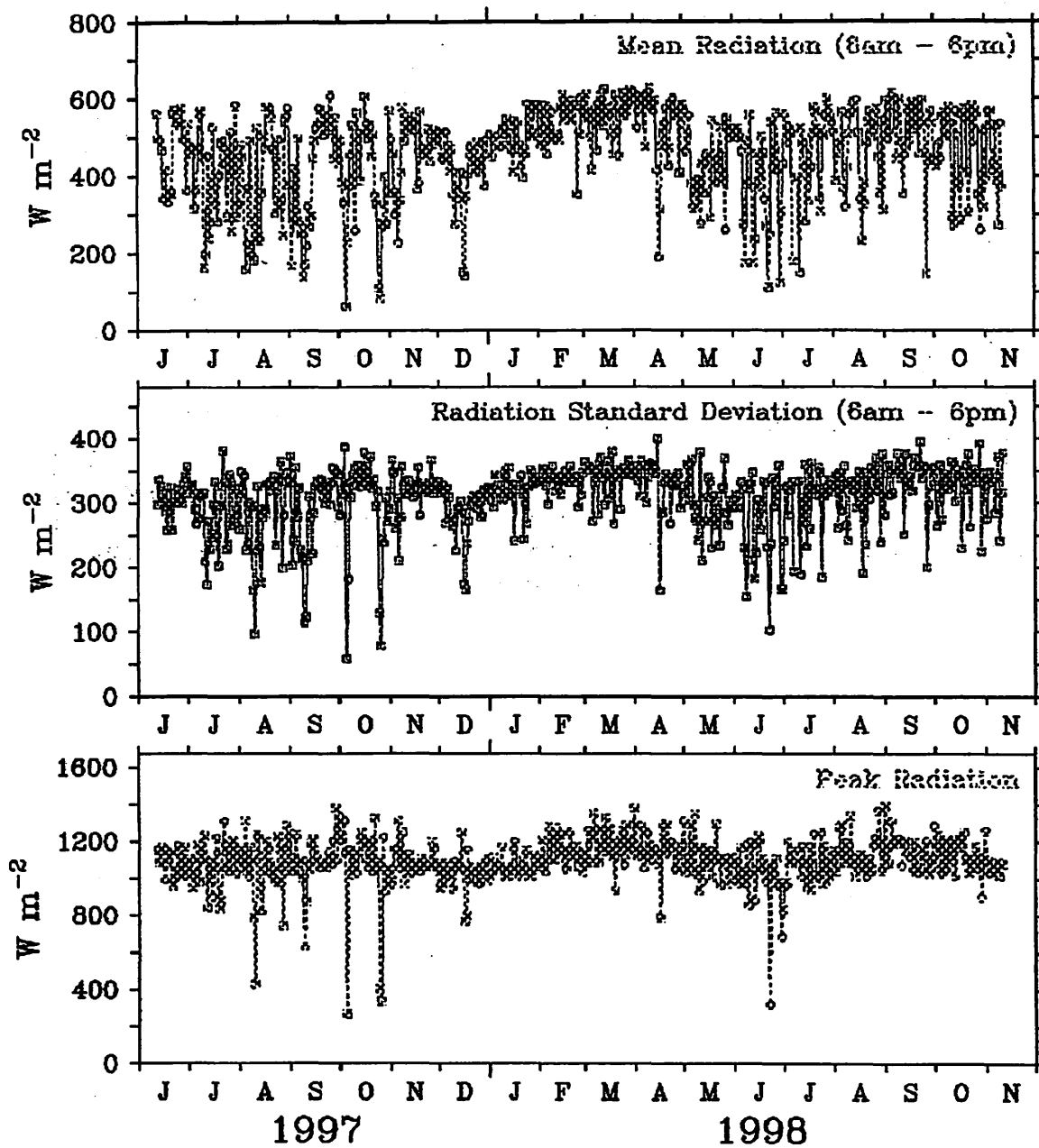


Figure 2a: Daily shortwave radiation data telemetered from a Next Generation ATLAS mooring.

### ATLAS II Rainfall Data for 5n165e

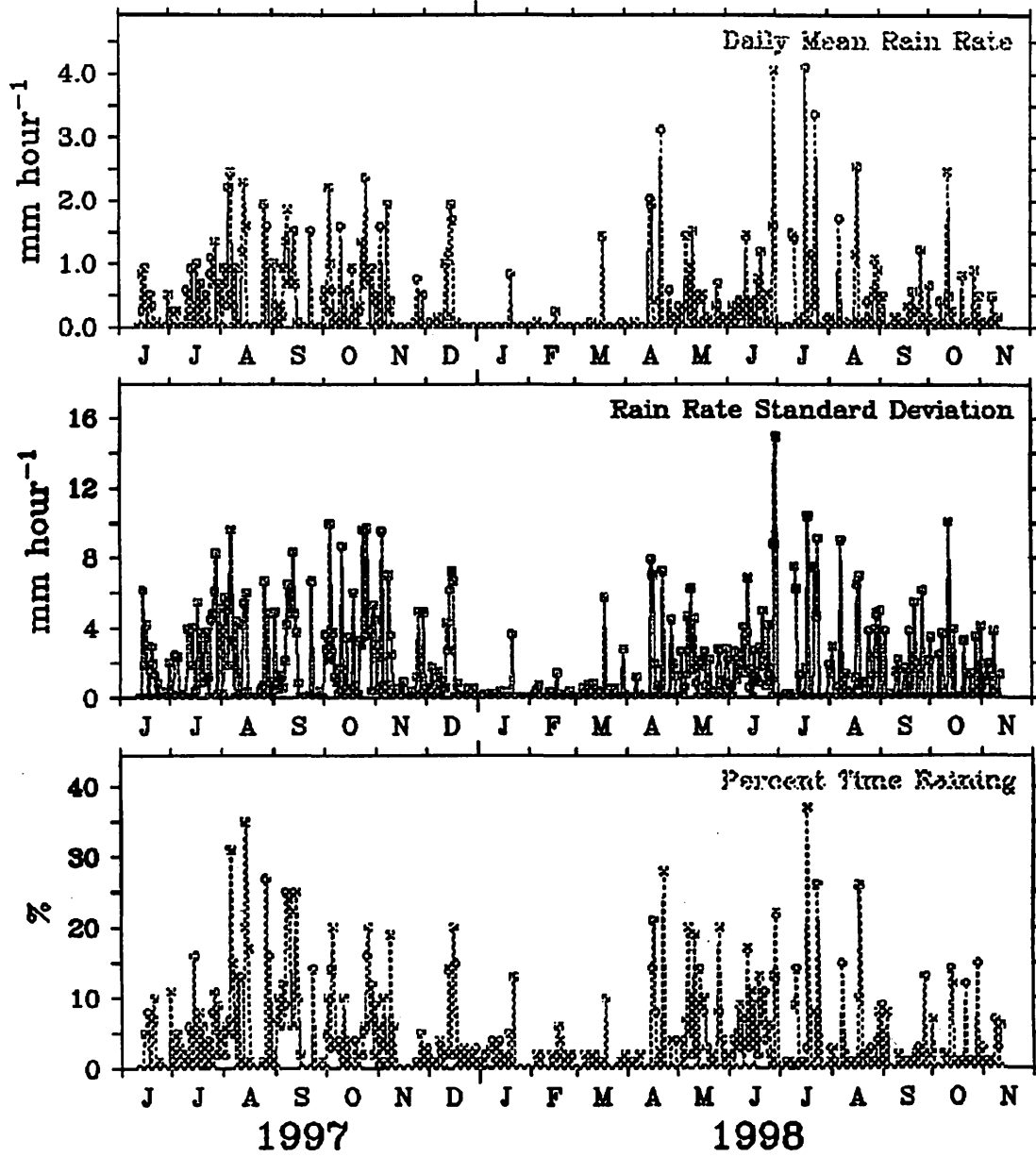
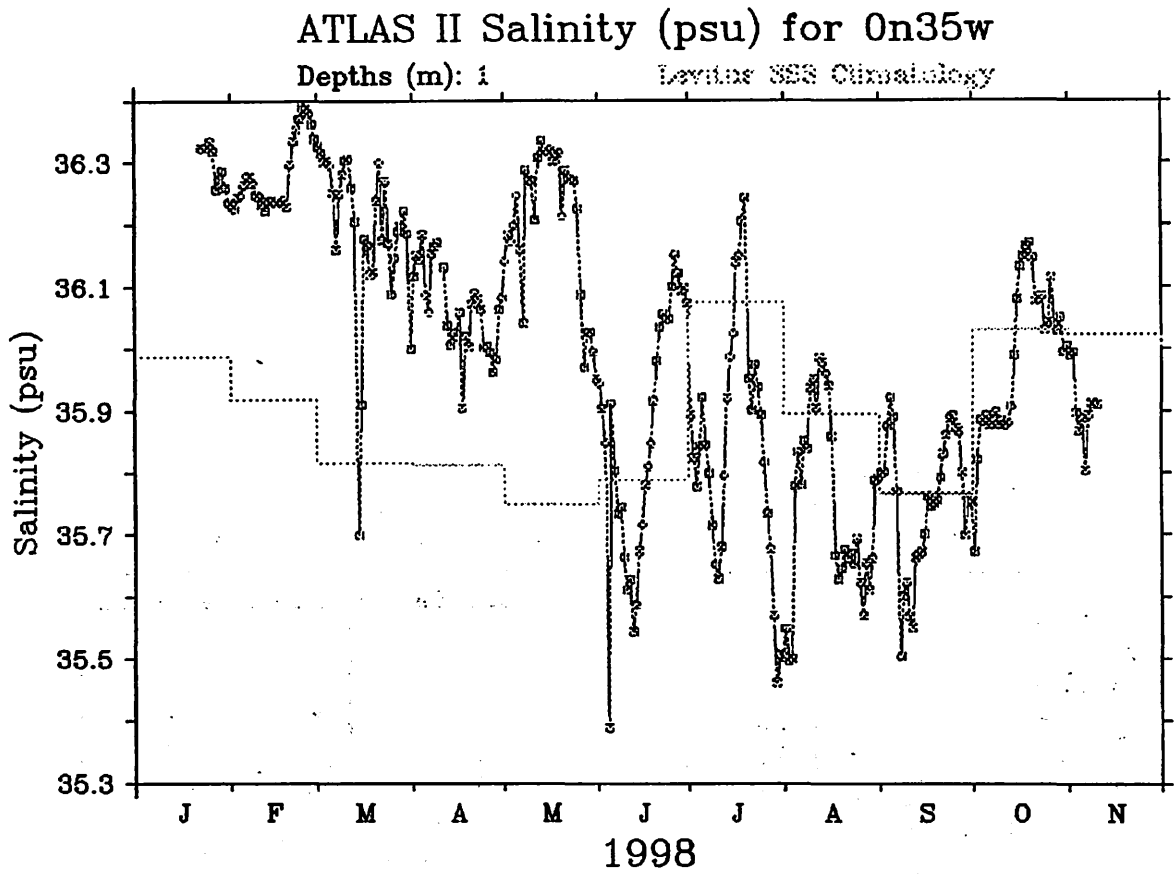


Figure 2b: Daily rainfall data telemetered from a Next Generation ATLAS mooring.

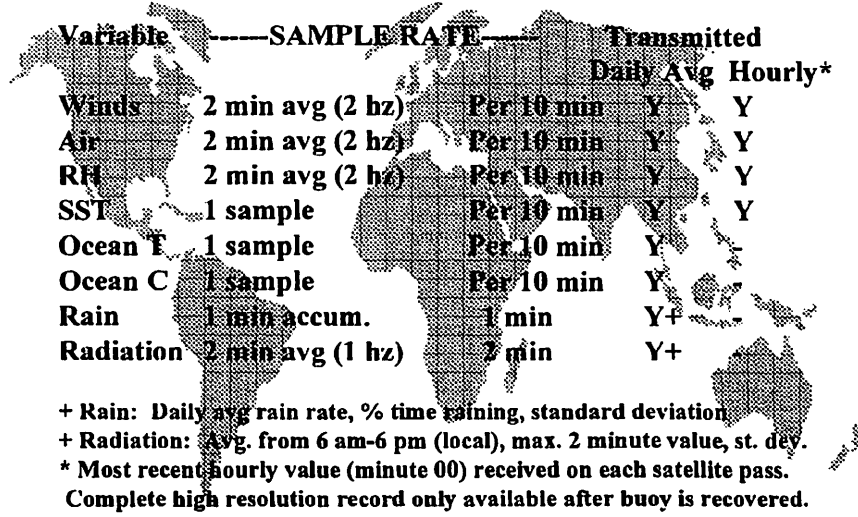


TAO Project Office/PMEL/NOAA

Nov 12 1998

Figure 2c: Daily salinity data telemetered from a Next Generation ATLAS mooring.

## Next Generation ATLAS



Variable	SAMPLE RATE		Transmitted	
			Daily Avg	Hourly*
Winds	2 min avg (2 hz)	Per 10 min	Y	Y
Air	2 min avg (2 hz)	Per 10 min	Y	Y
RH	2 min avg (2 hz)	Per 10 min	Y	Y
SST	1 sample	Per 10 min	Y	Y
Ocean T	1 sample	Per 10 min	Y	-
Ocean C	1 sample	Per 10 min	Y	-
Rain	1 min accum.	1 min	Y+	-
Radiation	2 min avg (1 hz)	2 min	Y+	-

+ Rain: Daily avg rain rate, % time raining, standard deviation  
 + Radiation: Avg. from 6 am-6 pm (local), max. 2 minute value, st. dev.  
 \* Most recent hourly value (minute 00) received on each satellite pass.  
 Complete high resolution record only available after buoy is recovered.

Figure 3: Data sample rates and transmitted data from Next Generation ATLAS moorings.

# ATLAS NextGen Corrections ( $^{\circ}\text{C}$ ) for 5n140w

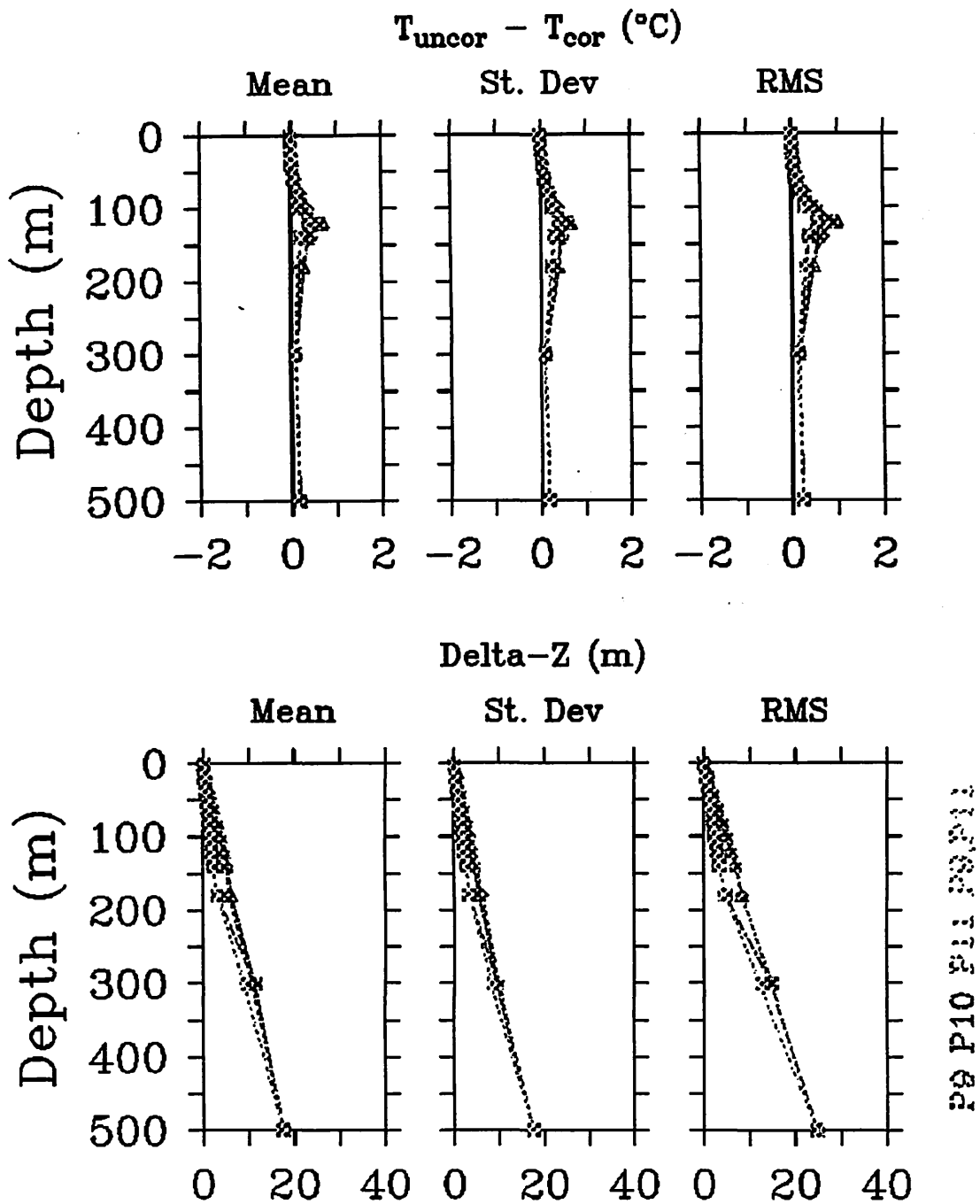


Figure 4: Lower panels: Mean standard deviation and RMS depth variation of ATLAS modules on a reverse catenary mooring. Pressure was measured at 180m, 300m and 500m, and extrapolated upward. Alternate depth profiles were computed for cases when one or more measured pressures were not available. Upper panel: Temperature corrections computed from depth profiles and vertical temperature gradients.

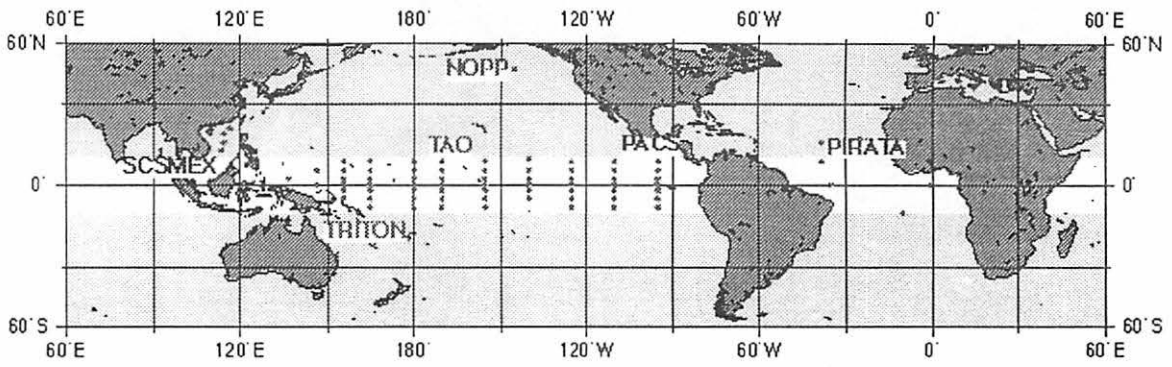


Figure 5: Expansions of TAO mooring technology.

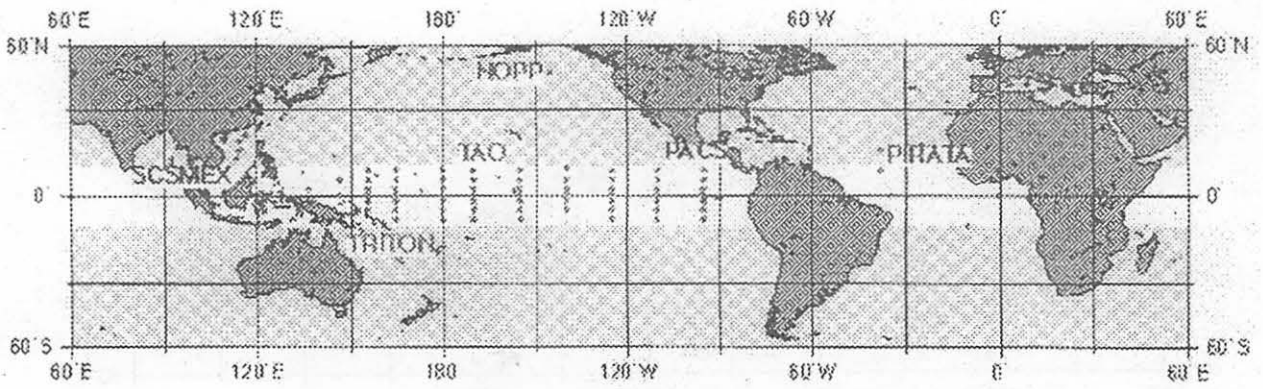


Figure 5: Expansions of TAO mooring technology.



**Data Buoy Co-operation Panel, Fourteenth Session  
Technical Workshop  
(Marathon, Florida, USA, 12-13 October 1998)**

**LIST OF PARTICIPANTS**

**Mr Robert Bassett**  
NOAA/NESDIS  
Direct Services Division  
E/SP3, Rm. 3320, FB-4  
4200 Auth Road  
SUITLAND, MD 20746-4304  
USA  
Telephone: +1-301 457 5681  
Telefax: +1-301 457 5620  
E-mail: rbassett@nesdis.noaa.gov

**Mr A.N. Bentley**  
The Meteorological Office  
London Road  
Beaufort Park, Easthampstead  
WOKINGHAM, Berkshire RG40 3DN  
United Kingdom  
Telephone: +44-1344 855 603  
Telefax: +44-1344 855 897  
E-mail: anbentley@meto.gov.uk

**Mr K. Berger-North**  
Axys Consulting, Ltd.  
P.O. Box 2219  
2045 Mills Road  
SIDNEY, B.C. V8L 3S8  
Canada  
Telephone: +1-205 656 0881  
Telefax: +1-205 656 4789  
E-mail: kberger@axys.com

**Dr Peter G. Black**  
NOAA/AOML  
4301 Rickenbacker Cswy  
MIAMI, FL 33149-1026  
USA  
Telephone: +1-305 361 4320  
Telefax: +1-305 361 4402  
E-mail: Peter.Black@noaa.gov

**Mr Mark Blaseckie**  
Meteorological Systems

**Axys Environmental Systems**  
2045 Mills Road  
P.O. Box 2219  
SIDNEY, BC  
Canada  
Telephone: +1-250 656 0881  
Telefax: +1-250 656 0316  
E-mail: mblaseckie@axys.com

**Mr Paul-André Bolduc**  
Marine Environment Data Service  
Department of Fisheries and Oceans  
200 Kent Street  
OTTAWA, Ontario, K1A 0E6  
Canada  
Telephone: +1-613 990 0231  
Telefax: +1-613 993 4658  
E-mail: bolduc@ottmed.meds.dfo.ca

**Mr Graeme Brough**  
Chairman, DBCP  
Bureau of Meteorology  
G.P.O. Box 1289 K  
MELBOURNE, Vic. 3001  
Australia  
Telephone: +61-3 9669 4163  
Telefax: +61-3 9669 4168  
E-mail: g.brough@bom.gov.au

**Mr Hal Brown**  
National Data Buoy Center (NWS/NOAA)  
Bldg. 1100  
STENNIS SPACE CENTER, MS 39529-  
6000  
USA  
Telephone: +1-228 688 2439  
Telefax: +1-228 688 3153  
E-mail: hbrown@ndbc.noaa.gov

**Mr Terry E. Bryan**  
Chairman, JTA  
Argos JTA Program Manager

NOAA Office of Global Programs  
1100 Wayne Avenue, Suite 1210  
SILVER SPRING, MD 20910-5603  
USA  
Telephone: +1-301 427 2089 ext. 147  
Telefax: +1-301 427 2222  
E-mail: bryan@ogp.noaa.gov

Mr John Burman  
Measurements Standards Engineer  
MetService NZ Ltd  
Tahi Road Extension  
PARAPARAUMU  
New Zealand

Mr Mark Bushnell  
Manager, Global Drifter Center  
R/E/AO/PHOD  
NOAA/AOML, R/E/AO/PHOD  
4301 Rickenbacker Causeway  
Virginia Key  
MIAMI, FL 33149-1026  
USA  
Telephone: +1-305 361 4353  
Telefax: +1-305 4582  
E-mail: bushnell@aoml.noaa.gov

Ms Christine Caruso  
NOAA/NWS/NCEP/Central Operations  
Data Management and Quality  
Assessment Branch  
5200 Auth Road, Room 100  
CAMP SPRINGS, MD 20746  
USA  
Telephone: +1-301 763 8000 ext. 7160  
Telefax: +1-301 763 8381  
E-mail: chris.caruso@noaa.gov

Mr Etienne Charpentier  
Technical Coordinator, DBCP  
c/o CLS/Service Argos  
8-10 rue Hermes  
Parc Technologique du Canal  
F-31526 RAMONVILLE SAINT-AGNE  
France  
Telephone: +33-5 61 39 47 82  
Telefax: +33-5 61 75 10 14  
E-mail: charpentier@cls.cnes.fr  
Web: http://dbcp.nos.noaa.gov/dbcp

Ms Monique Ciccione  
Météo-France  
Boîte postale 645  
97262 FORT DE FRANCE Cédex  
Martinique  
France  
Telephone: +596 63 99 65  
Telefax: +596 63 99 55  
E-mail: monique.ciccione@meteo.fr

Dr P. David Cotton  
James Rennell Division  
Southampton Oceanography Centre  
European Way  
SOUTHAMPTON SO14 3ZH  
United Kingdom  
Telephone: +44-1703 596411  
Telefax: +44-1703 596400  
E-mail: d.cotton@soc.soton.ac.uk

Dr Peter E. Dexter  
Chief, Oceanic Affairs Division  
World Weather Watch Department  
World Meteorological Organization  
41, avenue Giuseppe-Motta  
Case postale No 2300  
CH-1211 GENEVE 2  
Switzerland  
Telephone: +41-22 730 82 37  
Telefax: +41-22 733 02 42  
E-mail: dexter@www.wmo.ch  
Telex: 41 41 99 OMM CH

Dr Rex J. Fleming  
Program Manager, Climate Observations  
NOAA/ERL  
3300 Mitchell Lane, Suite 175  
BOULDER, CO 80301  
USA  
Telephone: +1-303 497 8165  
Telefax: +1-303 497 8158  
E-mail: fleming@ncar.ucar.edu

Mr H. Paul Freitag  
NOAA/PMEL  
7600 Sandpoint Way, NE  
BIN C15700  
SEATTLE, WA 98115-0070

**USA**

Telephone: +1-206 526 6727  
Telefax: +1-206 526 6744  
E-mail: Paul.H.Freitag@noaa.gov

**Mr François Gérard**  
Vice-chairman, Joint IOC-WMO-UNEP  
Intergovernmental Committee for GOOS  
Chef du Département "réseau" de la  
Direction générale des opérations de  
Météo-France  
1,quai Branly  
75340 PARIS Cédex 07  
France  
Telephone: +33-1 45 56 70 24  
Telefax: +33-1 45 56 70 05  
E-mail: francois.gerard@meteo.fr  
Telex: 202876

**Mr David B. Gilhousen**  
National Data Buoy Center (NWS/NOAA)  
Bldg. 1100  
STENNIS SPACE CENTER, MS 39529-  
6000  
USA  
Telephone: +1-228 688 2840  
Telefax: +1-228 688 3153  
E-mail: dgilhousen@ndbc.noaa.gov

**Mr A.T. Frank Grooters**  
Observations and Modelling Department  
Royal Netherlands Meteorological Institute  
P.O. Box 201  
3730 AE DE BILT  
Netherlands  
Telephone: +31-30 220 6691  
Telefax: +31-30 221 0407  
Telex: 47 096 nl  
E-mail: grooters@knmi.nl

**Mr Jim Hanlon**  
Vice President - Principal  
Seimac Limited  
271 Brownlow Avenue  
DARTMOUTH, Nova Scotia  
Canada B3B 1W6  
Telephone: +1-902 468 3007  
Telefax: +1-902 468 3009  
E-mail: jhanlon@seimac.com

**Mr Paul Hill**  
Instruments Sales Manager  
Seimac Limited  
271 Brownlow Avenue  
DARTMOUTH, Nova Scotia  
Canada B3B 1W6  
Telephone: +1-902 468 3007  
Telefax: +1-902 468 3009  
E-mail: phill@seimac.com

**Mr Hreinn Hjartarson**  
Icelandic Meteorological Office  
Bústaðavegur 9  
150 REYKJAVIK  
Iceland  
Telephone: +354 560 0600  
Telefax: +354 552 8121  
E-mail: hreinn@vedur.is

**Ms Elizabeth Horton**  
U.S. Naval Oceanographic Office  
NAVOCEANO: N-31  
Stennis Space Center  
SSC, MS 39529-5001  
USA  
Telephone: +1-601 688 5725  
Telefax: +1-601 688 4589  
E-mail: ehorton@navo.navy.mil

**Dr Ngoc Huang**  
NAL Research Corporation  
14318 Montverd Ct  
CENTREVILLE; VA 20121  
USA  
Telephone: +1-703 803 1418  
Telefax: +1-703 803 7435  
E-mail: hoang@bitmotel.com

**Mr Michael Johnson**  
NOAA OGP  
1100 Wayne Avenue, Suite 1220  
SILVER SPRING, MD 20910  
USA  
Telephone: +1-301 427 2089 ext. 62  
Telefax: +1-301 427 2073  
E-mail: johnson@ogp.noaa.gov

**Mr D. Wynn Jones**  
Chairman, EGOS  
The Meteorological Office  
London Road  
Beaufort Park, Easthampstead  
WOKINGHAM, Berkshire, RG40 3DN  
United Kingdom  
Telephone: +44-1344 855 603  
Telefax: +44-1344 855 897  
E-mail: dwjones@meto.gov.uk

**Mr K. Prem Kumar**  
Programme Director  
National Data Buoy Programme  
National Institute of Ocean Technology  
Department of Ocean Development  
IC & SR Building  
IIT Campus  
CHENNAI-600 036  
India  
Telephone: +91-44 230 0521  
Telefax: +91-44 230 0537  
E-mail: prem@niot.ernet.in

**Dr Joao Lorenzetti**  
National Institute for Space Research  
Av. Dos Astronautas  
1758 J. Da Granja  
CEP 12227-010  
SAO JOSE DOS CAMPOS, S.P.  
Brazil  
E-mail: loren@lagavulin.itid.inpe.br

**Mr Greg Maki**  
Engineer  
Technocean, Inc.  
820 NE 24th Lane, Unit 112  
CAPE CORAL, FL 33909  
USA  
Telefax: +1-941 574 5613

**Mr Svend-Aage Malmberg**  
Marine Research Institute  
Skúlagata  
121 REYKJAVIK  
Iceland  
Telephone: +354 552 0240  
Telefax: +354 562 3790  
E-mail: svam@hafro.is

**Mr Ron McLaren**  
Head, Marine Operations  
Atmospheric Environment Branch Pacific  
and Yukon Region  
Environment Canada  
Suite 700-1200 West 73rd Avenue  
VANCOUVER, B.C., V6P 6H9  
Canada  
Telephone: +1-604 664 9188  
Telefax: +1-604 664 9195  
E-mail: ron.mclaren@ec.gc.ca

**Mr Eric A. Meindl**  
National Data Buoy Center  
Bldg. 1100  
STENNIS SPACE CENTER, MS 39529-  
6000  
USA  
Telephone: +1-601 688 1717  
Telefax: +1-601 688 3153  
E-mail: emeindl@ndbc.noaa.gov

**Mr David Meldrum**  
Vice-chairman, DBCP  
Dunstaffnage Marine Laboratory  
PO Box 3  
OBAN, Argyll, PA34 4AD  
Scotland  
United Kingdom  
Telephone: +44-1631 567 873  
Telefax: +44-1631 565 518  
E-mail: dtm@dml.ac.uk

**Dr Robert L. Molinari**  
Physical Oceanography Division  
NOAA-AOML, R/E/AO/PHOD  
4301 Rickenbacker Causeway  
Virginia Key  
MIAMI, FL 33149-1026  
USA  
Telephone: +1-305 361 4344  
Telefax: +1-305 361 4582  
E-mail: molinari@aoml.noaa.gov

**Dr Peter Niiler**  
Scripps Institution of Oceanography  
LA JOLLA, CA 92093-0230  
USA

Telephone: +1-619 534 4100  
Telefax: +1-619 534 7931  
E-mail: pniiler@ucsd.edu

Mr Christian Ortega  
CLS/Service Argos  
8-10 rue Hermès  
31526 RAMONVILLE ST AGNE  
France  
Telephone: +33-5 61 39 47 70  
Telefax: +33-5 61 75 10 14  
E-mail: ortega@cls.cnes.fr  
Telex: 531 752F

Mr Derek J. Painting  
DBCP Consultant  
5 The Sycamores  
Darby Green  
Blackwater  
CAMBERLEY  
United Kingdom  
Telephone: +44-1252 876804  
Telefax: +44-1252 645612  
E-mail: 101527.1533@compuserve.com  
Mobile: +44-385 250377

Dr Stephen Pazan  
Ocean Prospects  
204 N. El Camino Real, Suite 619  
ENCINITAS, CA 92024  
USA  
Telephone: +1-760 753 9328  
Telefax: +1-760 436 0338  
E-mail: spazan@cts.com

Mr Jack Ploeg  
4696 Gail Crescent  
COURTENAY, B.C.  
Canada  
Telephone: +1-250 338 1604  
E-mail: jjploeg@ireland.net

Mr Jean Rolland  
Météo-France  
13 rue du Chatellier  
29273 BREST CEDEX  
France  
Telephone: +33-2 98 22 18 53

Telefax: +33-2 98 22 18 49  
E-mail: jean.rolland@meteo.fr

Mr Simon Skey  
Axys Consulting, Ltd.  
P.O. Box 2219  
2045 Mills Road  
SIDNEY, B.C. V8L 3S8  
Canada  
Telephone: +1-250 656 0881  
Telefax: +1-250 656 4789  
E-mail: sskey@axys.com

Mr John Stadler  
NOAA/AOML  
4301 Rickenbacker Cswy  
MIAMI, FL 33149-1026  
USA  
Telephone: +1-305 361 4322  
Telefax: +1-305 361 4442  
E-mail: John.Stadler@noaa.gov

Dr Mark Swenson  
Chairman, GDP  
Director, Global Drifter Center  
NOAA - AOML - R/E/AO/PHOD  
4301 Rickenbacker Causeway  
MIAMI, FL 33149-1026  
USA  
Telephone: +1-305 361 4363  
Telefax: +1-305 361 4582  
E-mail: swenson@aoml.noaa.gov  
Telex: 6507457601

Mr Michel Taillade  
General Manager, CLS/Service Argos  
8-10 rue Hermes  
Parc Technologique du Canal  
31526 RAMONVILLE ST AGNE  
France  
Telephone: +33-5 61 39 47 02  
Telefax: +33-5 61 75 10 14  
E-mail: taillade@cls.cnes.fr

Mr H. Tanner  
The Meteorological Office  
London Road  
Beaufort Park, Easthampstead

WOKINGHAM, Berkshire RG40 3DN  
United Kingdom  
Telephone: +44-1344 855 603  
Telefax: +44-1344 855 897  
E-mail: htanner@meto.gov.uk

Mr Peter Thomas  
Principal Lecturer  
Department of Software & Electronic  
Engineering  
Central Institute of Technology  
P.O. Box 40 740  
UPPER HUTT  
New Zealand  
Telephone: +64-4 527 6383  
Telefax: +64-4 527 6374  
E-mail: BRENDA@ee2.ee.cit.ac.nz

Mr Yves Tréglos  
Assistant Secretary  
Intergovernmental Oceanographic  
Commission  
1, rue Miollis  
75732 PARIS Cédex 15  
France  
Telephone: +33-1 45 68 39 76  
Telefax: +33-1 45 56 93 16  
E-mail: y.treglos@unesco.org

Mr Hedinn Valdimarsson  
Marine Research Institute  
Skulagata  
121 REYKJAVIK  
Iceland  
Telefax: +354 562 3790

Mr W.C.M. van Dijk  
Vice-chairman, EGOS  
Observations and Modelling Department  
Royal Netherlands Meteorological Institute  
P.O. Box 201  
3730 AE DE BILT  
Netherlands  
Telephone: +31-30 220 6324  
Telefax: +31-30 221 0407  
Telex: 47 096 nl

Mr Louis Vermaak  
South African Weather Bureau  
Private Bag X97  
PRETORIA 0001  
South Africa  
Telephone: +27-12 309 3834  
Telefax: +27-12 309 3020  
E-mail: vermaak@cirrus.sawb.gov.za

Mr W. Gary Williams  
Clearwater Instrumentation Inc.  
304 Pleasant Street  
WATERTOWN, MA 02472  
USA  
Telephone: +1-617 924 2708  
Telefax: +1-617 924 2724  
E-mail: wgwill@clearwater-inst.com

Mr Jeffrey L. Wingenroth  
General Manager  
Technocean, Inc.  
820 NE 24th Lane, Unit 112  
CAPE CORAL, FL 33909  
USA  
Telephone: +1-941 772 9067  
Telefax: +1-941 574 5613  
E-mail: jlwing@gate.net

Mr William E. Woodward  
Vice-chairman, DBCP  
NOAA/AOML, R/E  
SSMC #3, Room 11142  
1315 East-West Highway  
SILVER SPRING, MD 20910  
USA  
Telephone: +1-301 713 2790 ext. 180  
Telefax: +1-301 713 4499  
E-mail: William.e.woodward@noaa.gov

## TECHNICAL DOCUMENTS ISSUED WITHIN THE DATA BUOY COOPERATION PANEL SERIES

No.	Title	Year of issue
1	Annual Report for 1994	1995
2	Reference Guide to the GTS Sub-system of the Argos Processing System	1995
3	Guide to Data Collection and Location Services using Service Argos	1995
4	WOCE Surface Velocity Programme Barometer Drifter Construction Manual	1995
5	Surface Velocity Programme - Joint Workshop on SVP Barometer Drifter Evaluation	1996
6	Annual Report for 1995	1996
7	Developments in Buoy Technology and Enabling Methods - Technical Presentations Made at the Eleventh Session of the DBCP	1996
8	Guide to Moored Buoys and Other Ocean Data Acquisition Systems	1997
9	Annual Report for 1996	1997
10	Developments in Buoy and Communications Technologies	1997
11	Annual Report for 1997	1998
12	Developments in Buoy Technology and Data Applications	1998
13	Annual Report for 1998	1999
14	Variety in Buoy Technology and Data Applications	1999

**These publications can be ordered from: Etienne Charpentier, Technical Coordinator of the DBCP, CLS/Service Argos, 8-10 rue Hermès, Parc Technologique du Canal, F-31526 Ramonville Saint-Agne, France - *Internet mail:* charpentier@cls.cnes.fr - *Telefax:* +33-5 61 75 10 14 *Telephone:* +33-5 61 39 47 82**

